

***Molecular mechanism of homo and hetero
interactions of human Guanylate Binding Protein
isoforms***

Dissertation zur Erlangung des akademischen Grades
eines Doktors der Naturwissenschaften
der Fakultät für Chemie und Biochemie
an der Ruhr-Universität Bochum

vorgelegt von

Semra Ince

aus Dortmund

Bochum, 2015

Die vorliegende Arbeit wurde in der Zeit von Februar 2015 bis September 2015 in der Fakultät für Chemie und Biochemie der Ruhr Universität Bochum unter der Leitung von Herrn Prof. Dr. Christian Herrmann angefertigt.

1. Gutachter: Prof. Dr. Christian Herrmann
2. Gutachter: Prof. Dr. Raphael Stoll

Table of content

1.	Introduction.....	1
1.1.	Principles of the interferon controlled immune system	1
1.2.	Classification of human guanylate binding proteins	4
1.3.	Specifications of hGBPs	7
1.4.	Structure of hGBP-1.....	12
1.5.	Nucleotide dependent self-assembly and self-assembly stimulated GTPase activity of hGBPs.....	14
1.6.	Intramolecular motions of hGBP-1.....	21
1.7.	Dimerization dependent subcellular localization of the hGBPs	23
1.8.	Biological function of hGBPs.....	25
1.9.	Objectives	29
2.	Materials and Methods	31
2.1.	Materials.....	31
2.1.1.	Chemicals.....	31
2.1.2.	Enzymes/ Proteins	31
2.1.3.	Vectors.....	31
2.1.4.	Oligonucleotides.....	31
2.1.5.	Antibiotics.....	33
2.1.6.	E. coli strains.....	34
2.1.7.	Growth media.....	34
2.1.8.	Buffers and solutions.....	34
2.1.9.	Nucleotides.....	35
2.1.10.	Fluorophores	36
2.2.	Molecular biological methods	36
2.2.1.	Isolation of plasmid-DNA from E. coli cells.....	36
2.2.2.	Agarose gel electrophoresis	36

2.2.3.	Gene amplification via Polymerase Chain Reaction (PCR) and purification of reaction products	37
2.2.4.	Restriction digestion with BamHI and Sall.....	37
2.2.5.	DNA extraction from agarose gel.....	38
2.2.6.	DNA ligation	38
2.2.7.	Colony PCR.....	38
2.2.8.	Site directed mutagenesis.....	39
2.2.9.	Preparation of competent E. coli cells.....	40
2.2.10.	Heat shock transformation of E. coli cells	40
2.2.11.	DNA Sequencing	40
2.3.	Biochemical and biophysical methods.....	41
2.3.1.	Synthesis of recombinant hGBPs in E. coli.....	41
2.3.2.	Cell lysis via sonication and purification of recombinant hGBPs.....	41
2.3.3.	Concentrating protein by precipitation and ultrafiltration	42
2.3.4.	Determination of protein concentration by absorption spectroscopy at 280 nm	43
2.3.5.	SDS-PAGE for analysis of protein samples	43
2.3.6.	Nucleotide binding: Equilibrium fluorescence titration	44
2.3.7.	Nucleotide binding: Stopped-flow kinetics.....	45
2.3.8.	GTPase activity assay	46
2.3.9.	Long term GTP and GDP hydrolysis assay.....	47
2.3.10.	Analytical size exclusion chromatography.....	47
2.3.11.	Labelling of hGBPs with Alexa fluorophores.....	48
2.3.12.	Time dependent inter- and intramolecular FRET measurements	51
3.	Results.....	53
3.1.	hGBP-1	53
3.1.1.	Nucleotide binding dynamics of hGBP-1 under physiological salt conditions.....	53
3.1.2.	GTP hydrolysis and product formation catalyzed by hGBP-1 under physiological salt conditions	56

3.1.3.	Nucleotide dependent oligomerization of hGBP-1	60
3.2.	Studies on mutants effecting GMP production of hGBP-1.....	75
3.2.1.	Correlation between C-terminal flexibility and capability of hGBP-1 to catalyze GDP hydrolysis.....	75
3.2.2.	Particular role of C-terminal helix α 13 in GMP production assessed by truncation mutant hGBP-1 $\Delta\alpha$ 13.....	77
3.2.3.	Contribution of conserved phenylalanines to basic properties of hGBP-1.....	86
3.2.4.	GMP defective hGBP-1 mutant K76A	104
3.2.5.	Intramolecular opening of α 12 and α 13 in presence of different interaction partners	120
3.3.	Biochemical properties of hGBP-2, hGBP-3 and hGBP-5 in comparison to hGBP-1 .	123
3.3.1.	Protein expression and purification	124
3.3.2.	Enzymatic activity of hGBP-1, hGBP-2 and hGBP-3.....	126
3.3.3.	Nucleotide binding properties of hGBP isoforms.....	137
3.3.4.	Nucleotide dependent homo interactions of hGBPs - analytical SEC	144
3.4.	Homo and hetero interactions of hGBPs measured by intermolecular FRET	150
3.4.1.	Unspecific labelling of hGBP LG domains with fluorescent dyes	151
3.4.2.	Nucleotide dependent homo dimerization of 1-LG	155
3.4.3.	GDP·AlF _x dependent homo and hetero dimerization of LG domains.....	157
3.4.4.	GTP γ S dependent homo and hetero dimerization of LG domains.....	164
3.4.5.	Competitive FRET studies to address domain involvement in hGBP interactions	173
4.	Discussion	176
4.1.	Physiological salt conditions do affect the oligomerization but not the catalytic activity of hGBP-1	176
4.2.	GDP·AlF _x bound hGBP-1 most likely forms voluminous dimers rather than tetramers..	177
4.3.	Dimerization of hGBP-1 relies on mutual regulation of the subdomains LG and GED which is nucleotide dependent.....	183

4.4.	Formation of GMP upon hGBP-1 catalyzed GTP hydrolysis is controlled by helical motions	184
4.5.	Additional structural elements in the LG domain of hGBP-1 mediate intramolecular motions	190
4.6.	Substrate specificity and product formation serve as indicator for the structural ground state of hGBP-1.....	193
4.7.	Characterization of the isoforms hGBP-2, hGBP-3 and hGBP-5	195
4.7.1.	Purification.....	195
4.7.2.	Individual biochemical fingerprint for each isoform	196
4.7.3.	Lacking GMP production of hGBP-2 is in apparent contradiction to the previously published data	200
4.8.	GTPase activity of hGBP-3 is controlled by the C-terminus.....	201
4.9.	LG domains do not only mediate homo but also hetero dimerization of hGBPs	205
4.10.	Cellular concentration of hGBPs as critical determinant for GTP dependent dimerization	210
	Summary	217
	Bibliography	219
	Acknowledgement	234
	Curriculum vitae.....	235

1. Introduction

1.1. Principles of the interferon controlled immune system

Being permanently exposed to pathogens and infectious agents, vertebrates evolved several mechanisms to protect against. They are primarily equipped with physical and chemical barriers that prevent a majority of bacteria, viruses and parasites from entering the organism but once pathogens succeed to evade those barriers the immune system comes into play. In humans, the innate and the adaptive immune system built the two major constituents which upon pathogen recognition cooperate in a highly balanced manner to confer an efficient immune response to combat and eliminate foreign invaders with the major aim to restore physiological conditions. Cellular and humoral components of the innate system (figure 1-1) establish a rapid immune response after recognizing pathogen-associated molecular patterns (PAMPs) which include conserved structures present on many microorganisms. Phagocytes such as macrophages bind PAMPs via cognate surface receptors which in turn induces pathogen uptake with subsequent degradation and elimination. The complement system encompassing a set of soluble plasma proteins can destroy foreign organisms either directly by inducing cell lysis or indirectly by opsonizing and attracting macrophages and neutrophils for subsequent phagocytosis (Janeway, et al., 2001).

The adaptive immune system builds on the activity of T lymphocytes and B lymphocytes (T cells and B cells, figure 1-1) which give a slower but highly antigen-specific and enhanced immune response. Clonal selection, random recombination of variable receptor gene segments, and pairing of different variable chains generates a huge repertoire of lymphocytes (each with single antigen-specificity) that altogether can recognize virtually any antigen. However, T cells can recognize antigens only when presented on molecules of the major histocompatibility complex (MHC). This can be fulfilled by dendritic cells (DCs), a subgroup a phagocytic innate cells which thus have an essential role in linking the innate and adaptive immune system. Activated by this interaction, T cells can proliferate and differentiate into a subset of mature cells having a variety of essential functions; for instance, cytotoxic T cells can expel cytolytic granules to initiate apoptosis of infected cells, regulatory T cells can regulate an immune response counteracting host damage, and helper T cells can activate innate cells to provide more efficient phagocytosis as well as B cells to differentiate into plasma cells enabled to produce and secrete antibodies specific to the antigen that elicited the immune response. Binding antibodies in turn can agglutinate, neutralize or label antigens altogether supporting

Introduction

the innate system to recognize and eliminate the foreign invaders (Janeway, et al., 2001). Although developing from lymphoid progenitors, natural killer (NK) cells do not act through specific receptors against antigens but rather by recognition of 'missing self' which is equivalent to the absence of MHC molecules. There are certain situations where degenerated or virus infected cells are modified to produce reduced levels of MHC in order to prevent the cell from being recognized by the immune system. However, receiving reduced MHC levels as activating signal NK cells represent an efficient arm of the immune system to rapidly destroy not only foreign cells but also modified host cells (Dranoff, 2004) (Kumar, et al., 2005).

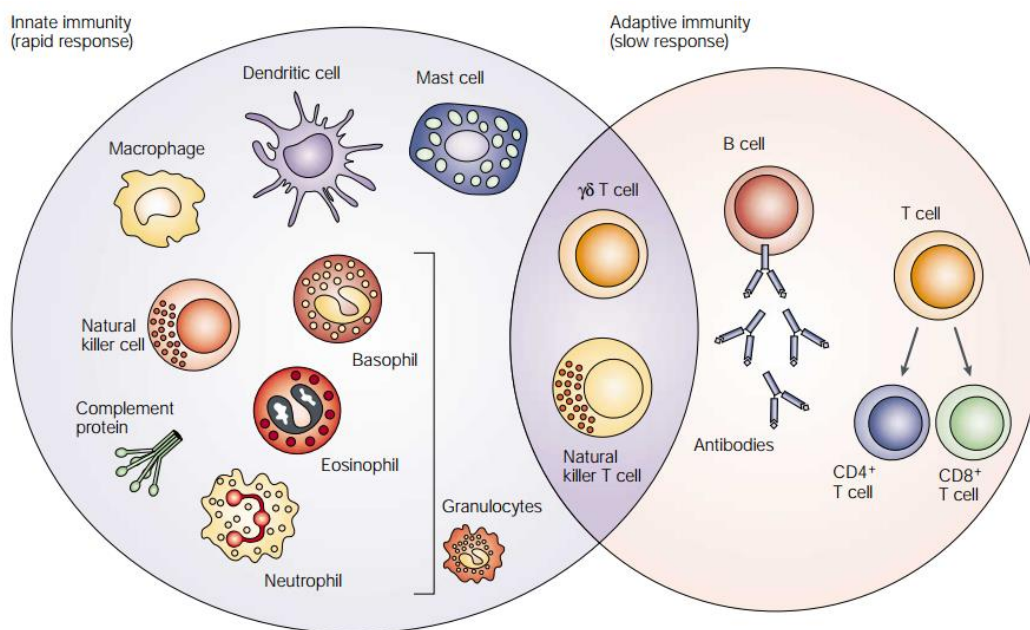


Figure 1-1: Overview on major components of the innate and adaptive immune response. Functioning fast and unspecific, the innate immune response consists of complement proteins and cellular components including mast cells, granulocytes (basophils, eosinophils and neutrophils), phagocytes (macrophages, dendritic cells) and natural killer cells which provide cytolytic activity. Emerging slower but manifested highly specific, the adaptive immune response consists of T cells, B cells and the antibodies they produce. The large subset of differentiated T cells is summarized by their surface glycoproteins CD4⁺ (for example at helper T cells) or CD8⁺ (for example at cytotoxic T cells) that serve as co-receptors for the antigen-specific T cell receptors (TCR). Natural killer T cells and $\gamma\delta$ T cells are specialized cytotoxic lymphocytes comprising specific characteristics from both constituents of the immune system (adapted from Dranoff, 2004).

The immensely complex immune system as only roughly outlined above importantly relies on cytokines to initiate, coordinate and regulate an immune response tailored to the type of host invader. Cytokines comprise a large group of small proteins encircling chemokines, tumor necrosis factor, interleukins and interferons that are able to influence nearly every biological process through signaling activity that aids cell to cell communication (Dinarello, 2007).

Introduction

Interferons (IFNs) first discovered in 1957 and termed by their ability to confer viral interference are recognized as key components of the innate immunity and the first line of defense against viral infection and a broad spectrum of other pathogens (Isaacs, et al., 1957) (Pestka, 2007) (Ding, et al., 2014). Three different types of interferons are distinguished based on their structure, cognate receptors, and biologic activities: type I interferons including IFN- α and IFN- β , type II interferon solely consisting of IFN- γ , and type III interferons comprising three different IFN- λ molecules designated IFN- λ 1, IFN- λ 2 and IFN- λ 3 (Kotenko, et al., 2003) (Pestka, et al., 2004) (Robb, et al., 2012). IFN- λ exhibits potent antiviral activity similar to IFN- α/β but other than ubiquitously expressed IFN- α/β receptors expression of the IFN- λ receptor is restricted to epithelial cells (Ding, et al., 2014). IFN- γ also known to mediate antiviral activity is better known to confer defense strategies against bacterial and protozoal infections (MacMicking, 2012). The common mechanism by which different interferons exert their particular function is the transcriptional regulation of immunologically relevant genes (figure 1-2): IFN binding to receptor leads to activation of Janus kinases (JAKs) which subsequently activate members of the signal transducer and activator of transcription (STAT) family. Phosphorylated STATs form homo or hetero complexes that migrate into the nucleus and bind to specific DNA regions to initiate transcription of downstream genes (Darnell, et al., 1994) (Li, et al., 2009) (MacMicking, 2012). In total, IFNs regulate more than 1000 genes (Li, et al., 2009).

Human guanylate binding proteins (hGBPs) that are focused in the present work are responsive to type I but most prominently to type II interferons; they represent the most abundant group being upregulated in response to IFN- γ accounting for 20 % of the total product (Cheng, et al., 1983) (Kim, et al., 2012). While the molecular mechanism is yet poorly understood, in fact, the majority of functions reported for hGBPs belong to the diverse array of effector functions elicited by IFN- γ , strongly suggesting a mediating role of these proteins (see paragraph 1.8.). Just to mention a few effector functions, IFN- γ inhibits cell growth and proliferation, enhances antigen presentation of infected or transformed cells by upregulating MHC expression, activates macrophages which includes enhanced receptor mediated phagocytosis, production of reactive oxygen species and upregulation of lysosomal enzymes, and moreover IFN- γ upregulates different enzymes including hGBPs with antiviral activity (Schroder, et al., 2004).

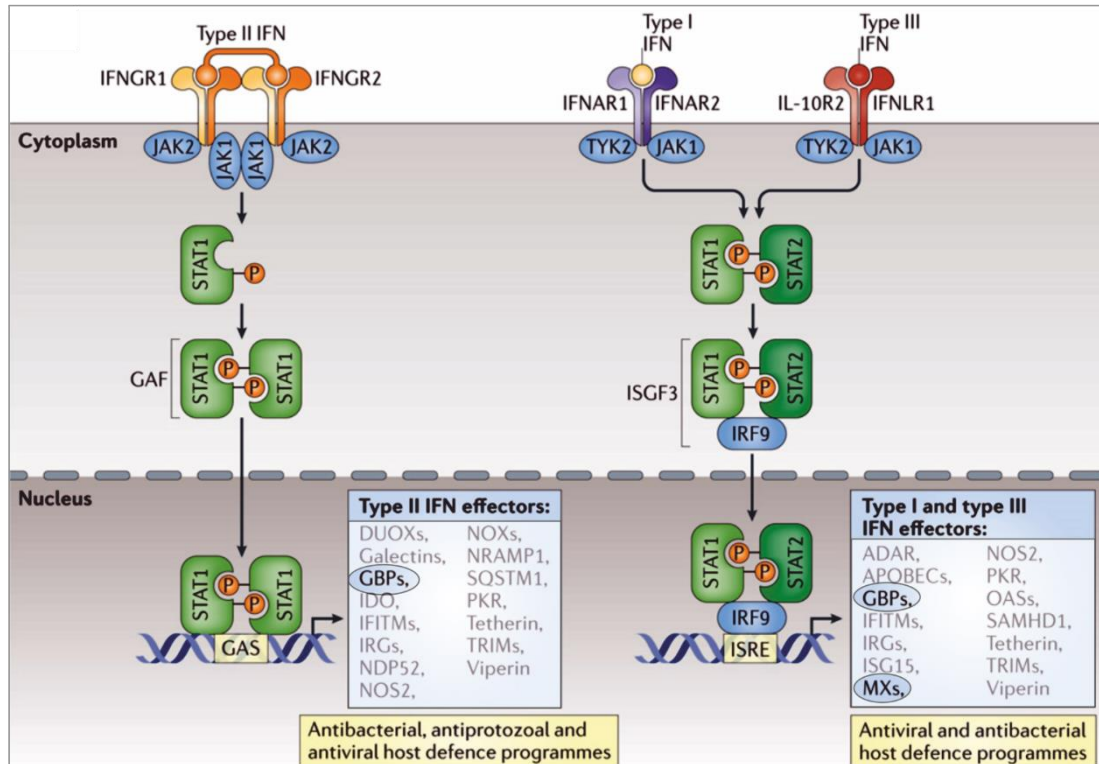


Figure 1-2: Interferon signaling through the JAK-STAT pathway. Different types of interferons bind to particular receptor complexes that in the cytoplasmic tail associate with members of the Janus tyrosine kinases (JAK1, JAK2 and TYK2). Associated with type I and type III interferons, JAK1 and JAK2 are involved in activating STAT1 and STAT2 that together with the interferon regulatory factor 9 (IRF9) build the IFN-stimulated gene factor 3 (ISGF3). ISGF3 migrates into the nucleus and binds the promoter element called IFN-stimulated response element (ISRE) to initiate transcription of accordingly controlled genes. IFN- γ signaling occurs through STAT1 homodimers (also called gamma-interferon activating factor, GAF) that bind to the gamma-interferon activating site (GAS). Selected interferon effectors are listed in the box; highlighted Mx and hGBPs represent the interferon regulated subgroup of dynamin related large GTPases (adopted and modified from MacMicking, et al., 2012).

1.2. Classification of human guanylate binding proteins

The large family of guanine nucleotide binding proteins (G-proteins) regulate important cellular processes such as intracellular signal transduction, protein synthesis, organization of the cytoskeleton and vesicular transport (Bourne, et al., 1990) (Wittinghofer, et al., 2011). They are identified by conserved sequence motifs, termed G1 to G5, that in the three-dimensional structure mediate specific, Mg^{2+} dependent binding of guanine nucleotides and hydrolysis of guanosine triphosphate (GTP) to guanosine diphosphate (GDP) and inorganic phosphate (P_i) (Bourne, et al., 1991) (Wittinghofer, et al., 2011). Designated G domain, this structural unit represents the basic functional subdomain of almost 38,000 G-proteins discovered in all kingdoms of life (Wittinghofer, et al., 2011). Insertions and additional

Introduction

structural elements in the G domain as well as additional subdomains apart from the G domain account for structural and functional diversity among all members (Vetter, et al., 2001).

Representing the largest group of G proteins with over 100 members, small GTPases act as molecular switches typically cycling between a GDP bound inactive state ('off' state) and a GTP bound active state ('on' state). Latter one grounds on GTP induced conformational changes, in particular stabilization of two flexible regions called switch I and switch II that allow the protein to interact with its cognate effector to cause a biological effect; once GTP is hydrolyzed and P_i is released the same regions relax into the GDP bound 'off' conformation (Vetter, et al, 2001) (Wennerberg, et al., 2005). Due to both slow dissociation of GDP and slow intrinsic GTPase activity, the GTP turnover cycle of small GTPases like Ras (rat sarcoma) relies on interactions with regulatory proteins (figure 1-3 a). In this process, guanine nucleotide exchange factors (GEFs) enhance the dissociation of GDP and thus allow GTP to replace GDP. On the other hand, GTPase-activating proteins (GAPs) provide a catalytic residue, mainly an 'arginine finger', and stabilize the active site of the protein, thereby accelerating the intrinsically slow GTPase reaction by orders of magnitude (Schweins, et al., 1995) (Ahmadian, et al., 1997) (Scheffzek, et al., 1997) (Gasper, et al., 2009).

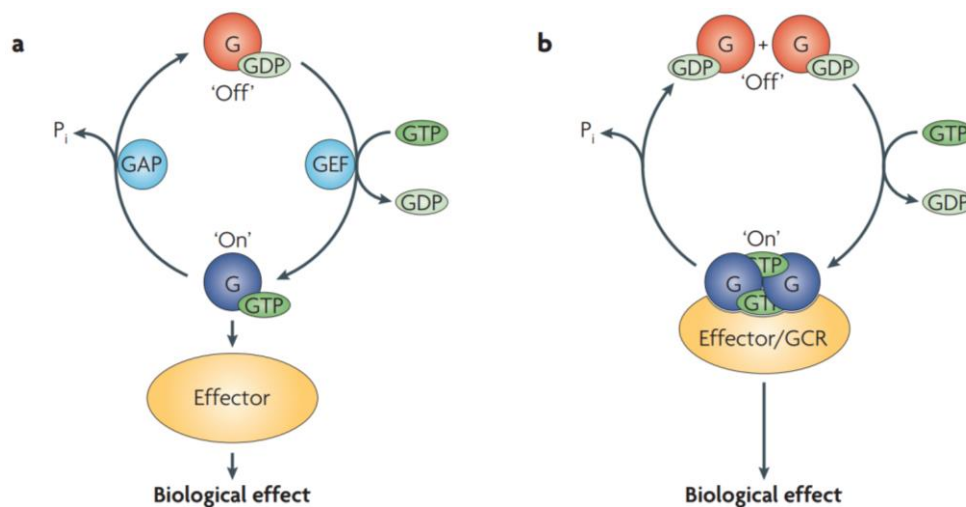


Figure 1-3: Differential regulation mechanisms of the GTPase cycle. (a) Activation and inactivation of Ras-like small GTPases is controlled by guanine nucleotide-exchange factors (GEFs) and GTPase-activating proteins (GAPs), respectively. GEFs induce GDP exchange for GTP establishing a conformation capable of effector binding, whereas GAPs act to accelerate the otherwise slow GTPase reaction to terminate effector binding. (b) The other type of GTPases including members of the dynamin superfamily has low affinity for nucleotides which allows exchange of GDP for GTP in the absence of GEFs. These proteins are capable to form GTP dependent homo assemblies which on the one hand establish the 'on' conformation for effector binding and, on the other hand, accelerate the GTPase activity sufficient to terminate the reaction in the absence of GAPs. G denotes the G domain (adopted from Gasper, et al., 2009).

Introduction

In this work, the family of human guanylate binding proteins (hGBPs) is further elucidated which together with classical dynamins, Myxovirus resistance (Mx) proteins and atlastins belong to the dynamin superfamily of large GTPases (Prakash, et al., 2000a) (Praefcke, et al., 2004b). Members of the dynamin superfamily share common structural and biochemical properties by which they clearly distinguish from other G proteins, in particular from small GTPases. Being 60-100 kDa in size, they have a characteristic multi-domain architecture including at least a conserved but elongated G domain (LG domain), a middle domain (MD) and a GTPase effector domain (GED). Being involved in different intracellular fusion and fission events, some of the members are additionally equipped with pleckstrin homology domains, transmembrane domains or signal sequences all of which act to mediate membrane association and particular targeting of the protein (figure 1-4; Praefcke, et al., 2004b).

Members of the dynamin superfamily have the particular ability to form self-assemblies, or homo complexes, which appears as a conventional and important mechanism to accomplish their diverse array of functions, such as antiviral activity of Mx proteins. In principle, self-assembly involves at least guanine nucleotide dependent LG domain dimerization but also other subdomains to form higher ordered homo complexes (Praefcke, et al., 2004b) (Gao, et al., 2011) (Faelber, et al., 2011). Remarkably, GTP dependent LG domain dimers represent the biologically active conformation of dynamin related proteins which at the same time function to stimulate the GTPase activity, sufficient to terminate the reaction in a self-regulatory manner (Gasper, et al., 2009). Moreover, these protein have a low affinity for nucleotides being in the micromolar range and thus weaker by almost six orders of magnitude as compared with Ras like proteins (Praefcke, et al., 2004b). As a result of both self-assembly stimulated GTPase activity and weak nucleotide affinity, members of the dynamin superfamily do not require additional GAPs and GEFs. Instead, they establish a regulation mechanism of a GTPase cycle which is distinct from the conventional switching cycle of Ras like GTPases (figure 1-3 b) (Danino, et al., 2001) (Praefcke, et al., 2004b) (Gasper, et al., 2009).

Introduction

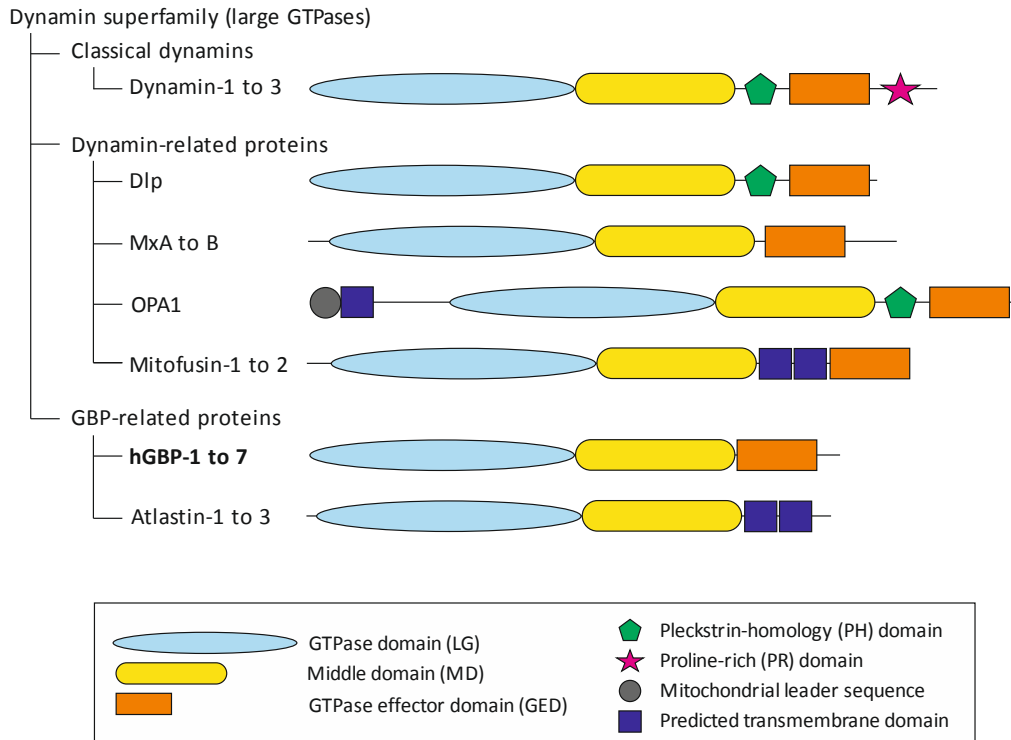


Figure 1-4: Multi-domain architecture of members of the dynamin superfamily. Besides an N-terminal elongated G domain (LG domain) all members contain a middle domain (MD) and a GTPase effector domain (GED, except for atlastins). Some of the members have additional elements such as a pleckstrin homology domain (PH), transmembrane domains or a mitochondrial leader sequence that mediate protein targeting to particular compartments (adopted and modified from Praefcke, et al., 2004b).

1.3. Specifications of hGBPs

Although being part of the dynamin superfamily and sharing characteristic features like low affinity binding of nucleotide, nucleotide dependent self-assembly and self-assembly stimulated GTPase activity, hGBPs define a subgroup with additional features not found in other members of the superfamily. Furthermore, most of the results about hGBPs ground on studies performed on hGBP-1 which is biochemically and structurally the best characterized member to date. Designated hGBP-1 to hGBP-7, seven hGBP isoforms have been identified in human. Being approximately 70 kDa in size, hGBP isoforms share are high sequence homology (identities range up to 88 % between hGBP-1 and hGBP-3) which is mostly pronounced for the N-terminal LG domain (figure 1-5) (Olszewski, et al., 2006) (Vestal, et al., 2011). Despite the sequence homology, initial biochemical studies on the isoforms hGBP-2 and hGBP-5 revealed particular features distinguishing from that of hGBP-1 (Neun, et al., 1996) (Wehner, et al., 2010), altogether suggesting that differences do not only exist between hGBPs and other groups of proteins but also between isoforms within the hGBPs as will be documented below.

Introduction

Similar binding affinities to all guanine nucleotides, GTP, GDP as well as GMP, is one of the unique characteristics by which the GBPs were originally identified and designated (Cheng, et al., 1983) (Cheng, et al., 1985). Basically, the binding of GMP was exploited to initially purify hGBPs from fibroblasts by using GMP-agarose (Cheng, et al., 1985). Later experiments with recombinant hGBP-1 synthesized in *E. coli* allowed to characterize nucleotide binding affinities in detail; while confirming previous results, binding affinities of GMP, GDP and non-hydrolysable GTP analogs were found to be in the micromolar range, mainly resulting from fast dissociation of nucleotides (Praefcke, et al., 1999) (Praefcke, et al., 2004) (Kunzelmann, et al., 2005). However, biochemical characterization of hGBP-5 revealed that GMP binding is not a feature that applies to all isoforms as there was no indication for GMP binding in the micromolar range (Wehner, et al., 2010). The binding affinities of hGBP-2 and guanine nucleotides have not been quantified in detail but estimated by the ability of different nucleotides to interfere with the GTPase reaction. While GDP potently inhibited GTP turnover GMP had only poor effect, thus, authors deduced a significantly lower binding affinity for GMP (Neun, et al., 1996). As the remaining isoforms have not been characterized yet, hGBP-1 remains the only member with efficient GMP binding activity.

The first cloning and sequential analysis of hGBP-1 and hGBP-2 revealed the sequence elements ⁴⁵GLYRTGKS⁵², ⁷⁵T, and ⁹⁷DTEG¹⁰⁰ that fit the consensus motifs GxxxxGK(S/T) (G1), the invariant threonine (G2) and DxxG (G3), respectively (figure 1-5) (Cheng, et al., 1991). These motifs responsible for GTP binding and hydrolysis are present and moreover identical in all hGBPs (see 1-5). However, all hGBPs lack the consensus motif (N/K)TxD (G4) which provides the guanine base specificity (Cheng, et al., 1991) (Olszewski, et al., 2006). Initially, this appeared contradictory since GBPs were shown to specifically bind guanine-nucleotides but not ATP or other nucleotides tested (Cheng, et al., 1991). However, later studies demonstrated that hGBP-1 has the alternative residues ¹⁸³RD¹⁸⁴ to provide base specificity (Praefcke, et al., 1999). Indeed, mutation of D184 dropped the guanine specificity remarkably (Praefcke, et al., 1999) (Praefcke, et al., 2004) and solved crystal structures of hGBP-1 moreover confirmed that both residues R183 and D184 form contacts to the guanine base while the preceding residues T181 and L182 apparently do not (Prakash, et al., 2000b) (Ghosh, et al., 2006). Also the RD sequence is identical in all hGBPs (figure 1-5), in conclusion, yielding no obvious reason for the altering GMP binding capacity of the investigated isoforms hGBP-1, hGBP-2 and hGBP-5.

Introduction

Like other members of the dynamin superfamily also hGBPs associate with membranes, yet not knowing the biological function. Therefore, hGBPs unlike other members undergo post-translational modification (Praefcke, et al., 2004) (Britzen-Laurent, et al., 2010). Only three of the human GBPs, hGBP-1, hGBP-2 and hGBP-5, are equipped with a C-terminal CaaX motif (C: cysteine; a: aliphatic amino acid; X: terminal amino acid) that serves as signal for prenylation (figure 1-5) (Britzen-Laurent, et al., 2010). Prenylation is sort of post-translational modification in eukaryotic cells that comprises either farnesylation or geranylgeranylation, both of which enable the target protein to associate with membranes or other proteins, thereby regulating localization and/or function of matured proteins (Novelli, et al., 2012). For some small GTPases owing such a motif, in particular, prenylation has been shown as an essential requirement for developing full functionality (Gao, et al., 2009) and so have altered or deficient prenylation been found to be the basis for severe human diseases such as cancer (Novelli, et al., 2012). Farnesylation and geranylgeranylation is initiated by the two enzymes farnesyltransferase (FTase) and geranylgeranyl transferase I (GGTase I), respectively (Casey, et al., 1996). These recognize the CaaX sequence and promote respective transfer of a C15 farnesyl or a C20 geranylgeranyl moiety to the cysteine. The terminal CaaX residue (X) is assumed to serve as determinant for the type of attached moiety since there is evidence that FTase recognizes rather CaaX motifs with a Ser, Gln, Met or Ala at the terminal X position, whereas GGTase I prefers a Leu instead (Casey, et al., 1996) (Gao, et al., 2009).

The CaaX sequences of hGBP-1 (CTIS), hGBP-2 (CNIL) and hGBP-5 (CVLL) have been demonstrated as target for prenylation. As predicted by the terminal serine residue, hGBP-1 is the one member being attached with a farnesyl anchor *in vitro* and *in vivo*, as well (Schwemmle, et al., 1994) (Nantais, et al., 1996) (Modiano, et al., 2005) (Fres, et al., 2010). Although not quantified to which share cellular hGBP-1 exists in the farnesylated form, hGBP-1 revealed as the most abundant prenylated protein in IFN- γ treated human cells having a concentration equal to or greater than Ras. Assessed by cellular fractionating, moreover, farnesylated hGBP-1 appeared predominantly in the cytosol while merely 15 % associated with membranes (Nantais, et al., 1996). By immunofluorescence staining of HeLa cells, furthermore, Modiano et al. described a diffuse staining pattern of hGBP-1 which majorly was restricted to the cytosolic fraction (Modiano, et al., 2005). Although results imply that hGBP-1 even upon farnesylation does not gain the capability to tightly interact with membranes, however, supplement of aluminum fluoride (AlF_x), which in combination with GDP is believed to capture the transition state of GTP hydrolysis, causes a significant redistribution of hGBP-1 to the Golgi apparatus suggesting that membrane localization requires GTPase activity. Reciprocally, when

Introduction

farnesylation is inhibited, either by FTase inhibitors or a mutation in the CaaX motif (C589S), hGBP-1 constitutively remains cytosolic (Modiano, et al., 2005). Upon AIF_x treatment, not only Golgi targeting but also accumulation of farnesylated hGBP-1 to granular, so far not identified vesicle-like structures was reported (Tripal, et al., 2007) (Britzen-Laurent, et al., 2010). These structures, however, are not formed by the CaaX truncated and hence non-farnesylated protein (Britzen-Laurent, et al., 2010). Also *in vitro* farnesylated hGBP-1 has been shown to be capable of liposome binding while unmodified hGBP-1 was not (Fres, et al., 2010).

Likewise have the remaining isoforms hGBP-2 and hGBP-5 been shown to incorporate a prenyl anchor in cell culture which was not the case when the respective CaaX sequences were truncated (Britzen-Laurent, et al., 2010). Similar to hGBP-1, hGBP-2 and hGBP-5 associate with the Golgi apparatus only in their prenylated form, however, hGBP-5 constitutively resides at the Golgi, while hGBP-2 translocates there by the aid of AIF_x (Britzen-Laurent, et al., 2010) (Tripal, et al., 2007). Since inhibition of GGTase but not FTase abrogated the constitutive Golgi localization of hGBP-5, hGBP-5 was supposed to be geranylgeranylated which is in accordance with the terminal predictor leucine. However, assignment of the prenyl moiety attached to hGBP-2 was not that clear, as cellular localization pattern of hGBP-2 did not alter by any of both inhibitors (Tripal, et al., 2007) (Britzen-Laurent, et al., 2010). Containing also a terminal leucine residue, hGBP-2 like hGBP-5 might likely be a target of geranylgeranylation. In sum, these studies clearly indicate that all hGBPs containing a CaaX motif indeed are prenylated and that prenylation transforms the proteins capable of interacting with membranes.

Introduction

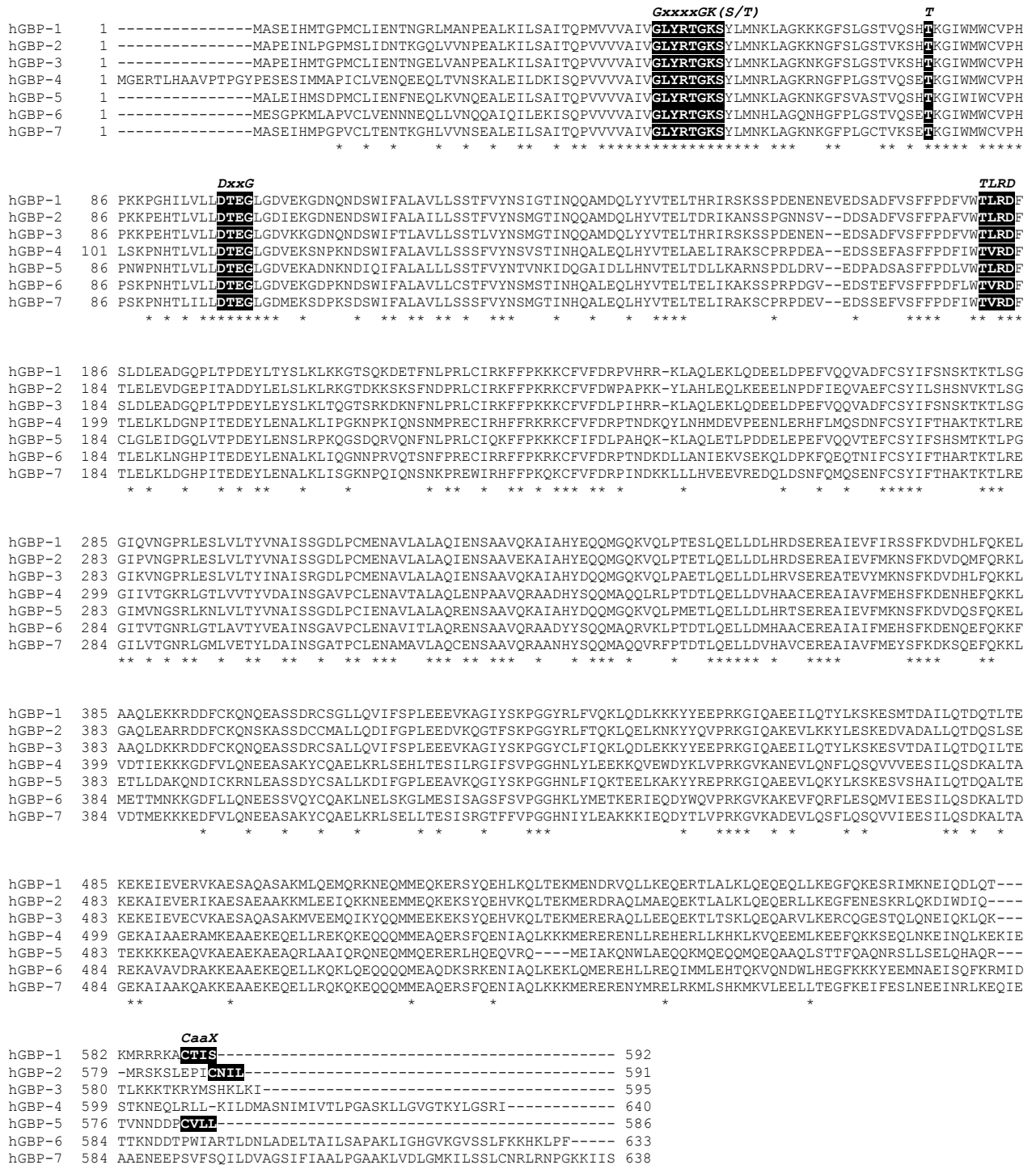


Figure 1-5: Primary sequence alignment of the hGBP isoforms. Alignment was performed with sequences of hGBP-1 (AAA35871.1), hGBP-2 (NP_004111.2), hGBP-3 (NP_060754.2), hGBP-4 (AAL02054.1|AF288814_1), hGBP-5 (NP_443174.1), hGBP-6 (NP_940862.2) hGBP-7 (NP_997281.2) using Clustal W. Asterisks indicate identical amino acids. Conserved motifs for GTP binding as described in the text as well as the C-terminal prenylation motif CaaX are highlighted in black.

1.4. Structure of hGBP-1

First crystal structures of full-length hGBP-1 solved in the nucleotide free form and in complex with the non-hydrolysable GTP analog GppNHp gave detailed insights into the structural organization (Prakash, et al., 2000a) (Prakash, et al., 2000b). Human GBP-1 consisting of 592 amino acids has a domain architecture consistent with that of dynamin-related large GTPases (Praefcke, et al., 2004b); a globular large GTP binding domain (LG domain; aa 1-278) is followed by an elongated purely α -helical domain (aa 311-592). Both are connected by a short intermediate region (aa 279-310) consisting of an α -helix and a two stranded β -sheet (Prakash, et al., 2000a). The helical domain subdivides into the middle domain (α 7-11) and the C-terminal domain (α 12-13) classically referred to as GTPase effector domain (GED) in large GTPases (Prakash, et al., 2000a) (Prakash, et al., 2000b) (Praefcke, et al., 2004b). Figure 1-6 presents the color coded structure of hGBP-1 in complex with the non-hydrolysable GTP analog GppNHp (pdb: 1f5n).

The LG domain of hGBP-1 (figure 1-6, light blue) including all GTP binding motifs G1, G2, G3 and a modified G4, builds on the canonical folding of Ras but is extended by several insertions that make a difference of approximately 100 amino acids (Prakash, et al., 2000a). While Ras consists of six β -strands and five α -helices, hGBP-1 with additional structural elements comprises eight β -strands surrounded by nine α -helices. Two of the five identified insertions I1 and I2 render the switch I (containing G2: Thr75) and switch II (containing ⁹⁷DxxG¹⁰⁰) regions of hGBP-1 larger as compared with Ras (Prakash, et al., 2000a); figure 1-6 C, magenta and green). The switch I of hGBP-1 is also named phosphate cap since it shields the phosphate binding site from solvent so that a potential external GAP cannot approach (Prakash, et al., 2000b). Upon insertions I3 and I4 do two additional α -helices develop, α 3' and α 4', that stabilize the C-terminal helix α 12 by four direct and eight water mediated contacts (Prakash, et al., 2000a). Insertion 5 (I5; aa 239-259) is comparatively large and comprises the so-called guanine cap. By arranging parallel to the flat side of the guanine base it forms a hydrophobic pocket and similar to the action of the phosphate cap it mostly covers the guanine base from the solvent (Prakash, et al., 2000 a; figure 1-6 C, yellow). Thus, both the phosphate and the guanine cap of hGBP-1 are unique elements that arrange a nucleotide binding site not found in canonical G-proteins (Prakash, et al., 2000b).

Introduction

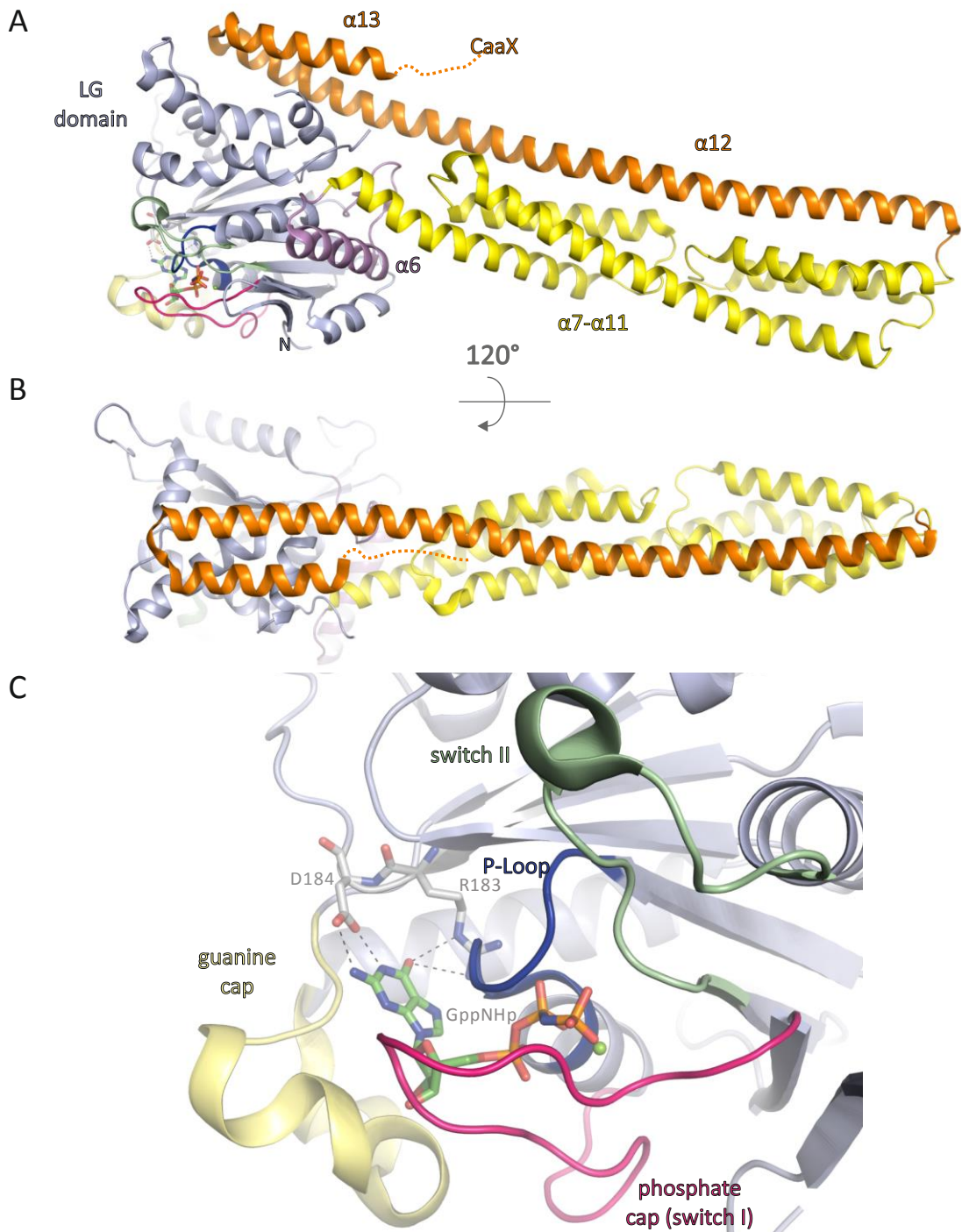


Figure 1-6: Crystal structure of the human guanylate binding protein 1 (hGBP-1). (A) Based on the GppNHp bound structure (pdb:1f5n) hGBP-1 subdomains are colored as following: LG domain (light blue), intermediate connecting region including $\alpha 6$ (violet), middle domain $\alpha 7-11$ (yellow), C-terminal domain $\alpha 12-13$ (orange). The non-resolved terminal amino acids 584-592 including the CaaX motif are indicated as dotted line. The nucleotide binding pocket with GppNHp (sticks) and the colored structural elements being involved are focused and assigned in (C). The guanine base specificity provided by hGBPs is demonstrated by a stick presentation of $^{183}\text{RD}^{184}$ and the related contacts (dashed black lines). (B) The illustration is derived from a 120° rotation of structure (A) allowing a view on the C-terminal domain.

The middle domain (α 7-11, figure 1-6 A, yellow) accounts for the overall elongated shape of hGBP-1. It is arranged in two triple-helix-bundles with the longest helix α 9 being part of both (Prakash, et al., 2000a). The C-terminal domain (figure 1-6 A and B, orange) starts with helix α 12 which has a length of approximately 120 Å and flanks the entire protein. By a helical turn, α 12 moves into helix α 13 that makes a coiled-coil type of interaction with α 12 (Prakash, et al., 2000a). Both, α 13 and the C-terminal end of α 12 mediate contacts to the LG domain, particularly established by salt bridges (Prakash, et al., 2000a) (Vöpel, et al., 2010). Since not solved in any structure, the last 10 amino acids including the prenylation motif are indicated by a dotted line (figure 1-6 A and B).

1.5. Nucleotide dependent self-assembly and self-assembly stimulated GTPase activity of hGBPs

Not only the particular ability to bind GTP, GDP and GMP with similar affinities, but also the GTP hydrolysis catalyzed by hGBP-1 occurred unique since both GDP and GMP yielded as reaction products. For several reasons, the authors deduced that GTP hydrolysis catalyzed by hGBP-1 is accomplished in two consecutive cleavage steps of single phosphate groups; first, hGBP-1 failed to hydrolyze GDP coming from bulk solution, second, no pyrophosphate could be detected as GTP hydrolysis product, and third, hGBP-1 did not succeed to hydrolyze GTP analogs with a cleavage resistant bond between the β - and γ -phosphate (Schwemmler, et al., 1994) (Praefcke, et al., 1999).

Furthermore, as a member of the dynamin superfamily characteristically hGBP-1 exhibits high intrinsic GTPase activity which upon self-assembly is accelerated up to 80-95 min⁻¹ (37°C) (Prakash, et al., 2000a) (Praefcke, et al., 2004) (Kunzelmann, et al., 2005). Although 37°C was determined as optimum temperature for the enzymatic activity of hGBP-1 (Schwemmler, et al., 1994), for protein stability reasons measurements were performed at 25°C, as well. Reduced reaction temperatures had some noteworthy effects; although the cooperative mechanism remained the maximum activity of approximately 20 min⁻¹ appeared with a ten-fold higher dimer affinity compared to results at 37°C; dimer dissociation constants were 0.03 μ M and 0.4 μ M, respectively (Kunzelmann, et al., 2005) (Wehner, et al., 2012). Also did the temperature have an effect on the product ratio: while GMP accounted for 90 % of total product at 37°C, its proportion decreased to 40 % at 25°C or lower (Schwemmler, et al., 1994) (Praefcke, et al., 2004) (Vöpel, et al., 2010). Due to suboptimal temperature conditions below 37°C, Schwemmler and others suggested a premature release of GDP from the enzyme prior to the second phosphate cleavage step (Schwemmler, et al., 1994). Noteworthy, monomeric

Introduction

hGBP-1 is not capable to form any GMP, thus, GMP production absolutely requires dimerization of the protein (Kunzelmann, 2006) (Abdullah, et al., 2010).

Irrespective of the temperature, GTP dependent self-assembly - as suggested from the protein concentration dependent stimulation of the GTPase activity - was confirmed by analytical size exclusion chromatography (SEC). In the nucleotide free form or when bound to GTP hydrolysis products GMP or GDP, hGBP-1 eluted as monomer, whereas either GTP analog GppNHp or GDP·AlF_x induced the formation of protein complexes (Prakash, et al., 2000a) (Ghosh, et al., 2006) (Praefcke, et al., 2004). Interestingly, the GppNHp bound complex (93 kDa) was classified as dimer but the apparent molecular weight was increased by only 50 % as compared to the monomeric species (62 kDa). Being approximately three-fold as large as the monomer, nevertheless, the GDP·AlF_x bound complex with 175 kDa was proposed to be a tetramer rather than a trimer since a transient assembly of two GTP-bound dimers into one tetramer seemed more reasonable (Kunzelmann, et al., 2005). The same nucleotide dependent species of monomeric, dimeric and tetrameric hGBP-1 have been identified with dynamic light scattering exploiting the diffusion coefficient as a measure for protein size (Vöpel, et al., 2010). However, there is no structure of a full-length dimer or tetramer available. Although believed to induce dimerization, also GppNHp bound hGBP-1 crystallized as monomer with an overall arrangement very similar to the nucleotide free form (Prakash, et al., 2000b). The mechanism of how the unique GTPase activity including two hydrolysis steps is regulated was mainly enlightened by crystal structures of isolated LG domains (Ghosh, et al., 2006).

The isolated amino-terminal LG domain of hGBP1 (1-LG) retains the main enzymatic properties of the full-length protein. More precisely, 1-LG performs cooperative GTP hydrolysis with slightly increased maximum activity (110 min⁻¹ at 37°C). An apparent K_d value of 0.3 μM versus 0.4 μM for full-length protein indicates similar dimer affinities and further suggests that dimerization is initially mediated by LG domain contacts. In contrast to full-length hGBP-1, 1-LG was not found to form higher complexes than a dimer as shown by analytical SEC in presence of either GTP analog GppNHp or GDP·AlF_x (Ghosh, et al., 2006). Likewise did 1-LG in complex with GppNHp or GDP·AlF_x crystallize as dimer (figure 1-7 A) while the protein in complex with GMP remained monomeric (Ghosh et al., 2006). Representing successive steps along the GTP binding and hydrolysis cycle, comparative analysis of GppNHp and GDP·AlF_x and GMP bound 1-LG structures revealed remarkable conformational changes within the flexible loop regions switch I and switch II as well as the guanine cap. In other G-proteins the conformational

Introduction

changes of the switches are responsible for effector binding, in hGBP-1 they turned out to be involved in dimer formation. Until hydrolysis of GTP to GMP is completed, they stay mostly buried in the dimer interface and thus are inaccessible for binding to any putative effector proteins (Ghosh, et al., 2006). A substantial role of the guanine cap in dimer formation has been proven by mutational analysis; substitution of either arginine Arg240 or Arg255 by an alanine led to considerable decrease of the dimer affinity by up to 100-fold as derived from a concentration dependent GTPase activity assay (Wehner, et al., 2012).

Homo dimerization of hGBP-1, once established, generates a conformation in which an arginine finger and a serine residue are oriented for efficient catalysis of GTP hydrolysis which creates the molecular basis for self-assembly stimulated activity. As shown in figure 1-7 C, Arg48 from the P-loop being solvent exposed in the monomeric state, flips into the active site upon dimerization such that it can participate in catalysis. This internal catalytic residue corresponds to the arginine finger that for accelerated GTPase activity of small GTPases is supplied by cognate GAPs (Ghosh, et al., 2006). Ser73 in switch I is the second catalytically important residue being reoriented upon dimerization. In turn, Ser73 is enabled to contact the nucleophilic water and functions to position and/or to activate the water for nucleophilic attack. Mutational analysis demonstrated the catalytic importance of both residues, substituting either residue by an alanine caused complete abolishment of the cooperative GTP hydrolysis mechanism and yielded an intrinsic activity reduced by 10-fold in case of S73A and even 100-fold in case of R48A as compared with wt (Ghosh, et al., 2006). The same impairment was observed when corresponding positions of the full-length protein were mutated emphasizing that full-length hGBP-1 like 1-LG is subject to the same mechanism (Ghosh, et al., 2006) (Praefcke, et al., 2004). Accordingly, LG domain contacts were sufficient and required to mediate catalytically competent dimers of full-length hGBP-1 in which, moreover, both of the molecules were found to be catalytically active (Kunzelmann et al., 2006). Of note, construct 1-LG discussed here ranges from amino acid 1-317 which other than the LG domain by definition (aa 1-278, Prakash, et al., 2000a) additionally contains the connecting region (see figure 1-6 A, violet). Partwise deletion of the connection region has been proposed to encounter the GTPase activity by negatively influencing dimerization capacity of the protein, however, nucleotide binding that might be affected in the first instance has not been investigated explicitly (Abdullah, et al., 2009) (Abdullah, et al., 2010).

Introduction

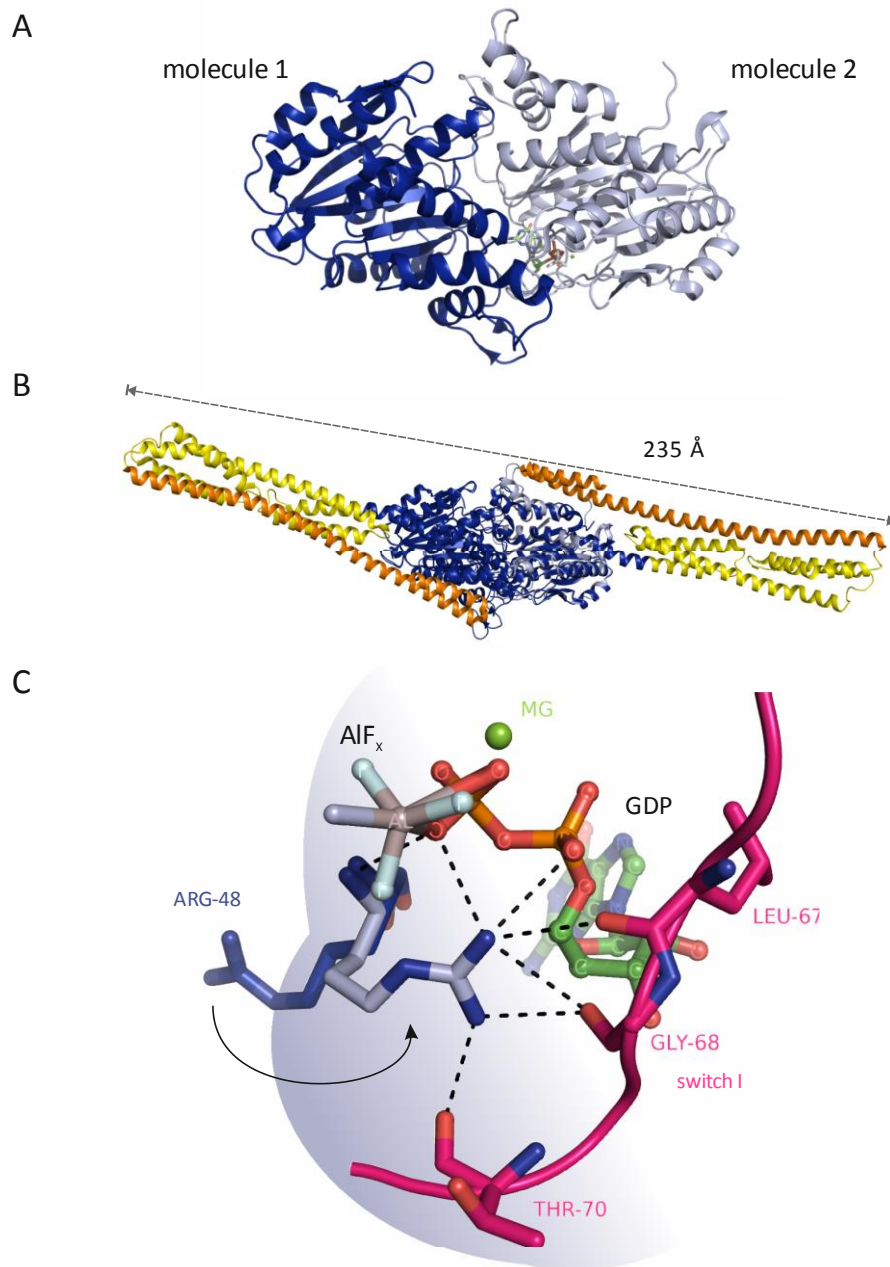


Figure 1-7: Dimer structure of the isolated hGBP-1 LG-domain in complex with GDP-ALF_x. (A) Cartoon presentation of the GDP-ALF_x bound LG domain dimer (pdb: 2b92) with involved molecules displayed in dark and light blue. (B) Full-length hGBP-1 molecules aligned to the dimer from (A) revealed a putative arrangement of an extended dimer being 235 Å in length. (C) The enlarged view on the nucleotide binding pocket of molecule 2 demonstrates the solvent exposed orientation of Arg48 in the monomeric state (dark blue) which upon dimerization flips into the catalytic center (arrow) and contacts phosphate groups of the nucleotide as well as residues from switch I (magenta). Ligand GDP-ALF_x is indicated by stick presentation, cofactor Mg²⁺ by a green sphere.

Introduction

Emerging from C-terminal truncation, 1-LG (aa 1-317) different to full-length hGBP-1 has the additional ability to employ not only GTP but also GDP as substrate which is likewise converted in a cooperative manner yielding similar stimulated activity up to 150 min^{-1} at 37°C . However, GDP-dependent dimers are approximately 30-fold weaker than the GTP-dependent dimers as reflected by the dimer dissociation constants being $9 \mu\text{M}$ versus $0.3 \mu\text{M}$. Consequently, stimulated GDPase activity occurs at much higher protein concentrations. Consistent with the cooperative hydrolysis of GDP, 1-LG dimerized in presence of $\text{GMP}\cdot\text{AlF}_x$ which as GDP analog is supposed to trap the transient state of GDP hydrolysis. The $\text{GMP}\cdot\text{AlF}_x$ bound 1-LG also crystalized as dimer such that comparison with the GppNHp and $\text{GDP}\cdot\text{AlF}_x$ bound dimers provided fundamental insights into the mechanism of consecutive GMP production during GTP turnover. Most remarkably, the GDP intermediate was found to be shifted and coordinated within the active center such that the same catalytic machinery as for the first hydrolysis step could be exploited also for the second hydrolysis step. The change in nucleotide conformation occurs at the ribose that keeps the guanine base interactions intact and repositions the phosphates. In consequence, β -phosphate occupies the previous γ -phosphate binding site and likewise does the α -phosphate shift into the canonical position of the β -phosphate keeping the coordination with the P-Loop and Mg^{2+} . With respect to the cooperative catalytic activity, critical mutants R48A and S73A had the same effect on the GDPase activity as observed on the GTPase activity which confirms that γ - and β -phosphate cleavage involves the same cluster of residues after GDP repositioning (Ghosh, et al., 2006). Considering dimerization and involvement of particular structural elements and residues as described above, figure 1-8 A illustrates a schematic overview on a whole GTP turnover cycle catalyzed by LG domain dimers of hGBP-1 (adapted from Ghosh, et al., 2006)

Kunzelmann and others carried out kinetic analyses of the individual steps of stimulated GTP hydrolysis catalyzed by dimeric hGBP-1 at 25°C (Kunzelmann, et al., 2006). They further considered preceding steps like GTP binding and dimer formation, following steps such as dimer dissociation and product release, as well as the occurrence of potential intermediate steps all of which are schematically drawn in figure 1-8 B (Kunzelmann, et al., 2006). Substrate binding with $k_{\text{on}} = 2.5 \mu\text{M}^{-1}\text{s}^{-1}$ and dimer formation were found to be fast. Extracting the rates for the first (k_1) and second hydrolysis step (k_2) under single turnover conditions required the consideration of an additional inactivating step, namely dissociation of the GDP bound dimer intermediate (k_3) releasing GDP as final product and thus preventing from further hydrolysis to GMP. Fitting the data accordingly, the second hydrolysis step with $k_2 = 2.2 \text{ s}^{-1}$ turned out to be even faster than the first one ($k_1 = 0.45 \text{ s}^{-1}$) which suggests that repositioning of GDP within the

Introduction

binding pocket is fast. Moreover, the ratio of k_3/k_2 ($0.87 \text{ s}^{-1}/2.2 \text{ s}^{-1}$) expected to define the ratio of GDP/GMP indeed applied to the experimentally obtained shares of the nucleotide products. Upon increasing the temperature to 37°C , k_2 was accelerated by approximately 4-fold (8.0 s^{-1}) while k_3 was decelerated by 2-fold (0.4 s^{-1}) (Kunzelmann, et al., 2006). The yielded ratio of 5/95 for GDP/GMP is in perfect agreement with previously obtained values (Kunzelmann, et al., 2006) (Praefcke, et al., 2004) (Prakash, et al., 2000a). The slower dissociation at 37°C indicates that the half-life of the GDP-bound intermediate strongly depends on the temperature and thus occurs as a putative key mechanism that regulates the particular GDP/GMP composition at defined temperatures. Since both GMP and GDP bound hGBP-1 dimers arise only temporarily and dissociate irreversibly in the course of GTP hydrolysis (figure 1-8 B), the stability or the half-life of the dimeric complexes could not be addressed directly. However, researchers found that increasing temperature had stabilizing effect on the GDP bound monomer of hGBP-1, a fact which may apply also to the dimeric form (Rani, et al., 2012).

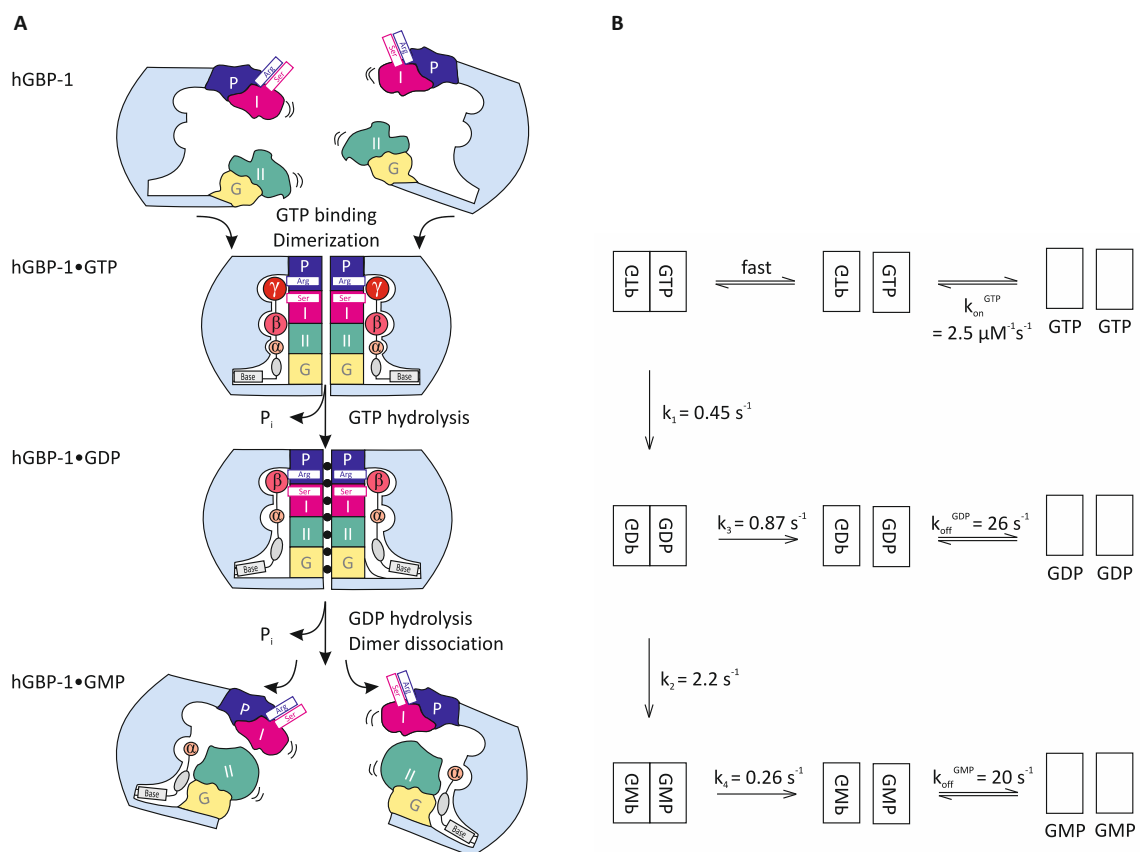


Figure 1-8: Scheme of the cooperative GTPase reaction catalyzed by hGBP-1. (A) The drawing adapted from Ghosh, et al. (2006) grounds on different nucleotide bound structures of 1-LG and mutational analyses of critical residues. The scheme involves the consecutive events following GTP binding: dimerization, cleavage of the γ -phosphate, shift of the GDP, cleavage of the β -phosphate with subsequent dissociation of the dimers. Corresponding structural changes within the P-loop (P), the switch I including R48 (I, Arg), the switch II including

Introduction

S73 (II, Ser), and the guanine cap (G) are considered, accordingly. (B) The model adopted from Kunzelmann, et al. (2006) extends the same cycle in (A) by pre- and proceeding steps with the kinetic parameters as described in the text. Importantly, an additional step (k_3) not considered in (A) was required to appropriately fit the two hydrolysis steps (k_1 and k_2). Recognizing the irreversible dissociation of GDP bound dimers (k_3) as a competing step to the β -phosphate cleavage (k_2) is in reasonable agreement with the defined mixture of GDP and GMP experimentally obtained from the GTPase reaction. All constants refer to a temperature of 25°C. Each rectangle denotes a hGBP-1 molecule either with or without nucleotide.

Until now, only hGBP-5 beside hGBP-1 was investigated with respect to the cooperative GTP hydrolysis mechanism (Wehner, et al., 2010). By aid of an HPLC based GTPase assay at 25°C, indeed, a concentration-dependent self-activation was observed also for hGBP-5. However, the results yielded remarkable differences as compared with hGBP-1. First, self-assembly induced activation of GTP hydrolysis was significantly weaker than observed for hGBP-1; at maximal levels, GTP hydrolysis occurred with 3.2 min^{-1} which compared to the basal activity is accelerated by merely two-fold. Second, also self-assembly of hGBP-5 characterized by a dimer dissociation constant of $4 \mu\text{M}$ appeared to be ten times weaker than the GTP dependent self-assembly of hGBP-1. In consistence with its deficient GMP-binding activity, above all, hGBP-5 did not yield any GMP from GTP hydrolysis. Even increasing the reaction temperature to 37°C did not enhance the GMP production. As suggested from the cooperative enzymatic activity, nucleotide dependent hGBP-5 homo complexes were investigated via analytical SEC. Indeed, both analogs GppNHp and GTP γ S forced hGBP-5 to form apparently twice as large complexes (450 and 400 kDa) as obtained in the nucleotide free or GDP bound form (250 and 220 kDa). Due to the large molecular weights in contrast to the theoretical weight of 67 kDa authors proposed that nucleotide free hGBP-5 unlike hGBP-1 preexists rather as constitutive dimer than as monomer. Upon GTP binding and hydrolysis, thus, hGBP-5 was assumed to cycle between the dimeric and tetrameric state. Since a putative monomeric state could be observed only in case of the C-terminal truncation hGBP-5ta, Wehner et al. (2010) proposed that the constitutive dimeric state of full-length hGBP-5 was established via C-terminal contacts. Of note, hGBP-5 displayed only weak binding to AlF_x , consequently, analytical SEC runs in presence of $\text{GDP}\cdot\text{AlF}_x$ most probably monitored the GDP bound species only (220 kDa) (Wehner, et al., 2010).

Also hGBP-2 has been reported to hydrolyze GTP in an efficient manner; at 37°C, a turnover number of 22 min^{-1} has been obtained (Neun, et al., 1996). Although the cooperative mechanism of GTP hydrolysis has not been subjected to date, it is suggested by the high catalytic activity of hGBP-2 as well as its capability to dimerize when bound to GppNHp (Neun, et al., 1996) (Abdullah, et al., 2010). Human GBP-2 other than hGBP-5 was further shown to

generate also GMP as GTP hydrolysis product resembling the hydrolysis mechanism catalyzed by hGBP-1. However, at 37°C, hGBP-1 yields 90 % GMP while hGBP-2 yields only 13 % which is a crucial difference (Neun, et al., 1996) (Praefcke, et al., 2004). Moreover, GMP production of hGBP-2 like hGBP-1 strongly requires dimer formation. When proteins were immobilized to trap the monomeric state, GDP but clearly not GMP emerged from GTP hydrolysis (Abdullah, et al., 2010).

1.6. Intramolecular motions of hGBP-1

GTP dependent dimerization of hGBP-1 through LG domain contacts was found to be one of the most crucial mechanisms triggered by the substrate (Praefcke, et al., 1999). But the same LG domain mediated dimerization was found to induce substantial conformational changes at intramolecular basis proposed as an important prerequisite for the release of an additional interface to facilitate tetramer formation and/or membrane association (Vöpel, et al., 2010) (Syguda, et al., 2012). Already by solving the full-length structure of hGBP-1 an area between the LG domain and the GED (α 12-13) was proposed to maintain the contacts for the safety pin like, closed folding (Prakash, et al., 2000a). Structural analyses of the isolated LG domain clearly indicated intramolecular conformational changes depending on the loaded nucleotide and the oligomeric state (Ghosh, et al., 2006). Among others, a noteworthy shift of helix α 4' was observed in different dimer structures of the isolated LG domain. Helix α 4' is a structural element of hGBP-1 not found in the canonical G domain architecture of Ras and Ras-like proteins. It is encoded by the sequence insertion 4 (I4) which together with I3 is predicted to be involved in intramolecular interactions with the helical domain (Prakash, et al., 2000a). Indeed, superimposition of the LG dimer structure with the monomeric full-length structure clearly indicated that the dimeric conformation of α 4' was not compatible with the attached α 12-13 in the monomeric full-length structure such that authors proposed a α 4' induced release of the latter (Ghosh, et al., 2006).

First experiments towards assessing intramolecular changes in solution were performed exploiting the nine cysteine residues distributed all over the protein and a thiol-reactive reagent used to quantify the number of solvent exposed, accessible cysteines. A series of mutational studies identified a cysteine (C225) within the LG domain that was buried in the closed conformation and became accessible only in the course of GTP hydrolysis, consequently serving as potent indicator for GED release. Considering that the GED stretches over the entire LG and middle domain, areas of the middle domain were also expected to get solvent exposed accordingly. In fact, introduction of an additional cysteine residue into the middle domain

Introduction

yielded the same nucleotide dependent alterations in the accessibility and thus confirmed that helices α_{12-13} were likely to move apart as a rigid unit (Vöpel, et al., 2009). These findings were further corroborated by extensive studies based on fluorescence resonance energy transfer (FRET); numerous fluorescently labeled hGBP-1 constructs were generated to monitor relative distance changes between two subdomains within one molecule. As a result, the release of the GED was found to account for major structural changes that hGBP-1 undergoes in the course of GTP binding and hydrolysis. Noteworthy, the structural changes of hGBP-1 were investigated under conditions that ensured complete dimerization of the protein, in sum, indicating intramolecular as well as intramolecular interactions as two interdependent processes (Hengstenberg, 2013).

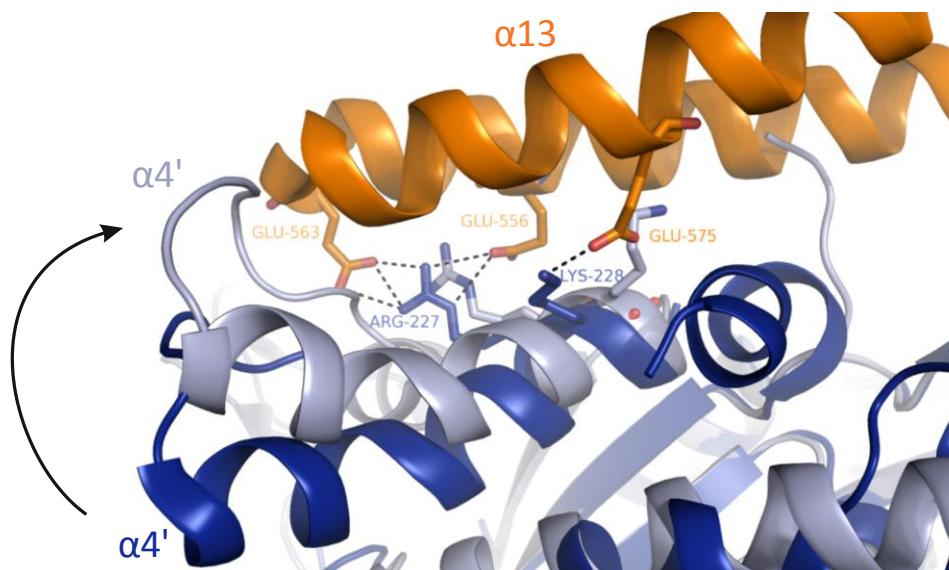


Figure 1-9: Intramolecular interactions between the subdomains LG (blue) and the GED (orange) of hGBP-1. The electrostatic contacts that the positively-charged $\alpha_{4'}$ residues R227 and K228 (dark blue) establish with E556 and E563 from α_{12} and E575 from α_{13} are indicated by dashed lines on basis of a monomeric full-length structure (pdb: 1f5n). The conformational change helix $\alpha_{4'}$ undergoes upon GTP dependent dimerization and/or hydrolysis (indicated by an arrow) is illustrated by superimposition with the dimeric structure of 1-LG in complex with GDP·AlF_x (light blue). The so caused reorientation of both R227 and K228 are supposed to interrupt the contacts consequently leading to weaker attachment and release of α_{12-13} .

In accordance with previous predictions grounding on structural analyses, it has been proven experimentally that $\alpha_{4'}$ has an important role in transmitting GTP dependent structural changes of the LG domain towards the GED. More precisely, two key residues R227 and K228 have been identified and proposed to control the attachment and release of the GED according to following scenario: in the nucleotide free monomeric form, R227 and K228

establish several ionic contacts involving glutamic acids on the C-terminal helices α_{12} and α_{13} to contribute to a closed conformation of the protein. Upon GTP binding and LG domain dimerization, LG domain undergoes conformational changes including a shift of $\alpha_{4'}$ towards the GED which results in disruption of the electrostatic contacts and in turn facilitates the release of the GED (figure 1-9) (Vöpel, et al., 2010). This release uncovers an interface within α_{12-13} that at least allows the interaction with the same subdomain of another molecule which together with the LG domain dimer ends up in a tetramer (Syguda, et al., 2012).

1.7. Dimerization dependent subcellular localization of the hGBPs

Three of the hGBPs, hGBP-1, hGBP-2 and hGBP-5 undergo posttranslational modifications that are absolutely required to enable those proteins to interact with membranes, as shown in cell culture. However, in the absence of certain stimuli or conditions proteins remain mainly cytosolic although effectively farnesylated (hGBP-1) or geranylgeranylated (hGBP-2 and hGBP-5) (Nantais, et al., 1996) (Modiano, et al., 2005) (Tripal, et al. 2007) (Britzen-Laurent, et al., 2010). These certain stimuli include additional treatment of the cells with aluminum fluoride (AlF_x) and IFN- γ , whereby AlF_x in complex with cellular GDP acts to capture the transition state of GTP hydrolysis and IFN- γ acts to upregulate the array of IFN- γ inducible products in the background (Modiano, et al., 2005). It was evidently shown that simultaneous treatment of the cells with AlF_x and IFN- γ is required to redistribute both isoform hGBP-1 and hGBP-2 to the Golgi apparatus which, importantly, is not the case when either one stimulus is missing (Modiano, et al., 2005) (Tripal, et al., 2007). So, what are the implications? With respect to biochemical characterization of hGBP-1, $\text{GDP}\cdot\text{AlF}_x$ induces homo complex formation and also release of the GED which harbors the farnesyl group (Vöpel, et al., 2010) (Hengstenberg, 2013). Fusing this knowledge with the observations in cell culture, it appears likely that hGBP-1 in the course of GTP binding and hydrolysis exposes its farnesyl group and anchors itself selectively to the cytosolic face of the Golgi (Modiano, et al., 2005). Although comparable data for hGBP-2 are not available to date, an almost identical behavior in cell culture suggests a molecular mechanism similar to that of hGBP-1 (Tripal, et al., 2007). To enlighten the particular role of IFN- γ in the process of Golgi translocation, Tripal and others (2007) delivered the important fact that neither IL-1 β nor TNF- α instead of IFN- γ were capable to induce hGBP-1 or hGBP-2 redistribution from the cytosolic fraction. In sum, to accomplish Golgi translocation both isoforms hGBP-1 and hGBP-2 revealed to require an additional factor exclusively induced by IFN- γ . To this end, other isoforms of the hGBP family, namely hGBP-4

Introduction

and hGBP-5, occurred as potential candidates as they were remarkably upregulated by IFN- γ but not by either IL-1 β or TNF- α (Tripal, et al., 2007). In particular, hGBP-5 was shown to be the only isoform with a considerable fraction constitutively residing at the Golgi requiring only its geranylgeranyl tail but no additional stimuli (Tripal, et al., 2007) (Britzen-Laurent, et al., 2007). Consequently, hetero interaction of the hGBP isoforms appeared as a possible mechanism by which coordinated subcellular redistribution of the members might occur.

In fact, homo and hetero dimerization could be shown between all isoforms hGBP-1 to hGBP-5 using co-immunoprecipitation, bimolecular fluorescence complementation and also yeast two-hybrid assay (Britzen-Laurent, et al., 2010). Furthermore, by pairwise transfection of vectors encoding for any isoform Britzen-Laurent and others instead of monitoring a single isoform ultimately investigated homo and hetero dimers in the absence of AIF $_x$ or IFN- γ . Thus, proteins were neither trapped in the GTP bound state nor were other IFN- γ dependent factors upregulated in the background. As a result, homo dimers of prenylated isoforms were found to locate to specific and distinct compartments: hGBP-1 with vesicle-like, granular structures in the cytosol particularly accumulated in the periplasm, hGBP-2 having also granular appearance accumulated around the nucleus but did not colocalize with the endoplasmic reticulum (ER) or the Golgi, and hGBP-5 being enriched in the perinuclear region other than hGBP-2 associated with the Golgi. Also both of the non-prenylated isoforms hGBP-3 and hGBP-4 were shown to form homo dimers but these dimers did not associate with membranes at all; instead, they were evenly distributed throughout the cytoplasm. A fraction of hGBP-4 was additionally found in the nucleus as observed also for hGBP-2 (Tripal, et al., 2007) (Britzen-Laurent, et al., 2010).

Consistent with the assumption that hetero interaction with hGBP-5 might be necessary to direct particular hGBPs to the Golgi, any dimer containing hGBP-5 as interaction partner was indeed shown to colocalize with the Golgi. Only in the case of hGBP-5 and hGBP-1 the situation appeared ambiguous since hetero dimer localization strongly depended on the farnesylation state of hGBP-1: when hGBP-1 was farnesylated the hetero dimers located to cytoplasmic granular compartments like hGBP-1 homo dimers, but when hGBP-1 was non-farnesylated (nf-hGBP-1) hetero dimers were found at the Golgi (Britzen-Laurent, et al., 2010). Latter one seems in contradiction to the assumption that Golgi targeting of hGBP-1 absolutely requires farnesylation (Modiano, et al., 2005) but is probably not when considering differences in experimental setups: data from Modiano, et al. (2005) demonstrate that nf-hGBP-1 does not associate with the Golgi even though hGBP-5 should be assumed upregulated upon IFN- γ

treatment (Modiano, et al., 2005). Importantly, IFN- γ does not only upregulate hGBP-5 but also the other isoforms hGBP-1 to hGBP-4 all of which are potent to interact with either nf-hGBP-1 or hGBP-5, probably with even higher affinity to abolish the complex of nf-hGBP-1 and hGBP-5. In contrast, the setup from Britzen-Laurent et al. (2010) allows detecting the interaction nevertheless, as there is no IFN- γ stimulation and thus no proteins competing for the interaction.

Likewise have all the remaining combinations of hetero dimers tested for their subcellular localization (table 1-1). Taken together, homo and hetero interactions likely to emerge with different affinities seem to be crucially important for a dynamic distribution of the hGBPs within the cell enabling also non-prenylated forms like hGBP-3 and -4 to target membranes. The dimer dependency of membrane targeting was additionally supported by the hGBP-1 mutant K51A which disabled to dimerize remains cytosolic regardless of prenylation and interaction partner offered (Britzen-Laurent, et al., 2010).

Table 1-1: Homo and hetero dimer dependent cellular localization and appearance of hGBP isoforms. (On basis of prenylated forms of hGBP-1, hGBP-2 and hGBP-5; after Britzen-Laurent, et al., 2010)

	<i>hGBP-1</i>	<i>hGBP-2</i>	<i>hGBP-3</i>	<i>hGBP-4</i>	<i>hGBP-5</i>
<i>hGBP-1</i>	Cytoplasm, granular	Cytoplasm, granular	Cytoplasm, granular	Cytoplasm, granular	Cytoplasm, granular
<i>hGBP-2</i>	Cytoplasm, granular	Around the nucleus, granular	Around the nucleus, granular	Around the nucleus, granular	Golgi
<i>hGBP-3</i>	Cytoplasm, granular	Around the nucleus, granular	Cytoplasm, diffuse	Cytoplasm, diffuse	Golgi
<i>hGBP-4</i>	Cytoplasm, granular	Around the nucleus, granular	Cytoplasm, diffuse	Cytoplasm, diffuse	Golgi
<i>hGBP-5</i>	Cytoplasm, granular	Golgi	Golgi	Golgi	Golgi

1.8. Biological function of hGBPs

Human guanylate binding proteins were initially identified as the most abundant proteins in response to IFN- γ (Cheng, et al., 1983) (Cheng, et al., 1985). However, hGBPs comprise seven members that in later studies have been demonstrated to have distinguishing promoter elements and accordingly specific expression profiles (Olszewski, et al., 2006) (Tripal, et al., 2007). In endothelial cells, for instance, only isoforms hGBP-1 to hGBP-5 were significantly

Introduction

upregulated in response to IFN- γ while hGBP-1 to hGBP-3 were additionally responsive to inflammatory cytokines (IC) including interleukin 1 β (IL-1 β) and tumor necrosis factor α (TNF- α) (Lubeseder-Martellato, et al., 2002) (Tripal, et al., 2007).

Until now, various cellular functions of hGBPs, particularly hGBP-1 have been reported that closely associate with the known effects of inducing cytokines. For instance, inflammatory cytokines IFN- γ , IL-1 β TNF- α are known to have inhibitory effects on cell proliferation, invasion and migration. Accordingly, hGBP-1 significantly induced by the same set of cytokines has been reported to inhibit proliferation and invasion of endothelial cells (Guenzi, et al., 2001) (Lubeseder-Martellato, et al., 2002) (Guenzi, et al., 2003). Further, hGBP-1 was found to be necessary and sufficient to inhibit also proliferation, migration and invasion of colorectal carcinoma cells altogether acting to suppress tumor progression (Britzen-Laurent, et al., 2013). This is in reasonable agreement with previous studies reporting that expression of hGBP-1 in stroma cells of colorectal cell carcinoma correlate with improved prognosis as compared with hGBP-1 negative cells (Naschberger, et al., 2008).

Besides these activities, hGBPs have been identified to participate in host defense strategies against some bacteria and viruses. Although the mechanism of actions is only poorly understood, GTP binding and/or hydrolysis seems be crucial in many cases (Vestal, et al., 2011).

The first time hGBPs appeared in the context of bacterial infections was the recognition of significantly increased hGBP-1 concentrations in the cerebrospinal fluid of patients with bacterial meningitis as compared to control patients. Whilst not knowing the particular function of the protein in the course of infection, actively secreted hGBP-1 was anticipated as a clinically important marker for diagnosis of bacterial meningitis (Naschberger, et al., 2006). Both isoforms hGBP-1 and hGBP-2 have been further identified in the context of *Chlamydia trachomatis* infection. *C. trachomatis* are obligate intracellular bacteria that reside in so called inclusions by which they facilitate nutrient supply from the infected host cell whilst preventing the same cell from recognition, attack and elimination by host defense mechanisms (Zhong, 2009). These factors contaminant with a non-fusogenic nature of the inclusions counteracting lysosomal degradation contribute to chlamydia survival and replication in host cells (Al-Zeer, et al., 2013). In infected HeLa cells, hGBP-1 and hGBP-2 localization to inclusion membranes suggested a particular role of the proteins in the course of chlamydial infection. In fact, hGBP-1 and hGBP-2 have been identified to convey and even to potentiate the inhibitory effect of IFN- γ on chlamydial growth in a manner that at least required GTP binding of hGBP-1. Cells

Introduction

transfected with both hGBP isoforms showed significantly smaller inclusions than neighboring non-transfected cells, whereas knockdown of either isoform by shRNA reversed the inhibitory effect (Tietzel, et al., 2009). In later studies performed on *C. trachomatis* infected macrophages, Al-Zeer and others (2013) identified hGBP-1 and hGBP-2 as key players in mediating IFN- γ induced fusion of inclusions with lysosomes and the activation of autophagic flux in order to eliminate infection from host cells.

Interferons after binding to cell surface receptors of responsive cells are capable of establishing an immune response and an antiviral state (MacMicking, 2012). The role of particular IFN regulated proteins such as Mx in mediating antiviral effects against a broad range of viruses is well-documented (Haller, et al., 2015). However, there is accumulating evidence that also hGBPs participate in IFN regulated host defense mechanisms against some viruses. Already in the course of developing human GBPs almost four decades ago, researchers proposed a potential correlation between the hGBPs being strongly upregulated after IFN- γ treatment and a higher resistance of those cells to vesicular stomatitis viruses (VSV; Knigh, et al., 1979). To explore the antiviral role of hGBP-1, HeLa cells constitutively expressing hGBP-1 were infected with either VSV or encephalomyocarditis virus (EMCV). As a result, significantly less cytopathic effects and reduced viral load (50 %) could be observed in hGBP-1 positive cells as compared with hGBP-1 negative cells. Treating the cells with IFN- γ while silencing hGBP-1 reversely abrogated the antiviral effects emphasizing the role of hGBP-1 as mediator of the IFN- γ induced response against VSV and EMCV (Anderson, et al., 1999).

Further, hGBP-1 appeared as one of the IFN stimulated genes with potential activity against hepatitis C virus (HCV; Itsui, et al., 2006). While upregulation of hGBP-1 significantly suppressed the expression of subgenomic HCV replicon and also the viral replication in cell culture, the opposite was observed upon hGBP-1 silencing (Itsui, et al., 2006) (Itsui, et al., 2009). Further studies revealed that hGBP-1 inhibited viral replication by a specific interaction with the non-structural protein NS5B which is the RNA-dependent RNA polymerase and part of the viral replication complex. As shown by a GTPase deficient mutant of hGBP-1, a functional GTPase domain of hGBP-1 was required to suppress the viral polymerase activity. However, vice versa NS5B was shown to counteract the GTPase activity of hGBP-1 resulting in continuous intracellular replication of HCV (Itsui, et. al., 2009). Similar mutual effects of viral non-structural protein 1 (NS1) and hGBP-1 have been observed in the context of influenza A virus (Zhu, 2013); once entered the nucleus, NS1 interacts with host components to potently evade immune mechanisms and thus to establish IAV infection (Fernandez-Sesma, 2007). However,

Introduction

hGBP-1 prevents NS1 from entering the nucleus and thus antagonizes IAV replication by direct interaction. This process requires GTPase activity of hGBP-1 which is mutually antagonized by NS1 (Zhu, et al., 2013). Besides hGBP-1, hGBP-3 has been identified as another isoform with antiviral activity against VSV, EMCV and IAV. In particular, the recently identified splice variant of hGBP-3, hGBP-3 Δ C, revealed the most potent activity against IAV. Although the molecular mechanism was not further elucidated, the presence of a functional GTPase domain was absolutely required and sufficient to provide the function (Nordmann, et al., 2012).

1.9. Objectives

The human guanylate binding proteins (GBPs) related to the dynamin superfamily of large GTPases provide anti-pathogenic and anti-proliferative activity which to date is only poorly assigned to molecular mechanisms of the proteins. Although GBPs comprise characteristic features of large GTPases, however, additional properties render them unique. The ability of the first member hGBP-1 to hydrolyze GTP to GDP and GMP in two successive steps is one of these unique properties. From previous studies it is known that after the first phosphate cleavage step GDP in the intermediate dimer is rearranged such that it occupies the original position of the GTP. Further hydrolysis to GMP, thus, occurs with aid of the residues from the first cleavage step. Furthermore, GTP is never completely converted to GMP, as would be expected after passing the entire hydrolysis cycle. It is believed that the dissociation rate of the GDP bound dimer competitively engages into the complete hydrolysis cycle and so defines the product composition consisting of both GDP and GMP. However, it is not known which structural elements or mechanisms are responsible for GDP repositioning or the lifetime of the GDP bound dimer intermediate.

The binding and hydrolysis of GTP triggers a chain of events that turn hGBP-1 into a highly dynamic system. These events primarily include the LG domain mediated intermolecular self-assembly, which in turn stimulates the GTPase activity and influences intramolecular interactions of the subdomains. In particular, additional interfaces in the C-terminal domain become uncovered for further intermolecular homo interactions –including polymerization in the case of farnesylated hGBP-1-, or association to membranous cell compartments. GTP hydrolysis to both products GDP and GMP cause that hGBP-1 gradually returns to the initial monomeric state which is controlled by the dissociation of both product bound hGBP-1 complexes as well as the release of individual products. This and due to similar nucleotide binding affinities also the local concentration of all nucleotides- changing after each GTPase cycle- are criteria decisive about to which share and at which time hGBP-1 is available for the next GTPase cycle.

This simplified and yet not fully clarified representation of the protein dynamics bases on studies ultimately focusing hGBP-1 in an isolated manner. However, more recent studies reveal that also other human GBP isoforms are capable of engaging into this system, since they were shown to form not only homo but also hetero complexes. Latter one causing cellular translocations of the interaction partners in a coordinated manner, indicates that hetero-interactions might be crucial for the full development of the GBP functions and thus need to be

Introduction

considered appropriately. Understanding the biological activity of GBPs, taken together, requires both the characterization of individual hGBP members as well as their interactions. Biochemical studies as a fundamental prerequisite for insights into molecular details, however, have been performed only on hGBP-1 and hGBP-5 and rudimentary also on hGBP-2 while entirely lacking for the remaining members. Despite the large sequence homology among all hGBPs which suggests similar biochemical properties, already hGBP-5 shows remarkable differences compared with hGBP-1.

Towards completing the picture of GBPs intracellular networking and in accordance with the above mentioned points, the objective pursued in this work can be subdivided into three major points:

1. What are the structural requirements for the unique mechanism of hGBP-1 to hydrolyze GTP also to GMP? Contributions of structural elements and residues will be challenged by mutational analysis.
2. What is the molecular basis for the differences in biochemical and biological behavior of the closely related hGBP isoforms? Full-length and isolated subdomains of not yet characterized isoforms hGBP-2 and hGBP-3 will be generated to work out their specific function, particularly concerning nucleotide binding, nucleotide dependent oligomerization and enzymatic activity.
3. As observed in cellular studies, interaction and colocalization of various hGBP isoforms revealed crucial for their biological function. Intending to get insights into the interplay of the isoforms, fluorescently labelled hGBPs will be used to characterize homo and hetero interactions in quantitative terms.

2. Materials and Methods

2.1. Materials

2.1.1. Chemicals

All chemicals were purchased from Applichem (Germany), J.T. Baker (Netherlands), Fluka (Germany), Merck (Germany), Qiagen (Germany), Roth (Germany), Serva (Germany), Sigma-Aldrich (Germany) if not indicated otherwise.

2.1.2. Enzymes/ Proteins

KOD HotStart DNA-Polymerase	Novagen (USA)
Restriction endonucleases (<i>Bam</i> HI, <i>Sall</i> , <i>Dpn</i> I)	Fermentas (Germany)
T4 DNA-Ligase	Fermentas (Germany)
Protein Molecular Weight Marker (116-14 kDa)	Fermentas (Germany)
Bovine serum albumin (BSA) – Fraction V	Sigma-Aldrich (Germany)

2.1.3. Vectors

For cloning and expression, pQE vectors from Qiagen were used. Both pQE9 and pQE80L contain an IPTG-inducible T5-promoter/ lac-operon element, a gene for ampicillin resistance and an identical multiple cloning site (MCS) the follows a coding regions for an amino-terminal hexa-histidine tag.

2.1.4. Oligonucleotides

All oligonucleotides were purchased from MWG-Biotech. Adjusting to a final concentration of 100 pmol/μl, lyophilisates were dissolved in ddH₂O and stored at -20°C. For subsequent cloning via restriction endonucleases, sense and antisense primers for gene amplification were consistently designed with overhanging sites for *Bam*HI and *Sall*, respectively (underlined). Italics indicate additional bases recommended for efficient restriction endonucleases.¹ Primers for site directed mutagenesis have the exchanged codons highlighted in bold type. For desired constructs, template DNA is listed together with respective oligonucleotide sequences in 5'-3' direction.

¹ New England BioLabs, 2002-03 Catalog & Technical Reference

Materials and Methods

1-LG (hGBP-1 aa 1-327)

Template DNA pQE80L-hGBP-1
Sense primer CGC GGA TCC ATG GCA TCA GAG ATC CAC
Antisense primer GAG AGA GTC GAC TTA TCA TGC AGC TGA GTT CTC TAT

hGBP-1 $\Delta\alpha 13$ (hGBP-1 aa 1-564)

Template DNA pQE80L-hGBP-1
Sense primer CGC GGA TCC ATG GCA TCA GAG ATC CAC
Antisense primer CGC GTC GAC TCA TCC CTC TTT TAG TAG TTG CTC

3-Phe Δ (hGBP-1 aa 1-481 F171A/F174A/F175A)

Template DNA pQE80L-hGBP-1 F171A/F174A/F175A (3-Phe)
Sense primer CGC GGA TCC ATG GCA TCA GAG ATC CAC
Antisense primer GAG AGA GTC GAC TTA TCA AGT CTG GTC TGT CTG GAG

LG-76 (hGBP-1 aa 1-327 K76A)

Template DNA pQE80L-hGBP-1 K76A
Sense primer CGC GGA TCC ATG GCA TCA GAG ATC CAC
Antisense primer GAG AGA GTC GAC TTA TCA TGC AGC TGA GTT CTC TAT

A76 (hGBP-1 Cys9/N18C/K76A/Q577C)

Template DNA pQE80L-hGBP-1 Cys9/N18C/Q577C
Sense primer G CAG TCT CAC ACT **GCA** GGA ATC TGG ATG
Antisense primer CAT CCA GAT TCC **TGC** AGT GTG AGA CTG C

B76 (hGBP-1 Cys9/K76A/Q344C/V540C)

Template DNA pQE80L-hGBP-1 Cys9/Q344C/V540C
Sense primer G CAG TCT CAC ACT **GCA** GGA ATC TGG ATG
Antisense primer CAT CCA GAT TCC **TGC** AGT GTG AGA CTG C

3-Phe (hGBP-1 F171A/F174A/F175A)

Template DNA pQE80L-hGBP-1
Sense primer GAG GAT TCA GCT GAC **GCG** GTG AGC **GCG GCG** CCA GAC TTT GTG
TGG
Antisense primer CCA CAC AAA GTC TGG **CGC CGC** GCT CAC **CGC** GTC AGC TGA ATC
CTC

hGBP-1 F171A

Template DNA pQE80L-hGBP-1
Sense primer G GTT GAG GAT TCA GCT GAC **GCG** GTG AGC TTC TTC CCA GAC
Antisense primer GTC TGG GAA GAA GCT CAC **CGC** GTC AGC TGA ATC CTC AAC C

hGBP-1 F175A

Template DNA pQE80L-hGBP-1
Sense primer GCT GAC TTT GTG AGC TTC **GCG** CCA GAC TTT GTG TGG AC
Antisense primer GT CCA CAC AAA GTC TGG **CGC** GAA GCT CAC AAA GTC AGC

Materials and Methods

hGBP-1 F229A

Template DNA	pQE80L-hGBP-1
Sense primer	G CCC AGA CTC TGT ATC CGG AAA GCG TTC CCA AAG AAA AAA TGC
Antisense primer	GCA TTT TTT CTT TGG GAA CGC TTT CCG GAT ACA GAG TCT GGG C

2-LG (hGBP-2 aa 1-327)

Template DNA	pQE9-hGBP-2
Sense primer	GC <u>GGA TCC</u> ATG GCT CCA GAG ATC AAC
Antisense primer	CGC <u>GTC GAC</u> TCA TCA CAC TGC GGC TGA GTT CTC

hGBP-3

Template DNA	pcDNA/myc-His (+)- hGBP-3
Sense primer	CGG <u>GAT CCA</u> TGG CTC CAG AGA TCC ACA TGA CAG GCC
Antisense primer	GGC TGC <u>AGG TCG ACT</u> TAG ATC TTT AGC TTA TGC G

hGBP-3 (aa 1-481)

Template DNA	pQE80L-hGBP-3
Sense primer	CGG <u>GAT CCA</u> TGG CTC CAG AGA TCC ACA TGA CAG GCC
Antisense primer	CGC <u>GTC GAC</u> TCA TGT GAG AAT CTG GTC

3-LG (hGBP-3 aa 1-327)

Template DNA	pQE80L-hGBP-3
Sense primer	CGG <u>GAT CCA</u> TGG CTC CAG AGA TCC ACA TGA CAG GCC
Antisense primer	CGC <u>GTC GAC</u> TCA TTG CAC TGC GGC TGA

5-LG (hGBP-5 aa 1-327)

Template DNA	pQE80L-hGBP-5
Sense primer	GTA TCA CGA GGC CCT TTC GTC (pQE sense)
Antisense primer	CGC <u>GTC GAC</u> TCA TCA CAC TGC GGC TGA GTT CTC

Newly generated constructs were sequenced with pQE vector primers:

Sense primer	GTA TCA CGA GGC CCT TTC GTC
Antisense primer	CAT TAC TGG ATC TAT CAA CAG GAG.

2.1.5. Antibiotics

Ampicillin (Roth) was used for selection of pQE vector containing cells. Stock solutions having a concentration of 100 mg/ml were prepared with ddH₂O, sterile filtered (0.2 µm) and stored in 1 ml aliquots at -20°C. Bacterial growth media and LB-agar plates were supplemented with a target concentration of 100 µg/ml ampicillin.

2.1.6. *E. coli* strains

Plasmid replication was carried out in the *E. coli* strain Veggie NovaBlue Singles, whereas Rosetta (DE3) or BL21-CodonPlus® (DE3)-RIL were used for recombinant protein synthesis. Respective genotypes are as follows:

Rosetta (DE3) (Novagen)

$F^- ompT hsdS_B(r_B^- m_B^-) gal dcm$ (DE3) pRARE (Cam^R)

BL21 - CodonPlus (DE3)- RIL (Stratagene)

E. coli B $F^- ompT hsdS(r_B^- m_B^-) dcm^+ Tet^r gal \lambda$ (DE3) *endA Hte* [*argU ileY leuW* Cam^r]

Veggie NovaBlue Singles (Novagen)

endA1 hsdR17 ($r_{K12}^- m_{K12}^+$) *supE44 thi-1 recA1 gyrA96 relA1 lac F*'[*proA^+ B^+ lacI^q*ZΔM15::Tn10] (Tet^R)

2.1.7. Growth media

LB medium

10 g/l bacto tryptone, 5 g/l yeast extract, 10 g/l NaCl, 5 mM NaOH, pH 7.3-7.5

LB agar

LB medium plus 12 g/l agar (antibiotics added when agar solution was cooled to 45-50°C)

TB medium

12 g/l bacto tryptone, 24 g/l yeast extract, 4 ml/l glycerol, 0.17 mM KH₂PO₄, 0.072 mM K₂HPO₄

2.1.8. Buffers and solutions

Buffer for preparation of competent cells (0.2 μm filter sterilized)

TSS-Buffer 85% (v/v) LB-medium without NaOH (pH not adjusted); 10% (w/v) PEG 8,000; 5% (v/v) DMSO, 50 mM MgCl₂

Buffers and solutions for agarose gel electrophoresis

1% agarose gel 1% (w/v) agarose in electrophoresis buffer (TAE)
 Electrophoresis buffer 40 mM Tris, 20 mM acetic acid, 1 mM EDTA, pH 8.0 (= 1x TAE)
 (TAE)
 Ethidium bromide 0.5 μg/ml ethidium in ddH₂O (diluted from a 10 mg/ml stock, Roth)
 solution

Buffer for protein purification and analysis (0.2 μm filter sterilized, degassed and cooled to 4°C)

Lysis buffer Buffer A + 1 mM PMSF
 Buffer A 50 mM Tris-HCl (pH 7.9), 5 mM MgCl₂, 10% glycerol (v/v), 500 mM NaCl
 Buffer B₅ 50 mM Tris-HCl (pH 7.9), 5 mM MgCl₂, 150 mM NaCl, 5 mM Imidazole
 Buffer B₁₅₀ 50 mM Tris-HCl (pH 7.9), 5 mM MgCl₂, 150 mM NaCl, 150 mM Imidazole
 Buffer C 50 mM Tris-HCl (pH 7.9), 5 mM MgCl₂, 150 mM NaCl
 Buffer C_{AIF} (*) 10 mM NaF, 300 μM AlCl₃ in buffer C

Materials and Methods

Buffer for protein concentration determination (0.2 µm filter sterilized)

Gua-buffer 6M Guanidine-HCl, 50 mM potassium phosphate, pH 6.5

Buffers for protein labelling (0.2 µm filter sterilized and degassed prior to use)

Buffer low salt 50 mM Tris-HCl, 5 mM MgCl₂, (pH 7.4)
Buffer high salt 50 mM Tris-HCl, 5 mM MgCl₂, 500 mM NaCl, (pH 7.4)
Buffer L 50 mM Tris-HCl, 5 mM MgCl₂, 150 mM NaCl, (pH 7.4)

Buffers and solutions for SDS-PAGE

Polyacrylamide 30 % (w/v) acrylamide solution with 0.8 % (w/v) bis-acrylamide (Roth)
Upper Tris 500 mM Tris-HCl, 4 g/l SDS, pH 6.8
Lower Tris 1.5 M Tris-HCl, 4 g/l SDS, pH 8.8
Sample buffer (2x) 126 mM Tris-HCl, 20 % (v/v) glycerol, 4 % (w/v) SDS, 0.02 % (w/v) bromophenol blue, pH 6.8. Basically, 1 ml of buffer was freshly supplemented with 10 µl β-mercaptoethanol.
Electrophoresis buffer 25 mM Tris, 192 mM glycine, 0,1 % (w/v) SDS, pH 8.3
Staining solution 40 % (v/v) ethanol, 10 % (v/v) acetic acid, 0.1 % (w/v) Coomassie R250
Destaining solution 20 % (v/v) ethanol, 10 % (v/v) acetic acid
Fixation solution 40 % (v/v) ethanol, 10 % (v/v) acetic acid

Buffer for HPLC

Buffer_{HPLC} 10 mM TBA-Br, 30 mM K₂HPO₄ 70 mM KH₂PO₄, 0.2 mM sodium azide, pH 6.5. Addition of 2 % (v/v) acetonitrile after filter sterilization and degassing.

(*) To form the complex of GDP·AlF_x, GDP was added into buffer C already containing AlF. Individual stock solution of NaF (0.5 M) and AlCl₃ (0.3 M) were prepared in ddH₂O. From those, 200 µl and 10 µl, respectively, were added to 10 ml buffer C yielding a final concentration of 10 mM NaF and 300 µM AlCl₃. Routinely, the buffer was applied to sterile filtration (0.2 µm) and degassing prior to usage. Due to instability of the solutions, both stock solutions and buffer C_{AlF} were freshly prepared and used only one day.

2.1.9. Nucleotides

All nucleotides were purchased from Jena Biosciences. Mant-nucleotides were delivered as 10 mM stock solutions (in H₂O), whereas non-modified nucleotides (GTP, GppNHp, GTPγS, GDP and GMP) were shipped in lyophilized form. Adjusting the final concentration to 50-150 mM, lyophilisates were dissolved in 100 mM Tris-HCl (pH 7.4) and stored in 20-50 µl aliquots at -20°C. Actual nucleotide concentration was derived from absorption measurements at 252 nm ($\epsilon_{252} = 13,700 \text{ M}^{-1}\text{cm}^{-1}$) using Beer-Lambert law (eq. 1).

2.1.10. Fluorophores

For fluorescent labelling of hGBPs, Alexa dyes 488 C₅ maleimide (Alexa488, Invitrogen) and 647 C₂ maleimide (Alexa647, Invitrogen) were used. By thiol-reactive maleimide groups fluorescent dyes were covalently coupled with cysteine residues of the protein. The dyes provided as lyophilisates (1 mg) were dissolved in an equimolar mixture of DMF and DMSO (50 μ l). After preparing serial dilutions in H₂O (1:2000 to 1:4000), absorption of Alexa488 and Alexa647 was measured at 491 nm and 651 nm, respectively. Using the molar extinction coefficients $\epsilon_{491} = 71,000 \text{ M}^{-1}\text{cm}^{-1}$ and $\epsilon_{651} = 268,000 \text{ M}^{-1}\text{cm}^{-1}$ (Hengstenberg, 2013) actual concentrations were calculated according to Beer-Lambert law (eq. 1).

2.2. Molecular biological methods

2.2.1. Isolation of plasmid-DNA from *E. coli* cells

For replication of plasmid-DNA, 5-10 ml LB-medium was inoculated with a single colony of transformed *E. coli*. At 37°C, the culture was agitated for 15-18 h. The plasmid-DNA was extracted and prepared using the GeneJET Plasmid Miniprep Kit (Thermo Scientific) according to manufacturer's instruction. The procedure is based on alkaline lysis of bacterial cells with subsequent precipitation of proteins and chromosomal DNA. Plasmid-DNA remaining in the supernatant was then applied to spin columns containing a silica gel membrane. After several washing steps, plasmid-DNA was eluted in a 1:1 mixture of ddH₂O and elution buffer (30 μ l-50 μ l). DNA concentration was determined by measuring absorbance at 260 nm (NanoDrop 2000, Thermo Scientific) and considering that one absorbance unit equals 50 ng/ μ l double stranded DNA. Usually, 50-150 ng/ μ l plasmid-DNA was obtained from 2 ml bacterial cell culture.

2.2.2. Agarose gel electrophoresis

Agarose gel electrophoresis is a method which is used for separating DNA molecules according to their length. In this work, it was used for both analytic (see 2.2.7.) and preparative purposes (see 2.2.5.). In both cases, 1 % (w/w) agarose gels were prepared using TAE buffer as solvent. TAE was also used as electrophoresis buffer. DNA samples were applied and electrophoretic separation was carried out at constant voltage (100-120 V) for approximately 45 minutes. To visualize separated DNA fragments by UV light, the gel was soaked in ethidium bromide solution (0.5 μ g/ml) for 15 minutes and subsequently rinsed and destained with H₂O for additional 15 minutes.

2.2.3. *Gene amplification via Polymerase Chain Reaction (PCR) and purification of reaction products*

Gene fragments coding for truncated hGBP isoforms were amplified by polymerase chain reaction (PCR) carried out in a PCR cycler (Mastercycler Eppendorf, Germany). The desired gene fragment was derived from template DNA using an appropriate primer pair as listed in 2.1.4. Having a final volume of 50 μ l, a PCR mixture was prepared as follows:

1 μ l	Template-DNA (Mini-Prep)	(~ 100 ng/ μ l)
1.5 μ l	5'-primer	(100 pmol/ μ l)
1.5 μ l	3'-primer	(100 pmol/ μ l)
5 μ l	KOD Hot Start DNA Polymerase buffer	(10x)
3 μ l	MgSO ₄	(25 mM)
5 μ l	dNTPs	(2 mM)
32 μ l	ddH ₂ O	
1 μ l	KOD Hot Start DNA Polymerase	(1U/ μ l).

After an initial denaturation step (95°C, 2 min), a three-step-cycle of denaturation (95°C, 20 sec), annealing (55-60°C, 15 sec), and elongation (70°C, 40 sec) was repeated 40 times in order to ensure considerable amounts of target DNA which due to particular design of the primers uniformly contained *Bam*HI and *Sal*I restriction sites. For efficient restriction digestion, PCR products were purified using the QIAquick gel extraction kit (Qiagen) according to manufacturer's instruction. The DNA adsorbed to the membrane of spin columns was washed and subsequently eluted with a 1:1 mixture of ddH₂O and elution buffer (30 μ l).

2.2.4. *Restriction digestion with BamHI and SalI*

To introduce the purified gene fragment yielded from PCR reaction into the bacterial expression vector pQE80L, both were digested with *Bam*HI and *Sal*I creating single stranded cohesive ends by which recombination of vector and insert could be achieved. The reaction mixture was prepared according to following composition and restriction digestion was carried out at 37°C for 20 minutes.

	<i>pQE80L</i>	<i>PCR product (insert)</i>
ddH ₂ O	37 μ l	19 μ l
10 x FastDigest® Green buffer	5 μ l	3 μ l
DNA	5 μ l (~0.5 μ g)	15 μ l (~0.2 μ g)
FastDigest® enzyme <i>Bam</i> HI	1 μ l	1 μ l
FastDigest® enzyme <i>Sal</i> I	2 μ l	2 μ l
Total volume	50 μ l	40 μ l

Due to using Green buffer, subsequent addition of sample buffer was eliminated. Reaction mixtures were entirely subjected to 1 % agarose gel electrophoresis for subsequent extraction of linearized vector and insert DNA.

2.2.5. DNA extraction from agarose gel

After restriction digestion, DNA was separated via agarose gel electrophoresis and stained with ethidium bromide. Linearized vector pQE80L and insert gene fragments of hGBPs identified at the correct height (comparison with DNA ladder) were isolated using the QIAquick gel extraction kit (Qiagen). Basically, gel slices containing the target DNA were excised with a scalpel and weighed for addition of 3 volumes of buffer QG to 1 volume of gel (considering 100 mg \approx 100 μ l). The mixture was incubated at 50°C until the gel slice was completely dissolved (~10 min). Resulting solution was applied to QIAquick spin columns. After several washing steps, DNA was eluted with a 1:1 mixture of ddH₂O and elution buffer (30 μ l). DNA concentration was determined by measuring absorbance at 260 nm (NanoDrop 2000, Thermo Scientific) and considering that one absorbance unit equals 50 ng/ μ l double stranded DNA.

2.2.6. DNA ligation

To recombine *Bam*HI/*Sall* cleaved pQE80L and insert DNA by their cohesive ends, T4-DNA-Ligase was added to a 1:1 or 1:5 mixture of pQE80L and insert.

Linearized pQE-80L	50 ng
Insert DNA	50 ng / 250 ng
10 x T4 DNA Ligase buffer	2 μ l
T4-DNA-Ligase	1 μ l
ddH ₂ O	ad 20 μ l
Total volume	20 μ l

Ligation was carried out at 17°C for 15 hours with following heat inactivation of T4-DNA-Ligase (80°C, 5 min). *E. coli* cells Veggie NovaBlue Singles were transformed with 5 μ l of the ligation mixture and plated on ampicillin containing LB-agar plates.

2.2.7. Colony PCR

After ligation, circularized empty vector as well recombinant insert DNA containing vector can confer ampicillin resistance resulting in positive selection on agar plates. To screen bacterial colonies for their DNA content, colony PCR was performed enabling to specifically select those colonies harboring successfully inserted gene fragments into the vector. Therefore, a small amount of bacterial cells was picked from a single colony and transferred

into the bottom of PCR tubes. After disruption of the cells in a microwave for 1-2 minutes, PCR was performed according to a typical setup as described in paragraph 2.2.3. As a difference, cells replaced the template DNA and vector primers pQE sense and antisense were used that flank the multiple cloning site. Thus, resulting PCR products analyzed by agarose gel electrophoresis yielded either copies of successfully inserted gene fragments or no detectable fragments due to empty vector. Only the positive colonies were then used to inoculate mini-cultures for replication of recombinant vector, isolation and analysis by sequencing.

2.2.8. Site directed mutagenesis

Site directed mutagenesis was performed to introduce particular mutations into the sequence of hGBP-1 using primers with modified codon sequence at desired amino acid position (indicated by bold type in section 2.1.4.). Primers were designed and the polymerase chain reaction was carried out according to Stratagene's QuickChange site directed mutagenesis kit which allows amplifying the entire plasmid by appropriately adjusted elongation time. Secondary structure formation coming along with extended length of mutagenesis primers was encountered by addition of DMSO into the PCR mixture. Also, template DNA and primer concentration was reduced as compared with the concentrations for amplification of gene fragments.

1 µl	Template-DNA (Mini-Prep)	(10-20 ng/µl)
1.5 µl	Sense primer	(10 pmol/µl)
1.5 µl	Antisense primer	(10 pmol/µl)
5 µl	KOD Hot Start DNA Polymerase buffer	(10 x)
5 µl	MgSO ₄	(25 mM)
5 µl	dNTPs	(2 mM)
2.5 µl	DMSO	
27.5 µl	ddH ₂ O	
1 µl	KOD Hot Start DNA Polymerase	(1U/µl)

After an initial denaturation step (95°C, 2 min), a three-step-cycle of denaturation (95°C, 20 sec), annealing (T_m of the primer pair reduced by 5-10°C, 15 sec), and elongation (70°C, 4 min) was repeated 25 times. To subsequently eliminate non-mutated template DNA, 1 µl of restriction enzyme *DpnI* specifically digesting methylated DNA was added to the PCR product. After incubation at 37°C for 1.5 to 2 hours, *DpnI* was heat inactivated at 80°C for 5 minutes. *E. coli* cells Veggie NovaBlue Singles were transformed with 5 µl of the reaction and plated on ampicillin containing LB-agar plates. Single colonies were multiplied in LB medium and plasmid DNA was isolated and checked by DNA sequencing.

2.2.9. Preparation of competent *E. coli* cells

Competent *E. coli* cells were derived from purchased strains and prepared according to the DMSO or CaCl₂ method adapted and modified from (Chung, et al., 1989) or (Mandel, et al., 1970). Basically, both procedures are largely overlapping except for the solutions used for washing and storage of the cells. From an overnight culture (5 ml LB medium inoculated with desired *E. coli* strain) 1 ml was used to inoculate 100 ml LB medium. Cells were grown at 37°C until an optical density (600 nm) of 0.3 - 0.4 was reached. After chilling at 4°C for 30 minutes, cells were harvested at 1.500 rcf and 4°C for 5 minutes. For washing, the cell-sediment was gently resuspended in 50 ml TSS-buffer or CaCl₂ solution (100 mM) and centrifuged in the same way as before. Subsequently, cells were resuspended in 10 ml TSS or CaCl₂ (1/10 of the initial culture volume) and left for incubation at 4°C for 15 hours. The suspension was finally supplemented with 15 % (v/v) glycerol, subdivided into 100 µl aliquots and snap frozen in liquid nitrogen for storage at -80°C.

2.2.10. Heat shock transformation of *E. coli* cells

One aliquot of *E. coli* (100 µl) was gently thawed on ice, supplemented with plasmid-DNA and incubated at 4°C for 10-30 minutes. The volume and amount of DNA varied depending on the preparation method: 5 µl was used from either site directed mutagenesis or ligation product, or 1-2 µl of plasmid-DNA from mini preparation. For incorporation of external DNA, *E. coli* cells were exposed to 42°C for 45 seconds and immediately chilled on ice. The whole suspension was then transferred onto LB-agar plates that for selection contained 100 µg/ml ampicillin. The plates were incubated at 37°C for 15-18 hours.

2.2.11. DNA Sequencing

Successful cloning and mutagenesis was verified by DNA sequencing with a 3130xl sequencer (Applied Biosystems, USA). Therefore, vector primers pQE sense (5'-GTA TCA CGA GGC CCT TTC GTC-3') and pQE antisense (5'-CAT TAC TGG ATC TAT CAA CAG GAG-3') were used.

2.3. Biochemical and biophysical methods

2.3.1. Synthesis of recombinant hGBPs in *E. coli*

Genes coding for hGBP isoforms and their mutants were inserted into bacterial expression vectors pQE9 or pQE80L having additional coding regions for six histidine residues upstream of the MCS. Thus, target hGBPs contained a hexa-histidine tag at the N-terminus. Expression and synthesis of either construct were carried out in *E. coli* strain Rosetta (DE3) or BL21 CodonPlus (DE3) RIL. Cells containing plasmids were grown in TB-Medium with 100 µg/ml ampicillin at 37°C until optical density at 600 nm (OD_{600}) was between 0.4 and 0.6 (full-length hGBPs) or between 0.9 and 1 (truncated constructs). Subsequently, temperature was reduced to 25°C and expression was uniformly induced with 100 µM Isopropyl β-D-1-thiogalactopyranoside (IPTG) for 16-18h. Cells were harvested at 5,000 rcf and 4°C for 15 minutes and pellets were transferred into plastic bags for storage at -80°C. Successful synthesis of target protein was verified by SDS-PAGE using samples before and after induction. For optimal gel loading, sample volumes were adjusted to the cell density: A cell pellet resulting from 1 ml of cell suspension having $OD_{600} = 1$ was resuspended in 100 µl of 1 x sample loading buffer.

2.3.2. Cell lysis via sonication and purification of recombinant hGBPs

Following steps were carried out on ice or in a refrigerated cabinet where the purification columns were placed. Also, buffers used in these step were cooled to 4°C for at least 15 hours. Basically, recombinant hGBPs were purified in two steps altogether yielding highly pure and monomeric target protein: Exploiting the (His)₆-tag of the protein, first, affinity chromatography was performed using a column packed with HisPur Cobalt resin (Thermo Fisher Scientific, column volume (CV) ≈ 30 ml). Second, affinity purified protein was separated through size exclusion chromatography (also termed gel filtration chromatography, S200 26/60, GE Healthcare, CV ≈ 320 ml) to remove both remaining contaminations and unspecifically formed protein complexes larger than monomeric target protein.

To release successfully synthesized recombinant protein from *E. coli*, 10 g of frozen cell pellet was poured with lysis buffer (buffer A + 1 mM PMSF, ad 100 ml) and thawed under stirring. Cells were disrupted via sonication (Sonoplus HD 2200, Bandelin) for in total 10 minutes, whereas process was paused every one to two minutes to encounter heat production and hence denaturation of liberated proteins. Pause intervals were adjusted such that temperature of the lysate was always kept below 8°C. To remove cell debris, lysates were

centrifuged at 15,000 rcf and 4°C for 1 hour. The clear supernatant containing the fraction of soluble proteins was further applied to a HisPur Cobalt column which was previously equilibrated with at least 2 CV of buffer A. Flowrate for efficient binding of His-tagged proteins was reduced to 2 ml/min whereas remaining steps were carried out at 4 ml/min. After loading, column was sequentially washed with 5-10 CV of buffer A and 3-5 CV of buffer B₅. His-tagged recombinant protein specifically bound to the column material was eluted with 2 CV of buffer B₁₅₀ yielding 30 - 50 ml protein containing eluate. Eluted protein was precipitated with 3 M of ammonium sulfate and centrifuged. Resulting pellet was stored at -80°C.

For the second purification step, gel filtration column was equilibrated with buffer C. Ammonium sulfate pellet of protein was resolved in maximum 5 ml of buffer C and subjected to the column. At a flowrate of 2 ml/min, protein was eluted with 320-400 ml of buffer C and collected in 4 ml fractions. After SDS-PAGE analysis, monomeric fractions with the highest purity were pooled and concentrated by ultrafiltration up to 0.6 to 1.8 mM of target protein. In small aliquots, proteins were snap frozen and stored at -80°C.

2.3.3. Concentrating protein by precipitation and ultrafiltration

Uniformly, 3 M ammonium sulfate (J. T. Baker) was used to precipitate hGBPs after affinity chromatography. Therefore, 10 ml of protein solution was supplemented 4 g of ammonium sulfate (= 3 M) and stirred until solid material was completely dissolved. Transferring into 50 ml tubes, precipitated protein was centrifuged at 7,000 rcf and 4°C for 15-20 minutes. Supernatant was discarded and protein pellet was stored at -80°C.

After preparative gel filtration chromatography yielding approximately 20-25 ml target protein containing eluate, VivaSpin concentrators (Sartorius) with defined pore size (10 kDa cutoff) and 20 ml capacity were used to reduce the volume and thereby to increase the concentration of protein solution. To protect both target protein and filter membrane, ultrafiltration was performed at maximum 4,000 rcf. Usually, total volume was reduced by 100-fold after 1-2 hours. Small aliquots were prepared, snap frozen and stored at -80°C.

2.3.4. Determination of protein concentration by absorption spectroscopy at 280 nm

Concentration of isolated hGBPs was determined by absorption spectroscopy exploiting the capacity of aromatic amino acids to absorb light at 280 nm. Protein samples were diluted in denaturing Gua-buffer (6 M guanidinium hydrochloride and 20 mM phosphate, pH 6.5) and measured in a UV/Vis photometer (Specord 200, Analytic Jena). Dilution factor was adjusted such that absorption could be measured in the linear range between 0.3 and 0.9. Measurements were repeated in at least triplicate. The molar extinction coefficient (ϵ_{280}) of each protein was calculated using the online tool Protcalc² (hGBP-1 wt, hGBP-1 $\Delta\alpha13$ and point mutants: 43,240 M⁻¹cm⁻¹, hGBP-1 mutant 3-Phe Δ : 41,960 M⁻¹cm⁻¹, hGBP-2: 52,060 M⁻¹cm⁻¹, hGBP-3: 47,080 M⁻¹cm⁻¹, 1-LG: 34,280 M⁻¹cm⁻¹, 2-LG: 38.690 M⁻¹cm⁻¹, 3-LG: 34,280 M⁻¹cm⁻¹ and hGBP-3 (aa 1-481): 43,240 M⁻¹cm⁻¹). The actual concentration was determined according to the Beer-Lambert law (equation 1); c is the calculated concentration in mol/l (M), A is the absorbance at 280 nm, ϵ_{280} is the molar extinction coefficient in M⁻¹cm⁻¹, l is the path length of the cuvette in cm, and df is the dilution factor.

eq. 1
$$c = \frac{A}{\epsilon_{280} \cdot l} \cdot df$$

2.3.5. SDS-PAGE for analysis of protein samples

Eliminating structural effects on mobility, denaturing sodium dodecyl sulfate (SDS)-polyacrylamide gel electrophoresis (PAGE) was performed to analyze protein samples. Binding of SDS does not only denature proteins but also applies an even distribution of negative charges to the linearized chain. In an electric field, this consistent charge to mass ratio among proteins allows migration of protein molecules to the cathode whereby separation occurs by mass alone.

One-dimensional discontinuous gel systems containing a stacking gel with low pH (6.8) and low polyacrylamide percentage (3.9 %) and a separation gel with higher pH (8.8) and polyacrylamide percentage (10 or 12.5 %) were prepared (see below). Protein samples for analysis were diluted in 2 x sample loading buffer (1:1) and boiled at 95°C for 5 minutes. β -mercaptoethanol in the sample loading buffer functioned to reduce disulfide bonds. Using electrophoresis buffer composed of 25 mM Tris, 192 mM glycine and 0.1 % (w/v) SDS (pH 8.3)

² <http://www.justbio.com/index.php?page=protcalc>

SDS-PAGE was performed at a constant current of 32 mA (Bio-Rad PowerPac 200 Electrophoresis Power Supply) for 45-60 minutes.

	Separation gel		Stacking gel
	10 %	12 %	3.9 %
<i>Acrylamide</i>	2.5 ml	3.1 ml	0.65 ml
<i>Lower Tris ,pH 8.8</i>	1.9 ml	1.9 ml	
<i>Upper Tris, pH 6.8</i>			1.25 ml
<i>H₂O</i>	3.1	2.5 ml	3.1 ml
<i>10% APS</i>	100 µl	100 µl	50 µl
<i>TEMED</i>	5 µl	5 µl	5 µl

APS stands for ammonium persulfate and TEMED stands for N,N,N',N'-Tetramethylethane-1,2-diamine.

2.3.6. *Nucleotide binding: Equilibrium fluorescence titration*

Mant (mant 2'/3'-O-(N-methylanthraniloyl)) labelled nucleotides were used as fluorescent probes as they exhibit protein binding properties similar to those of non-modified nucleotides (Praefcke, et al., 1999). Binding of mant-labelled nucleotides to proteins yielded considerable increase of fluorescence which was exploited to characterize protein and nucleotide interactions (Kunzelmann, et al., 2005). The mant-nucleotides used in this study were mGMP, mGDP, mGppNHp and mGTPγS (Jena Bioscience, Germany). At 25°C, fluorescence measurements were done in a Kontron SFM 25 fluorimeter (Kontron Instruments Ltd, Watford, UK). All solutions were prepared in buffer C. In titration experiments, 0.5 µM of mant-nucleotide was placed in a cuvette (700 µl) and mant-group was excited at 366 nm whereas emitted fluorescence was monitored at 435 nm. 250 µl of titrant was prepared with at least 50 µM of hGBP and additional 0.5 µM of the same mant-nucleotide to eliminate dilution effects. Until saturation, titrant was added to the cuvette in small portions ensuring stepwise increase of protein and thus complex concentration of protein and nucleotide reflected by proportional increase of fluorescence. At each step, fluorescence values were averaged over 30-60 seconds. The equilibrium dissociation constant K_d was obtained by drawing a fit to the data as described earlier (equation 2, Kunzelmann, et al., 2005).

$$\text{eq. 2} \quad F = F_{\min} + (F_{\max} - F_{\min}) \frac{A_0 + B_0 + K_d - \sqrt{(A_0 + B_0 + K_d)^2 - 4A_0B_0}}{2B_0}$$

A_0 denotes the increasing total concentration of protein and B_0 denotes the constant mant-nucleotide concentration in the cuvette. F is the measured fluorescence and F_{\min} and F_{\max} are the approached minimum and maximum fluorescence values, respectively.

2.3.7. Nucleotide binding: Stopped-flow kinetics

To get further insights into dynamics of hGBP interactions with guanine nucleotides, kinetic measurements were performed in a *stopped-flow* device (Biologic SFM 400, France). Either reaction partner was diluted in buffer C and applied to distinct syringes of the *stopped-flow* apparatus. Using a flowrate of 14 ml/s, reaction partners were rapidly mixed with a 1:1 ratio. For several seconds, fluorescence changes were recorded under usage of appropriate excitation wavelength and emission filters. Kinetic data were obtained from the average of four to eight single experiments. All measurements were performed at 25°C.

Experiments were performed having either protein or mant-nucleotide at fixed concentration between 0.25 and 0.5 μ M, whereas the interaction partner was supplied in varying concentrations starting from an at least 10-fold molar excess to maintain pseudo first order conditions. Excitation wavelength was adjusted considering the experimental setup: when protein was the constant compound and nucleotide was in excess, tryptophan residues were excited (295 nm) and fluorescence resonance energy transfer (FRET) to the mant-group was detected through a 420 nm cutoff filter. When nucleotide concentration was constant and protein was in excess, mant-group was excited directly at 366 nm and again emission was detected through a 420 nm cutoff filter. Due to pseudo first order kinetics, increasing fluorescence was fitted single exponentially yielding an observed rate constant for each reaction (k_{obs}). A plot of k_{obs} versus concentration of excess compound yielded a linear dependency, thus, slope and intercept of a linear fit to the data denoted association (k_{on}) and dissociation rate constant (k_{off}) of the particular interaction of protein and mant-nucleotide (equation 3). The equilibrium constant of the interaction (K_d) was obtained by equation 4.

$$\text{eq. 3} \quad k_{obs} = k_{on}[\text{excess compound}] + k_{off}$$

$$\text{eq. 4} \quad K_d = \frac{k_{off}}{k_{on}}$$

Dissociation rate constants carry a high inaccuracy when the values are close to zero, thus, k_{off} values were corroborated by additional displacement experiments. Therefore, 1000 to 2000-fold molar excess of non-modified nucleotide was rapidly mixed with a preformed complex of protein and mant-nucleotide. The large molar excess of non-modified nucleotide ensured fast association with protein and quasi-irreversible dissociation of mant-nucleotide thereby resulting in a single exponential decrease of fluorescence intensity with the obtained k_{obs} value directly equaling k_{off} . For distinguishing purpose, k_{off} values obtained from

displacement experiments were marked with an asterisk (k_{off}^*). Accordingly, K_d values were indicated by K_d^* when the calculation based on the ratio $k_{\text{off}}^*/k_{\text{on}}$.

2.3.8. GTPase activity assay

GTPase activity of hGBPs was investigated by *reversed-phase* HPLC (rp-HPLC) as previously described (Kunzelmann, et al., 2005). If not indicated otherwise, all reactions were carried out at 25°C using buffer C including 50 μM of BSA to maintain protein stability (particularly relevant for protein concentrations in the submicromolar range). The GTPase reaction was started by mixing GTP and protein solution in equal ratio, whereby GTP concentration was kept constant (500 μM) and protein concentration was varied between 10 nM and 20 μM . During GTPase reaction, aliquots were removed at different time points and subjected to the HPLC system which was sufficient to terminate the reaction. Using buffer_{HPLC} (4 ml/min) the mixture of nucleotides in each aliquot (GTP being the remaining substrate as well as emerging products GDP and GMP) was separated through a C18 column (Chromolith® Performance RP-18e, 100-4.6 mm) and nucleotide absorption was detected at 254 nm (Jasco MD 2010). As retention of nucleotide grounds on interaction between stationary phase and phosphate groups, GMP having a single phosphate eluted the first and was followed by GDP and GTP. In total, three distinct peaks occurred which were integrated to quantify the concentration of each nucleotide considering a total concentration of 500 μM . Accordingly, time traces of GTP turnover and product formation could be drawn. Initial rate of GTP turnover ($\leq 50\%$ of GTP hydrolyzed) was derived from the slope of a linear fit to the respective kinetics. Normalizing initial rate by protein concentration yielded specific activity (s) of GTP turnover at the particular protein concentration. For any tested hGBP, protein concentration dependent plot of specific GTPase revealed increasing values with increasing protein concentration, suggesting self-assembly stimulated GTPase activity. As described by Kunzelmann et al. (2005), a quadratic equation (equation 5) modeling GTPase stimulation by dimer formation was used to obtain maximal stimulated activity (s_2) and the dimer dissociation constant (K_d).

Not only GTP turnover but also GDP and GMP formation occurred in a protein concentration dependent manner. Thus kinetics of product formation was evaluated analog to substrate turnover and equation 5 was also used to yield maximal specific activity for GDP or GMP formation. To distinguish, resulting s_2 values were denoted s_{GTP} , s_{GDP} , and s_{GMP} .

$$\text{eq. 5} \quad s = s_1 + (s_2 - s_1) \frac{E_0 + \frac{K_d}{4} - \sqrt{(E_0 + \frac{K_d}{4})^2 - E_0^2}}{E_0}$$

E_0 stands for enzyme concentration. s_1 and s_2 denote basal and maximal stimulated activity performed by monomeric and dimeric enzyme, respectively. K_d represents the dissociation equilibrium constant.

2.3.9. Long term GTP and GDP hydrolysis assay

In buffer C with 50 μM BSA, GTP or GDP hydrolysis catalyzed by either hGBP isoform was studied after 24 hours of incubation at 25°C. Serial dilutions of protein was prepared (10 nM-200 μM) and mixed with 500 μM substrate GTP or GDP to initiate hydrolysis reaction. The reaction was terminated by addition of buffer_{HPLC} (30 μl into 20 μl reaction volume). Nucleotide composition at each protein concentration was analyzed via rp-HPLC as described in paragraph 2.3.8. A plot of nucleotide proportions against protein concentration revealed protein concentration ranges for efficient GTP or GDP hydrolysis and also particular product patterns resulting from GTP hydrolysis.

2.3.10. Analytical size exclusion chromatography

Homo complex formation of hGBP isoforms and mutants were investigated by analytical size exclusion chromatography (SEC) in the absence and presence of nucleotides. Therefore, size exclusion column S200 PC 3.2/30 (2.4 ml, GE Healthcare) was equilibrated with two column volumes (CV) of running buffer which was only buffer C or buffer C with either GTP analog GDP·AlF_x, GTP γ S or GppNHp (250-320 μM). 20 μM of investigated protein was diluted in the respective buffer and incubated at 4°C for 10-30 minutes prior to injection to the column. As the column was placed in a refrigerated cabinet, each run was performed at 10-13°C. From chromatograms recorded at 280 nm elution volumes (V_e) were derived and used to calculate the molecular weight (MW_{SEC}) of each homo complex according to a calibration curve. The calibration curve was generated using elution volumes of protein standards (in buffer C) which covered a range between 29 kDa and 669 kDa (Carbonic Anhydrase, Albumin, Ovalbumin, Conalbumin, Alcohol Dehydrogenase, β -Amylase, Apoferritin, and Thyroglobulin).

2.3.11. Labelling of hGBPs with Alexa fluorophores

2.3.11.1. Unspecific labelling of hGBP isoforms for intermolecular FRET measurements

For intermolecular FRET measurements, hGBP-1 and mutants 3-Phe and K76A were labelled with donor fluorophore Alexa488 or acceptor fluorophore Alexa647, both of which harbour a maleimide group for specific coupling to cysteine residues. Keeping the dye in under-excess, 160 μ M fluorophore and 200 μ M protein were combined in buffer L (total volume of 100 μ l) to initiate the labelling reaction carried out on ice for 20 minutes. To remove unbound fluorophores, to exchange buffer, and also to exclude unspecific protein complexes putatively emerging during labelling reaction, the entire reaction mixture was applied to a semi-preparative gel filtration column (S200 10/30, GE Healthcare) previously equilibrated with the target buffer C + 2 mM DTT. The monomeric protein fraction was collected and concentrated by ultrafiltration (4000 rcf, 4°C) using 4 ml VivaSpin columns with a 10 kDa cutoff (Sartorius) until a final volume smaller than 100 μ l was reached.

For labelling of isolated LG domains of hGBP-1, -2, -3, and -5, two to three fold molar excess of either Alexa fluorophore over 50-100 μ M protein were mixed in buffer L. After incubation on ice for 30 to 60 minutes, reaction mixtures were applied to desalting spin columns (ZebaSpin, 2 ml, Pierce) or centrifugal concentrators (VivaSpin, 10 kDa cutoff, 4 ml, Sartorius) in order to accomplish buffer exchange to buffer C + 2 mM DTT and also to remove unbound fluorophores.

2.3.11.2. Sequential labelling of hGBP-1 for intramolecular FRET measurements

Intramolecular FRET construct of hGBP-1 carrying both donor fluorophore Alexa488 and acceptor fluorophore Alexa647 within one molecule was generated by sequential supplement of fluorophores, exploiting differential accessibility of cysteines (in total nine residues in hGBP-1). As C-terminal C589 revealed as initial target of dye attachment, initial labelling step was carried out with acceptor fluorophore only (the same as for intermolecular labelling construct, 160 μ M Alexa647 and 200 μ M hGBP-1 in buffer L, 20 minutes on ice) to ensure that most of the C589 positions were occupied. Only then was 420 μ M Alexa488 added to the same reaction mixture incubating for additional 20 minutes. The entire reaction mixture was applied to a semi-preparative gel filtration column (S200 10/30, GE Healthcare) previously equilibrated with the target buffer C containing 2 mM of DTT. The monomeric protein fraction was

collected and concentrated by ultrafiltration (4000 rcf, 4°C) using 4 ml VivaSpin columns with a 10 kDa cutoff (Sartorius) until a final volume smaller than 100 µl was obtained.

2.3.11.3. Sequential labelling of Cys9 based intramolecular FRET constructs using anion exchange chromatography

Sequential labelling of either hGBP1 mutant A76 (Cys9/C18/C577/K76A) or B76 (Cys9/C344/C540/K76A) was performed as described earlier (Hengstenberg, 2013). In these proteins all natural cysteines were replaced by an alanine or serine residue. Instead, exactly two cysteine residues were introduced into desired subdomains defining the specific position for fluorophore attachment (Hengstenberg, 2013). For the first labelling step, 100-300 µM protein and 1.5-fold molar excess of Alexa647 were diluted in buffer L (total 1 ml) and incubated on ice for 1 hour. Meanwhile anion exchange column (ResourceQ, 6 ml, GE Healthcare) was equilibrated with low salt buffer. Upon covalent binding of Alexa647, hGBP-1 adopts a more negative charge linearly increasing with the number of dyes. This was exploited to separate single labelled protein molecules from non-labelled and double-labelled species by anion exchange chromatography (AEC). Therefore, 1 ml of labelling mixture was diluted with 4 ml of low salt buffer and the total volume of 5 ml was subjected to the column (1 ml/min) through an injection loop. After washing with 6 CV of low salt buffer, high salt buffer was connected to start a gradient from 0 to 500 mM NaCl over a length of 120 ml. Eluate was collected in 2 ml fractions. By the chromatogram recorded at 280 nm different protein species were identified and corresponding fractions were analyzed according to their labelling efficiency (LE, for determination see 2.3.11.4.). Those fractions having a LE close to one, i.e. protein species carrying a single dye per molecule, were collected and used for the second labelling step. Therefore, protein concentration was determined to add a 4-fold molar excess of Alexa488 ensuring that the remaining cysteine residue was attached with a donor dye. After an additional hour of incubation on ice, labelling mixture was again separated by AEC and the concentration of the target FRET construct was increased by ultrafiltration (VivaSpin concentrator, 4 ml, 10 kDa cutoff, Sartorius). At a resulting volume smaller than 100 µl, 4 ml buffer C + 2 mM DTT was added and left for centrifugation. To accomplish buffer exchange, this procedure was repeated two more times. After determining protein concentration and labelling efficiency, small aliquots were prepared, shock frozen in liquid nitrogen and stored at -80°C.

2.3.11.4. Determination of labelling efficiency

In principle, labelling efficiency (LE) reflects the number of covalently attached fluorescent molecules per protein molecule that can be easily calculated by the ratio [fluorophore]/[protein]. The fluorophores Alexa488 and Alexa647 used in this work have absorption maxima at 491 nm and 651 nm, respectively. These are sufficiently distinct and allow determination of protein and fluorophore concentrations by absorption spectroscopy. However, both fluorophores do also absorb at 280 nm to certain extent which influences appropriate calculation of the protein concentration. Thus, correction factors 0.11 (Alexa488) and 0.03 (Alexa647) were considered to determine the protein concentration resulting in equation 6 which was used to calculate the labelling efficiency.

$$\text{eq. 6} \quad LE = \frac{\frac{A_{491 \text{ or } 651}}{\epsilon_{491 \text{ or } 651}}}{\frac{A_{280} - 0.11 \cdot A_{491} - 0.03 \cdot A_{651}}{\epsilon_{280}}}$$

Other than described in paragraph 2.3.4., here, proteins were not denatured prior to absorption spectroscopy. Instead, absorption measurements were performed in buffer C + 2 mM maintaining native folding of the protein. Relevant extinctions coefficients are listed below; ϵ_{280} was obtained from (Gasteiger, et al., 2005) considering H₂O as solvent.

Fluorophore/Protein	ϵ_{280} $M^{-1} cm^{-1}$	ϵ_{491} $M^{-1} cm^{-1}$	ϵ_{651} $M^{-1} cm^{-1}$
Alexa488		71,000	
Alexa647			268,000
hGBP-1 wt and point mutants	45,400		
1-LG	35,410		
2-LG	39,420		
3-LG	35,410		
5-LG	30,940		

2.3.11.5. Trypsin digestion of fluorophore labelled hGBP-1 and dye assignment

Trypsin digestion of hGBP-1 with subsequent SDS-PAGE analysis was performed for two reasons: firstly, to check altering structural arrangement of mutants as compared with wt hGBP-1 (reflected by different patterns of cleavage products), secondly, to identify localization of Alexa dyes at particular subdomains of hGBP-1 after labelling (Hengstenberg, 2013). For the latter one, experimental procedure is described in detail as it has an additional step to create fluorescence images of the SDS gel.

In buffer C, 1 g/l Alexa labelled hGBP-1 was mixed with 0.005 g/l trypsin (total 50 μ l) to initiate the cleavage reaction at 25°C. To monitor the time course of cleavage reaction (0-30 min) by subsequent SDS-PAGE analysis, samples were taken at different time points: 5 μ l of the mixture was supplemented with 15 μ l sample loading buffer (1 x) and subsequently boiled at 95°C for 5 min. 10 μ l of each sample was separated by SDS-PAGE using a 12.5 % gel. Prior to coomassie staining, fluorescence images were generated. Therefore, the gel was soaked in fixation solution for 15 minutes and subsequently placed in the BioSpectrum Imaging System (UVP, UK) which was equipped with the BioLite MultiSpectral Light source (UVP, UK). Using appropriate excitation and emission filters, fluorescence of Alexa dyes could be captured in images. Afterwards, the same gel was stained with coomassie. Comparison or merging of fluorescence and coomassie gels enabled to assign the fluorescent dye to the C-terminal region of hGBP-1 or to the N-terminal LG domain.

2.3.12. Time dependent inter- and intramolecular FRET measurements

All measurements were carried out in an LS55 fluorescence spectrometer (Perkin Elmer, USA). Irrespective of inter- or intramolecular FRET measurements, uniformly, donor fluorophore Alexa488 was excited at 498 nm, whereas emission of the acceptor fluorophore Alexa647 was monitored at 664 nm. Excitation and emission slits were set to 10 and 15 nm, respectively, and the voltage was set to 775 mV. If not indicated otherwise, all measurements were performed at 25°C using buffer C or buffer C+AIF for investigating the complex GDP-AIF_x as GTP analog. Basically, Alexa labelled proteins were mixed and monitored during a preincubation period of 2-5 minutes until a stable basal fluorescence signal was obtained. Only then were nucleotides added (0.2-1.5 mM) to trigger any inter- or intramolecular interactions which were reflected by changes in FRET efficiency relative to the initial fluorescence signal.

Intramolecular motions of hGBP-1 subdomains induced by different nucleotides were monitored using appropriately double labelled proteins. For intramolecular FRET measurements, 0.1-0.5 μ M labelled intramolecular FRET constructs (LP) were always mixed with an at least ten-fold molar excess of non-labelled protein (NLP) to ensure nucleotide dependent formation of mixed LP:NLP complexes and hence to encounter putative intermolecular FRET effects emerging in LP:LP complexes. Any change in FRET efficiency exclusively reported relative distance changes between donor and acceptor dyes within one protein molecule. Depending on particular localization of fluorophores within the protein, changes in FRET efficiency consequently reported relative changes of particular subdomains to

Materials and Methods

each other. An increase of fluorescence reported subdomains coming closer and a decrease reciprocally indicated that subdomains moved apart.

Intermolecular FRET studies were performed on C-terminally labelled wild-type hGBP-1 and point mutants (3-Phe, K76A) testing different buffer and temperature conditions. Also, homo and hetero dimerization of isolated LG domains of different hGBP isoforms were investigated via intermolecular FRET measurements. In principle, a pair of donor and acceptor labelled protein was mixed in equimolar ratio and nucleotide dependent intermolecular complex formation was deduced from increasing FRET efficiency. In competitive FRET studies, different types of NLPs were supplemented to the system. A reduced FRET efficiency as compared with control measurements in the absence of NLPs was exploited as semi-quantitative measure for LP:NLP formation interfering with the maximum amount of FRET compatible and thus detectable LP:LP complexes.

3. Results

3.1. hGBP-1

Basic properties of hGBP-1, such as nucleotide binding, GTPase activity and nucleotide dependent oligomerization, were investigated extensively until now. However, temperature and buffer conditions used for the studies have not always been the same, which indeed complicates comparison of the data. Moreover, the biochemical characterization of other hGBP isoforms and their intermolecular interactions, also with hGBP-1, is a main topic of this thesis. Thus, it was a major concern to establish consistent conditions that ground the basis for reliable comparisons. In order to stabilize the proteins and also to simulate physiological salt conditions, we decided to perform all measurements in buffer C consisting of 50 mM Tris-HCl (pH 7.9), 5 mM MgCl₂ and additional 150 mM NaCl. Temperature of 25°C was chosen as a compromise between protein stability and sufficiently fast reaction kinetics. First, hGBP-1 was characterized under given conditions serving as reference.

3.1.1. Nucleotide binding dynamics of hGBP-1 under physiological salt conditions

Human GBP-1 was originally identified by its feature to bind GMP, GDP and GTP with similar affinities (Cheng, et al., 1983) (Cheng, et al., 1985). Binding to different nucleotides which naturally appear and disappear upon GTP turnover were further investigated and found to regulate inter- and intramolecular interactions of hGBP-1 (Ghosh, et al., 2006) (Vöpel, et al., 2009).

To investigate the effect of 150 mM NaCl on nucleotide binding properties of hGBP-1, stopped-flow experiments with mant-(2'/3'-O-(N-Methyl-anthraniloyl) labeled nucleotides were performed. Stopped-flow measurements and processing data to obtain kinetic parameters are exemplified on binding of non-hydrolysable GTP-analog mant-GppNHp (mGppNHp) to hGBP-1 (figure 3-1). Protein and nucleotide were diluted in buffer C containing 150 mM NaCl. Mant group of the nucleotide was excited at 366 nm and its emission was detected through a 420 nm cutoff filter. Maintaining pseudo first order conditions, 0.5 µM mGppNHp was rapidly mixed with 5 µM, 7.5 µM, 12.5 µM and 15 µM hGBP-1, respectively. Fluorescence increase upon nucleotide binding to protein was fitted by a single exponential equation (figure 3-1 A, red lines) that yielded observed rate constants (k_{obs}) for each protein concentration. The slope and intercept of a linear regression to k_{obs} values as a function of hGBP-1 yielded rate constants for mGppNHp association (k_{on}) and dissociation (k_{off}) being

Results

$0.26 \mu\text{M}^{-1} \text{s}^{-1}$ and 1.1s^{-1} , respectively (figure 3-1, B). Obtained k_{off} value was additionally checked by a displacement experiment (figure 3-1, C); for that, preformed complex of $0.5 \mu\text{M}$ mGppNHp and $5 \mu\text{M}$ hGBP-1 was mixed with a 2000-fold molar excess of non-modified GMP over mant-nucleotide. Verifying k_{off} obtained from linear intercept (1.1s^{-1}), $k_{\text{off}}^* = 0.96 \text{s}^{-1}$ was derived from fluorescence decrease upon quasi-irreversible dissociation of mGppNHp. By the ratio of $k_{\text{off}}^*/k_{\text{on}}$ lastly, equilibrium dissociation constant (K_{d}^*) of $3.8 \mu\text{M}$ was calculated for hGBP-1-mGppNHp in presence of 150 mM NaCl buffer compound.

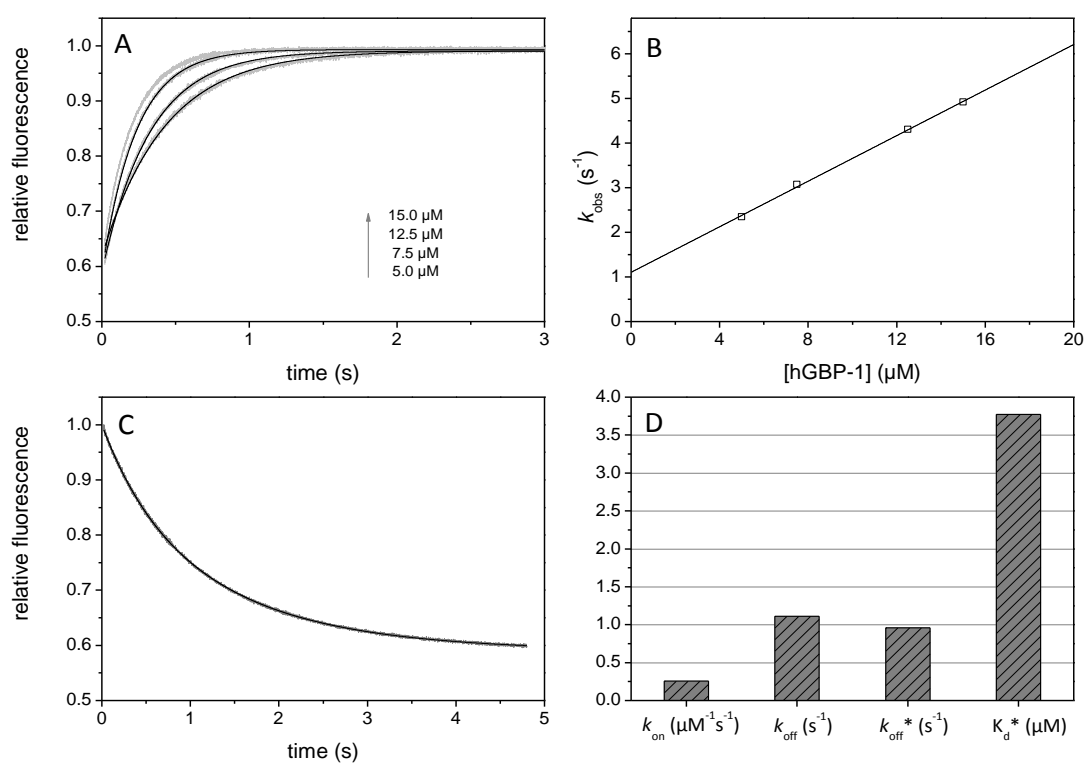


Figure 3-1: Binding of hGBP-1 and mGppNHp measured by stopped-flow. Stopped-flow measurements were performed in buffer C containing 150 mM NaCl. Mant group of GppNHp was excited at 366 nm and its emission was detected through a 420 nm cutoff filter. (A) Association kinetics of $0.5 \mu\text{M}$ mGppNHp and hGBP-1 with indicated concentrations were normalized by maximum intensities. Rate constants (k_{obs}) for association were derived from single exponential fits (black lines). (B) k_{obs} values were plotted against protein concentration and fitted by linear regression (straight line) yielded $k_{\text{on}} = 0.26 \mu\text{M}^{-1} \text{s}^{-1}$ (slope) and $k_{\text{off}} = 1.1 \text{s}^{-1}$ (intercept). (C) As a control for k_{off} from intercept, $k_{\text{off}}^* = 0.96 \text{s}^{-1}$ was obtained from displacement of mGppNHp with 1 mM of GMP. (D) Kinetic parameters and equilibrium dissociation constant $K_{\text{d}}^* = k_{\text{off}}^*/k_{\text{on}}$ of mGppNHp and hGBP-1 interaction are presented in bars.

Results

Exactly as described for mGppNHp binding, rate and equilibrium constants were determined also for binding of mGMP and mGDP to hGBP-1. All obtained parameters are summarized in table 3-1. In figure 3-2 values are plotted with corresponding parameters in the absence of 150 mM NaCl (adapted from Praefcke, et al., 2004). Comparison showed that increased salt content decelerated both association and dissociation rates to different extent, except for mGDP dissociation which was even slightly faster. Although resulting K_d values under physiological salt conditions were slightly higher, they did not remarkably distinguish from corresponding values under no salt conditions; 0.63 μM instead of 0.25 μM (mGMP), 5.4 μM instead of 4.1 μM (mGDP), and 3.8 μM instead of 1.7 μM (mGppNHp). Also the order of mGMP being the most tightly bound nucleotide followed by mGppNHp and mGDP, remained the same.

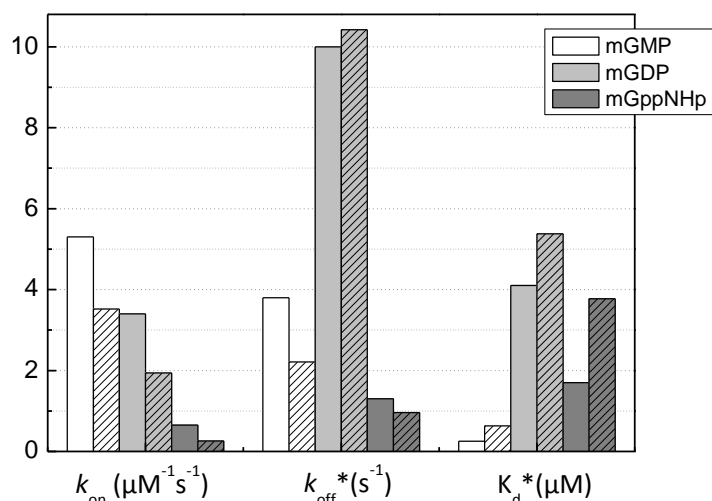


Figure 3-2: Kinetic parameters of hGBP-1 and mant-nucleotide interaction in the absence and presence of 150 mM NaCl. Corresponding k_{on} , k_{off}^* , and K_d^* values for mGMP (white), mGDP (light gray), mGppNHp (gray) binding are plotted as non-hatched bars (low salt conditions) and hatched-bars (physiological salt conditions), respectively.

Non-hydrolysable GTP-analogs GppNHp and GDP- AlF_x are typically used to analyze hGBP-1 in the GTP-bound state. Both analogs are believed to capture different steps in GTP binding and hydrolysis. An analog is expected to mimic properties of the natural substrate as similar as possible except for the feature to be hydrolyzed. However, some studies give hints towards GppNHp might not be an appropriate GTP analog for hGBP-1. For instance, kinetics of GppNHp induced hGBP-1 inter- and intramolecular interactions were shown to be decelerated by orders of magnitude. Also, excessive concentrations of protein ($> 100 \mu\text{M}$) were necessary to

Results

facilitate partial self-assembly of hGBP-1 (Hengstenberg, 2013). Altering behavior of GppNHp compared to GTP was shown to appear already at the stage of binding to hGBP-1; a weaker interaction of hGBP-1 and mGppNHp than hGBP-1 and mGTP as a result of slower association rate (Kunzelmann, 2007). Exhibiting more similar properties to GTP, GTP γ S has become a frequently used GTP-analog in hGBP-1 studies (Hengstenberg, 2013). Since also applied in this work, dynamics of mGTP γ S and hGBP-1 binding were determined under physiological salt conditions. With regards to an obtained rate of 3.3 $\mu\text{M}^{-1}\text{s}^{-1}$, mGTP γ S associated with hGBP-1 more than ten times faster than mGppNHp did (table 3-1). Dissociating also slightly slower than GppNHp, the complex of hGBP-1 and mGTP γ S had an almost 20-fold higher affinity than hGBP-1·mGppNHp.

Table 3-1: Kinetic and equilibrium constants of hGBP-1 and mant-nucleotides in buffer containing 150 mM NaCl. Dissociation rate constants were obtained either from linear intercept of association experiments (k_{off}) or directly from mant-nucleotide displacement experiments (k_{off}^*). Dissociation constant K_d^* was calculated by the ratio of $k_{\text{off}}^*/k_{\text{on}}$. Since k_{off}^* of mGTP γ S was not determined (--), K_d value of mGTP γ S·hGBP-1 was obtained by the ratio of $k_{\text{off}}/k_{\text{on}}$.

	k_{on} ($\mu\text{M}^{-1}\text{s}^{-1}$)	k_{off} (s^{-1})	k_{off}^* (s^{-1})	K_d^* (μM)
mGMP	3.5	2.2	2.2	0.63
mGDP	1.9	9.8	10.4	5.4
mGppNHp	0.26	1.1	0.96	3.8
mGTPγS	3.3	0.69	--	0.21

3.1.2. GTP hydrolysis and product formation catalyzed by hGBP-1 under physiological salt conditions

Human GBP-1 is a large GTPase that efficiently catalyzes GTP hydrolysis in a cooperative manner and yields both products GDP and GMP in two consecutive cleavage steps (Schwemmler, et al., 1994). Wehner and others showed that higher salt conditions, namely 200 mM NaCl, elevate hGBP-1 dimer dissociation constant by almost one order of magnitude, whereas effects on the maximum specific activity could not be identified (Wehner, et al., 2012). Here, for the sake of completeness, we investigated hGBP-1 catalyzed GTP hydrolysis in presence of 150 mM NaCl. As described in paragraph 2.3.8., substrate multi-turnover as well as product formation were analyzed at varying hGBP-1 concentrations and 500 μM GTP. Initial rates normalized by protein concentration yielded specific activities (s) for both GTP conversion and product formation. Data plotted as a function of protein concentration (figure

Results

3-3) were evaluated according to equation 5, whereby minimum specific activity was set to zero for 0 μM protein concentration. Obtained maximum activity for GTP turnover (s_{GTP}) and dimer dissociation constant (K_d^{GTP}) were determined to 19.1 min^{-1} ($\pm 0.6 \text{ min}^{-1}$) and $0.20 \mu\text{M}$ ($\pm 0.03 \mu\text{M}$), respectively. Being in line with published data, physiological salt conditions did not significantly alter s_{GTP} but did weaken dimer formation.

Besides GTPase activity, also maximum specific activities for GDP and GMP formation were obtained, namely $s_{\text{GDP}} = 12.2 \text{ min}^{-1}$ and $s_{\text{GMP}} = 6.9 \text{ min}^{-1}$ (eq. 5). Both s_{GDP} and s_{GMP} almost exactly add up to $s_{\text{GTP}} = 19.1 \text{ min}^{-1}$. That implicates two important facts: First, there is no production of pyrophosphate, thus, products GDP and GMP emerge upon successive cleavage. Second, any other reaction such as taking up product GDP for further hydrolysis can be excluded. Consequently, ratios $s_{\text{GDP}}/s_{\text{GTP}}$ and $s_{\text{GMP}}/s_{\text{GTP}}$, respectively, were considered as a measure of product composition, revealing 64% GDP and 36% GMP. Similar product composition found under no salt conditions (Vöpel, et al., 2010) indicates that additional salt does not affect the product ratio.

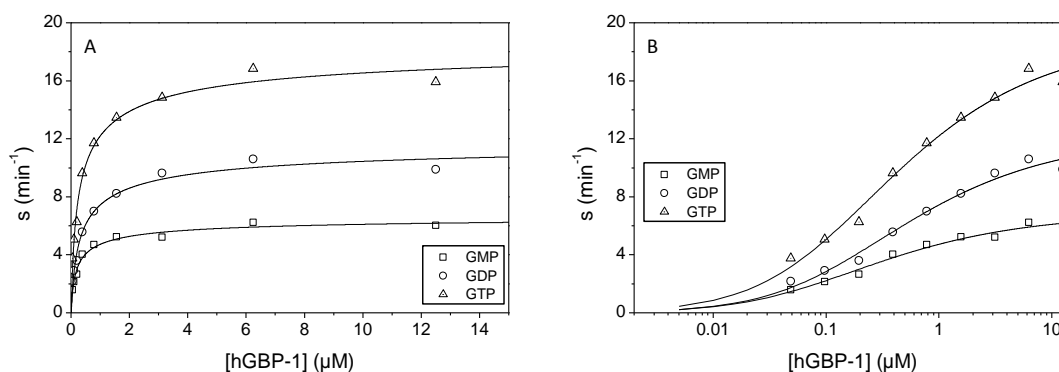


Figure 3-3: Specific activity of GTP hydrolysis and product formation catalyzed by hGBP-1 under physiological salt conditions. Concentration dependent increase of specific activities was evaluated according to equation 5 (straight lines), revealing maximum activities 19.1 min^{-1} , 12.2 min^{-1} and 6.9 min^{-1} for GTP turnover and GDP and GMP formation, respectively. Dimer dissociation constant K_d^{GTP} in presence of 150 mM NaCl was $0.20 \mu\text{M}$. The same dataset is plotted either linearly (A) or logarithmically (B).

3.1.2.1. Long term GTP and GDP hydrolysis assay: Screening concentration dependent substrate consumption and product formation

In a concentration dependent manner, GTP-bound hGBP-1 dimerizes which in turn leads to stimulated GTPase activity. During GTP hydrolysis, γ - and β -phosphate are cleaved in two successive steps yielding both GDP and GMP as products. The product ratio is controlled by two competing processes: After the first phosphate cleavage step (cleavage of γ -phosphate) GDP-bound hGBP-1 dimer either remains and β -phosphate cleavage proceeds, or GDP-bound dimer dissociates and releases GDP as final product (Kunzelmann, et al., 2006) (Rani, et al., 2012). GMP is the major product at 37°C (90 %) but declines to 40 % at 25°C (Praefcke, et al., 2004) (Vöpel, et al., 2010) suggesting a longer lifetime of the GDP-bound intermediate and thus elevated GMP production at higher temperatures (Rani, et al., 2012). In the previously shown experiment (paragraph 3.1.1.), product formation was investigated also at 25°C but under physiological salt conditions. Still, 36 % GMP was obtained which is similar to the results under low salt conditions performed at the same temperature. Consequently, reaction temperature rather than salt concentration might be a critical factor for the GDP-bound hGBP-1 dimer and thus for specific product levels.

To further elucidate substrate turnover and product composition, another HPLC based setup was established, namely long term nucleotide hydrolysis assay. For 24 hours, varying concentrations of protein were incubated with 500 μ M GTP at 25°C. The same was repeated by applying GDP as substrate instead in order to address any GDPase activity which indeed becomes relevant for some hGBP-1 mutants. For instance, the isolated LG domain (aa 1-327) of hGBP-1, referred to as 1-LG from now on, is one of the mutants capable of utilizing also GDP as substrate. For direct comparison, 1-LG was assayed in the same manner as full-length hGBP-1. Nucleotide composition was then analyzed and plotted against protein concentration (figure 3-4).

Reflecting the concentration dependent self-stimulation of hGBP-1's GTPase activity, decreasing amounts of substrate and increasing amounts of products were detected at increasing protein concentration (figure 3-4 A). After 24 hours of incubation, half amount of GTP was turned over at approximately 0.1 μ M of hGBP-1. Although matching very well with the previously obtained dimer dissociation constant (0.20 μ M, paragraph 3.1.2.), noteworthy, altering incubation times can result in different curve progression such that the value is not suitable to replace the K_d value derived from kinetic experiments. At concentrations below

Results

0.1 μM , where hGBP-1 is believed to be mainly monomeric, just a small fraction or even no GTP was converted. In view of the long incubation time, one can get an idea about how slowly monomeric protein can hydrolyze GTP. These findings particularly demonstrate that determining initial rates for GTP turnover at very low protein concentrations is highly error-prone. As done in the last paragraph, thus, setting minimum specific activity to zero for protein concentration approaching zero might be the most appropriate choice to evaluate respective data. Derived from this long term hydrolysis assay, the proportion of GMP constitutes 43 % of total product. Having an upwards deviation by only seven percentage points compared to the GMP amount derived from hydrolysis activity assay (36 %), long term hydrolysis assay represents a suitable approach for product determination. Applying GDP as substrate (figure 3-4 B) confirmed that hGBP-1 hydrolyzes GDP only as intermediate but not from bulk solution. Only at concentrations above 10 μM some decrease of GDP amounts could be detected, indicating that efficient GDP hydrolysis might occur at even higher protein concentrations.

Isolated 1-LG in contrast to full-length hGBP-1 is capable of catalyzing not only GTP but also GDP hydrolysis (Ghosh, et al., 2006). More precisely, GDP resulting as product from GTP hydrolysis can also serve as substrate for a second hydrolysis reaction consequently yielding GMP as major product. Here, investigating 1-LG catalyzed long term hydrolysis of GTP and GDP illustrated a novel view how strictly both reactions are controlled by protein concentration (figure 3-4 C and D). The development of GTP amounts upon hydrolysis by either 1-LG or full-length protein was very similar (figure 3-4 A and C); no considerable turnover at monomer concentrations, remarkable decrease reaching half amount between 0.1 and 0.2 μM , and complete consumption of GTP at 0.45 μM and higher protein concentrations. Further, amounts of GDP as substrate for 1-LG developed in the same manner as substrate GTP (figure 3-4 D), reflecting very well dimer-dependent stimulation of also GDPase activity (Ghosh, et al., 2006). However, efficient GDP turnover in comparison to GTP turnover occurs at approximately 10-fold higher protein concentrations suggesting a correspondingly weaker 1-LG·GDP dimer. Nevertheless, already before GDPase activity became relevant (< 0.45 μM), up to 70 % GMP arose from GTP turnover only, indicating clearly that elevated GMP amounts produced by 1-LG are not due to additional GDP hydrolysis reaction. Since 1-LG and hGBP-1 distinguish only by the carboxy-terminal domain, the lack of it might cause either accelerated β -phosphate cleavage or prolonged lifetime of the GDP-bound dimer intermediate, both effects capable of shifting the product ratio in favor of GMP as major product.

Results

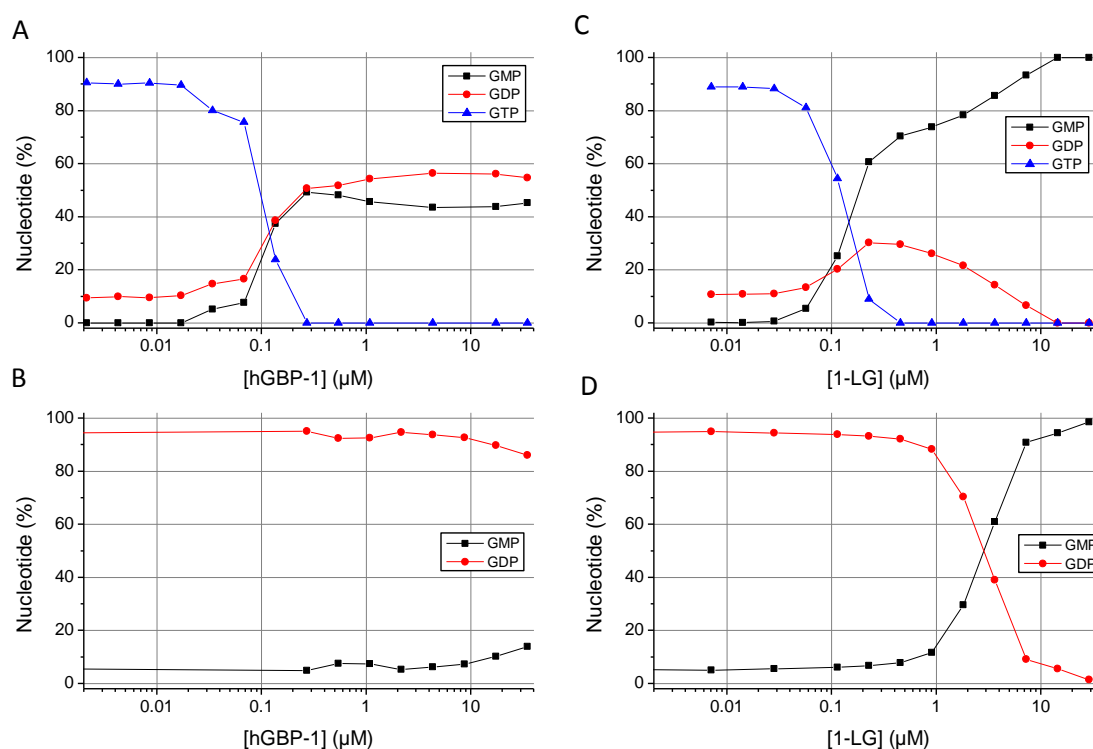


Figure 3-4: Long term GTP and GDP hydrolysis catalyzed by hGBP-1 and its isolated LG domain (1-LG). 500 μM of substrate (GTP or GDP) was mixed with different protein concentrations. After 24 hours incubation at 25°C, samples were analyzed via reversed-phase HPLC. Concentration dependent nucleotide compositions are depicted for following reaction mixtures: (A) hGBP-1 + GTP, (B) hGBP-1 + GDP, (C) 1-LG + GTP, and (D) 1-LG + GDP.

3.1.3. Nucleotide dependent oligomerization of hGBP-1

3.1.3.1. Analytical size exclusion chromatography

Analytical size exclusion chromatography (SEC) was performed to investigate nucleotide-dependent homo complex formation of hGBP-1 under physiological salt conditions. In order to evaluate the size of each complex by correspondingly obtained elution volumes (V_e), a calibration curve with protein standards was generated. Covering a range between 29 kDa and 669 kDa (table 3-2), each protein standard was applied to the gel filtration column S200 PC 3.2/30 (GE Healthcare) previously equilibrated with buffer C. Using Blue Dextran, a void volume (V_0) of 0.96 ml was determined. Logarithmic values of known molecular weights (MW) were then plotted against the ratio of V_e/V_0 (figure 3-5). The linear dependency described by equation $f(x) = -1.860 \cdot x + 4.880$ was further used to determine the size of assayed protein complexes (MW_{SEC}).

Results

Table 3-2: Protein standards analyzed by gel filtration column S200 PC 3.2/30. The list includes molecular weights (MW) of standard proteins, their logarithmic values (log MW) and obtained elution volumes (V_e) in buffer C. Using Blue Dextran, the void volume (V_0) of the column was determined to be 0.96 ml which then was used to calculate V_e/V_0 .

	MW (kDa)	log MW	V_e (ml)	V_e/V_0
<i>Carbonic Anhydrase</i>	29	1.46	1.79	1.86
<i>Albumin</i>	66	1.82	1.55	1.62
<i>Ovalbumin</i>	43	1.63	1.64	1.71
<i>Conalbumin</i>	75	1.88	1.55	1.61
<i>Alcohol Dehydrogenase</i>	150	2.18	1.43	1.49
<i>β-Amylase</i>	200	2.30	1.33	1.39
<i>Apo ferritin</i>	443	2.65	1.18	1.23
<i>Thyroglobulin</i>	669	2.83	1.04	1.08
<i>Blue Dextran</i>	2,000	3.30	0.96	1.00

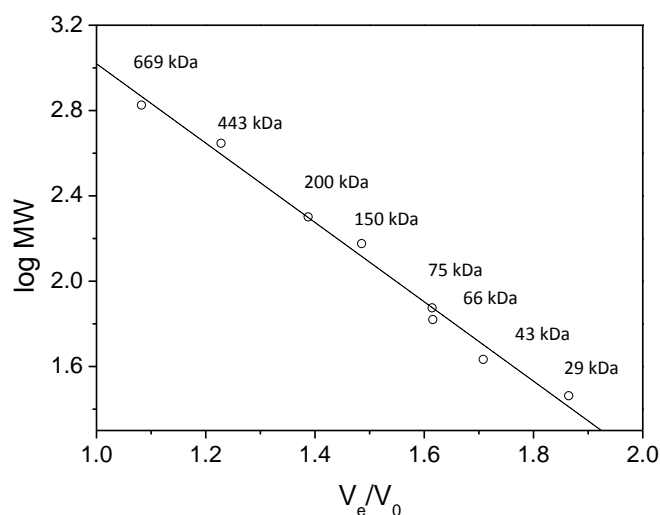


Figure 3-5: Calibration curve of gel filtration column Superdex 200 PC 3.2/30 (2.4 ml, GE Healthcare). Logarithmic values of proteins' molecular weight (corresponding values depicted in kDa within the graph) as a function of according V_e/V_0 value was fitted by linear regression which in turn yielded the equation $f(x) = -1.860 \cdot x + 4.880$.

GTP dependent homo interactions, particularly homo dimerization of hGBP-1 is known to be an essential feature, at least for self-stimulation of enzymatic activity. To further explore the nature of hGBP-1 complexes analytical SEC in presence of different nucleotides was performed in previous studies. Accordingly, hGBP-1 being monomeric in the nucleotide free, GMP and GDP bound state, was believed to form dimers and also tetramers when bound to

Results

GTP analogs GppNHp and GDP·AlF_x, respectively (Kunzelmann, et al., 2005). Here, we did the same to investigate whether increased salt conditions (150 mM NaCl) had any effects on hGBP-1s self-assembly. Elution behavior of hGBP-1 was tested in absence of any nucleotide and also in presence of the GTP-analogs GDP·AlF_x, GppNHp, and GTPγS. In contrast to previous studies, not three but only two hGBP-1 species could be identified (figure 3-6); one being the monomeric fraction and the other representing a hGBP-1 homo complex. Interestingly, only in presence of GDP·AlF_x did the homo complex with a corresponding size of 274 kDa occur. In presence of both other GTP analogs GppNHp and GTPγS, hGBP-1 remained monomeric instead. Respective values of 97 kDa and 90 kDa were almost identical to that of nucleotide free protein (MW_{SEC} = 94 kDa), thus no evidence for complex formation was given.

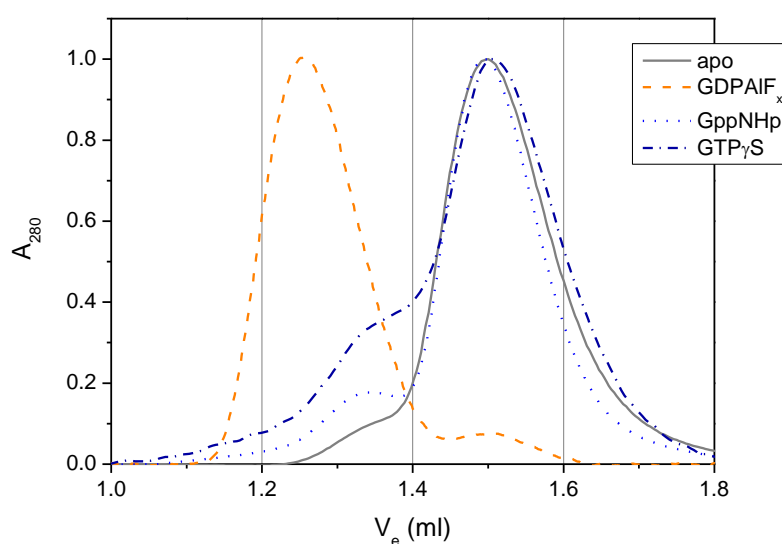


Figure 3-6: Analytical SEC of hGBP-1 under physiological salt conditions. Each run was normalized by maximum value. Nucleotide free (apo) as well as GppNHp and GTPγS bound hGBP-1 remained monomeric (MW_{SEC} = 94 kDa, 97 kDa and 90 kDa). Only when bound to GDP·AlF_x, hGBP-1 was enabled to form a complex with an apparent size of 274 kDa.

Especially due to GppNHp dependent complex formation of hGBP-1 which obviously does not arise under increased salt conditions, same experiments were repeated also in buffer C without NaCl. For comparison, corresponding runs were plotted in figure 3-7. In the absence of NaCl and independent from the nucleotide added, remarkably, protein peaks occurred much broader and due to a greater tailing also less symmetrical. This specific shape indicates that protein under low salt conditions might provide weak interactions that lead to more than one single species overlapping in the detected peak. Protein peaks being narrower and more

Results

defined under physiological salt conditions might thus be a result of salt dependent diminishing of those interactions. However, presence and absence of NaCl revealed shifted elution volumes for each nucleotide state which was mostly pronounced for the GppNHp bound state.

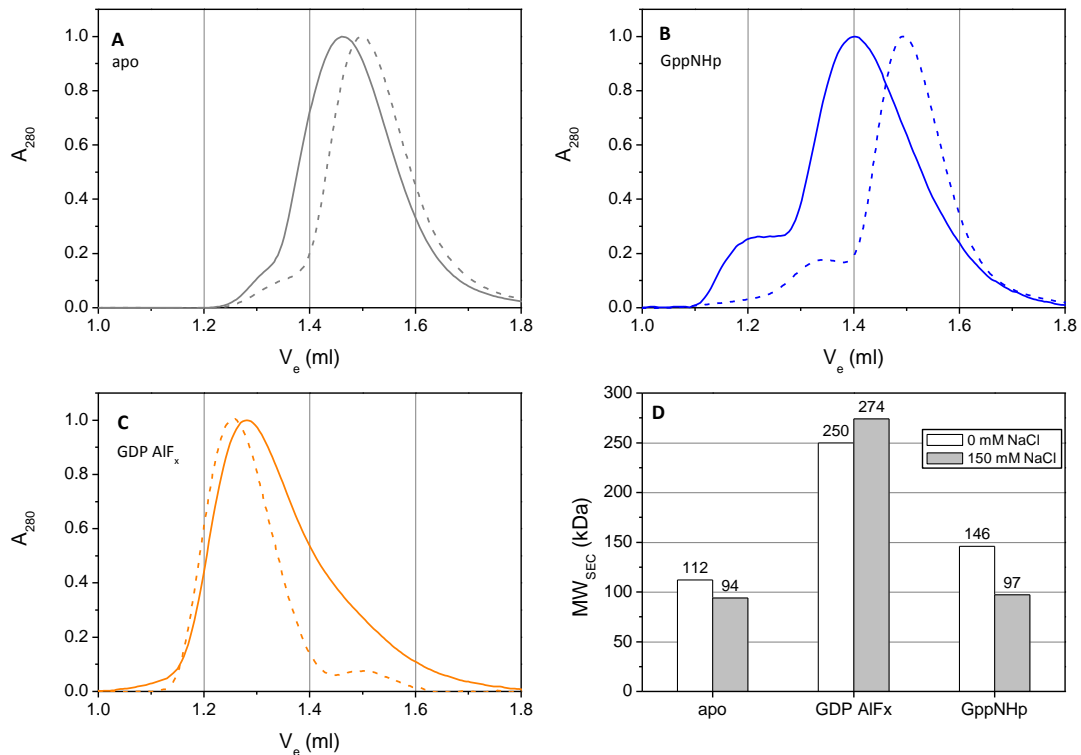


Figure 3-7: Salt dependent analytical SEC of hGBP-1. Oligomerization behavior of hGBP-1 was explored in either buffer C containing 0 mM (straight lines) or 150 mM NaCl (dashed line). Runs were performed in absence of any nucleotide (A, gray), in presence of GppNHp (B, blue) and in presence of GDP-AIF_x (C, orange). Each curve was normalized by its maximum value. Panel (D) gives an overview of all obtained molecular weights (MW_{SEC}) with indicated values in kDa.

Based on the amino acid sequence, hGBP-1 has a molecular weight of 68 kDa. However, the shape of the protein and its hydrodynamic radius are critical parameters for size exclusion experiments. Already demonstrated by the nucleotide free monomer under physiological salt conditions, hGBP-1 eluted with an apparent size of 94 kDa which compared to the theoretical value is enlarged by almost 40 %. In the absence of NaCl, nucleotide free protein eluted even earlier, corresponding to a molecular weight of 112 kDa. Like monomeric protein, also GDP-AIF_x bound complex deviated by approximately 20 kDa upon different salt conditions. While GppNHp bound hGBP-1 under physiological salt conditions eluted almost identical to the

Results

nucleotide free monomer, in the absence of NaCl, most remarkably, it appeared as a 146 kDa species being significantly smaller than the GDP·AlF_x induced complex but taller than the corresponding monomer (figure 3-7 B and D). Dividing $MW_{SEC}=146$ kDa by the theoretical monomer weight of 68 kDa, indeed, reveals two protein molecules being involved in the supposed dimer. However, in view of the monomer protein which upon SEC yields already 112 kDa, it is highly questionable to assign that species to a hGBP-1 dimer. Accordingly, also hGBP-1 complex emerging upon GDP·AlF_x binding and so far handled as tetramer needs to be revisited.

For a more reliable assignment of putative dimers and tetramers we performed an SDS-PAGE coupled analytical SEC. For that, a hGBP-1 point mutant was chosen (introduced later in paragraph 3.2.3.) that has the unfavourable tendency to form covalent homo complexes. The mutant was perfectly suitable as covalently formed complexes remain also under denaturing SDS conditions. In buffer C, the protein was diluted to 20 μM and applied to both SDS-polyacrylamide gel (SDS-PAAG) and gel filtration column, respectively. After separation, SDS-PAAG revealed three different bands with different intensities (figure 3-8 A). Reflecting the 68 kDa hGBP-1 monomer, the most intensive band occurred at the level of 66 kDa standard. The second band slightly higher than the 116 kDa marker is most likely the covalently dimerized protein which is expected to have a molecular weight of 136 kDa (=2·68 kDa). Having a similar intensity, the last band just hardly migrated into the separation gel and thus assigned a higher order oligomer of the protein.

Corresponding SEC yielded an elution profile that comprised also three different species, partly overlapping, but also having different intensities (figure 3-8 B). A fit to multiple peaks with Gaussian model unraveled elution volumes and proportions of each. Starting from the smallest molecule that consequently elutes the latest, molecular weights of 101 kDa, 268 kDa and 429 kDa were obtained. In the same order, they comprised 68%, 16% and 15% of total protein, which compared to the SDS-PAAG reflects very well the band intensities. Molecular weights of approximately 101 kDa and 268 kDa, of note, were typically obtained for hGBP-1 monomer and GDP·AlF_x bound hGBP-1 homo complex. While latter one was claimed to be a tetramer, however, combined analysis with SDS-PAGE revealed that it is most likely the dimer (>116 kDa SDS-PAAG) which elutes at a corresponding size of approximately 270 kDa. For analytical SEC studies on hGBP-1, in conclusion, any obtained molecular weight in between the range of 100 and 270 kDa might represent altering shapes of monomer or dimer, or even an equilibrium of both. This is particularly relevant for GppNHp bound hGBP-1 that under low salt

Results

conditions eluted earlier than the nucleotide free monomer and thus suggested an apparently higher molecular weight.

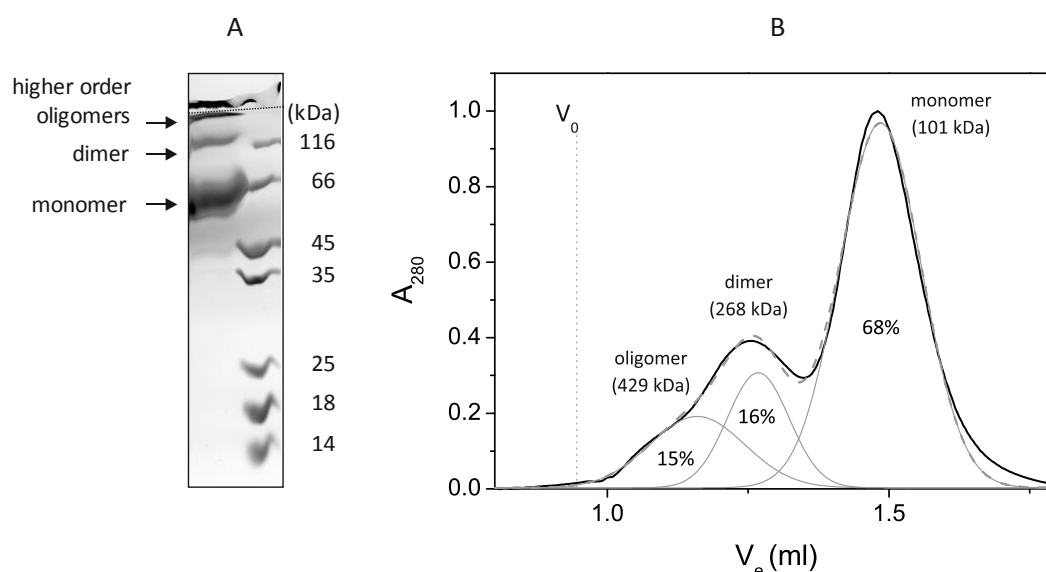


Figure 3-8: Coupled SDS-PAGE and SEC analysis of a mutant variant of hGBP-1. 20 μ M of hGBP-1 point mutant (3-Phe, see paragraph 3.2.3.) was applied to both SDS-PAAG (A) and gel filtration column in the absence of any nucleotide (B). (A) Coomassie stained SDS-PAAG revealed monomeric, dimeric and oligomeric protein. (B) According to a Gaussian model, three peaks (gray lines adding up to resulting dashed curve) were fitted to elution diagram (black line) yielding V_e and proportion of each species as indicated. According to SDS-PAGE analysis, obtained molecular weights (MW_{SEC} in brackets) could be assigned to monomer, dimer and oligomer species of hGBP-1.

3.1.3.2. Inter- and intramolecular FRET measurements with hGBP-1

Analysis of hGBP-1 via analytical size exclusion chromatography revealed that GDP- AlF_x was the only GTP-analog that clearly induced complex formation of the protein. We could assume the complex to be rather tight since same results were obtained irrespective of salt content of the buffer system (0 mM and 150 mM NaCl). Coupled analysis of SEC and SDS-PAGE, moreover, revealed that the hGBP-1 complex formed upon GDP- AlF_x binding is more likely a dimer than a formerly supposed tetramer.

In contrast, we could figure out a dependency between NaCl composition of buffer and the elution profile of hGBP-1 when bound to GppNHp. While clearly eluting as monomer when buffer contained 150 mM NaCl, a shift to lower V_e was observed when NaCl was missing, raising two questions. First: Does GppNHp to some extent induce weak dimer formation of hGBP-1 that upon increased salt levels is vanished? Second: Does GppNHp bound hGBP-1 constitute a more 'open' monomer state that due to altered hydrodynamic radius apparently

Results

elutes earlier than nucleotide-free monomer does? From the result of combined SDS-PAGE analysis and SEC, at least, a dimer was expected to elute significantly earlier.

However, to further address the question whether specific nucleotides do induce dimerization or not, we decided to switch to a more sensitive method, namely Förster Resonance Energy Transfer (FRET). Using fluorescently labelled hGBP-1 and considering increase in FRET efficiency as reporter for protein interaction, different nucleotides, buffer conditions and temperatures were assayed for the potential effects on dimerization. At least, we intended to figure out whether the claimed hGBP-1·GppNHp dimer under no NaCl conditions could be detected by FRET.

3.1.3.2.1. Labelling efficiency and dye assignment

For intermolecular FRET measurements, hGBP-1 was labelled with donor fluorophore Alexa488 or acceptor fluorophore Alexa647, both harbouring a maleimide group for specific coupling to cysteine residues. Keeping the dye in under excess, 160 μ M fluorophore and 200 μ M hGBP-1 (total volume of 100 μ l) were mixed for the labelling reaction that was carried out on ice for 20 minutes. To remove unbound fluorophores, to exchange buffer (target buffer C containing 2 mM DTT) and also to specifically collect the monomeric protein fraction, all reaction mixture was applied to gel filtration column (S200 10/30, GE). Remarkably, no oligomers or aggregates were formed upon labelling, both proteins eluted as monomers (figure 3-9). Respective fractions were concentrated via centrifugal concentrators (10 kDa cutoff) to a final volume smaller than 100 μ l. Protein and fluorophore concentration and labelling efficiency determined as described in paragraph 2.3.11.2 are summarized in table 3-3. Labelling efficiencies were 0.87 and 0.62 for donor labelled (wt-D) and acceptor labelled hGBP-1 (wt-A), respectively. Assuming the fluorophores to be equally distributed within a protein molecule, maximum 87 % wt-D and 62 % of wt-A molecules were assumed to carry a single dye while the rest remained unlabelled.

Human GBP-1 contains nine cysteine residues, whereby six are located in the LG domain (amino acid position 12, 82, 225, 235, 270, and 311), two are located in the middle domain (amino acid position 396 and 407) and the last one is located in the C-terminal CaaX-motif (Cys589). In general, some of the LG domain cysteines and also the CaaX-box cysteine have been found to be solvent exposed and thus mostly accessible (Vöpel, et al., 2009).

Results

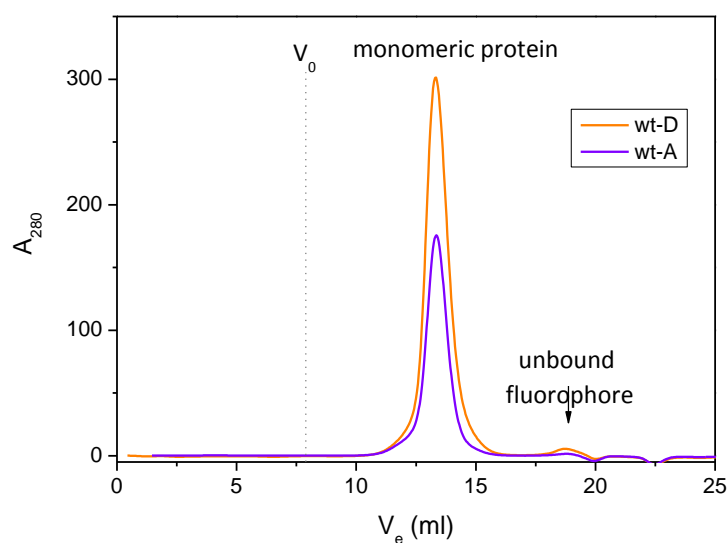


Figure 3-9: Size exclusion chromatography of Alexa labelled hGBP-1. Elution of donor labelled hGBP-1 (wt-D, orange) and acceptor labelled hGBP-1 (wt-A, blue) was detected at 280 nm. According to a calibration curve both proteins exclusively elute as monomers. Void volume (V_0) indicates that no aggregations or higher oligomers were formed upon labelling.

To figure out the hGBP-1 domain at which Alexa dyes upon unspecific labelling were localized, we performed trypsin digestion with subsequent SDS-PAGE analysis like established in (Hengstenberg, 2013). For that 1 g/l Alexa labelled hGBP-1 (wt-D or wt-A) were mixed with 0.005 g/l trypsin. Cleavage was monitored over time by taking samples at defined time points. After sample separation via SDS-PAGE, fluorescence images of the gels were created using appropriate excitation and emission filters for donor and acceptor dye, respectively. Afterwards, the same gels were also stained with coomassie. In figure 3-10, coomassie gel (left panel), fluorescence gel (right panel) and their overlay (middle panel) are illustrated for both donor (A) and acceptor labelled hGBP-1 (B).

Comprising 77 cleavage sites (Gasteiger, et al., 2005), Lys252 of hGBP-1 has been shown to be the first target of trypsin (Hengstenberg, 2013) (Praefcke, 2001). As a consequence, first cleavage yields two hGBP-1 fractions, a smaller one from amino acid (aa) 1 to 252 constituting major parts of the LG domain and a bigger one (aa 259-592) constituting the C-terminal rest including the CaaX motif. Here, already after two minutes of trypsin digestion, both fractions could be identified on the coomassie stained gels. They appeared at corresponding heights of 35 kDa and 45 kDa marker, respectively, and stably remained for almost ten minutes before additional cleavage products occurred (figure 3-10, A and B, left panels). Fluorescence images

Results

confirmed successful labelling since a clear fluorescence signal was obtained for both donor and acceptor fluorophore (figure 3-10 A and B, right panels, lane 0'). Trypsin digested hGBP-1 fractions revealed, moreover, that both fluorophores were attached to the C-terminal domain (aa 253-592). Within the domain, CaaX-box cysteine C589 is highly accessible and thus most probably carries the dye. Also the fact that fluorescence signal disappeared significantly after six minutes, while according coomassie stained protein fraction remained almost at same height, provided further evidence for C589 being the labelled position. These findings particularly indicated that, first, without significantly affecting overall size only terminal and small parts of the domain were further cleaved and, second, that these parts above all contained fluorescent dyes. Since terminal localization in first line applies to C589, taken together, that residue was assumed to harbour both Alexa dyes.

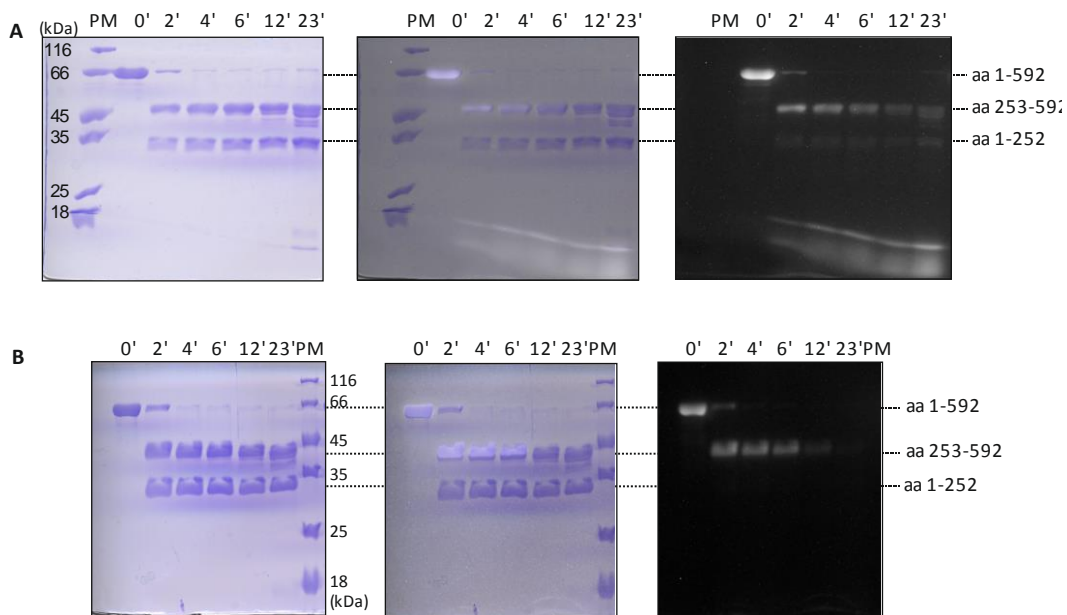


Figure 3-10: SDS-PAGE analysis of fluorescently labelled hGBP-1 after trypsin cleavage. At 25°C and in buffer C, 1 g/l donor or acceptor labelled hGBP-1 was digested with 0.005 g/l trypsin. Samples taken before (0') and during cleavage reaction (after 2', 4', 6', 12' and 23') were separated through a 15% SDS gel. From each gel either containing wt-D samples (A), or wt-A samples (B), three images were derived illustrating coomassie stained protein (left panel), dye fluorescence (right panel) and an overlay of both (middle panel). PM: Molecular weight marker with indicated standards covering a range from 18 to 116 kDa.

Concerning a putative rearrangement of hGBP-1 upon GppNHp binding which might lead to the apparently higher molecular weight under no salt conditions, we were also interested in a construct suitable to monitor intramolecular motions. Thus, an intramolecular FRET construct (wt-intra) was generated carrying both, donor fluorophore Alexa488 and acceptor fluorophore Alexa647 in a single hGBP-1 molecule. The major challenge was to position the

Results

fluorophores such that two requirements were satisfied. First, fluorophores had to be localized at two distinct hGBP-1 domains that upon GTP turnover are known to undergo intramolecular movements. Second, relative distant between donor and acceptor fluorophore had to be in a detectable range around 52 Å which is the according Förster radius. That could be best met by attaching one dye to the C-terminal helix α 13, more specifically to residue C589, and the other dye to any accessible cysteine residue within the LG domain. Profiting from high accessibility of cysteines at mentioned positions and moreover exploiting that Alexa fluorophores primarily targeted C589 (see above), we established a successive labelling procedure.

In the first step, labelling was carried out with acceptor fluorophore only (the same as for intermolecular labelling construct, 160 μ M Alexa647 and 200 μ M hGBP-1, 20 minutes of incubation on ice) to ensure that most of the C589 positions were occupied. Only then donor fluorophore could be successfully redirected to LG-domain cysteines. In the second step, 420 μ M Alexa488 was added to the same reaction mixture. After additional 20 minutes of incubation, labelled intramolecular construct (wt-intra) was processed in the same manner as both intermolecular constructs wt-D and wt-A. Determined protein concentrations as well as respective labelling efficiencies are listed in table 3-3.

Table 3-3: Protein concentration and labelling efficiency (LE) of fluorophore labelled hGBP-1. Wt hGBP-1 was labelled either with donor Alexa488 (wt-D), with acceptor Alexa647 (wt-A), or with both (wt-intra). Protein and fluorophore concentrations were obtained according to the Beer-Lambert law using molecular extinction coefficients $\epsilon_{280} = 45,400 \text{ M}^{-1}\text{cm}^{-1}$, $\epsilon_{491} = 71,000 \text{ M}^{-1}\text{cm}^{-1}$, and $\epsilon_{651} = 268,000 \text{ M}^{-1}\text{cm}^{-1}$ (Hengstenberg, 2013) for hGBP-1, donor dye and acceptor dye, respectively.

<i>Protein</i>	<i>Protein concentration</i> (μM)	<i>LE</i> (<i>donor</i>)	<i>LE</i> (<i>acceptor</i>)	ϵ_{280} ($\text{M}^{-1} \text{cm}^{-1}$)
wt-D	103	0.87	--	
wt-A	147	--	0.62	45,400
wt-intra	157	1.99	0.51	

3.1.3.2.2. Temperature and salt dependent intermolecular FRET measurements

Since size exclusion chromatography was performed at approximately 10°C, we first investigated whether temperature is a critical parameter for hGBP-1 dimerization. Thus, time dependent runs were performed at either 10°C, simulating condition during SEC, or 25°C, the temperature at which any other study like nucleotide binding or enzyme activity assay was performed. Equimolar ratio of both hGBP-1 labelled with donor fluorophore Alexa488 (wt-D), or acceptor fluorophore Alexa647 (wt-A) were diluted to a final concentration of 2 μ M total protein. The buffer used for the experiments (buffer C) contained 150 mM NaCl. Donor was excited at 498 nm and acceptor fluorescence was monitored at 664 nm. After a stable signal was obtained within 2-5 minutes, GTP analogs GDP·AlF_x, GppNHp or GTP γ S were added and time trace of FRET was detected for additional 5-15 minutes (figure 3-11 A). Indicating a clear intermolecular interaction independent from temperature, fluorescence signals increased up to 2.8-fold when GDP·AlF_x was applied (left panel). Only the kinetic was faster at higher temperature (orange). Addition of GppNHp, in contrast, did not induce any change (middle panel). At both temperatures, fluorescence intensity remained at identical level of initial fluorescence before nucleotide addition ($t_0 = 0$ seconds). Almost same effect was observed when GTP γ S instead of GppNHp was used. A minor difference was a fast and narrow increase to 1.1-fold over initial fluorescence (right panel) which by means of interaction is not noteworthy. Detecting nucleotide dependent hGBP-1 interaction under salt conditions via FRET, taken together, mirrored the same observations on complex formation already obtained by analytical SEC. In both approaches, only GDP·AlF_x induced some significant effects. Here, we could observe that also increased temperature did not promote enhanced interactions.

In order to likewise elucidate salt effects, same experiments were repeated in buffer without NaCl and at 25°C. Corresponding FRET traces in presence and absence of NaCl are illustrated in figure 3-11 B. In general, all nucleotides except for GTP γ S induced same effects also in absence of NaCl. A lower maximum fluorescence value for GDP·AlF_x driven hGBP-1 interaction (left panel) might be a result of altering fluorophore arrangement under reduced salt conditions. For GppNHp, fluorescence level in absence of salt was very slightly increased (middle panel), however, it is highly questionable if this difference reflects the shifted elution volume in SEC. Lastly, GTP γ S in absence of NaCl induced a continuous increase in fluorescence suggesting that hGBP-1 to some extent dimerizes (right panel). Due to both a slow kinetic and an increase up to 1.4-fold only, GTP γ S driven hGBP-1 dimers might have a much weaker affinity than the GDP·AlF_x driven ones.

Results

Of note, due to fluorophore positions at C589 obtained FRET traces exclusively reported distance changes between C-termini and probably also their interaction which in fact was shown on basis of isolated α 12-13 (Benscheid, 2005). Although interactions through LG domain contacts cannot be excluded at this point, for sure, one can deduce a clear correlation between interactions provided by the helical domain and the complex occurring on analytical SEC. Since recently published data give evidence for α 13: α 13 interactions being involved in LG mediated hGBP-1 dimerization (Vöpel, et al., 2014), we can conclude with the data above that merely in presence of GDP·AlF_x α 13 interactions come into play. Particularly only then a hGBP-1 dimer is established that is tight enough to remain during analytical size exclusion.

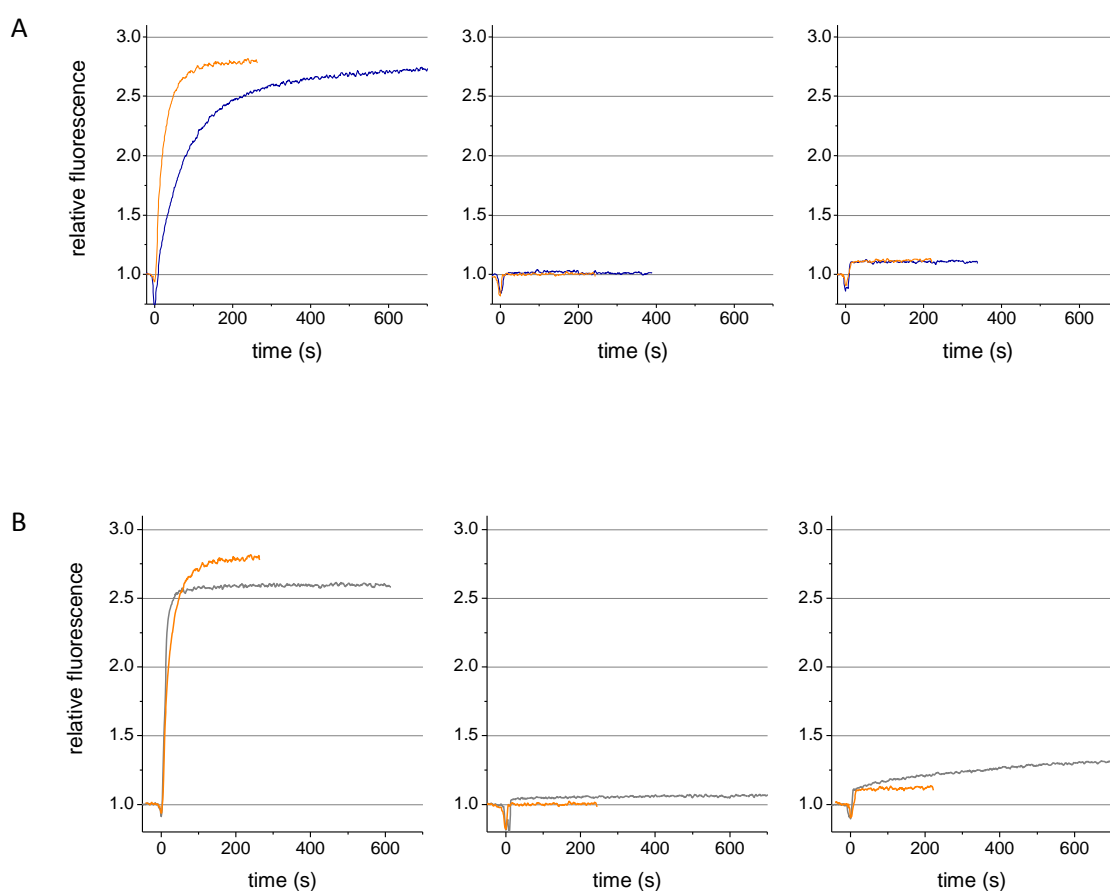


Figure 3-11: Temperature and salt dependent intermolecular FRET measurements of hGBP-1. 1 μ M donor and 1 μ M acceptor labelled hGBP-1 were mixed and monitored for 2-5 minutes until fluorescence signal was stable. Donor was excited at 498 nm, acceptor emission was detected at 664 nm. Dimerization reported by an increase of fluorescence was started by addition of nucleotide at $t_0 = 0$ s; 250 μ M GDP·AlF_x (left), 250 μ M GTP γ S (middle), 500 μ M GppNHp (right). For comparison, each trace was divided by initial values. (A) Runs were performed at 10°C (blue) and 25°C (orange) using buffer C containing 150 mM NaCl. (B) At 25°C, solvents buffer C with (orange) and without 150 mM NaCl (gray) were compared.

3.1.3.2.3. Salt dependent intramolecular FRET measurements

With given hGBP-1 constructs wt-D and wt-A, FRET measurements were performed to elucidate different conditions for intermolecular interactions. None of the tested conditions gave clear evidence for any helical interaction induced by GppNHp. To remind, SEC analysis of GppNHp bound hGBP-1 under reduced salt conditions led to a shift of elution volume revealing apparently higher molecular weight, in former studies handled as dimer. In contrast, GppNHp bound hGBP-1 under physiological salt conditions clearly remained monomeric. Supposed to ground the basis for increased hydrodynamic volume, finally, nucleotide dependent intramolecular interactions of hGBP-1 were investigated. Using wt-intra (donor and acceptor labelled construct), at 25°C both salt conditions and all GTP analogs were assayed for their effects on intramolecular opening. To maintain protein concentration from previous experiment and also to prevent interfering intermolecular FRET effects, 0.1 μ M wt-intra and 1.9 μ M non-labelled hGBP-1 were mixed. The same procedure as before, protein was monitored for several minutes and nucleotide was added to start the reaction. Upon nucleotide addition, all intramolecular FRET traces displayed a relative decrease in FRET efficiency, suggesting fluorophores move apart accordingly (figure 3-12). Due to localization of FRET couple within the protein, most likely opening of helix α 13 relative to LG-domain was recorded. Depending on applied nucleotide and also on salt condition, α 13 released to different extent.

Like in intermolecular FRET studies, also in intramolecular FRET studies GDP·AIF_x among all GTP analogs forced the greatest effect (figure 3-12, left panel). Independent from buffer composition, opening of hGBP-1 when bound to GDP·AIF_x occurred with almost same rates to almost same levels. Interestingly, also GDP·AIF_x driven dimerization in the previous study was controlled by almost same rate, thus concluding that dimerization and opening are highly dependent processes.

Although GppNHp controlled hGBP-1 dimerization could not be detected by intermolecular FRET measurements, here, intramolecular opening could be identified nevertheless (middle panel). With a much slower kinetic than observed for GDP·AIF_x, in presence and absence of 150 mM NaCl fluorescence signals decreased to 95 % and 80 % of initial fluorescence, respectively. Under physiological salt conditions, moreover, the signal increased even slightly after nucleotide addition, only then decreasing behavior set in. An increase in fluorescence as a result of fluorophores moving closer would indicate that accordingly α 13 and LG domain upon nucleotide binding first come closer and then start to

Results

move apart slowly. However, even though overall change in fluorescence signal is not very large, in low salt it is anyhow more pronounced and thus probably gives an explanation for elution behavior of hGBP-1·GppNHp.

For GTP γ S, the overall change in fluorescence was larger than for GppNHp but still less than for GDP·AlF $_x$ (right panel). In presence and absence of NaCl signals decreased to 70 % and 60 % of initial fluorescence, respectively, suggesting GTP γ S induced hGBP-1 opening like GppNHp induced one is sensitive to salt content. With GTP γ S, analytical SEC under low salt conditions was not performed. But when the effect obtained for GppNHp is indeed linked to intramolecular opening seen here, consequently, GTP γ S bound hGBP-1 in absence of NaCl should also elute apparently enlarged on analytical SEC.

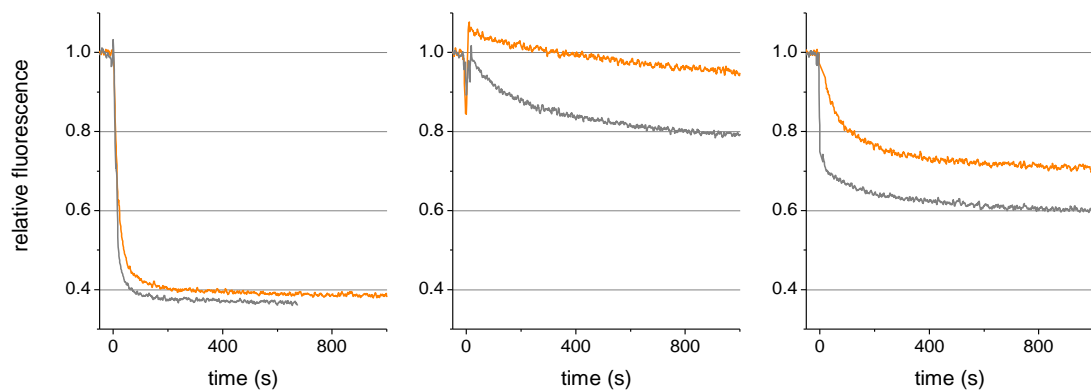


Figure 3-12: Salt dependent intramolecular FRET measurements of hGBP-1. 0.1 μ M wt-intra (donor and acceptor labelled hGBP-1) and 1.9 μ M non-labelled hGBP-1 were mixed and monitored for 2-5 minutes until fluorescence signal was stable. Donor was excited at 498 nm, acceptor emission was detected at 664 nm. Intramolecular opening reported by a decrease of fluorescence was started by addition of nucleotide at $t_0 = 0$ s (250 μ M GDP and GTP γ S, 500 μ M GppNHp). To obtain the complex GDP·AlF $_x$, protein was diluted in buffer additionally containing 10 mM NaF and 300 μ M AlCl $_3$, GDP was added at t_0 . Runs were performed 25°C using buffer C with (orange) or without 150 mM NaCl (gray). Panels from left to right depict corresponding runs with GDP·AlF $_x$, GppNHp and GTP γ S. For comparison, each trace was divided by initial values.

GppNHp and GTP γ S induced hGBP-1 motions displayed a pronounced dependency on salt content. Since intermolecular interactions of LG domains are known to be strongly driven by electrostatic contacts, different levels of opening might be linked to the same. Exemplary for GppNHp induced hGBP-1 opening, the same experiment from above was repeated with ten-

Results

fold higher concentration of non-labelled protein (NLP). When opening is due to concentration dependent LG domain interaction, consequently, altered fluorescence traces should be obtained. As depicted in figure 3-13, also high protein concentration did not induce larger opening or significant increase in kinetics. Thus, LG domain provided effects could be excluded. What we see is more likely an intramolecular rearrangement of a single hGBP-1 molecule exclusively resulting from GppNHp binding.

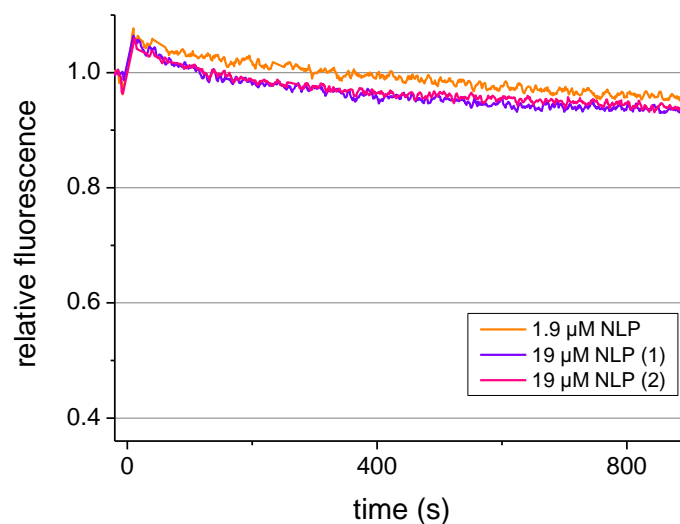


Figure 3-13: hGBP-1 concentration dependent intramolecular FRET induced by GppNHp. Experiments were performed as described in figure 3-12. Only buffer C with 150 mM was used and NLP concentrations were increased as indicated. Runs with 19 μM NLP were repeated twice ((1) and (2)), yielding almost identical traces not deviating remarkably from the previous one containing only one tenth of total protein.

3.2. Studies on mutants effecting GMP production of hGBP-1

3.2.1. Correlation between C-terminal flexibility and capability of hGBP-1 to catalyze GDP hydrolysis

Human GBP-1 is a GTPase capable of exhibiting cooperative GTP hydrolysis which by successive cleavage of phosphate groups yields a mixture of GDP and in particular GMP suggesting a unique hydrolysis mechanism (Schwemmler, et al., 1994). After the first hydrolysis step in which the hydrolysis competent hGBP-1 dimers cleave the γ -phosphate of GTP, protein molecules either dissociate to release GDP as product, or, they remain dimeric and perform the second hydrolysis step by cleavage of the β -phosphate. Although one could speculate that the second hydrolysis step might be required as an additional energy supplier, until now the biological relevance of that unique hydrolysis mechanism could not be clarified. Another remarkable feature of hGBP-1 is how it processes GDP: although hGBP-1 binds and also hydrolyses GDP when it is an intermediate product of GTP hydrolysis, it converts GDP only poorly when it is applied as substrate.

Up to now, a large number of site-directed as well as truncated mutants of hGBP-1 were generated to gain insights into the very specific enzyme machinery. Bringing specific mutants into a certain order, we could identify a putative correlation between the flexibility of the helical domain and the enhanced second hydrolysis step (figure 3-14). All the mutants were shown to accelerate GTP turnover upon dimerization via LG-contacts. The values depicted in the figure were adapted from (Vöpel, et al., 2010) and relate to the maximum activity provided when the protein is assumed to be completely dimerized. Serving as reference, wild type hGBP-1 converts GTP with a maximum catalytic activity of 23 min^{-1} and reveals 40 % GMP and 60 % GDP as final products. Direct hydrolysis of GDP, however, is reduced by three orders of magnitude (0.036 min^{-1}). The LG domain and C-terminal helices α 12-13 of hGBP-1 were proposed to be connected via salt bridges. Further rearrangements of the LG domain upon GTP turnover and dimerization were suggested to interrupt the salt bridges which in turn lead to a release of the α 12-13. A weakening of LG-helical contacts could be confirmed by the RK-mutant, where the salt bridge related amino acids R227 and K228 were substituted by charge reversed residues. In line with the hypothesis that a higher flexibility of the helical domain affects the second hydrolysis step, the RK-mutant in comparison to wild type (wt) showed an almost 22-fold increase in GDP turnover while the hydrolysis of GTP remained mainly unaffected. The exact opposite was achieved by the cross-linked (CL)-mutant: Here, two cysteines at positions 217 and 567 were introduced which subsequently were utilized to

Results

covalently connect the LG domain with the C-terminal $\alpha 13$ by the homobifunctional cross-linker DTME. As a result, any GTPase induced intramolecular motions between the LG and helical domain were blocked and neither significant GDPase activity (0.006 min^{-1}) nor significant GMP product amounts (4 %) were detected, emphasizing once more the essential role of the $\alpha 12$ -13 movement on the second hydrolysis step. An additional increase in GDPase activity by orders of magnitude was obtained for hGBP-1 $\Delta\alpha 12$ -13, a variant lacking the helices $\alpha 12$ -13, and finally becoming maximal for the isolated LG-domain (13 min^{-1}).

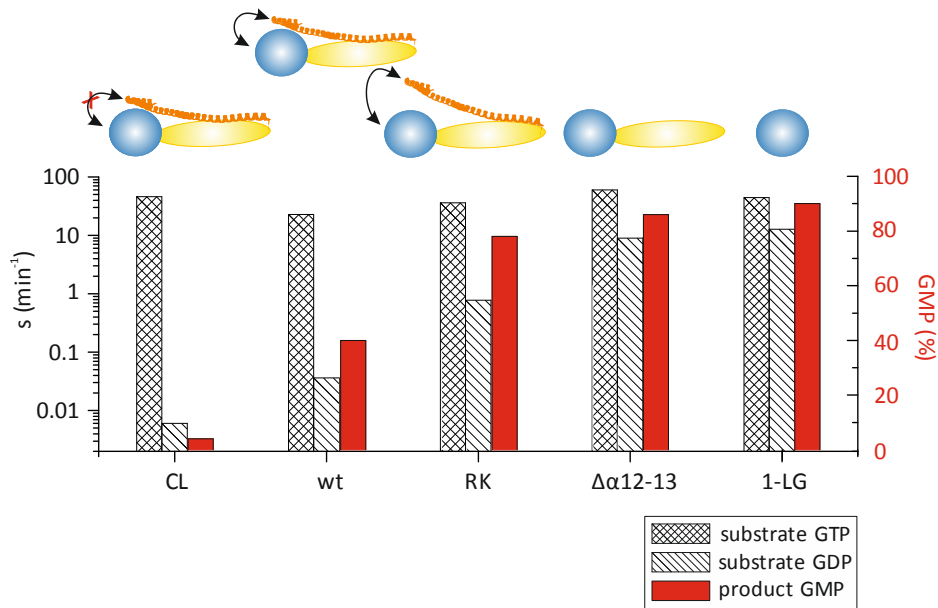


Figure 3-14: Overview on selected hGBP-1 mutants and their enzymatic properties. Specific GTPase/ GDPase activities were plotted logarithmically and the share of GMP on total product linearly (red). Mutants were sorted by increasing flexibility of the helices $\alpha 12$ -13 (left to right), whereby flexibility is blocked in the cross-linked (CL) mutant, becomes enhanced in the charge- reversed mutant (RK) and due to the truncation reaches even maximum in the mutants $\Delta\alpha 12$ -13 and isolated LG domain (1-LG). While all mutants perform similar GTPase activity, they show significant increase in GDPase activity and GMP production, suggesting that the C-terminus flexibility endorses the protein to cleave the β -phosphate more efficiently. Plotted data are according to results from (Vöpel, et al., 2010).

To sum up, as a result of enhanced opening or a higher flexibility of the helical domain, respectively, hGBP-1 gains the capacity to accept GDP as substrate, which in consequence yields GMP as major product. This in particular is true for the truncated variants. As they do not contain the helical domain at all, any inhibitory effects exerted by them is abolished, so that these variants can convert GDP most efficiently and the product composition is shifted almost exclusively to GMP.

3.2.2. Particular role of C-terminal helix α 13 in GMP production assessed by truncation mutant hGBP-1 $\Delta\alpha$ 13

The GTPase hGBP-1 consists of the globular LG domain as well as the elongated α -helical domain subdivided into the middle domain (α 7-11) and the C-terminal domain (α 12-13) which at the end is connected to the LG-domain via salt bridges. So far, dimerization mediated by LG contacts and its function to stimulate GTP hydrolysis is well understood. Beyond that, recent studies revealed a second interface located in α 12-13 which enables the protein to undergo further homo interactions or to interact with cellular compartments. Conformational rearrangements of the LG domains during GTP turnover and dimerization was identified as an essential mechanism that breaks the intramolecular salt bridges between the LG domain and the α -helices 12-13 and, therefore, makes α 12-13 release for further interactions (Vöpel, et al., 2010) (Syguda, et al., 2012). Homo-interactions of α 12-13, first proven by yeast two-hybrid experiments (Benscheid, 2005), were later shown to be accomplished by coiled-coil formation (Syguda, et al., 2012). Remarkably, homo interactions appeared mostly pronounced for α 12-13, whereas α 12 alone lacking α 13 remained mainly monomeric. Whether this is due to a decreased stability of α 12 in the absence of α 13, or due to the necessity of α 13 to induce helical interactions remains elusive (Benscheid, 2005).

Efforts were made to specify the second interface region, for instance, several crystal screenings with varying construct of hGBP-1 were set up. Dimer crystals were obtained with hGBP1 lacking the LG-domain (hGBP-1 α 7-13). The subsequent modeling procedure yielded two dimers with equal quality but great differences in spatial arrangement (Annamalai, 2013). Although biochemical data are still required to determine the definitive interface, most interestingly, all models showed an outstretching of helix α 13 as a common feature (figure 3-15, B and C). Moreover, DEER and FRET measurements demonstrated that two helices α 13 come in close proximity upon hGBP-1 dimerization, suggesting a substantial role of α 13 within the second interface. The authors proposed it to be important for the physiological membrane localization of hGBP-1 (Vöpel, et al., 2014).

Helix α 13 harbors the CaaX motif which is the target for hGBP-1's posttranslational farnesylation in eukaryotic cells (Modiano, et al., 2005). Farnesylated hGBP-1 in contrast to the non-farnesylated counterpart is enabled to associate to membranes but also to assemble to higher polymers in a nucleotide dependent manner. Prior to any interactions, again intramolecular movements, particularly the release of α 13 with the farnesyl tail are assumed to be required. That was found when the hydrophobicity of the labeled farnesyl tail was

Results

investigated. Indeed, the hydrophobic environment altered in presence of different nucleotides, which was suggested to be caused by nucleotide induced motions of the C-terminal domain and the farnesyl tail, respectively (Fres, et al., 2010) (Dovengerds, 2013) (unpublished data of Shydlovskiy).

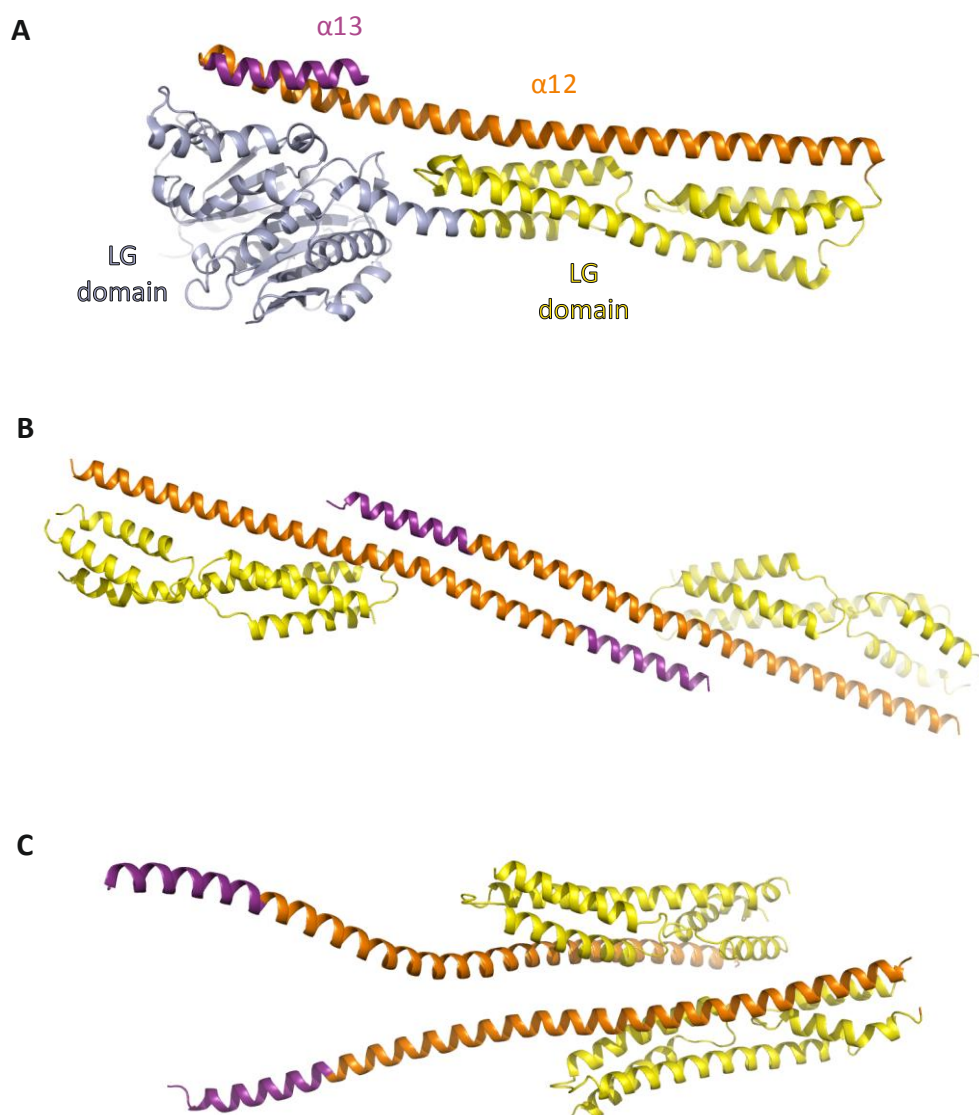


Figure 3-15: Outstretching of C-terminal helix $\alpha 13$ upon dimerization. Structural elements of hGBP-1 like LG domain (light blue), middle domain (yellow), $\alpha 12$ (orange), and $\alpha 13$ (purple) are highlighted in the full-length monomer structure (A; pdb: 1F5N), and in the putative $\alpha 7-13$ dimer structures, being either anti-parallel (B) or parallel (C); (B) and (C) adopted and modified from Annamalai (2013). While forming a bundle with $\alpha 12$ in the monomer structure, $\alpha 13$ swings out and forms a single continuous helix with $\alpha 12$ in the dimer structures.

In previous studies both helices $\alpha 12$ and $\alpha 13$ were considered as one unit performing their duties jointly. But at least the listed results above give rise to assume that both helices act very specifically in the complex enzyme machinery of hGBP-1. Here, we intended to address the distinct function of $\alpha 13$, thus a deletion mutants lacking the helix, namely hGBP-1 $\Delta\alpha 13$, was generated and investigated with respects to nucleotide binding affinities, GTPase and GDPase activity, as well as nucleotide dependent homo-complex formation.

3.2.2.1. hGBP-1 $\Delta\alpha 13$ hydrolyzes GTP in a cooperative manner

As described previously, GTPase activity assay was performed at 25°C using varying hGBP-1 $\Delta\alpha 13$ concentrations and 500 μM of GTP. Initial GTP turnover normalized by protein concentration yielded specific activities which plotted against protein concentrations illustrated a concentration dependent acceleration of GTPase activity, as known for any hGBP-1 construct containing a functional LG domain (figure 3-16). Likewise, initial rates of GMP or GDP production were processed yielding respective specific activities. Similar to the dimer stimulated GTP turnover, both GMP and GDP were formed in a protein concentration dependent manner, as well (figure 3-16).

Data fitted according to equation 5 yielded maximum specific activities for each substrate turnover and product formation and unraveled two remarkable deviations compared to full-length hGBP-1: First, maximum GTPase activity provided by hGBP-1 $\Delta\alpha 13$ was $s_{\text{GTP}} = 35.2 \text{ min}^{-1}$ (± 3.2) and thus almost two times higher than provided by full-length (19.1 min^{-1}). Second, GDP formation was significantly slower ($s_{\text{GDP}} = 7.7 \text{ min}^{-1}$ (± 1.0)) than GMP formation ($s_{\text{GMP}} = 27.9 \text{ min}^{-1}$ (± 2.4)) which is the opposite for hGBP-1. However, both deviations resemble rather GTP hydrolysis catalyzed by the isolated 1-LG (paragraph 3.3.2.2.). Of note, 1-LG lacks 265 C-terminal amino acids (helices $\alpha 7$ -13) while hGBP-1 $\Delta\alpha 13$ lacks only 28 amino acids; the enzymatic activity which is similar nevertheless emphasizes major contributions of helix $\alpha 13$.

Furthermore, apparent hGBP-1 $\Delta\alpha 13$ dimer dissociation constant was 0.80 μM (± 0.21) which is almost 4 times higher than obtained for hGBP-1 (0.20 μM). That might indicate an impact of $\alpha 13$ on the dimer formation or stability. Although hGBP-1 $\Delta\alpha 13$ still contains the fully GTPase competent LG domain that is sufficient to exert dimerization, moreover, our findings are probably in line with intermolecular interactions of two $\alpha 13$ helices which might contribute to dimer stabilization (Vöpel, et al., 2014). A lack of the appropriate region might lead to a weaker dimer formation, consequently reflected by an increased K_d value.

Results

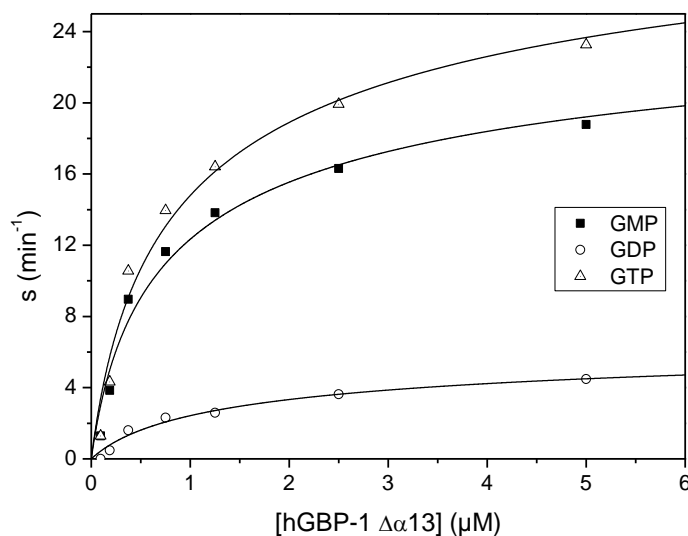


Figure 3-16: Concentration dependent GTPase activity and product formation of hGBP-1 Δα13. Specific activities of GTP turnover, as well as GDP and GMP formation were obtained from measurements at 25 °C using 500 μM GTP and protein concentrations as indicated. Data fitted according to equation 5 yielded specific activities of $s_{\text{GTP}} = 35.2 \text{ min}^{-1}$, $s_{\text{GDP}} = 7.7 \text{ min}^{-1}$ and $s_{\text{GMP}} = 27.9 \text{ min}^{-1}$, respectively. Apparent dimer dissociation constant was determined to 0.80 μM.

3.2.2.2. GMP is the major product of hGBP-1 Δα13 catalyzed GTP hydrolysis

Upon hGBP-1 Δα13 catalyzed GTP turnover, as illustrated in the previous experiment, specific activities of GDP and GMP formation significantly altered from full-length behavior. However, since $s_{\text{GDP}} = 7.7 \text{ min}^{-1}$ and $s_{\text{GMP}} = 27.9 \text{ min}^{-1}$ almost exactly add up to $s_{\text{GTP}} = 35.2 \text{ min}^{-1}$ still both product can be assumed to occur upon successive cleavage of GTP. Moreover, ratio of $s_{\text{GMP}}/s_{\text{GTP}}$ indicated that GMP had a share of 79 % on total product.

To analyze how GTP is processed in the absence of α13, we also performed a long term hydrolysis assay with varying concentrations of hGBP-1 Δα13 and 500 μM GTP. After 24 hours incubation at 25°C nucleotide compositions were analyzed and compared to corresponding data of wt hGBP-1 (figure 3-17). Both proteins showed almost same amounts of GTP at each concentration, hGBP-1 Δα13 converted slightly more GTP at even lower concentrations reflecting the higher GTPase activity. Resulting product amounts were roughly balanced for wt. In contrast, mutant hGBP-1 Δα13 converted GTP predominantly to GMP being approximately 75 % of the entire product. These data confirmed product composition of 79 % GMP and 21 % GDP derived from specific activities.

Results

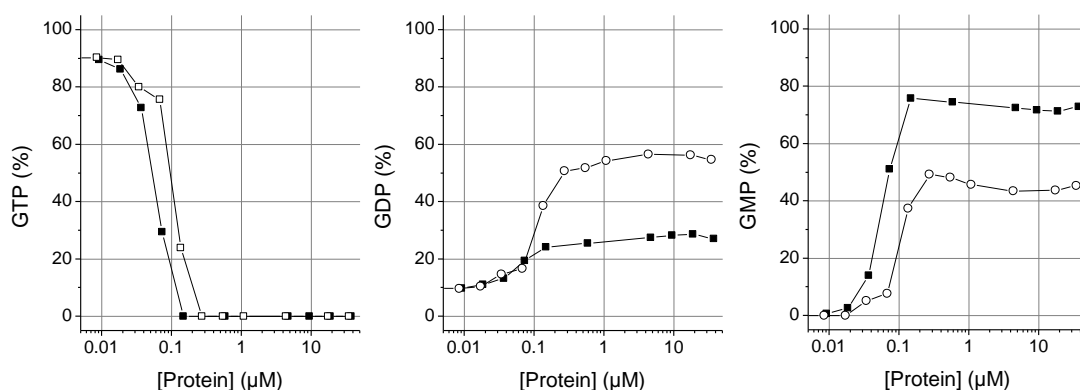


Figure 3-17: Nucleotide composition of hGBP-1 wt and hGBP-1 $\Delta\alpha 13$ in the course of long term GTP hydrolysis. Relative amounts of GTP (left), GDP (middle) and GMP (right) at each protein concentration were determined after 24 hours of incubation at 25°C. Corresponding data of wt hGBP-1 (open circles) and hGBP-1 $\Delta\alpha 13$ (closed squares) were plotted.

As shown for other mutants the product shift to GMP can be a consequence of additional feature to utilize GDP as substrate. For instance, truncation 1-LG being competent to produce elevated GMP amounts upon GTP hydrolysis, at certain protein concentrations started to consume also GDP which led to GMP being the exclusive product. Elevated GTPase activity and GMP production have already been figured out as features that both hGBP-1 $\Delta\alpha 13$ and 1-LG have in common. To finally elucidate whether truncation of $\alpha 13$ alters also GDPase capability, long term hydrolysis experiments were performed with 500 μM GDP. Nucleotide compositions were compared to that of full-length hGBP-1 and 1-LG (figure 3-18). As visible, GDP turnover catalyzed by either full-length or truncation $\Delta\alpha 13$ set in only at protein concentrations above 10 μM . The course of GDP indeed suggests that full-length as well as $\Delta\alpha 13$ are potentially capable of forming GDPase competent dimers, however, this might be only possible at much higher protein concentrations than assayed. In contrast, at concentrations around 10 μM isolated 1-LG converted GDP almost entirely to GMP suggesting that GDPase efficient 1-LG dimers have a significantly higher affinity.

To sum up, deletion of $\alpha 13$ resulted in enhanced GTPase activity as well as favored GMP production, both properties typical for 1-LG. Unlike 1-LG, deletion mutant hGBP-1 $\Delta\alpha 13$ like full-length hGBP-1 remained substrate-limited, more precisely, at protein concentrations within investigated range it was not capable of utilizing GDP as substrate. This suggests that more than just helix $\alpha 13$ must be missing so that efficient GDP hydrolysis can take place.

Results

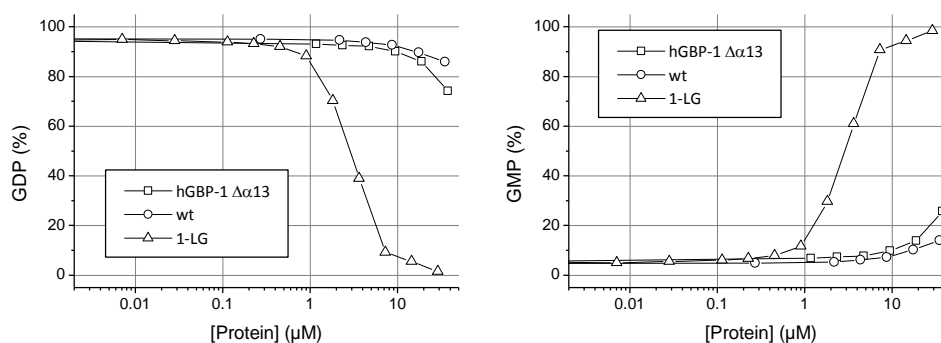


Figure 3-18: Nucleotide composition of hGBP-1 wt, hGBP-1 $\Delta\alpha13$ and 1-LG in the course of long term GDP hydrolysis. Relative amounts of GDP (left) and GMP (right) at each protein concentration were determined after 24 hours of incubation at 25°C. For comparison, corresponding data of either wt hGBP-1 (circle), hGBP-1 $\Delta\alpha13$ (square) and 1-LG (triangle) were plotted.

3.2.2.3. Nucleotide binding properties of hGBP-1 $\Delta\alpha13$

In order to exclude any effects on nucleotide binding properties caused by deletion of helix $\alpha13$, we primarily determined affinities by equilibrium fluorescence titration at 25°C. Therefore, 0.5 μM mant-nucleotide was titrated with increasing hGBP-1 $\Delta\alpha13$ concentration until fluorescence signal remained constant (figure 3-19, A). Mant-group was excited at 366 nm and fluorescence increase upon binding was detected at 435 nm. Fitting the data according to a quadratic binding equation 2 revealed K_d values of 0.81 μM , 3.6 μM and 4.3 μM for mGMP, mGDP and mGppNHp. Corresponding values for hGBP-1 were 0.63 μM , 5.4 μM and 3.7 μM , indicating that deletion of helix $\alpha13$ did not notably affect nucleotide binding properties.

Exemplary for mGDP binding, also kinetics were investigated via stopped-flow measurements. The slope of the linear fit of concentration dependent rate constants yielded an association rate constant of $k_{\text{on}} = 2.0 \mu\text{M}^{-1}\text{s}^{-1}$. Dissociation rate constant ($k_{\text{off}}^* = 9.9 \text{s}^{-1}$) was derived from a typical displacement experiment (see paragraph 3.1.1.). Both were similar to corresponding values obtained for full-length hGBP-1 ($k_{\text{on}} = 1.9 \mu\text{M}^{-1}\text{s}^{-1}$ and $k_{\text{off}}^* = 9.8 \text{s}^{-1}$). Consequently, calculated K_d^* value for hGBP-1 $\Delta\alpha13$ and mGDP was 4.9 μM and thus just slightly lower than the one for hGBP-1. That deletion of helix $\alpha13$ did not significantly alter nucleotide binding affinities is also visualized in figure 3-19 B.

Results

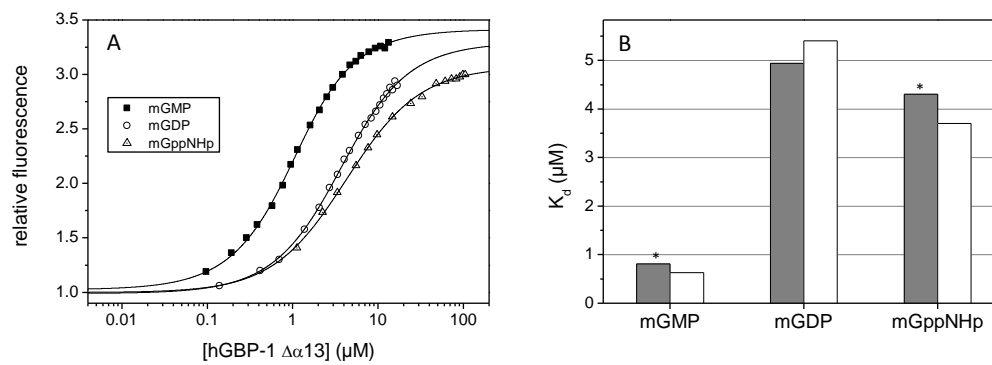


Figure 3-19: Nucleotide binding affinities of hGBP-1 $\Delta\alpha13$. (A) Fluorescence equilibrium titration of hGBP-1 $\Delta\alpha13$ and mant-labelled nucleotides denoted in legend. 0.5 μM mant-nucleotide was titrated with increasing protein concentrations. Mant-group was excited at 366 and fluorescence increase upon binding was detected at 435 nm. Data fitted according to equation 2 (straight lines) yielded equilibrium constants of 0.81 μM , 3.6 μM and 4.3 μM for mGMP, mGDP and mGppNHp, respectively. (B) Nucleotide binding affinities of hGBP-1 $\Delta\alpha13$ (gray) and full-length (white) in comparison. K_d values for indicated nucleotides were derived from stopped flow experiments, except for the ones labelled with asterisks which were taken from (A), instead.

3.2.2.4. Nucleotide dependent oligomerization of hGBP-1 $\Delta\alpha13$

In the next step, it was investigated whether deletion of the C-terminal helix $\alpha13$ had any effect on nucleotide dependent oligomerization of hGBP-1. Therefore, size exclusion chromatography was performed in the absence or presence of different GTP-analogs (figure 3-20). In the absence of any nucleotide, hGBP-1 $\Delta\alpha13$ eluted as monomer with a calculated size of 91 kDa. Like observed for wild-type, also here GDP·AlF_x was the analog that clearly made hGBP-1 $\Delta\alpha13$ assemble to a complex of 230 kDa. Considering the apparent size of a monomer, this complex would most likely correspond to a dimer.

As presented in paragraph 3.1.3.1, hGBP-1 bound to GppNHp or GTP γ S eluted in the same manner as nucleotide-free monomer, suggesting that none of the nucleotides could induce protein dimerization. In contrast, hGBP-1 $\Delta\alpha13$ bound to GppNHp eluted in two peaks, a major one representing monomeric protein and a minor one representing dimer at almost same elution volume as GDP·AlF_x bound complex. Probably protein concentration of 20 μ M was not sufficient to shift equilibrium entirely to dimer state indicating that GppNHp induced dimers are still weaker than GDP·AlF_x induced ones. Nevertheless, at least some hGBP-1 $\Delta\alpha13$ complex occurred giving evidence that hGBP-1 dimerization is more likely when helix $\alpha13$ is lacking. Similar results were obtained for GTP γ S bound protein but different than before the two species were barely separated so that resulting peak was rather an apparent single peak being twice as wide and having no clear maximum for elution volume assignment (figure 3-20). Altering elution diagrams might suggest different dynamics of either GppNHp or GTP γ S driven dimerization.

As a major difference to full-length hGBP-1, deletion of $\alpha13$ led to enhanced complex formation in presence of GppNHp and GTP γ S. Nevertheless, dimerization occurred only partly suggesting that GppNHp and GTP γ S bound hGBP-1 $\Delta\alpha13$ dimers were still weaker than the GDP·AlF_x induced ones and thus might require higher protein concentrations to establish a complete shift to dimer state.

Results

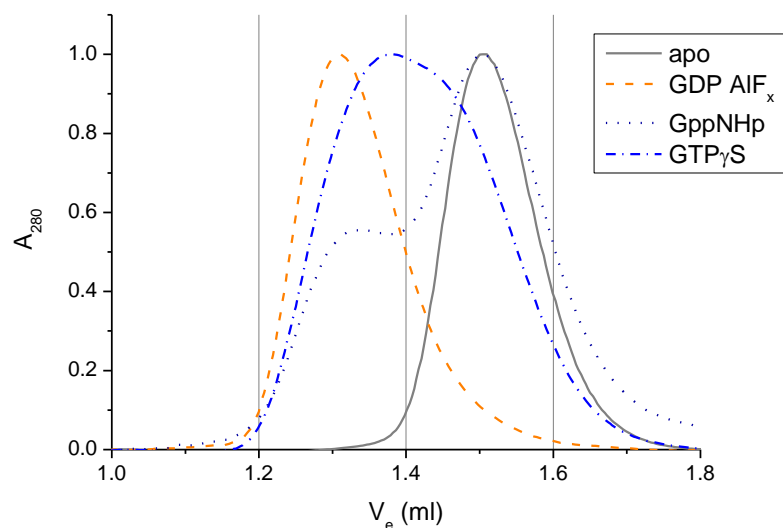


Figure 3-20: Nucleotide dependent oligomerization of hGBP-1 $\Delta\alpha13$ analyzed by SEC. Either no (apo) or 250-320 μ M of indicated nucleotide were used for SEC runs performed at 10-13°C. Prior to each run, 20 μ M protein was incubated with the respective nucleotide for at least 10 minutes. Each chromatogram was normalized by maximum value. Human GBP-1 mutant $\Delta\alpha13$ formed complexes in presence of GDP·AlF_x (218 kDa) and partly also in presence of GppNHp and GTP γ S. Obtained weight of nucleotide free monomeric protein (apo) was 91 kDa.

3.2.3. Contribution of conserved phenylalanines to basic properties of hGBP-1

3.2.3.1. Identification of a phenylalanine cluster with putative importance for hGBP-1 features

All seven members of human GBPs share a high sequence homology which is even more pronounced when the comparison is restricted to the enzymatically competent LG domain. In fact, all highly conserved and well characterized motifs responsible for guanine-nucleotide binding and hydrolysis are localized in the LG-domain. Interestingly, a detailed analysis of all human GBP sequences revealed another set of amino acids, namely phenylalanines, apparently distributed all across the proteins but being highly accumulated and conserved in the LG domains (figure 3-21).

In other contexts, numerous studies demonstrated the importance of phenylalanine residues on the structure and function of proteins. For instance, a single substitution of a phenylalanine in the immuno-active large GTPase MxA had great impact on virus recognition and, thus, on antiviral actions of the protein (Patzina, et al., 2014). Therefore, and due to the high degree of conservation within the human GBPs we presumed the phenylalanines to be greatly important for common characteristics of all family members, such as catalytic activity and nucleotide binding, as well as nucleotide-dependent oligomerization.

Until now, hGBP-1 is the best characterized member among all GBPs and the only one with solved crystal structures in complex with different nucleotides. Existing structures were utilized to further localize the phenylalanines, especially that ones being potentially critical for hGBP-1's enzymatic activity. Therefore, structures representing different states of GTP binding and hydrolysis were overlaid to select exactly that phenylalanines that in comparison clearly changed their spatial arrangements. While a majority of the phenylalanine residues hardly change their orientation, a hydrophobic cluster could be identified which harbors four phenylalanines that significantly do. All of them are localized in the LG domain but in immediate vicinity of the C-terminal domain α 12-13. While three of them (positions 171, 174 and 175) are part of helix α 3', the single phenylalanine F229 resides in α 4' (figure 3-22), the helix which previously was shown to undergo crucial conformational changes upon GTP binding and hydrolysis and thus might force release of α 12-13 for further interaction (Vöpel, et al., 2010). In the GppNHp bound state, residues are oriented towards the core of the LG domain. Probably as a result of α 3' becoming unstructured upon GDP·AlF_x binding, residues

Results

F174, F175 and particularly F171 move away from the core. Instead, F229 moves into the area where originally F175 was. Reorientations of mentioned residues are indicated by arrows in figure 3-22. The four phenylalanines are also highlighted in the sequence alignment (figure 3-21, black background).

Results

hGBP1	-----MASEIHMTGPMCLIENTNGRLMANPEALKILSAITQPMVVVAIVG	45
hGBP3	-----MAPEIHMTGPMCLIENTNGELVANPEALKILSAITQPVVVVAIVG	45
hGBP2	-----MAPEINLPGPMSLIDNTKQGLVNVNPEALKILSAITQPVVVVAIVG	45
hGBP5	-----MALEIHMSDPMCLIENTNEQLKVNQEAELISAITQPVVVVAIVG	45
hGBP4	MGERTLHAAVTPGYPESEIMMAPICLVENQEQLTVNSKALEILDKISQPVVVVAIVG	60
hGBP7	-----MASEIHMPGFVCLTENTKGLVNVNSEALEILSAITQPVVVVAIVG	45
hGBP6	-----MESGPKMLAPVCLVENNNEQLLVNQQAIIQLEKISQPVVVVAIVG	45
hGBP1	LYRTGKSYLMNKLAKKGGFSLGSTVQSHTKGIWMCVPHPKKPGHILVLLDTEGLGDVE	105
hGBP3	LYRTGKSYLMNKLAKKGGFSLGSTVKSHTKGIWMCVPHPKKPEHTLVLLDTEGLGDVK	105
hGBP2	LYRTGKSYLMNKLAKKGGFSLGSTVKSHTKGIWMCVPHPKKPEHTLVLLDTEGLGDIE	105
hGBP5	LYRTGKSYLMNKLAKKGGFVASTVQSHTKGIWICVPHPNWHTLVLLDTEGLGDVE	105
hGBP4	LYRTGKSYLMNKLAKKGGFPLGSTVQSETKGIWMCVPHLSKFNHTLVLLDTEGLGDVE	120
hGBP7	LYRTGKSYLMNKLAKKGGFPLGCTVKSETKGIWMCVPHSPKNHTLVLLDTEGLGDME	105
hGBP6	LYRTGKSYLMNKLAKKGGFPLGSTVQSETKGIWMCVPHSPKNHTLVLLDTEGLGDVE	105
hGBP1	KGDNQNDSWIFALAVLLSSTFVYNSIGTINQQAMDQLYVTELTTHRIRSKSSPDENENEV	165
hGBP3	KGDNQNDSWIFTLAVLLSSTLVYNSMGTINQQAMDQLYVTELTTHRIRSKSSPDENENE--	163
hGBP2	KGDNQNDSWIFALAILLSSTFVYNSMGTINQQAMDQLYVTELTDRIRKANSSP--GNNSV	163
hGBP5	KADNKNDIQIFALAILLSSTFVYNTVTKIDQGAIDLLHNVTETDILLKARNSP--DLDRV	163
hGBP4	KSNPKNDSWIFALAVLLSSSFVYNSVSTINHQAELQHYVTELAELIRAKSCP--RPDEA	178
hGBP7	KSDPKNDSWIFALAVLLSSSFVYNSMGTINHQAELQHYVTELTTELIRAKSCP--RPDEV	163
hGBP6	KGDPKNDSWIFALAVLLCSTFVYNSMSTINHQAELQHYVTELTTELIRAKSSP--RPDGV	163
hGBP1	EDSADFFVSFFPFDVWTLRDFSLDLEADGQPLTPDEYLTYSLKLLKGTSSQKDETFNLPRLC	225
hGBP3	EDSADFFVSFFPFDVWTLRDFSLDLEADGQPLTPDEYLYSLKLLKGTSSQKDETFNLPRLC	223
hGBP2	DDSADFFVSFFPFDVWTLRDFLELEVDGEPITADDYLESLKLLKGTSSQKDETFNLPRLC	223
hGBP5	EDPADSASFFPFDLWTLRDFCLGLEIDGQVLTPEYLENSLRPKQSDQQRVQNFNLPRLC	223
hGBP4	EDSSEFASFFPFDLWTLRDFLELEKLDGNPITDEYLENAKLLPKGNPKIQNSNMPPREC	228
hGBP7	EDSSEFVSFFPFDLWTLRDFLELEKLDGHPITDEYLENAKLLISGKNPQIQNSNKPREW	223
hGBP6	EDSTEFSFFPFDLWTLRDFLELEKLDGNPITDEYLENAKLLIQGNPNRQVTSNPPREC	223
hGBP1	IRKFFPKKCKVFDLPIHRR--KLAQLEKLQDEELDPEFVQQVADFCYSIFSNKTKTLTG	284
hGBP3	IRKFFPKKCKVFDLPIHRR--KLAQLEKLQDEELDPEFVQQVADFCYSIFSNKTKTLTG	282
hGBP2	IRKFFPKKCKVFDLPIHRR--KLAQLEKLQDEELDPEFVQQVADFCYSIFSNKTKTLTG	282
hGBP5	IQKFFPKKCKVFDLPIHRR--KLAQLEKLQDEELDPEFVQQVADFCYSIFSNKTKTLTG	282
hGBP4	IRHFFPKKCKVFDLPIHRR--KLAQLEKLQDEELDPEFVQQVADFCYSIFSNKTKTLTG	298
hGBP7	IRHFFPKKCKVFDLPIHRR--KLAQLEKLQDEELDPEFVQQVADFCYSIFSNKTKTLTG	283
hGBP6	IRRFFPKKCKVFDLPIHRR--KLAQLEKLQDEELDPEFVQQVADFCYSIFSNKTKTLTG	283
hGBP1	GIQVNGRPLESLVLTIVNAISSGDLPCMENAVLALAQIENSAAVQKAI AHYDQQMGQKQV	344
hGBP3	GIKVNGRPLESLVLTIVNAISSGDLPCMENAVLALAQIENSAAVQKAI AHYDQQMGQKQV	342
hGBP2	GIPVNGRPLESLVLTIVNAISSGDLPCMENAVLALAQIENSAAVQKAI AHYDQQMGQKQV	342
hGBP5	GIMVNGRPLESLVLTIVNAISSGDLPCMENAVLALAQIENSAAVQKAI AHYDQQMGQKQV	342
hGBP4	GIIVNGRPLESLVLTIVNAISSGDLPCMENAVLALAQIENSAAVQKAI AHYDQQMGQKQV	358
hGBP7	GILVNGRPLESLVLTIVNAISSGDLPCMENAVLALAQIENSAAVQKAI AHYDQQMGQKQV	343
hGBP6	GITVNGRPLESLVLTIVNAISSGDLPCMENAVLALAQIENSAAVQKAI AHYDQQMGQKQV	343
hGBP1	LPTESLQELLDLHRDREAEIEVFIKSDVDHLEFQKELAAQLEKRRDDFCQKQNEASS	404
hGBP3	LPAETLQELLDLHRDREAEIEVFIKSDVDHLEFQKELAAQLEKRRDDFCQKQNEASS	402
hGBP2	LPTETLQELLDLHRDREAEIEVFMKNSFKDQVDMFQKELAAQLEARRDDFCQKQNEASS	402
hGBP5	LPMETLQELLDLHRDREAEIEVFMKNSFKDQVDMFQKELAAQLEARRDDFCQKQNEASS	402
hGBP4	LPTDTLQELLDLHRDREAEIEVFMKNSFKDQVDMFQKELAAQLEARRDDFCQKQNEASS	418
hGBP7	FPTDTLQELLDLHRDREAEIEVFMKNSFKDQVDMFQKELAAQLEARRDDFCQKQNEASS	403
hGBP6	LPTDTLQELLDLHRDREAEIEVFMKNSFKDQVDMFQKELAAQLEARRDDFCQKQNEASS	403
hGBP1	DRCSGLLQVIFSPLEEEVKAGIYKPGGYRFLVQKLDLKKKYEEPRKGIQAEELIQTY	464
hGBP3	DRCSALLQVIFSPLEEEVKAGIYKPGGYRFLVQKLDLKKKYEEPRKGIQAEELIQTY	462
hGBP2	DCCMALLQVIFSPLEEDVKQGTFSKPGGYRFLVQKLDLKKKYEEPRKGIQAEELIKKY	462
hGBP5	DYCSALLQVIFSPLEEEVKAGIYKPGGHNLFIQKTEELKAKYREPRKGIQAEELQKY	462
hGBP4	KYCAELKRLSEHLTESILRGIKSVPGGHNLYLEEKQVWQVYKLVPRKGVKANEVLQNF	478
hGBP7	KYCAELKRLSEHLTESILRGIKSVPGGHNLYLEAKKIEQDYTLVPRKGVKANEVLQNF	463
hGBP6	QYCAELKRLSEHLTESILRGIKSVPGGHNLYLEAKKIEQDYTLVPRKGVKANEVLQNF	463
hGBP1	LKSKEVTDAILQTDQTLTEKEKEIEVERVKAESAQASAKMLQEMQRKNEQMMQEKERSY	524
hGBP3	LKSKEVTDAILQTDQTLTEKEKEIEVECVKAESAQASAKMVEEMQIKYQMMEEKEKSY	522
hGBP2	LESKEDVADAILQTDQTLSEKEKEIEVERIKAESAEAAKMLLEIQKNEEMMEQEKESY	522
hGBP5	LKSKEVSHAILQTDQALTEKKEKAEQVKAEEKAEQRLAAIQRQNEQMMQERERLH	522
hGBP4	LQSQVVEESILQSDKALTAGEKAI AAEERAMKAAEKEQLLEKQKEQQQMMEAQERSF	538
hGBP7	LQSQVVEESILQSDKALTAGEKAI AAKQAKKAAEKEQLLEKQKEQQQMMEAQERSF	523
hGBP6	LESQVVEESILQSDKALTDRKAVAVDRAKKAAEKEQLLEKQKEQQQMMEAQDKSR	523
hGBP1	QEHKQLTEKMENDRVQLLKEQERTLALKLQEQEQQLLKEGFQKESRIMKNEIQDLQTKMR	584
hGBP3	QEHVQLTEKMERERAQLLEEQEKTLSKLOEQARVLKERCQGESQTLQNEIQKLOKTKL	582
hGBP2	QEHVQLTEKMERDRAQLMAEQEKTLLKLEQEQEQQLLKEGFENESKRLQKDIWDIQ--MR	580
hGBP5	QEQVR---QMEIAKQNLAEQQKMQEQQMQEQQAQLSTTFQAQNRSLSELQHAQRTVN	578
hGBP4	QENIAQLKKMERERENLREHERLLKHLKLVQEQEMLKEEFQKKEQLNKEINQLKEKIE	598
hGBP7	QENIAQLKKMERERENYMLRELRKMLSHKMKVLEELLTEGFKEIFESLNNEINRLKEQIE	583
hGBP6	KENIAQLKELQMEREHLLEQIMMHEHTQVQNDWHEGFKKYEEMNAEISQFKRMD	583
hGBP1	RRKACTIS-----	592
hGBP3	KKTKRYMSHKLKI-----	595
hGBP2	SKSLEPICNIL-----	591
hGBP5	NDDPCVLL-----	586
hGBP4	STKNEQLRLL--KILDMASNIMIVTLPGASKLLGVGTYKLGSR-----	640
hGBP7	AAENEPSVFSQILDVAGSIFIAALPGAAKLVLDLGMKILSSLCNRLRNPQKGIIS	638
hGBP6	TTKNDTTPWIARTLDNLABELTALISAPAKLIGHGVKGVSSLFFKHKLPF-----	633

Figure 3-21: Conserved phenylalanine residues within the human guanylate binding proteins 1-7. Sequence alignment of hGBP-1 to hGBP-7 was performed with Clustal W. All phenylalanine residues are depicted in bold type. Critical residues that were mutated in hGBP-1 are highlighted with black background.

Results

Mentioned phenylalanine residues are highly conserved in all hGBP isoforms except for F171 which in hGBP-5 is a serine instead. However, to address their function and to investigate whether they are crucially involved in the basic features of hGBP-1, these phenylalanines were substituted by alanines yielding single mutants F171A, F175A, and F229A. Additionally, a triple mutant was generated in which all $\alpha 3'$ phenylalanines were replaced, namely hGBP-1 F171A/F174A/F175A, abbreviated as 3-Phe in the following.

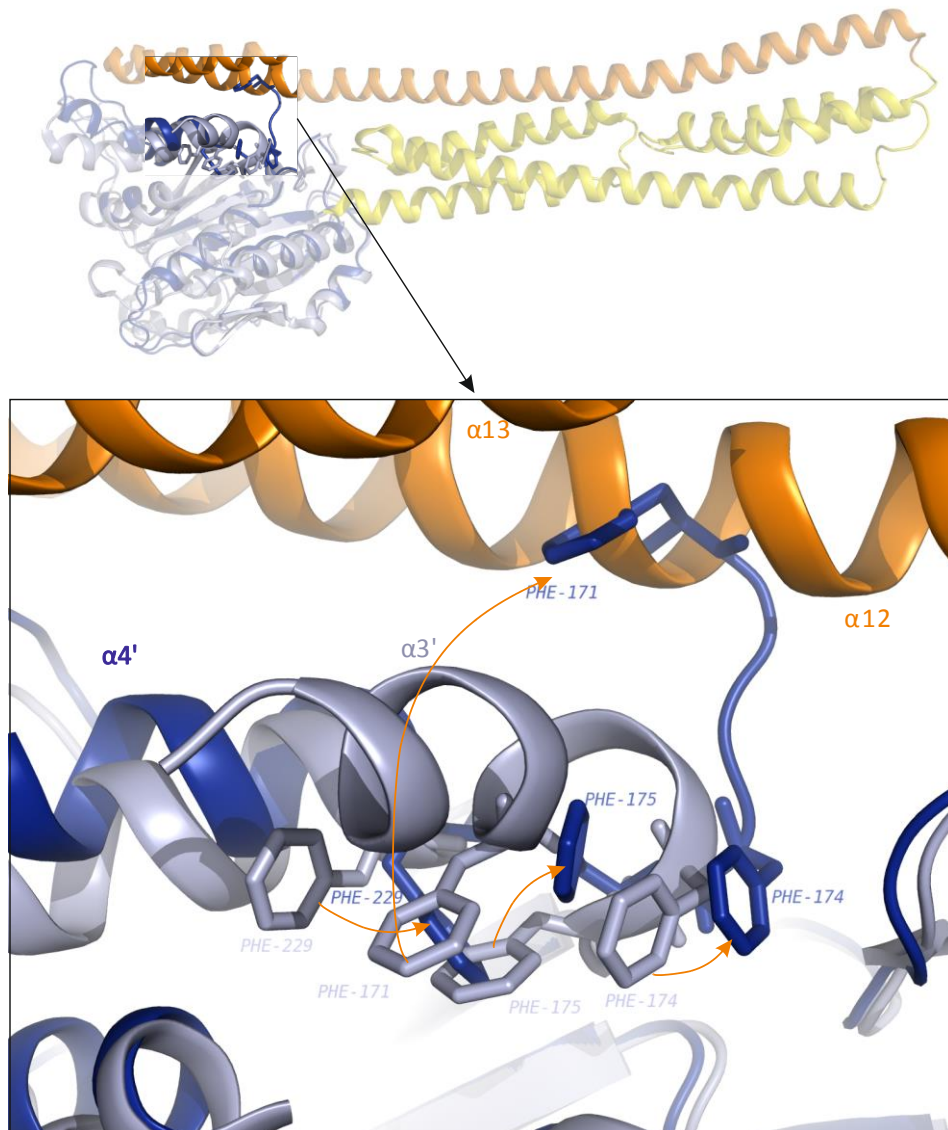


Figure 3-22: View on selected phenylalanine residues within different hGBP-1 structures. Full-length hGBP-1 structure in complex with GppNHp (pdb: 1FN5) consisting of LG domain (light blue), middle domain (yellow) and C-terminal $\alpha 12-13$ domain (orange) was superimposed with the GDP·AlF_x bound isolated LG domain (dark blue, pdb: 2B92). A zoom into the region where F171, F174, F175 and F229 are located illustrates nucleotide dependent spatial rearrangements of all phenylalanine residues. Arrows indicate changes from GppNHp structure to GDP·AlF_x structure which are proposed to represent the GTP binding and hydrolysis state, respectively.

3.2.3.2. Purification of phenylalanine mutants

Expression and purification of all phenylalanine mutants was carried out according to established protocols of wt hGBP-1. The procedure yielded high levels of overexpression, good solubility, and highly pure hexa-histidine tagged proteins after affinity chromatography. To selectively collect only monomeric fraction, lastly, proteins were applied to preparative size exclusion column (S200 26/60, GE). Elution chromatograms revealed that single point mutants like wt hGBP-1 predominantly existed as monomers. In contrast, elution profile of triple mutant 3-Phe differed from that of wt, suggesting that combined mutation had some considerable effects on the protein structure. Besides monomeric peak, two more peaks occurred at smaller elution volumes representing dimers or higher order oligomer which in sum dominated over monomer species (figure 3-23 A). Selected fractions b1 – b4 from SEC as well as sample before SEC were analyzed by SDS-PAGE (figure 3-23 C). The sample prior to SEC (lane a) contained already three bands, one at monomer level (68 kDa), another one slightly higher than 116 kDa, and a last one not even migrated into separating gel and thus representing a protein complex with much higher molecular weights. Notably, protein complexes were most likely covalently coupled since denaturing SDS-PAGE failed to break them up. However, due to significantly different sizes higher complexes could be excluded successfully at smaller elution volumes (lane b1 and b2). Consisting of highly pure target protein (lane b3 and b4) monomer fraction was collected and concentrated up to at least 500 μ M. SDS-PAGE analysis of concentrated final protein (lane c) revealed that formerly excluded bands at 116 kDa and higher appeared again so that the pattern was similar to that of protein solution prior to SEC (lane a) This observation suggested that covalent dimers (> 116 kDa) and higher order oligomers developed from the monomeric protein in a time dependent manner.

Content of purified 3-Phe was once again checked by analytical SEC. A portion was thawed and diluted to 20 μ M. Separation via analytical gel filtration column S200 3.2/30 revealed that still some higher ordered complexes were present but proportion of monomer species improved from 35 % (preparative SEC) to almost 70 % in the end (figure 3-23 B).

Results

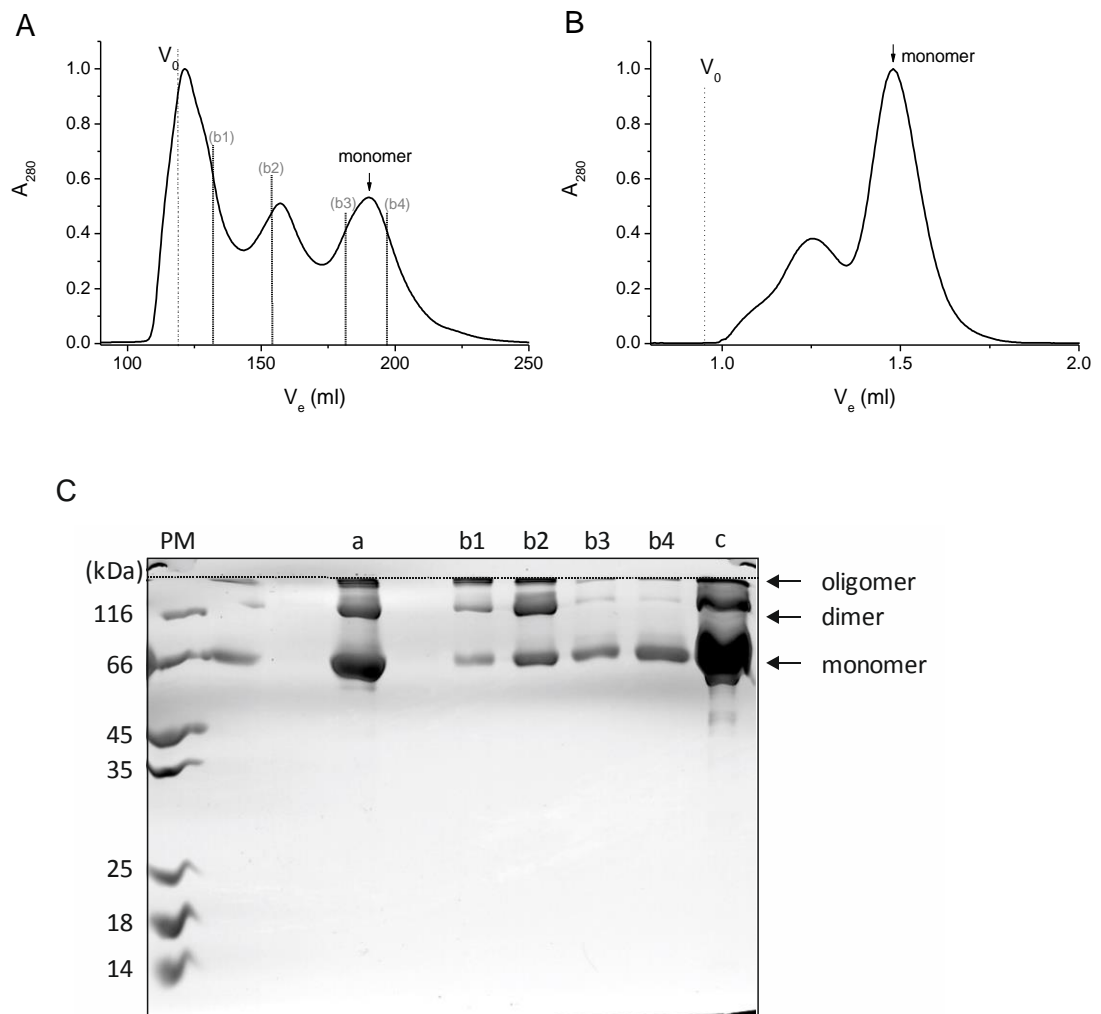


Figure 3-23: Purification of recombinant 3-Phe via preparative SEC. (A) Second step of protein purification using size exclusion column S200 26/60 (GE) revealed target monomeric fraction and also higher ordered complexes at smaller elution volumes. At designated positions samples b1-b4 were taken for SDS-PAGE analysis. (B) Analytical SEC of final protein revealed 70% monomeric 3-Phe species. (C) SDS-PAGE analysis unraveled protein contents at different steps of protein purification: (a) 3-Phe solution after affinity chromatography before loading to size exclusion column, (b1)-(b4) indicated samples from SEC, (c) concentrated final protein.

3.2.3.3. *GTPase activity of single and triple phenylalanine mutants*

Initially, GTPase activity of all phenylalanine mutants was investigated by standard HPLC assay using 1 μM protein and 500 μM GTP. Obtained specific activities for GTP turnover (s_{GTP}) were similar to that of wt hGBP-1. Values ranged between 12.0 min^{-1} (F171A) and 19.1 min^{-1} (F229A) suggesting that substitution by alanine residues did not impair GTPase activity. However, due to mutations a remarkable difference to wt hGBP-1 occurred with respect to product formation. While wt upon GTP hydrolysis showed faster formation of GDP rather than GMP, all mutants acted the other way around. Specific activity of GMP formation was always higher than that of GDP formation (figure 3-24). Thus, ratio $s_{\text{GMP}}/s_{\text{GTP}}$ giving a measure for GMP share on total product was 70-75 % for all mutants, whereas only 38 % for wt hGBP-1. As additional note, s_{GMP} and s_{GDP} in sum equaled s_{GTP} so that GMP production upon pyrophosphate cleavage could be excluded for any mutant. Since elevated GMP formation was also observed for truncation mutant hGBP-1 $\Delta\alpha 13$, inspected phenylalanine residues might at least contribute to coordination of helix $\alpha 13$.

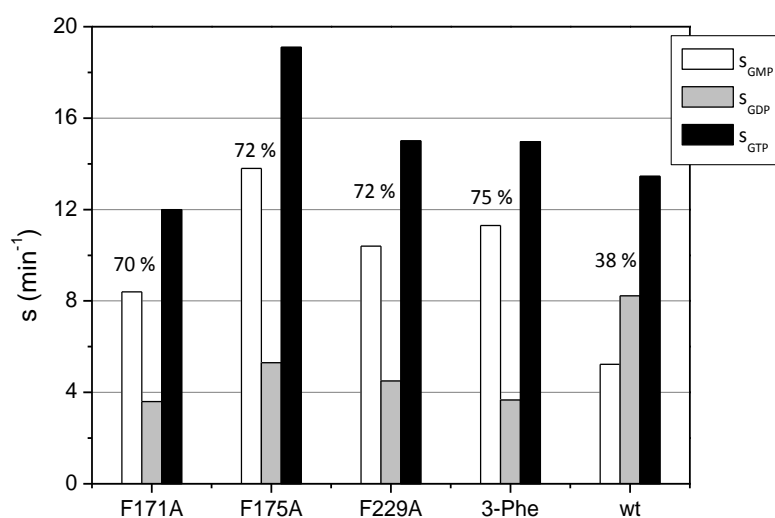


Figure 3-24: Enzymatic activities of phenylalanine mutants compared to wt hGBP-1. Specific activities of GTP turnover s_{GTP} (black) and product formation s_{GDP} (gray), s_{GMP} (white) were derived from hydrolysis assay with 1 μM protein (either single mutants F171A, F175A and F229A, triple mutant 3-Phe, or wt hGBP-1) and 500 μM GTP. Indicated proportion of GMP on total product (%) was calculated by the ratio $s_{\text{GMP}}/s_{\text{GTP}}$.

3.2.3.4. Long term hydrolysis of GTP or GDP catalyzed by single phenylalanine mutants

The common feature of all phenylalanine mutants to produce elevated GMP amounts was further explored with long term hydrolysis studies. In addition to GTP also substrate GDP was offered, each 500 μM . Figure 3-25 illustrates nucleotide composition of single phenylalanine mutants after 24 hours of incubation, except for F175A which was incubated for even 48 hours. Reflecting values from previous experiment, upon GTP hydrolysis GMP levels of around 70% were obtained for all mutants (figure 3-25, upper panels).

Within the assayed protein concentration range up to 100 μM , a second step in GMP and GDP progression could be observed in addition (visible by a kink in the upper panels of figure 3-25). Complete depletion of GDP levels accompanied by increasing GMP levels up to 100 % strongly suggested GDP hydrolysis from bulk solution which became relevant when the initial substrate GTP was used up. Indeed, applying GDP instead of GTP as substrate (figure 3-25, lower panels) clearly confirmed GDP hydrolysis at corresponding protein concentrations. Thus, the phenylalanine mutants were not only capable of producing enhanced GMP levels in the course of GTP hydrolysis but also capable of catalyzing efficient hydrolysis of external GDP which is a remarkable difference to the wt protein. While all mutants consumed half amount of GTP at similar protein ranges between 0.03 and 0.06 μM , however, more diverse protein concentration at which half amount of substrate GDP was consumed suggested differences in GDP dependent dimer affinities (provided that GDP hydrolysis like GTP hydrolysis is dimer dependent). In view of that, mutant F171A catalyzed GDP hydrolysis most efficiently since GDP turnover set in at only six times higher protein concentration than obtained for GTP turnover. For F175A according protein concentrations distinguished by a factor of 22 and for F229A even by a factor of 260.

These findings suggest that individual phenylalanine residues had particular contribution to the enzyme machinery of hGBP-1. While mutation F229A, the only representative of helix $\alpha 4'$, did not significantly alter GDPase activity of wt protein, indeed, mutations of $\alpha 3'$ phenylalanines 171 and 175 did. Assuming a GDP dependent dimerization of the protein required for stimulated turnover, alanine substitution of either F171 or F175 probably enabled hGBP-1 to dimerize with higher affinity.

Results

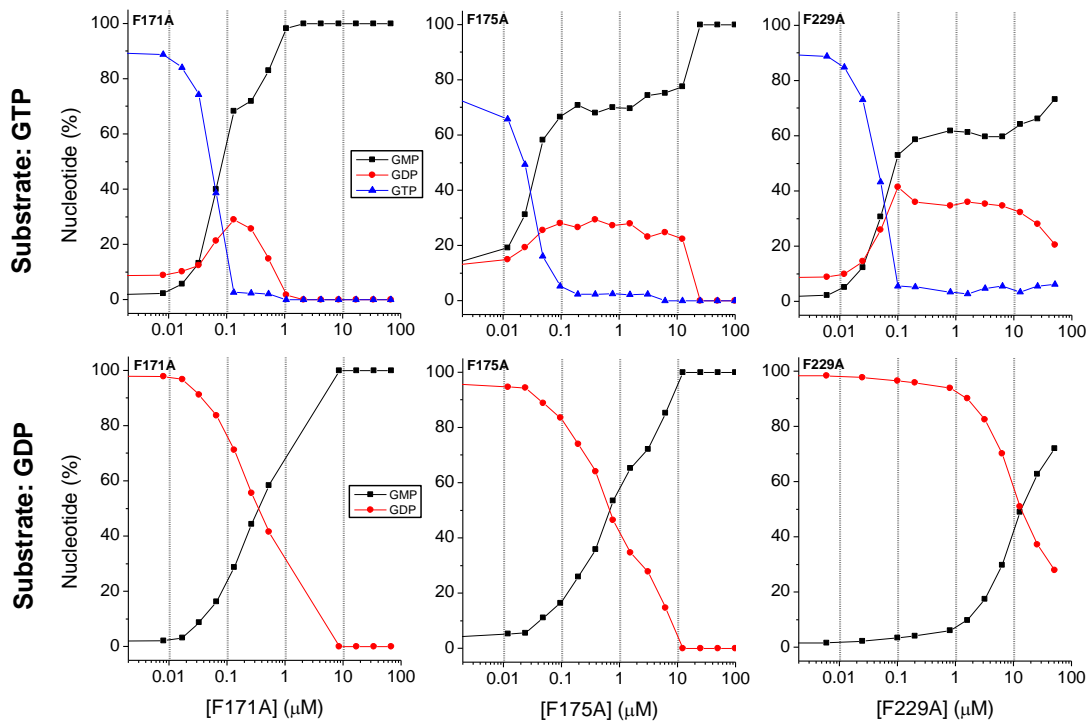


Figure 3-25: Long term GTP and GDP hydrolysis catalyzed by single phenylalanine mutants of hGBP-1. At 25°C and for 24 hours (48 hours for F175A), varying concentrations of F171A, F175A and F229A (panels from left to right) were incubated with either 500 μM GTP (upper panels) or 500 μM GDP (lower panels). Relative nucleotide amounts (GTP: blue, GDP: red), GMP: black) were derived from rp-HPLC analysis. Decrease and increase of substrates and products, respectively, occurred in concentration dependent manner.

3.2.3.5. GDP hydrolysis catalyzed by 3-Phe is subject to cooperative mechanism

Previous experiment demonstrated that single phenylalanine mutations within helix $\alpha 3'$ led to improved GDPase activity. Here, we quantified GDPase activity by performing time dependent measurements using 10 μM protein and 500 μM GDP. Besides single mutations, also triple mutation 3-Phe as well as GDPase active 1-LG was investigated. Protein and nucleotide were mixed and incubated at 25°C. At different time points, GDP turnover was analyzed by reversed-phase HPLC. Initial rates of GDP turnover derived from the slope of linear fit to the data (figure 3-26 A) were divided by protein concentration to obtain specific GDPase activity (s_{GDP} , figure 3-26 B).

Results

Obtained activity of 1-LG (1.6 min^{-1}) was significantly lower compared to published data showing that 1-LG exhibits almost ten-fold higher activity. The difference becomes even more striking when considering that the protein concentration was 2-5 times lower than we used (Vöpel, et al., 2010). As a major difference, the published data based on low salt conditions while here, measurements were consistently performed in presence of 150 mM NaCl. Additionally, activity deficiency can be excluded since the same batch of 1-LG was used to determine GTP turnover which revealed comparable values to the published data (see paragraph 3.3.2.2.). Thus, particularly GDP dependent dimerization of 1-LG might be affected by the salt content which consequently results in reduced, non-stimulated GDPase activity. However, determined activity of 1.6 min^{-1} was used for further comparisons with newly identified GDPase active phenylalanine mutants.

Upon long term hydrolysis studies, mutant F171A illustrated a similar nucleotide pattern as previously observed for 1-LG (see paragraph 3.1.2.1.). In line with that, also determined GDPase activity of 2.0 min^{-1} was similar, even slightly higher than for 1-LG. Although being only 50 % of F171A activity, also F175A performed efficient GDP turnover with 1.0 min^{-1} . Remarkably, GDPase activity was even synergized to 3.7 min^{-1} when both mutations were combined in 3-Phe. Being at least ten times slower than any assayed protein, single mutant F229A (helix $\alpha 4'$) provided GDPase activity was only 0.10 min^{-1} .

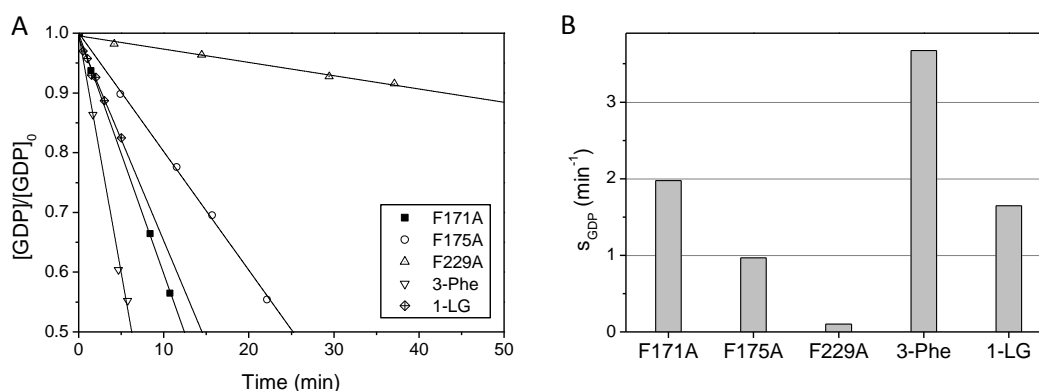


Figure 3-26: Specific GDPase activity provided by hGBP-1 phenylalanine mutants. Hydrolysis rates were measured with $10 \mu\text{M}$ protein and $500 \mu\text{M}$ GDP at 25°C . (A) Time course of GDP hydrolysis catalyzed by indicated mutants was fitted by linear regression (straight lines). (B) Slope of linear fits divided by protein concentration yielded specific GDPase activity of each mutant (s_{GDP}) that for comparison was plotted as column chart.

Results

Due to high activity, GDP hydrolysis catalyzed by mutant 3-Phe was further investigated with respect to concentration dependency. A typical hydrolysis experiment was performed with 500 μM GDP and varying 3-Phe concentrations. Obtained specific activities increased in a concentration dependent manner suggesting a cooperative GDP hydrolysis mechanism (figure 3-27). Moreover, plateau was reached at almost 1 μM indicating highly affine GDP bound 3-Phe dimers. Evaluating the data according to equation 5 yielded maximum specific activities of 4.1 min^{-1} and an apparent dimer dissociation constant of 0.06 μM .

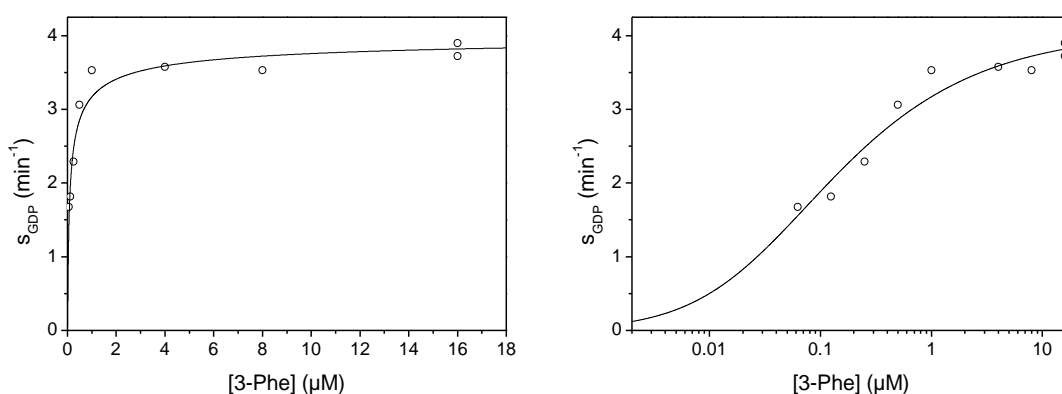


Figure 3-27: Concentration dependent GDP hydrolysis catalyzed by 3-Phe. Concentration dependent increase of specific activities was fitted according to equation 5 (straight lines), revealing maximum activity 4.1 min^{-1} for GDP turnover and an apparent dimer dissociation constant of 0.06 μM . The same dataset was plotted either linearly (left panel) or logarithmically (right panel).

3.2.3.6. GTP analog dependent dimerization of phenylalanine mutants determined by analytical SEC

All phenylalanine mutants were diluted to 20 μM and applied to analytical SEC to investigate their oligomeric states in the absence and presence of nucleotides. Particularly, their capacity to form complexes when bound to the GTP analogs GDP·AlF_x, GppNHp and GTPγS was explored. In the absence of any nucleotide all mutants subsisted as monomers (figure 3-28 A, apo). Similar to wild-type (wt) hGBP-1 (94 kDa) molecular weights obtained varied between 89 and 103 kDa, indicating slightly altering structural arrangements and thus hydrodynamic volumes of the mutants. As referred to previously (paragraph 3.2.3.2.), 3-Phe had a tendency to form covalent dimers which is reflected by a minor peak at elution volume $V_e = 1.28$ ml.

Results

Previous experiments in this work have shown that GTP analogs GppNHp and GTP γ S under given conditions were not capable of inducing wt complexes. A wt complex was found only in presence of GDP·AlF_x. These complexes upon coupled SDS-PAGE and SEC studies, moreover, were classified as putative dimers. As a remarkable difference to hGBP-1 wt, all phenylalanine mutants illustrated a clear shift to smaller V_e (1.26-1.31 ml) independent from the GTP analog offered (figure 3-28 A). These volumes correspond to molecular weights of 218-273 kDa which clearly indicate that particular phenylalanine substitutions enable hGBP-1 to dimerize easier in presence of any GTP analog. Possibly, given mutations altered hGBP-1 structure such that at least affinities of GppNHp and GTP γ S bound dimers improved. Only chromatogram of mutant F229A in presence of GppNHp revealed a dimer and a monomer peak with almost equal intensities, suggesting that K_d value of according dimer is significantly higher than that of other mutants. The column chart in figure 3-28 B gives an overview on molecular weights obtained for each run, clearly demonstrating different capacities of each mutant and wt to form nucleotide dependent complexes. Altering sizes of dimers probably being a result of nucleotide controlled different arrangements will not be considered further for the moment. All corresponding values can be found in table 3-4.

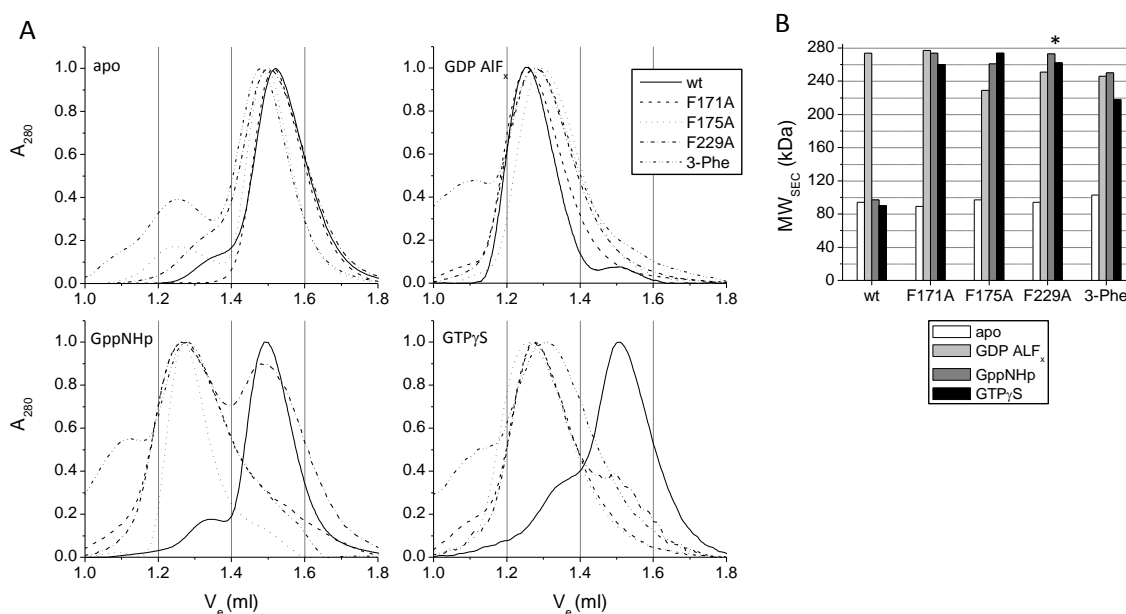


Figure 3-28: Analytical SEC of hGBP-1 phenylalanine mutants. Analytical SEC was performed with 20 μ M protein (denoted in legend) and buffer C containing either no nucleotide (apo) or 250-320 μ M GDP·AlF_x, GppNHp or GTP γ S. (A) Each chromatogram was normalized by its maximum value and plotted according to indicated nucleotides. (B) Molecular weights calculated with aid of calibration curve in paragraph 3.1.3.1. were plotted as columns. Although GppNHp bound mutant F229A had both monomer peak and dimer peak, here only dimer value was plotted (asterisk).

Results

Table 3-4: Results of analytical SEC performed with different hGBP-1 phenylalanine mutants. Elution volumes (V_e) of proteins in the absence or presence of indicated nucleotides were divided by the void volume (V_0) obtained with Blue Dextran. The ratio V_e/V_0 evaluated according to calibration in paragraph 3.1.3.1. yielded listed molecular weight (MW_{SEC}). The last column indicates the nature of the complex formed.

Nucleotide	Protein	V_e (ml)	V_e/V_0	MW_{SEC} (kDa)	Complex
No	<i>Wt</i>	1.50	1.56	94	Monomer
	<i>F171A</i>	1.51	1.57	89	Monomer
	<i>F175A</i>	1.49	1.56	97	Monomer
	<i>F229A</i>	1.50	1.56	94	Monomer
	<i>3-Phe</i>	1.48	1.54	103	Monomer
GDP·AlF_x	<i>Wt</i>	1.26	1.31	274	Dimer
	<i>F171A</i>	1.26	1.31	277	Dimer
	<i>F175A</i>	1.30	1.35	229	Dimer
	<i>F229A</i>	1.28	1.33	251	Dimer
	<i>3-Phe</i>	1.28	1.34	246	Dimer
GppNHp	<i>Wt</i>	1.49	1.55	97	Monomer
	<i>F171A</i>	1.26	1.31	274	Dimer
	<i>F175A</i>	1.27	1.32	261	Dimer
	<i>F229A (47%)</i>	1.51	1.57	90	Monomer
	<i>F229A (53%)</i>	1.26	1.31	273	Dimer
	<i>3-Phe</i>	1.28	1.33	250	Dimer
GTPγS	<i>Wt</i>	1.51	1.57	90	Monomer
	<i>F171A</i>	1.27	1.33	260	Dimer
	<i>F175A</i>	1.26	1.31	274	Dimer
	<i>F229A</i>	1.27	1.32	262	Dimer
	<i>3-Phe</i>	1.31	1.37	218	Dimer

3.2.3.7. Intermolecular FRET-studies on 3-Phe

Analytical SEC demonstrated that wt hGBP-1 dimerized in presence of GDP·AlF_x but not in presence of either GppNHp or GTPγS. This fact was further confirmed by intermolecular FRET studies using fluorescently labelled protein (paragraph 3.1.3.2.2.). More precisely, fluorophore dyes were positioned at the C-termini of hGBP-1 and thus increasing FRET was supposed to occur only when these domains came in closer proximity. In fact, a significant increase was detected in presence of GDP·AlF_x but not in presence of GppNHp or GTPγS. Thus, we

Results

hypothesized that only in the case that C-terminal interactions could be established according dimers were strong enough to be recorded as such also by SEC.

Mutant 3-Phe in contrast to wt hGBP-1 dimerized in presence of all investigated GTP analogs (SEC). To check the hypothesis, 3-Phe was subjected to intermolecular FRET studies, as well. For that, protein was labelled with either donor fluorophore Alexa488 (3-Phe-D) or acceptor fluorophore 647 (3-Phe-A) exactly as described in 3.1.3.2.1. Both 3-Phe-D and 3-Phe-A were diluted 1:1 to a total protein concentration of 2 μ M. Time dependent runs were performed at either 10°C, simulating condition during SEC, or 25°C. Donor was excited at 498 nm and acceptor fluorescence was monitored at 664 nm. When a stable signal was obtained after 2-5 minutes (figure 3-29), GTP analogs GDP·AlF_x (A), GppNHp (B) or GTP γ S (C) were supplemented. Irrespective of the nucleotide, all FRET traces significantly increased by almost 3.2-fold, confirming the hypothesis that C-terminal approach correlates with SEC-visible dimers. Only kinetics varied depending on the particular nucleotide and the temperature, e.g., GppNHp and GTP γ S dependent dimerization was remarkably faster than the GDP·AlF_x dependent one.

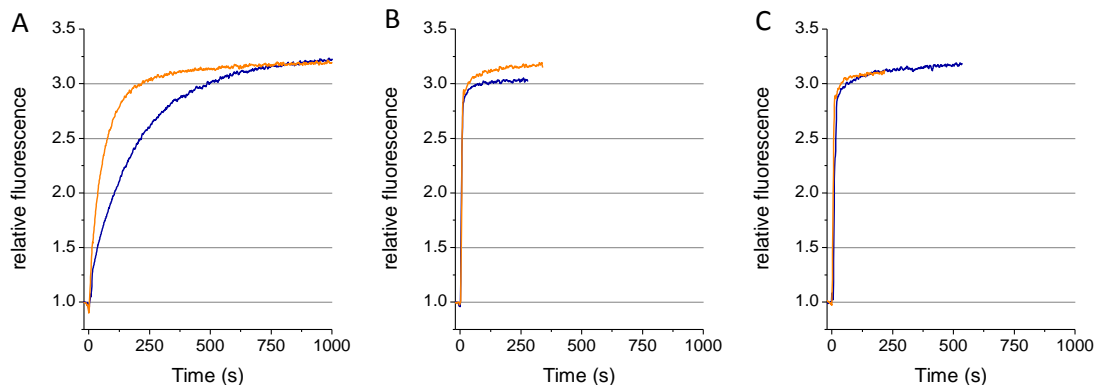


Figure 3-29: Intermolecular FRET measurements of hGBP-1 mutant 3-Phe. 1 μ M 3-Phe-D and 1 μ M 3-Phe-A were diluted in buffer C. Time dependent runs were performed at either 10°C (blue) or 25°C (orange). Donor was excited at 498 nm and acceptor fluorescence was monitored at 664 nm. At $t_0 = 0$ seconds GTP analogs GDP·AlF_x (A), GppNHp (B) or GTP γ S (C) were added to start dimerization. Each time trace was normalized by fluorescence intensity prior to nucleotide addition.

3.2.3.8. Truncation mutant 3-Phe $\Delta\alpha12-13$

Although being a mutant that retains full-length sequence, by exchange of three phenylalanine residues (F171A, F174A, and 175A) 3-Phe adapted particular features of truncated 1-LG. Besides GTPase activity with favoured GMP production, 3-Phe was found to perform also efficient GDPase activity which until now was unique for 1-LG. Likewise, mutant RK due to disrupted salt bridges to the LG domain was supposed to have a higher flexibility of the C-terminal $\alpha12-13$ domain. Also this mutant was shown to exhibit GDPase activity to some extent (see figure 3-14). However, determined activity was far not as enhanced as figured out for 3-Phe, suggesting that latter one may promote even higher flexibility of the C-terminal domain – presumably caused by a weaker attachment of $\alpha12-13$ already in the ground state.

Furthermore, other than wt hGBP-1 but again similar to 1-LG, 3-Phe succeeded to dimerize with all GTP analogues (see paragraph.3.1.3.1. and 3.3.4.2.). FRET studies additionally revealed that helical domains of wt hGBP-1 did not move closer upon GTP γ S or GppNHp binding while the same domains in 3-Phe did. One could assume that on intramolecular basis a release of helices $\alpha12-13$ must precede before further interaction can be provided to accomplish protein dimerization. Considering that, GTP γ S or GppNHp might not succeed to force the release in hGBP-1 due to tight attachment of $\alpha12-13$. Consequently, the same contacts are supposed to be weakened upon mutations in 3-Phe so that dimerization can occur more probably. In order to elucidate whether 3-Phe effects particular arrangement of the C-terminus $\alpha12-13$, a truncation mutant was generated (aa 1-481) that was specifically lacking helices $\alpha12-13$. Resulting mutant 3-Phe $\Delta\alpha12-13$ will be abbreviated as 3-Phe Δ from now on.

First of all, specific GTPase activity of 27.0 min⁻¹ was determined using 6 μ M 3-Phe Δ and 500 μ M GTP. Resulting product was composed of 72% GMP and 28% GDP, being similar to full-length 3-Phe. Long term hydrolysis studies were performed, as well (figure 3-30). Concentration dependent pattern of nucleotide composition was very similar for 3-Phe and 3-Phe Δ . Only GDP hydrolysis occurred at slightly higher 3-Phe Δ concentrations indicating a weaker GDP dependent dimer formation of truncation. Thus, presence of $\alpha12-13$ might facilitate GDP driven dimerization.

Further, nucleotide dependent dimerization of the protein was tested via analytical SEC. Being monomer in the nucleotide-free state (86 kDa), like its full-length counterpart also 3-Phe Δ dimerized with all GTP analogs. Obtained molecular weights were 140, 148 and 134 kDa upon binding to GDP \cdot AlF_x, GppNHp and GTP γ S, respectively.

Results

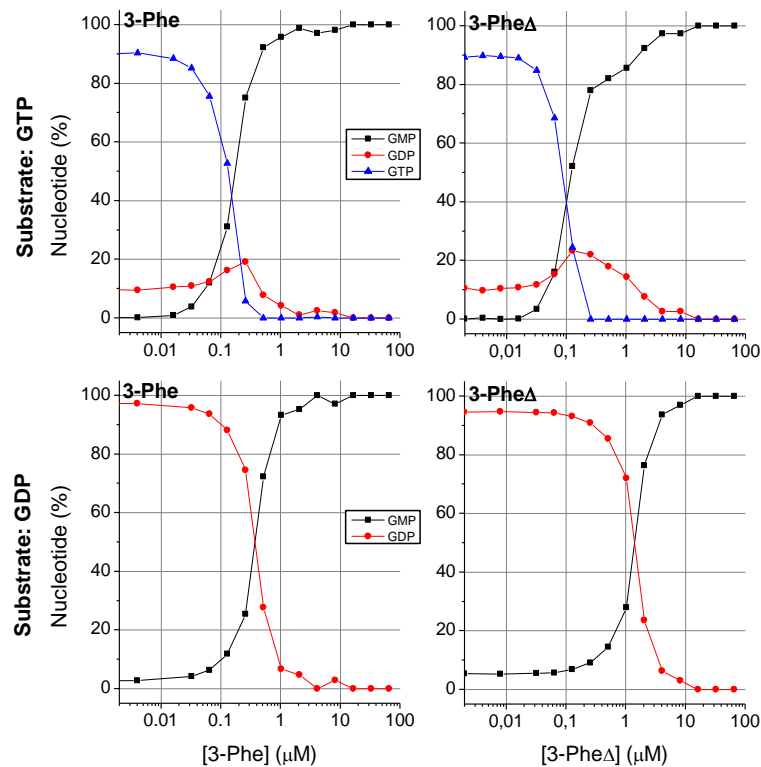


Figure 3-30: Long term GTP and GDP hydrolysis catalyzed by 3-Phe and 3-Phe Δ . At 25°C and for 24 hours varying concentrations of 3-Phe or 3-Phe Δ (panels from left to right) were incubated with either 500 μ M GTP (upper panels) or 500 μ M GDP (lower panels). Relative nucleotide amounts (GTP: blue, GDP: red, GMP: black) were derived from rp-HPLC analysis. Decrease and increase of substrates and products, respectively, occurred in a concentration dependent manner.

Finally, dynamics of 3-Phe provided mant-GDP binding was investigated by typical stopped-flow experiments. In addition to 3-Phe and 3-Phe Δ also another GDPase active hGBP-1 mutant, namely 1-LG was tested. Considering the GDPase activity of these proteins, this time protein concentration was kept fix (0.25 μ M or 0.5 μ M) and nucleotide concentrations being in at least ten time molar excess over protein were varied. Using 290 nm excitation wavelength and a 420 nm cutoff filter for emission, FRET between tryptophan residues and mant-group of nucleotide was detected. Usual processing of data yielded kinetic parameters k_{on} and k_{off} that served to determine the dissociation constant K_d of the complex mGDP·protein.

Results

Observed rate constants (k_{obs}) derived from a single exponential fit to association kinetics were plotted against protein concentration. For comparison with variants that are not GDPase active, also corresponding values of hGBP-1 and hGBP-1 $\Delta\alpha13$ were plotted (figure 3-31 A). Remarkably, when only viewing the graph it is clear that GDPase active and non-active proteins with respect to nucleotide binding differ significantly from each other. While hGBP-1 and hGBP-1 $\Delta\alpha13$ had almost identical traces, the same was true also for 3-Phe and its truncation 3-Phe Δ . Basically, 1-LG, 3-Phe and 3-Phe Δ did show much slower association and dissociation of mGDP than the GDPase inactive proteins. Obtained association rate constants (slope of linear fit) of $0.29 \mu\text{M}^{-1}\text{s}^{-1}$ (1-LG), $0.24 \mu\text{M}^{-1}\text{s}^{-1}$ (3-Phe), and $0.25 \mu\text{M}^{-1}\text{s}^{-1}$ (3-Phe Δ) were almost identical and thus nearly one order of magnitude smaller than for hGBP-1 ($1.9 \mu\text{M}^{-1}\text{s}^{-1}$) and hGBP-1 $\Delta\alpha13$ ($2.0 \mu\text{M}^{-1}\text{s}^{-1}$). In the same manner, dissociation rate constants were effected, k_{off} values were around 10 s^{-1} for hGBP-1 and hGBP-1 $\Delta\alpha13$ while only around 1 s^{-1} for both 3-Phe and 3-Phe Δ . Thus, rate constants compensated each other and resulting K_{d} values and thus binding affinities were similar. Only 1-LG having 3-fold higher k_{off} value, as a consequence, yielded an accordingly higher dissociation constant (figure 3-31 B).

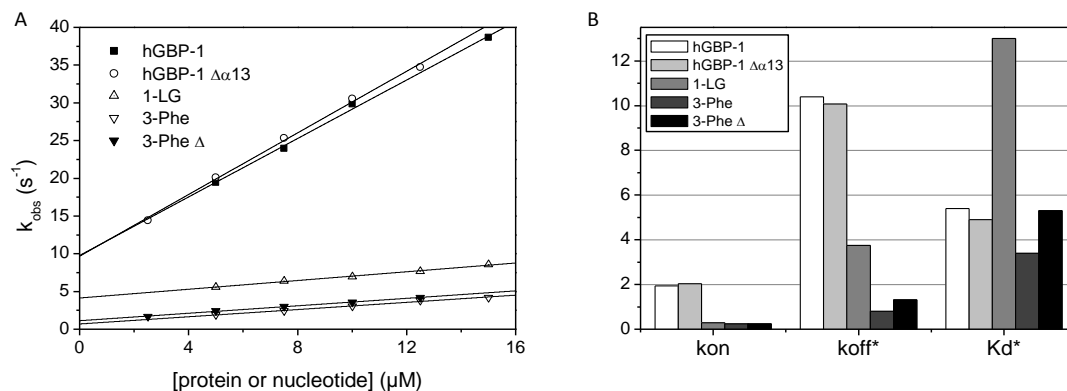


Figure 3-31: Binding of GDPase active hGBP-1 mutants to mGDP measured by stopped-flow. Experiments were performed at 25°C like described in the text. (A) Rate constants (k_{obs}) derived from a single exponential fit to concentration dependent fluorescence traces were plotted as a function of the variable concentration (either protein or nucleotide). Linear fits to the data (straight lines) yielded kinetic parameters k_{on} (slope) and k_{off} (intercept). (B) Both together with calculated K_{d} values (hGBP-1: 5.4 μM , hGBP-1 $\Delta\alpha13$: 4.9 μM , 1-LG: 13.0 μM , 3-Phe: 3.4 μM , 3-Phe Δ : 5.3 μM) were plotted as column chart.

However, these data clearly indicate that 3-Phe being a full-length construct also with respects to nucleotide binding behaves rather like truncated constructs lacking the C-terminal domain α 12-13 or even the entire helical part α 7-13 (1-LG). Thus, we can conclude that mutation of phenylalanines at positions 171, 174, 175 particularly contribute to C-terminal arrangement.

3.2.3.9. Trypsin digestion of 3-Phe

As a final experiment to address putative structural rearrangements caused by phenylalanine mutations, we performed trypsin digestion with either wild-type hGBP-1 or 3-Phe with subsequent SDS-PAGE analysis. Like also presented in paragraph 3.1.3.2.1 trypsin initially targets Lys252 of wild-type hGBP-1 yielding a smaller N-terminal fraction (aa 1-252) and a bigger C-terminal fraction (aa 253-592). Although sequence of hGBP-1 comprises up to 77 trypsin cleavage sites, virtually native folding of the protein shield a majority of sites from proteolytic action. This is at least true for adjusted conditions like buffer, temperature and concentration of each hGBP-1 (1 g/l) and trypsin (0.005 g/l) as well as reaction time of up to ten minutes. Incubation for longer time periods, indeed, resulted in further cleavage products. However, supposed altering structural arrangement of 3-Phe might cause also altering availability of other cleavage sites, consequently yielding different product pattern on SDS-PAGE compared to wt.

Under mentioned conditions hGBP-1 or 3-Phe were mixed with trypsin. Before trypsin addition (a) and after two (b) and six minutes (c) of digestion samples were taken for SDS-PAGE analysis (figure 3-32). Not digested proteins (a) appeared at expected levels of 66 kDa. Also as expected, hGBP-1 yielded two cleavage products at typical heights. These remained constant up to six minutes, indicating no further digest. Cleavage pattern of 3-Phe illustrated two remarkable differences: first, significantly reduced band intensities and, second, a larger number of product bands. Both indicate that much more cleavage sites were available so that trypsin digestion worked out more effective yielding a higher number of smaller fractions, particularly that small that they even ran out of the gel.

With respect to biochemical features, previous experiments unravelled great similarities between isolated 1-LG and full-length 3-Phe. It was discussed whether mutations of F171, F174 and F175 might lead to a weakening of α 12-13 attachment to the core protein. Deletion of the same (3-Phe Δ) did not cause significant differences to 3-Phe which strengthened the assumption even more. Finally, a higher number of available trypsin sites in 3-Phe compared to wt confirmed that 3-Phe indeed constitutes a more open state of hGBP-1.

Results

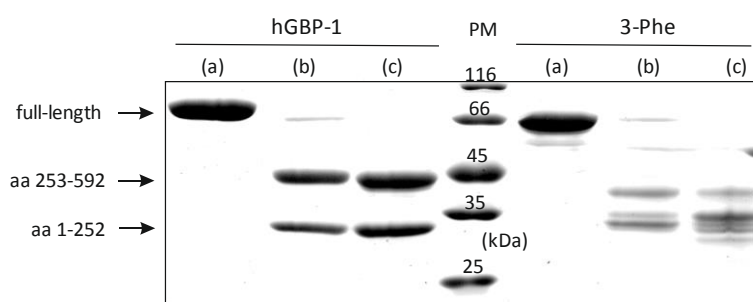


Figure 3-32: SDS-PAGE analysis of trypsin digested hGBP-1 and 3-Phe. At 25°C and in buffer C, 1 g/l protein was digested with 0.005 g/l trypsin. Samples taken before (a) and after 2 minutes (b) and 6 minutes (c) of trypsin digestion were separated through a 12.5 % SDS gel. Coomassie stained gel shows full-length proteins and cleavage products of hGBP-1 at indicated heights. Cleavage products of 3-Phe altered as described in the text. PM: Molecular weight marker with indicated standards covering a range from 18 to 116 kDa.

3.2.4. GMP defective hGBP-1 mutant K76A

In figure 3-14, we introduced a systematic overview on hGBP-1 mutants that with respect to GDPase activity and GMP production differ crucially. We further hypothesized that a higher flexibility of the C-terminus ('open' mutants) might enhance both GDPase activity and GMP formation while an impaired flexibility ('closed' mutants) might cause the opposite. In previous chapters we introduced novel hGBP-1 mutants that due to the biochemical properties most probably represent 'open' conformations. Finally, we wanted to prove the hypothesis using an appropriate mutant that unlike the others provides rather decelerated GDPase activity or reduced GMP production.

In former studies, several charged residues in the switch I and switch II regions of hGBP-1 were identified to be important for the proteins unique GTP hydrolysis mechanism yielding GDP and GMP as products. Substituting those by alanine residues remarkably abolished the proteins ability to form considerable amounts of GMP (Praefcke, et al., 2004). For our studies, we selected mutant K76A, referred to as FL-76 in the following, which in spite of being deficient in GMP formation maintained basic enzymatic properties of wt hGBP-1, such as cooperative GTP turnover with slightly reduced maximum activity.

3.2.4.1. GTP hydrolysis catalyzed by FL-76

First, we investigated FL-76 catalyzed GTP hydrolysis under buffer and temperature conditions that have been consistently applied in this work. Long term GTP hydrolysis was performed with varying FL-76 concentrations and 500 μM GTP at 25°C. The plot of nucleotide composition (figure 3-33 A) analyzed by reversed-phase HPLC illustrated the usual course of GTP turnover in a concentration dependent manner: rather inefficient turnover at protein concentrations below 0.1 μM , at which hGBP-1 is assumed to be mainly monomeric and thus performing only low basal activity, followed by set in of increased turnover at concentrations above 0.1 μM , most probably reflecting dimer formation and thus self-stimulation of GTPase activity. Remarkably, GTP was almost exclusively converted to GDP. Only low amounts of GMP were detected all over the range, revealing 3% to maximum 6% GMP at the highest protein concentration which is consistent with published data (Praefcke, et al., 2004).

Subsequently, catalytic activity was tested using 10 μM protein (wt or FL-76) and 500 μM GTP. Since dissociation constants of 0.28 μM and 0.15 μM , respectively, indicated even higher dimer affinity of FL-76 compared to wt (Praefcke, et al., 2004), at given concentration complete dimerization and thus maximum stimulation of GTPase was assumed to be established. However, we obtained a specific GTPase activity of 4.4 min^{-1} for FL-76 which compared to wt (16.4 min^{-1}) was almost four times reduced (figure 3-33 B). Previous data suggested that FL-76 activity was reduced by only 25 % (Praefcke, et al., 2004), thus, present salt conditions might either affect maximum turnover or dimer affinity of FL-76, probably having equilibrium not yet shifted to dimer entirely. Moreover, determined specific activities for GDP and GMP formation were 4.3 min^{-1} and 0.15 min^{-1} confirming a GDP favored product composition with 97% to 3%. Although FL-76 catalyzed GTP turnover rate was approximately four times reduced compared to wt hGBP-1, the main difference could be assigned to the rate of GMP formation which was even 40 times reduced (0.15 min^{-1} versus 6.1 min^{-1}) clearly indicating the impact of mutation K76A on the β -phosphate cleavage step.

Results

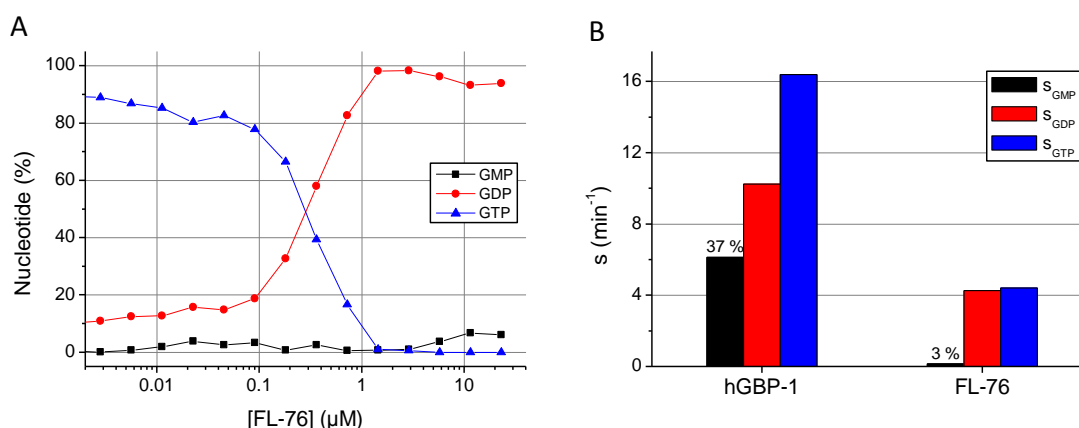


Figure 3-33: GTPase activity of GMP deficient hGBP-1 mutant FL-76. (A) Concentration dependent substrate and product composition was analyzed and plotted after long term GTP hydrolysis (500 μ M) catalyzed by FL-76 at 25°C. A concentration dependent decrease of substrate GTP was accompanied by an increase of product GDP while product GMP constantly remained at levels between 3-6%. (B) With 500 μ M GTP and 10 μ M hGBP-1 wt or mutant FL-76 specific activities for GTP turnover (s_{GTP} : blue) and product formation (s_{GDP} : red, s_{GMP} : black) were obtained. As indicated, share of GMP on total product calculated by the ratio s_{GMP}/s_{GTP} yielded 37% (hGBP-1) and 3% (FL-76).

3.2.4.2. Nucleotide binding properties of FL-76

Mutant FL-76 was reported to bind all mant-nucleotides with affinities similar to wt hGBP-1, except for mGppNHp which was bound at least 5-fold weaker (Praefcke, et al., 2004). For the sake of completeness, we examined nucleotide binding properties of FL-76 in buffer C (containing 150 mM NaCl) and at a temperature of 25°C. Binding of mGMP and mGDP was assessed by kinetic studies yielding respective association and dissociation rate constants (k_{on} and k_{off}^*). Comparable to wt hGBP-1, association and dissociation of FL-76 and mGMP occurred with $k_{on} = 2.3 \mu\text{M}^{-1}\text{s}^{-1}$ and $k_{off}^* = 2.9 \text{s}^{-1}$ which defined the dissociation constant $K_d^* = 1.3 \mu\text{M}$ (table 3-5). Also K_d^* value for mGDP (6.6 μM) was similar to wt (5.4 μM). With respect to almost abolished β -phosphate cleavage capability of FL-76, we were wondering whether accelerated dissociation rate of mGDP might limit the second hydrolysis step. However, with $k_{off}^* = 7.9 \text{s}^{-1}$ dissociation was even slightly slower than for wt (10.4 s^{-1}) and thus not the reason for GMP deficiency. Although hydrolyzing GTP almost exclusively to GDP, remarkably, FL-76 favored to bind mGMP rather than mGDP with almost 5-fold higher affinity. The same is true for wt hGBP-1, suggesting that the point mutation did not disturb

Results

corresponding binding regions but rather a communication step related to further processing of intermediate GDP.

Praefcke and other (Praefcke, et al., 2004) have found that FL-76 has the lowest affinity for the GTP analog mGppNHp ($K_d = 12 \mu\text{M}$). Also here, under physiological salt conditions, the weakest binding was obtained for mGppNHp: upon equilibrium titration of $0.5 \mu\text{M}$ mGppNHp with increasing FL-76 concentrations, a dissociation constant of $20 \mu\text{M}$ was determined. Displacement of mGppNHp from the preformed complex with FL-76 yielded a dissociation rate constant of 5.5 s^{-1} from which association rate of $0.28 \mu\text{M}^{-1}\text{s}^{-1}$ could be estimated. Thus, weaker binding of mGppNHp and FL-76 most probably results from an almost five times faster dissociation rate compared to wt (table 3-5).

Table 3-5: Kinetic and equilibrium constants of FL-76 and *mant*-nucleotides. Kinetic parameters were derived from stopped-flow experiments at 25°C : k_{on} (concentration dependent association experiments) and k_{off}^* (displacement experiments). Dissociation constant K_d^* was calculated by the ratio $k_{\text{off}}^*/k_{\text{on}}$. Only dissociation constant of GppNHp binding was determined by equilibrium titration (bold type) since association at tested protein concentration gave no reasonable change in fluorescence signal (--). For comparison, corresponding values of wt hGBP-1 are set in brackets.

	k_{on} ($\mu\text{M}^{-1}\text{s}^{-1}$)	k_{off}^* (s^{-1})	K_d^* (μM)
mGMP	2.3 (3.5)	2.9 (2.2)	1.3 (0.63)
mGDP	1.2 (1.9)	7.9 (10.4)	6.6 (5.4)
mGppNHp	-- (0.26)	5.5 (0.96)	20 (3.8)

3.2.4.3. *GTPase activity of truncated mutant LG-76*

The unique GTP hydrolysis mechanism of hGBP-1 seems to be impaired in the GMP production step when some mutations are introduced particularly into the conserved switch I and switch II loops. Due to the close proximity to the nucleotide binding pocket, one could assume that mentioned mutations could affect the appropriate coordination of the substrate for the nucleophilic attack. Based on structural analysis of GppNHp bound hGBP-1 the assumption appears likely, as certain switch I residues (aa positions 74-76) particularly provide contacts to the γ -phosphate of the substrate. In line with that, mutation of the residues resulted in weaker binding of GppNHp. Nevertheless, biochemical data revealed that the

Results

mutants are considerably capable of GTP hydrolysis achieved by cleavage of the γ -phosphate while only β -phosphate cleavage is affected significantly. Thus, restricted GMP production caused by mentioned mutations might result from altered translations of conformational changes upon the first cleavage step that in turn disturbs or interrupts initiation of the second phosphate cleavage step.

Being artificially restricted in C-terminal α 12-13 movement and also deficient in GMP production, the cross-linked hGBP-1 mutant (CL-hGBP-1, see figure 3-14) inspired us to investigate the GMP deficient mutant FL-76 with respect to helical movements. For a rough estimation whether mutation K76A hinders specifically the C-terminal flexibility, we introduced the same mutation K76A into the truncated hGBP-1 variant 1-LG which consists of the isolated LG domain and thus lacks the whole helical domain. By long term GTP hydrolysis assay, the resulting construct (termed LG-76) was investigated for its putatively altering enzymatic features. As usual, different LG-76 concentrations were mixed with 500 μ M GTP and incubated for 24 hours at 25°C. Resulting nucleotide composition, particularly, product ratio was significantly different to the full-length mutant FL-76 (figure 3-34 A). Upon GTP turnover, indicated by decreasing GTP amounts, not only GDP but also GMP emerged with significant share on total product. While FL-76 yielded a GMP:GDP ratio of 3:97, for LG-76 it was approximately 40:60. This finding impressively demonstrates that restricted GMP production as a result of mutation K76A is highly related to the C-terminus of hGBP-1 since truncation of the same mainly recovered wild-type properties.

The same plot, moreover, illustrated a further reaction step occurring at protein concentrations above 0.3 μ M when GTP was consumed entirely: here, GDP amounts decreased while accordingly GMP amounts increased up to 100%, indicating an additional feature of LG-76 to utilize also GDP as substrate when no more GTP was available. Applying 500 μ M GDP instead of GTP as substrate (figure 3-34 B) confirmed LG-76 catalyzed GDP hydrolysis setting in at protein concentrations above 0.3 μ M. Half of GDP amount was consumed at LG-76 concentrations between 2-3 μ M.

Taken together, truncated LG-76 in contrast to its full-length counterpart was able to produce considerable amounts of GMP upon GTP hydrolysis. Since both constructs distinguish only by the absence and presence of the C-terminal domain results indicate that FL-76 might constitute a 'closed' conformation of hGBP-1 that similar to the mutant CL-hGBP-1 is enabled to provide the release of α 12-13. LG-76, having no helical domain at all, is thus not restricted by any movements and can act like wild-type 1-LG.

Results

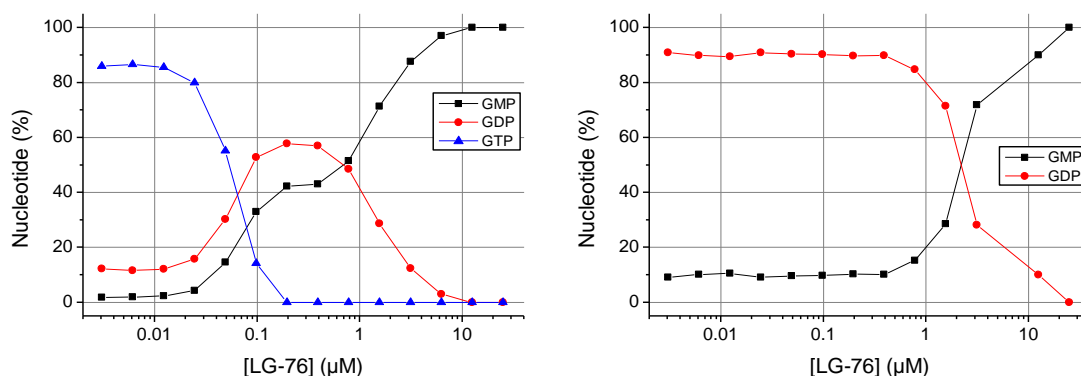


Figure 3-34: Long term GTP and GDP hydrolysis catalyzed by LG-76. 500 μM of substrate (GTP or GDP) was mixed with different LG-76 concentrations. After incubation for 24 hours at 25°C, samples were analyzed via reversed-phase HPLC. Concentration dependent nucleotide compositions are depicted for reaction mixtures with substrate GTP (A) or substrate GDP (B).

3.2.4.4. GTP analog dependent dimerization of FL-76 and LG-76

Human GBP-1 mutant FL-76 was shown to perform GTP hydrolysis in a cooperative manner (Praefcke, et al., 2004) which implies that FL-76 is at least capable to form homo dimers. Here, we investigated homo dimerization of FL-76 via analytical SEC in presence of different GTP analogs.

Like wt, FL-76 remained monomeric when bound to GppNHp ($MW_{SEC} = 94$ kDa) or GTPγS ($MW_{SEC} = 90$ kDa). GDP·AlF_x in contrast to GppNHp and GTPγS was the GTP analog most potent to force dimerization of wt hGBP-1 and any mutant tested. Interestingly, GDP·AlF_x binding yielded only a minor dimeric fraction of FL-76 while the majority of the protein remained monomeric (figure 3-35 A). Thus, we assumed that GDP·AlF_x controlled FL-76 dimers are prominently weaker than wt dimers. Attaching fluorescent dyes to the mutant (donor Alexa488 or acceptor Alexa647; labelling procedure according to paragraph 3.1.3.2.1.) allowed to investigate FL-76 dimerization by intermolecular FRET measurements. Therefore, 1 μM donor labelled FL-76 (76-D) and 1 μM acceptor labelled FL-76 (76-A) were mixed. Upon addition of GDP·AlF_x, a significant increase of fluorescence was monitored indicating dimerization of the protein (figure 3-35 C, orange trace). Not only total change in fluorescence but, more remarkably, kinetics being significantly reduced compared to wt hGBP-1 (gray trace) gave evidence for a weaker dimer affinity of the mutant.

Results

However, not only enzymatic activity but also oligomerization behavior was recovered upon deletion of the C-terminal domain, since LG-76 like its wt counterpart 1-LG dimerized in presence of any tested GTP analog (figure 3-35 B). GppNHp bound 1-LG dimer was plotted, as well, to assign the volume at which LG domain dimers are expected to elute. In presence of GDP·AIF_x, GppNHp and GTPγS obtained molecular weights of LG-76 dimers were 72 kDa, 76 kDa and 73 kDa, respectively. Only in the nucleotide-free state was the protein monomeric, comprising an apparent weight of 40 kDa.

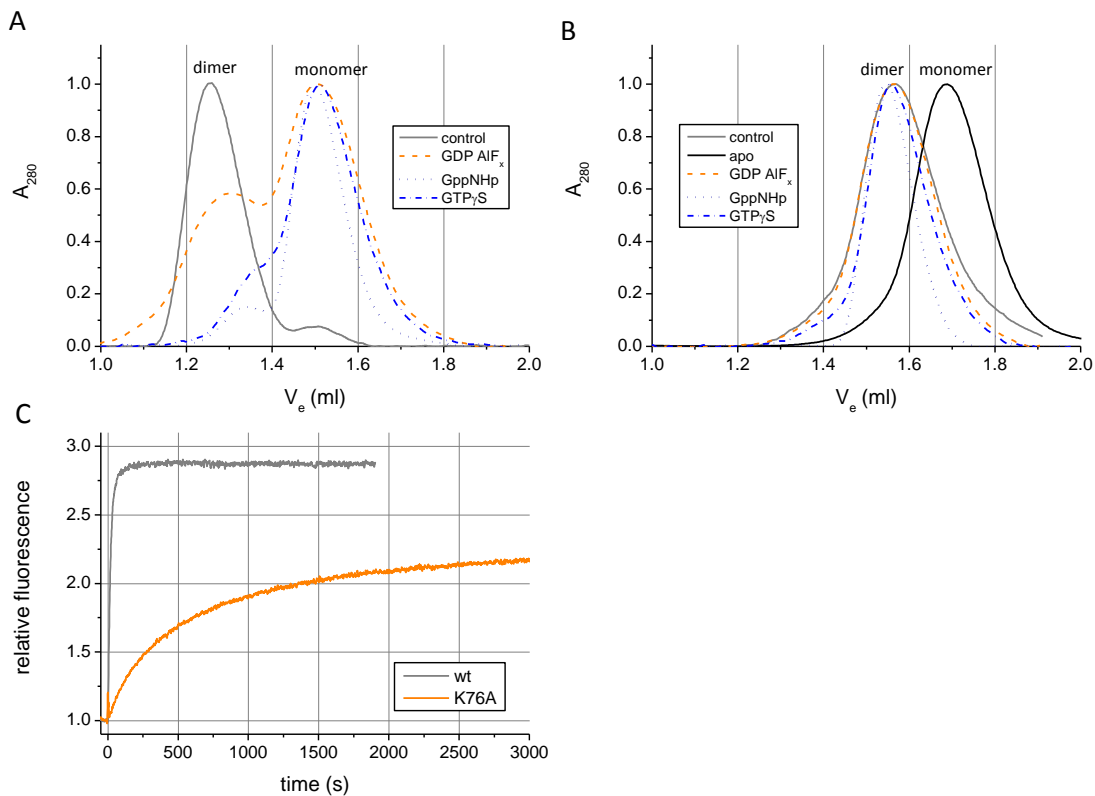


Figure 3-35: GTP analog dependent dimerization of FL-76 und LG-76. By analytical SEC, dimerization of 20 μ M FL-76 (A) or LG-76 (B) was investigated in presence of 250-320 μ M GDP·AIF_x, GppNHp, or GTPγS (color and line style as indicated). Elution chromatograms normalized by maximum values yielded only monomeric FL-76 (A) and just a small dimeric fraction arising in presence of GDP·AIF_x. Dimer of GDP·AIF_x bound wt was plotted for comparison (control). (B) In the absence of nucleotide, LG-76 eluted as monomer while in presence of any tested nucleotide protein eluted as dimer. GppNHp bound 1-LG dimer was plotted for comparison (control). (C) Intermolecular FRET measurements with 1 μ M donor and 1 μ M acceptor labelled protein (hGBP-1: gray; FL-76: orange) were performed at 25°C. GDP·AIF_x induced dimerization was triggered at $t_0 = 0$ s by addition of 250 μ M GDP. Traces were normalized by initial values.

Again, different properties of either truncated or full-length mutant suggested that full potential of mutation K76A unfolds only in cooperation with the helical domain. More precisely, assuming that dimerization of hGBP-1 requires a preceding release of α 12-13, results suggest that particularly this step becomes hampered upon K76A mutation.

3.2.4.5. *Cys-9 based FL-76*

To figure out the effect that mutation K76A putatively has on intramolecular conformational changes, particularly on the release of α 12-13, we decided to perform intramolecular FRET measurements. As already described in paragraph 3.1.3.2.1, we have established a labelling method to create a wt-based intramolecular FRET construct of hGBP-1. With that, however, only distances changes between the subdomains LG and α 13 were possible to monitor. Since we were also interested in exploring for example contributions of α 12 and the middle domain, we switched to Cys9 based hGBP-1 mutants that were particularly generated for intramolecular FRET studies (Hengstenberg, 2013). Basically, these mutant have all natural cysteines replaced by either alanine or serine residues. Instead, they harbor exactly two cysteines that depending on the investigated subdomains of hGBP-1 were introduced into appropriate positions for site-selective labelling with Alexa fluorophores. In former studies several combinations were generated, here, we selected two of them being suitable to report spatial changes between the LG domain and α 13 (figure 3-36 A) and also between the middle domain and α 12 (figure 3-36 B). Respective plasmid-DNA, kindly offered from Dr. Carola Hengstenberg, served as template to introduce K76A by site-directed mutagenesis. In accordance with figure 3-36 A and B, resulting Cys9-76 constructs were termed A76 and B76, respectively.

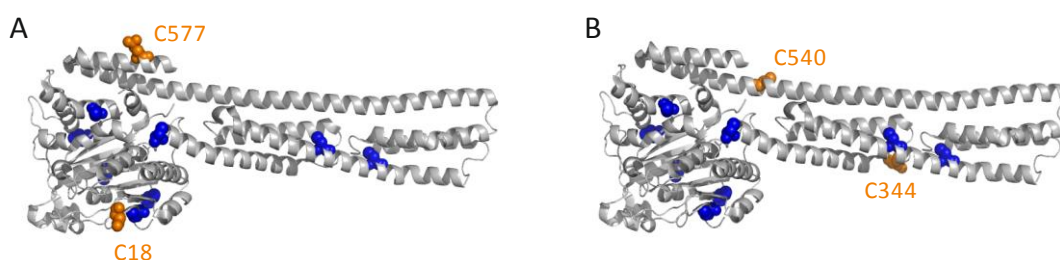


Figure 3-36: Schematic view on Cys-9 based hGBP-1 mutants for intramolecular FRET studies. The depicted constructs (pdb: 1f5n) with exactly two cysteine residues at indicated positions (orange spheres) are suitable to cover conformational changes between subdomains: (A) LG domain and α 13 ($C_{\alpha}(18)$ - $C_{\alpha}(577)$): 45 Å), (B) middle domain and α 12 ($C_{\alpha}(344)$ - $C_{\alpha}(540)$): 43 Å). Blue spheres indicate replaced natural cysteines.

3.2.4.5.1. Sequential labelling of hGBP-1 Cys9-76 constructs with Alexa fluorophores

Sequential labelling of either A76 (Cys9/C18/C577/K76A) or B76 (Cys9/C344/C540/K76A) was performed as described in materials and methods (paragraph 2.3.11.3.). After the first labelling step with acceptor dye Alexa647, single labelled proteins were isolated from non-labelled or double labelled proteins via anion exchange chromatography. Only to that fraction donor fluorophore Alexa488 was added to attach to remaining cysteine residue. Proteins were concentrated and quantified photometrically. Obtained values are listed in table 3-6. Figure 3-37 illustrates successful labeling of B76, since non-labelled, acceptor labelled, and both donor and acceptor labelled protein eluted with gradually higher NaCl concentration.

Table 3-6: Protein concentration and labelling efficiency (LE) of Alexa labelled hGBP-1 Cys9-76 constructs. In sequential manner, A76 and B76 were labelled with acceptor Alexa647 and donor Alexa488. Protein and fluorophore concentrations were obtained according to the Beer-Lambert law using molecular extinction coefficients $\epsilon_{280} = 45,400 \text{ M}^{-1}\text{cm}^{-1}$, $\epsilon_{491} = 71,000 \text{ M}^{-1}\text{cm}^{-1}$, and $\epsilon_{651} = 268,000 \text{ M}^{-1}\text{cm}^{-1}$ for protein, donor and acceptor, respectively (Hengstenberg, 2013).

<i>Protein</i>	<i>Protein concentration</i> (μM)	<i>LE</i> (<i>donor</i>)	<i>LE</i> (<i>acceptor</i>)	ϵ_{280} ($\text{M}^{-1} \text{cm}^{-1}$)
A76	75	0.76	0.70	45,400
B76	110	1.00	0.82	

Results

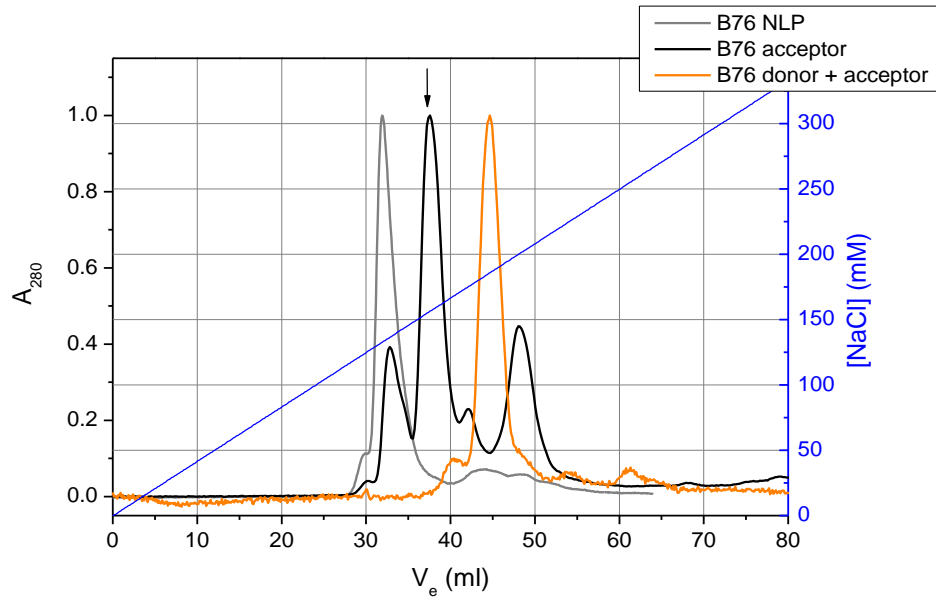


Figure 3-37: Anion exchange chromatography of B76 before and after sequential labelling with Alexa fluorophores. Non-labelled B76 applied to anion exchange column (ResourceQ, GE Healthcare) eluted with low concentrations of NaCl (gray). Labelling with Alexa647 yielded three fractions at different elution volumes, and thus protein species carrying either no, a single dye or two dyes (black). Single labelled protein (arrow) comprising the major fraction was collected for further labelling with Alexa488. Chromatogram revealed almost 100% labelling efficiency since previous peak was clearly shifted to higher elution volume (orange). Gradient of NaCl concentration is depicted in blue.

To investigate whether labelling had any effect on protein activity and also to ensure that GMP deficiency remained despite the large number of mutations, we checked GTPase activity with labelled A76. Using $2.7 \mu\text{M}$ of protein and $500 \mu\text{M}$ GTP, time course of substrate turnover as well as product formation was determined via reversed-phase HPLC (figure 3-38). Interestingly, obtained specific activity of substrate turnover was even 4 times larger than for wild-type based K76A mutant ($s_{\text{GTP}} = 17.6 \text{ min}^{-1}$ versus 4.4 min^{-1}) which suggest an activating effect based on mutated cysteine residues. Since ratio of $s_{\text{GMP}}/s_{\text{GTP}}$ yielded only 4 % GMP on total, however, enhanced GMP formation could be excluded.

Results

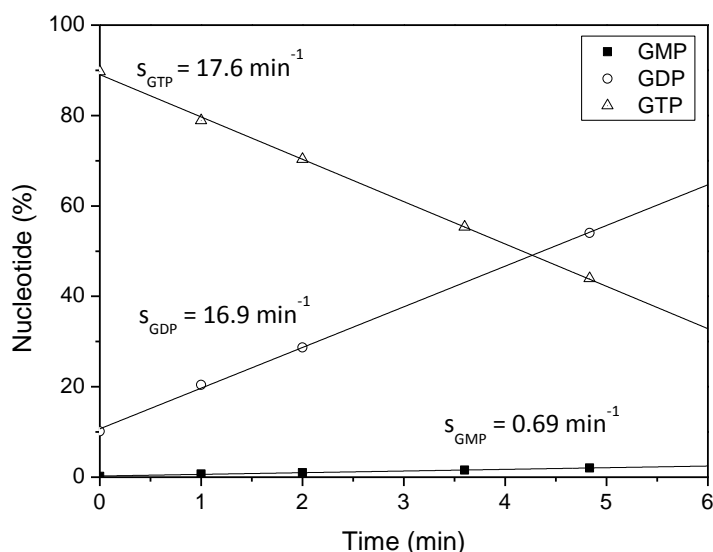


Figure 3-38: Kinetics of GTP turnover and product formation catalyzed by fluorophore labelled protein A76. At 25°C, 2.7 μ M protein was incubated with 500 μ M GTP. At defined time points, reaction was analyzed by reversed-phase HPLC. Initial rate of GTP turnover or product formation was derived from the slope of a linear fit to the data (straight lines) which divided by protein concentration yielded specific activities as indicated.

3.2.4.6. Nucleotide dependent intramolecular FRET measurements with A76 and B76

For not yet identified reasons, mutation K76A disables hGBP-1 to perform the second GTP hydrolysis step in the usual manner. Hampered cleavage of the β -phosphate, consequently, results in neglectable GMP product amounts (3-6 %). Data of hGBP-1 $\Delta\alpha$ 13 suggest a correlation between helix α 13 and the β -phosphate cleavage step. Containing α 13, hGBP-1 wt produces approximately 40 % GMP, whereas truncation of α 13 leads to GMP being the major product (75 %). On the other hand, covalent cross-linking of α 13 to the LG domain (CL-mutant), like mutation K76A, hinders the protein to produce regular amounts of GMP (3%). That is why the GMP deficiency of mutants like hGBP-1 K76A might be a consequence of an altered arrangement of helix α 13 relatively to the core protein.

By generating labelled construct A76, we intended to assess intramolecular distance changes between the structural elements LG domain and α 13. In the same manner, B76 was generated to report distance changes between the middle domain and helix α 12. All intramolecular FRET measurements were carried out at 25°C using buffer C. To ensure

Results

complete dimerization and to eliminate any intermolecular FRET effects, 0.25 μM labelled protein (LP) and 15 μM non-labelled protein (NLP) were mixed prior to nucleotide addition. Of note, used NLP was exactly the same protein constructs as LPs except for the fluorophores. Intramolecular movements were triggered with GTP analogues GTP γ S (250 μM), GppNHp (600 μM) and GDP·AlF $_x$ (250 μM). Donor fluorophore was excited at 498 nm and acceptor fluorescence was detected at 664 nm.

Addition of GTP γ S and GDP·AlF $_x$ resulted in significant decrease of both A76 and B76 fluorescence (figure 3-39 A, B). Indicating an according increase in relative distances between donor and acceptor, binding of nucleotides most probably induced opening or release of helices α 12-13. A similar picture was obtained also by reference measurements with the same protein constructs but without additional mutation K76A (Hengstenberg, 2013). The most striking difference was obtained for the GTP analogue GppNHp. Although kinetics of opening induced by GppNHp has already been shown to be very slow also for the reference measurement, total change in fluorescence was still more than 50%. Here, the fluorescence signal of A76 decreased by approximately 10% (panel A) while even less for B76 (panel B). A weaker binding of GppNHp and K76A ($K_d = 20 \mu\text{M}$) could be excluded as critical factor, since at given concentrations (15.25 μM and 600 μM of protein and GppNHp, respectively) more than 90 % of the protein should be in complex with nucleotide.

Due to significant signal changes upon GTP γ S and GDP·AlF $_x$ binding, for the time being, a supposed trapping of α 12-13 by K76A seemed to be falsified. To remind, we performed both experiments with non-labelled proteins that were the same Cys9-based K76A constructs as the labelled proteins. For control, we did an additional experiment with labelled protein A76, GTP γ S but wt based K76A as NLP (FL-76) in the background (figure 3-39 C). Astonishingly, fluorescence decrease was much less than obtained for NLP A76 (blue trace). Also increasing FL-76 concentration up to 150 μM did not yield any pronounced changes. Fluorescence traces with varying FL-76 concentrations were almost identical to the trace of LP only (without NLP, cyan blue) suggesting two possibilities: first, A76 and FL-76, at least in presence of GTP γ S, do not interact with each other or, second, they interact with each other but FL-76 other than A76 is not able to induce structural reorientation of monitored helix α 13. However caused, for sure A76 acted different than FL-76 assuming that numerous mutations of cysteines had already changed wt properties to some degree. That could be exposed also by analytical SEC of B76 in the absence or presence of GTP γ S (figure 3-39 D). Being monomeric in the nucleotide-free state, in presence of GTP γ S equilibrium of B76 was partly shifted to the dimeric state. This

Results

property is in contrast to previous data clearly demonstrating that neither wt hGBP-1 nor FL-76 was able to dimerize in presence of GTP γ S (figure 3-35).

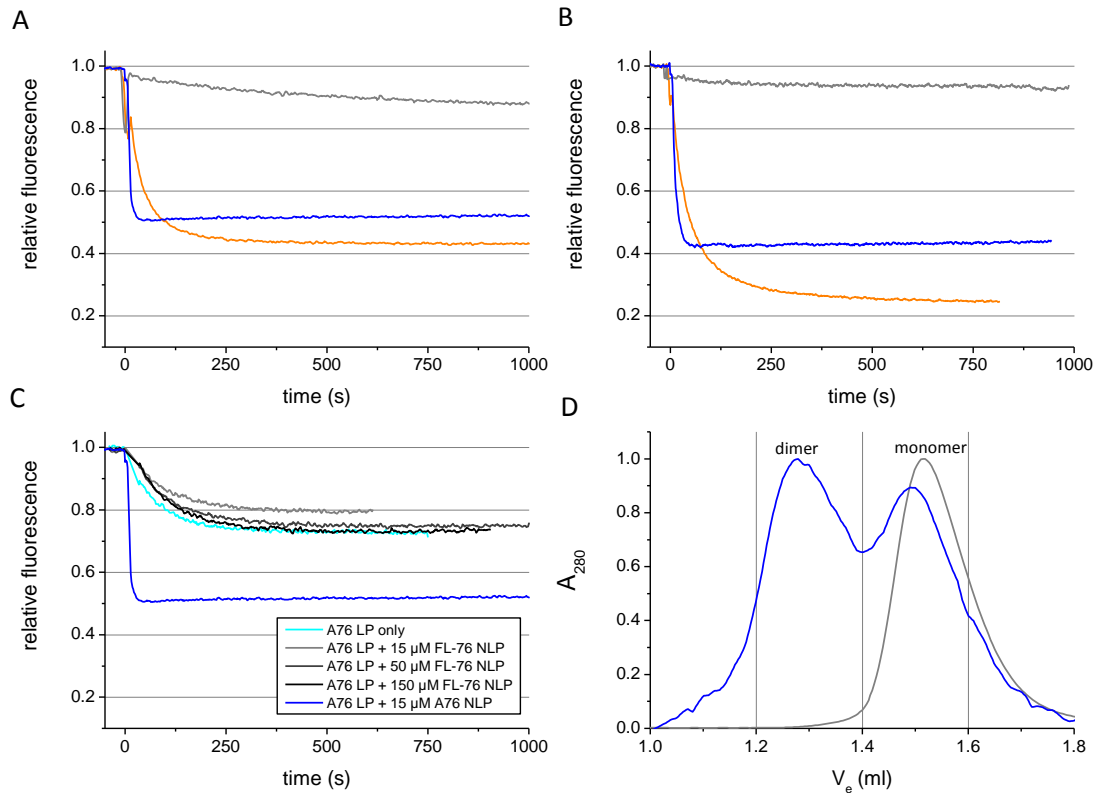


Figure 3-39: Nucleotide dependent intermolecular FRET measurements with hGBP-1 mutants A76 and B76.

At 25°C, (A) 0.25 μ M donor and acceptor labelled protein (LP) A76 and 15 μ M non-labelled protein (NLP) A76 were mixed and monitored for 2-5 minutes until fluorescence signal was stable. Donor was excited at 498nm, acceptor emission was detected at 664nm. Intramolecular movements were monitored in presence 250 μ M GDP·AlF $_x$ (orange), 600 μ M GppNHp (gray) and 250 μ M GTP γ S (blue), triggered at $t_0 = 0$ s by nucleotide addition. (B) The same as (A) using 0.25 μ M LP B76 and 15 μ M NLP B76. (C) GTP γ S driven intramolecular FRET measurements with 0.25 μ M LP A76 and varying NLPs as indicated in legend. Varying concentrations of wt based NLP FL-76 were tested. (D) Analytical SEC of B76 in the absence (gray) and presence of 250 μ M GTP γ S (blue). Monomer and dimer peaks are indicated.

Already GTPase activity assay gave evidence for altered features of the Cys9 bases mutant. Although reduced GMP production as a result of additional K76A was fulfilled, indeed GTP turnover was significantly faster. Cys9 based constructs used to enlighten intramolecular contributions of K76A were dominated by features originated from mutant Cys9 and, thus, not

Results

suitable to clearly assign K76A caused effects on intramolecular movements. However, for other purposes both mutants A76 and B76 will be taken up later (paragraph 3.2.5.).

In view of dominating features of Cys9, we went back to labelling of wt based FL-76 according to established labelling procedure in paragraph 3.1.3.2.1. Sequentially, acceptor fluorophore and after 20 minutes also donor fluorophore were added to FL-76, again, assuming that first CaaX cysteine is occupied by first dye so that the second dye was redirected to cysteines in the LG domain. Labelling was successful yielding wt based FL-76, named 76-intra, with a labelling efficiency of 0.60 for Alexa647 (acceptor) and 1.47 for Alexa 488 (donor), similar to wt intra (table 3-3).

Since 76-intra corresponds to Cys9 based A76 also having labelling positions in helix α 13 and the LG domain, we repeated the same nucleotide dependent FRET experiments for comparison. 0.25 μ M LP 76-intra was thus mixed with 15 μ M NLP FL-76, and GTP analog dependent intramolecular FRET traces were monitored (figure 3-40 A). Corresponding traces of A76 are depicted in figure 3-40 B. Both set of data illustrated several differences between 76-intra and A76 supporting previous findings related to Cys9. Only GDP·AlF_x induced fluorescence traces were comparable with a maximum decrease of signal by approximately 55%. This indicated a release of helix α 13 to same extent but with different rates since kinetics were significantly slower for 76-intra. Most crucially was the difference for GTP γ S controlled traces; A76 fluorescence dropped to almost 50 % of initial value (panel B) while recorded decrease was only 10% for 76-intra (panel A). Also GppNHp traces distinguished such that 10 % decrease but even a slight increase was obtained for A76 and 76-intra, respectively.

However, since all labelled proteins distinguish by labelling efficiency and also by labelling positions it is not easily possible to compare traces across proteins, but comparison within a protein species and different nucleotides rather is. Since GDP·AlF_x obviously caused the largest change in fluorescence signal we set final value to 100 % and adjusted remaining traces accordingly. More precisely, applying next equation to all traces from 3-40 A and B yielded corresponding traces in figure 3-40 A1 and B1, respectively.

$$\frac{\Delta F (nucleotide)}{\Delta F_{max} (GDP \cdot AlF_x)} = \frac{1 - F (nucleotide)}{1 - F_{min} (GDP \cdot AlF_x)}$$

Drawn columns in A1 and B1 assign maximum values from each run. The column presentation will be used further to evaluate traces like this.

Results

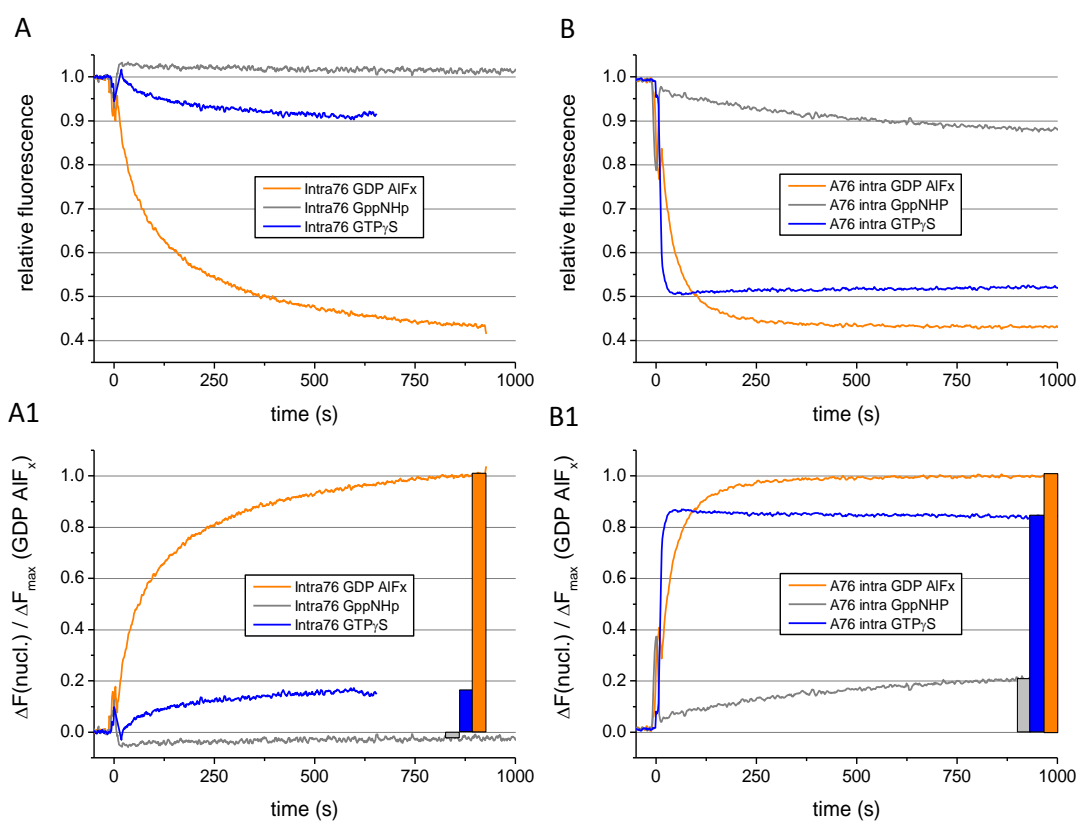


Figure 3-40: Nucleotide dependent intermolecular FRET measurements with hGBP-1 mutants A76 and 76-intra. At 25°C, (A) 0.25 μM donor and acceptor labelled protein (LP) intra-76 and 15 μM non-labelled protein (NLP) FL-76 were mixed and monitored for 2-5 minutes until fluorescence signal was stable. Donor was excited at 498 nm, acceptor emission was detected at 664 nm. Intramolecular movements were monitored in presence of 250 μM GDP·AIF_x (orange), 600 μM GppNHP (gray) and 250 μM GTP_γS (blue), triggered at $t_0 = 0$ s by nucleotide addition. (B) The same as (A) using 0.25 μM LP A76 and 15 μM NLP A76. (A1) and (B1) FRET traces from (A) and (B) were scaled according to the description in the text. Columns indicate final values of accordingly scaled fluorescence traces.

To finally figure out putative differences between intramolecular motions of wt hGBP-1 and FL-76, nucleotide dependent FRET measurements of both double labelled hGBP-1 (wt-intra) and 76-intra were compared (figure 3-41). Both proteins, due to labelling positions reporting distances between $\alpha 13$ and LG-domain, underwent largest conformational changes in presence of GDP·AIF_x. Although yielding almost similar changes in total fluorescence, decrease of fluorescence and hence moving apart of LG domain and $\alpha 13$ was significantly decelerated for the mutant 76-intra. Interestingly, similar time courses of fluorescence were obtained when GDP·AIF_x dependent dimerization of the proteins was investigated (see figure

Results

3-35 C). Considering that observed intramolecular opening might be coupled to simultaneous intermolecular dimerization, it remains elusive whether GDP·AIF_x controlled traces are suitable to identify intramolecular contributions exclusively resulting from mutation K76A.

With respect to total change in fluorescence, GppNHp and GTPγS yielded significantly different curves for wt-intra and 76-intra. Since GppNHp and GTPγS were not capable to force dimerization of either hGBP-1 or FL-76, obtained differences could be assigned to intramolecular changes in monomeric protein occurring upon nucleotide binding only. In view of that, FL-76 compared to wt hGBP-1 underwent only poor conformational changes. Values scaled according to maximum fluorescence change induced by GDP·AIF_x (figure 3-41 C) revealed that GTPγS caused a change of almost 50 % in wt-intra while not even 20 % in 76-intra. Addition of GppNHp initially led to a slight increase in fluorescence, in wt-intra as well as 76-intra, indicating that dyes came even closer. While that step was followed by a continuous decrease in wt, meaning that α13 and LG domain moved apart slowly, fluorescence signal of the mutant remained stably above 1. Even though a decrease was slightly indicated, kinetic compared to wt was significantly slower.

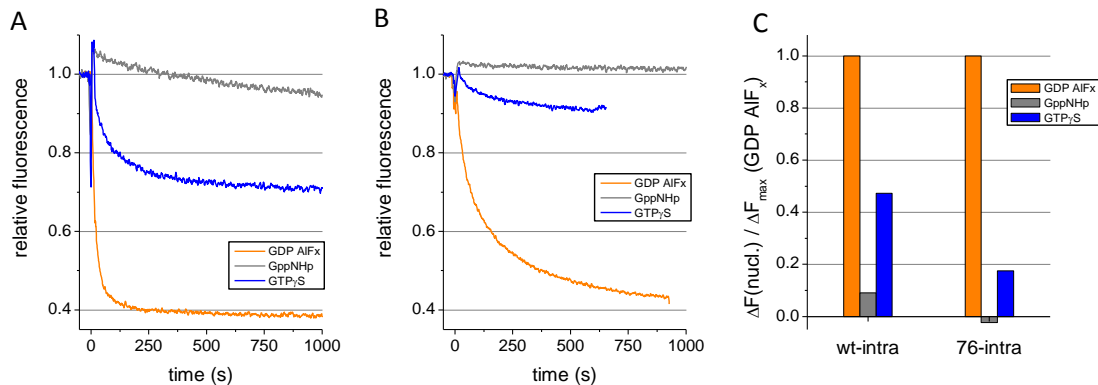


Figure 3-41: Nucleotide dependent intramolecular FRET measurements with wt-intra and 76-intra. At 25°C, (A) 0.25 μM LP wt-intra and 15 μM NLP hGBP-1 were mixed and monitored for 2-5 minutes until fluorescence signal was stable. Donor was excited at 498 nm, acceptor emission was detected at 664 nm. Intramolecular movements were monitored in presence 250 μM GDP·AIF_x (orange), 600 μM GppNHp (gray) and 250 μM GTPγS (blue), triggered at $t_0 = 0$ s by nucleotide addition. (B) The same as (A) using 0.25 μM LP 76-intra and 15 μM NLP FL-76, instead. (C) Final values of all traces were scaled relative to the maximum fluorescence change obtained with GDP·AIF_x.

Taken together, wt based labelling allowed to monitor relative changes between structural elements $\alpha 13$ and LG domain. By comparing nucleotide dependent FRET courses, indeed, we could see differences between wt and mutant, particularly suggesting that K76A was restricted to achieve the same opening of $\alpha 13$ as wt succeeded to do. However, the differences ground on experiments with GTP analogs mimicking the presence of also γ -phosphate, while deficiency of K76A affects the β -phosphate cleavage step.

3.2.5. Intramolecular opening of $\alpha 12$ and $\alpha 13$ in presence of different interaction partners

Previous FRET studies with Cys9 based A76 or B76 constructs have shown that it makes a difference whether the same Cys9 based or a wt based protein was used as non-labelled protein (paragraph 3.2.4.6). Inspired by that, we used labelled Cys9 based constructs and varying hGBP-1 mutants as NLP in the background to address their contribution to opening of either $\alpha 13$ (A76) or $\alpha 12$ (B76). We selected either truncated hGBP-1 mutants lacking C-terminal parts (1-LG, hGBP-1 $\Delta\alpha 13$ and 3-Phe Δ) or full-length mutant RK that was supposed to have weakened contacts between the LG domain and its C-terminus and thus to have a higher availability of helices $\alpha 12$ -13. Moreover, all mutants were able to dimerize in presence of GTP γ S. Using a mixture of 0.25 μ M labelled protein and 15 μ M NLP maintained that upon GTP γ S addition only mixed dimers were formed so that putative differences in fluorescence change could be easily assigned to particular NLP and its constitution.

Carrying its FRET pair in the LG domain and in the C-terminus $\alpha 13$, labelled protein A76 is a capable reporter of $\alpha 13$ movement relative to the LG-domain. Initially, a control measurement was performed with labelled protein (LP) A76 only. Within 500 seconds after GTP γ S addition, fluorescence signal dropped by almost 25 % of initial value. Applying different mutants as non-labelled interaction partners to A76, indeed, resulted in significantly deviating FRET traces indicating that movement of $\alpha 13$ was controlled by offered interfaces, as well (figure 3-42 A). While using non-labelled A76 caused a larger decrease in fluorescence, meaning 'opening' of the protein, it was even more pronounced when mutant RK was used instead. NLP hGBP-1 $\Delta\alpha 13$ lacking its C-terminus $\alpha 13$ was also sufficient to generate considerable opening of the LP. Isolated 1-LG lacking all helical structures $\alpha 7$ -13, as well as 3-Phe Δ lacking $\alpha 12$ -13, in contrast, facilitated even increase in fluorescence which implies two facts: First, mixed dimers

Results

of truncated hGBP-1 mutants and A76 had been established, otherwise fluorescence signal would remain as in control. Second, dimerization with truncated mutants made the structural elements $\alpha 13$ and LG move into closer proximity.

RK retaining all structural elements of full-length protein and particularly exhibiting a higher availability of $\alpha 12-13$ was the interaction partner that facilitated opening of A76 to highest level. Although deletion of $\alpha 13$ was obviously dispensable as still significant opening occurred, however, piecewise deletion of C-terminal ends diminished this capacity: deletion of either $\alpha 12-13$ (NLP: 3-Phe Δ) or $\alpha 7-13$ (NLP: 1-LG) resulted in even increasing fluorescence which indicates that the GED and LG domain came even closer. In conclusion, one could assume that opening of $\alpha 13$ is controlled by intermolecular interactions. According to the present data, the interaction partner needs to harbor at least $\alpha 12$ so that it can take up $\alpha 13$ from the other partner. If also $\alpha 12$ and more is missing, $\alpha 13$ virtually prefers intramolecular interactions by arranging even closer to the LG domain.

In the same manner as done for $\alpha 13$, using detectable FRET construct B76 which has a donor and acceptor fluorophore in the middle domain and $\alpha 12$, respectively, allowed to focus interaction partner dependent motions of $\alpha 12$ (figure 3-42 B). Similar to A76, also relative opening of $\alpha 12$ occurred most prominently in presence of RK. Opening controlled by either non-labelled B76 or deletion mutant hGBP-1 $\Delta\alpha 13$ were almost identical leading to a fluorescence decrease by more than 50 %. Further truncation represented by 3-Phe Δ and 1-LG had very poor or no effect on $\alpha 12$ movements since according fluorescence traces were similar to the control with LP only. In general, $\alpha 12$ being less flexible than $\alpha 13$ (indicated by control experiments) required the same constitution of interaction partner for opening as $\alpha 13$ did. Undergoing large distance changes when interaction partner harbored all domains up to $\alpha 12$, opening occurred only weakly or not at all when $\alpha 12$ and more elements were deleted. For comparison of $\alpha 13$ and $\alpha 12$ movements in dependency of varying dimer partners, final values of each trace were scaled according to the maximum fluorescence change obtained for respective control experiment (figure 3-42 C).

Results

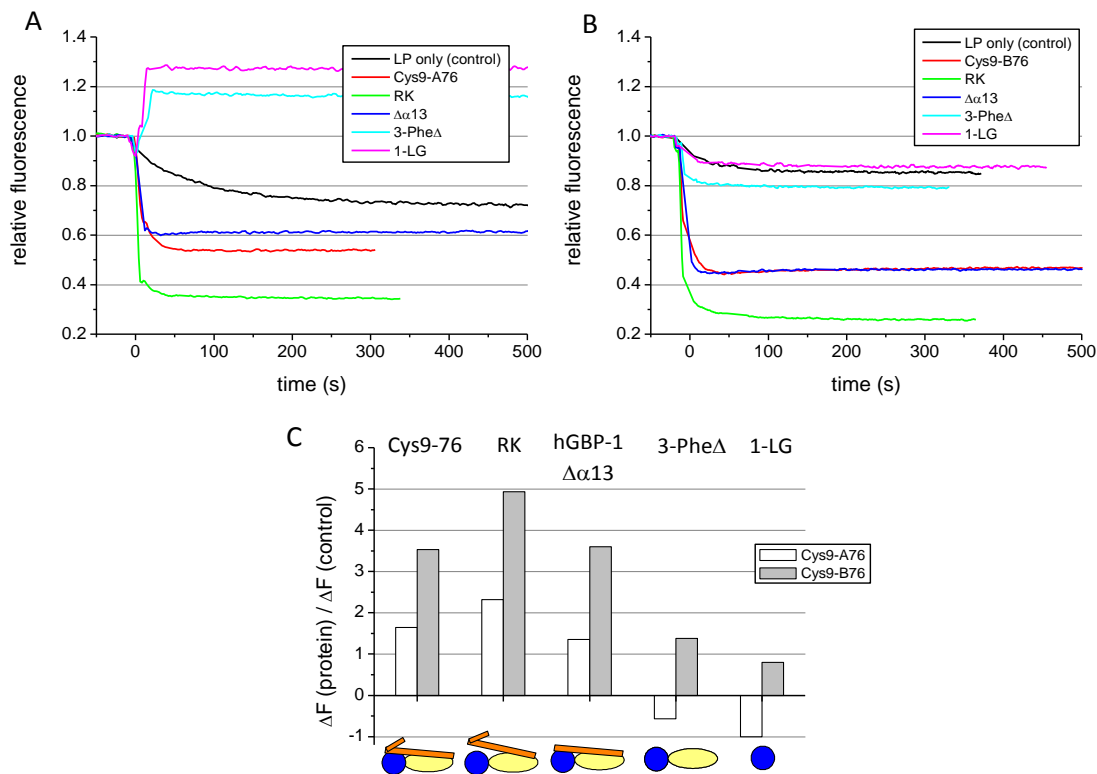


Figure 3-42: Intramolecular FRET studies focusing opening of α12 and α13 in presence of different interaction partners. At 25°C, (A) 0.25 μM LP A76 (LG:α13) and 15 μM NLP (indicated in legend) were mixed and monitored for 2-5 minutes until fluorescence signal was stable. Donor was excited at 498 nm, acceptor emission was detected at 664 nm. Intramolecular movements were monitored upon addition of 250 μM GTPγS ($t_0 = 0$ s). A control measurement was performed with LP only. (B) The same as (A) using 0.25 μM LP B76 (middle domain:α12), instead. (C) Final values of all traces were adjusted relatively to the maximum fluorescence change obtained with respective control experiment. Resulting values plotted against applied NLPs illustrate the extent of intramolecular opening (positive values) and closing (negative values). Constitutions of the NLPs were drawn schematically with LG domain (blue) middle domain (yellow) and α12-13 (orange).

3.3. Biochemical properties of hGBP-2, hGBP-3 and hGBP-5 in comparison to hGBP-1

Human GBPs (hGBP-1 to hGBP-7) are immuno-related proteins that are strongly upregulated in response to pathogenic infection and cytokine release, in particular IFN- γ . Several hGBPs have been shown to provide anti-pathogenic actions, among others, against vesicular stomatitis virus (VSV), encephalomyocarditis virus (EMCV), Influenza A virus (IAV), Hepatitis C virus (HCV), and also against the bacterium *Chlamydia trachomatis*. However, protein domains or properties necessary for pathogen combat were just marginally identified. In some cases LG domains and/or GTPase activity seemed to be relevant, in others C-terminal domain played a crucial role (Anderson, et al., 1999) (Itsui, et al., 2009) (Nordmann, et al., 2012). To understand intracellular actions provided by the hGBPs, also non-pathogen related *in vitro* studies were performed, reporting nucleotide dependent homo and hetero interactions among the isoforms hGBP-1 to hGBP-5. These interactions, most crucially, were shown to define the subcellular localization and translocation of the proteins in a hierarchal manner (Britzen-Laurent, et al., 2013). Therefore, homo and hetero interactions of the hGBPs might be an essential feature to fulfil the multiplicity of their so far identified physiological and pathophysiological roles. However, the understanding of the hGBPs' cellular networking demands quantitative data, basically with respects to individual biochemical properties. Thus, hGBPs sharing the highest sequence homology were focused in this work. Besides hGBP-1, recombinant proteins hGBP-2 and hGBP-3, to some extent also hGBP-5 were produced and characterized.

3.3.1. Protein expression and purification

Gene fragments of full-length or truncated variants of human GBP-1, GBP-2, GBP-3, and GBP-5 were amplified via PCR. With aid of restriction endonucleases *Bam*HI and *Sal*I, genes were cloned into vector pQE-80L encoding for an N-terminally hexa-histidine tagged target protein. All protein constructs with respective amino acid sequences and calculated parameters are listed in table 3-7.

Table 3-7: Theoretical parameters of human GBP constructs. For each construct, amino acid (aa) length, abbreviation (abbr.) of construct, amino acid sequences at N- and C-terminus and also calculated molecular weight (MW), isoelectric point (pI) and molar extinction coefficient at 280 nm (ϵ_{280}) are listed. Latter ones were calculated by the online tool ProtCalc³; ϵ_{280} apply to denaturing Gua-buffer (6 M Guanidine-HCl, 20 mM phosphate, pH 6.5) assuming all cysteines are reduced. Upon cloning via restriction enzyme BamHI, N-terminal hexa-histidine tag and starting methionine were connected by two additional residues, glycine and serine (HHHHHHGSM...).

Protein construct	Length (aa)	Abbr.	Sequence (N→C-terminus)	MW (kDa)	pI	ϵ_{280}
hGBP-1 full-length	1-592	hGBP-1	MASEIHM...KACTIS	67,903	5.97	43,240
hGBP-1 isolated LG domain	1-327	1-LG	MASEIHM...IENSAA	36,615	5.76	34,280
hGBP-2 full-length	1-591	hGBP-2	MAPEINL...PICNIL	67,209	5.53	52,060
hGBP-2 isolated LG domain	1-327	2-LG	MAPEINL...NSAAVE	36,257	5.38	38,690
hGBP-3 full-length	1-595	hGBP-3	MAPEIHM....SHKCLKI	68,143	6.22	47,080
hGBP-3 deletion of α 12-13	1-481	hGBP-3 (aa 1-481)	MAPEIHM...TDQILT	54,472	5.74	43,240
hGBP-3 isolated LG domain	1-327	3-LG	MAPEIHM...NSAAVQ	36,687	5.93	34,280
hGBP-5 isolated LG domain	1-326	5-LG	MALEIHM...ENSAAV	36,417	5.05	30,440

According to the standard protocol of hGBP-1 expression in *E. coli*, both strains Rosetta (DE3) and BL21 (DE3) CodonPlus RIL yielded considerable amounts of recombinant N-terminally hexa-histidine tagged hGBP constructs. Figure 3-43 exemplary illustrates levels of

³ <http://www.justbio.com/index.php?page=protcalc>

Results

hGBP-3 overexpression. Full-length hGBP-3 (a), C-terminally truncated (b) and LG domain protein (c) have molecular weights of 68 kDa, 54 kDa and 37 kDa, respectively. Induced cells compared to non-induced cells revealed prominent bands at corresponding heights.

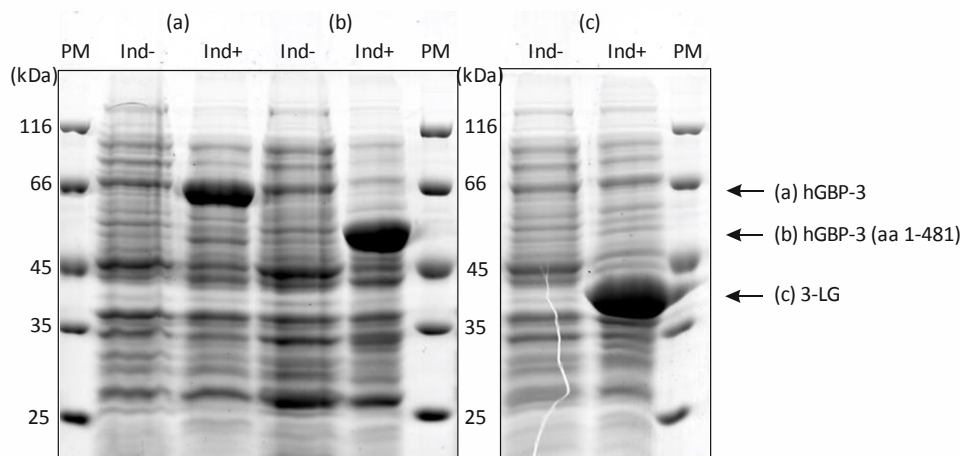


Figure 3-43: SDS-PAGE analysis of recombinant hGBP-3 expression in *E. coli*. *E. coli* cells Rosetta (DE3) transformed with pQE-80L plasmids containing full-length and truncated hGBP-3 genes were grown at 37°C until OD_{600nm} 0.4-0.6 was reached. Started by addition of 100 μ M IPTG, induction was performed for 16-18 hours at 25°C. Comparison of induced (Ind+) and not induced cells (Ind-) on a 10% SDS-PAAG revealed high levels of overexpression indicated by prominent bands at corresponding heights for hGBP-3 full-length (a), C-terminal truncated hGBP-3 (aa 1-481, (b)), and the isolated LG domain 3-LG (c).

Moreover, all proteins listed in table 3-7 were highly soluble. Protein purification and enrichment was performed in accordance with established hGBP-1 protocol. After affinity chromatography, protein was separated via size exclusion chromatography, revealing target monomer protein as major species. Taken together, one liter of *E. coli* culture yielded approximately 10 mg of highly pure monomeric protein.

Human GBP-3 in its full length variation was the only protein that deviated remarkably from the others. Although being soluble, full-length hGBP-3 had a high tendency to precipitate at some non-definable point, either during any protein purification step, during protein concentration or even during measurements. Precipitation virtually disappeared when for example up to 1 M NaCl was added to protein solution. For testing, buffer conditions were adjusted to 1 M NaCl along all purification steps; spontaneous precipitation at some stage occurred nevertheless. In the same manner, other buffer compounds such as glycerol or reducing DTT were tested, none of them considerably improved protein stability. Although

sharing the highest sequence homology with hGBP-1 and having a theoretical pI that does not considerably distinguish (6.22 versus 5.94), recombinant hGBP-3 obviously had some specific features that required stabilizing factors which could not be figured out so far. As an alternative, truncation mutant hGBP-3 (aa 1-481) was generated that compared to hGBP-1 structure corresponds to deletion of α 12-13. Interestingly, lack of the C-terminal domain enabled hGBP-3 to remain stable in solution. However, some amounts of full-length hGBP-3 was obtained and also assayed with respects to basic biochemical properties. Nevertheless, due to mentioned instability data need to be considered with care. In parallel, truncated hGBP-3 (aa 1-481) was investigated.

3.3.2. Enzymatic activity of hGBP-1, hGBP-2 and hGBP-3

3.3.2.1. hGBP-1, hGBP-2 and hGBP-3 hydrolyze GTP in a cooperative manner

The rate of GTP hydrolysis is a key factor for functional regulation of G proteins and their effector functions. Being a member of the dynamin family hGBP-1 shows accelerated GTPase activity in a self-stimulated manner without being dependent on extrinsic factors like GTPase activating proteins which are known to be essential for small GTPases (Gasper, et al., 2009). Another member of the human GBPs, namely hGBP-5, was reported to have a similar self-stimulating mechanism resulting in a maximum specific activity that was comparatively low (Wehner, et al., 2010). Also hGBP-2 was described to be an efficient GTPase (Neun, et al., 1996) but the self-stimulating mechanism was not further explored. Concentration dependence of GBPs enzymatic actions might be an important key regulator ensuring low levels of GTP hydrolysis at low protein concentration but a strong increase when GBP expression is significantly upregulated in response to interferons.

However, here GTP hydrolysis catalyzed by the first three full-length GBPs, namely hGBP-1, hGBP-2 and hGBP-3 was analyzed via reversed-phase HPLC. Similar to hGBP-1, both isoforms showed a significant increase in GTP turnover with higher protein concentrations indicating that enzymatic activity of the proteins was accelerated upon self-assembly (figure 3-44). Considering protein concentration dependent dimer formation, data was fitted with equation 5 which in turn yielded maximum specific activity (s_{GTP}) as well as apparent dimer dissociation constant K_d^{GTP} .

Results

Sharing the highest sequence homology among all human GBPs, hGBP-1 and hGBP-3 were found to hydrolyze GTP most efficiently with $s_{\text{GTP}} = 19.1 \text{ min}^{-1}$ and $s_{\text{GTP}} = 14.4 \text{ min}^{-1}$, respectively. However, hGBP-3 in contrast to hGBP-1 revealed a 22-fold lower homo dimer affinity. Obtained K_d^{GTP} values for hGBP-1 and hGBP-3 were $0.2 \mu\text{M}$ and $4.4 \mu\text{M}$, respectively. Similar to hGBP-3, hGBP-2 was also characterized by a significantly lower dimer affinity ($K_d^{\text{GTP}} = 2.0 \mu\text{M}$) as compared with hGBP-1. Other than hGBP-3, the GTPase activity of hGBP-2 was reduced as well; hGBP-2 converted GTP with $s_{\text{GTP}} = 7.4 \text{ min}^{-1}$ which is approximately two times slower than obtained for hGBP-3.

Taken together, hGBP-2 and hGBP-3 like hGBP-1 performed cooperative GTPase activity in comparable ranges, but unlike hGBP-1 they were attenuated to dimerize. In accordance with the obtained dimer dissociation constants, dimerization of hGBP-2 and hGBP-3 required at least ten times higher protein concentration than dimerization of hGBP-1.

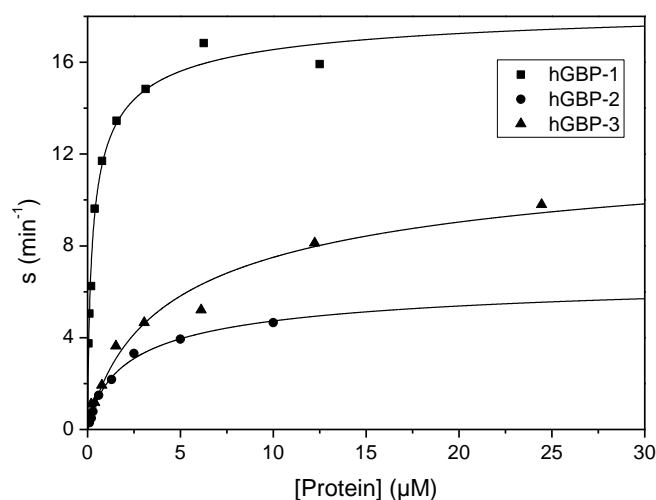


Figure 3-44: Concentration dependent GTP hydrolysis catalyzed by hGBP-1, -2 and -3. At 25°C , varying protein concentrations (20 nM-25 μM) and 500 μM GTP were incubated. At defined time points samples were applied to reversed-phase HPLC. GTP turnover plotted against time was fitted by linear regression. Initial turnover rate derived from linear slope was normalized by protein concentration and yielded specific activity s (min^{-1}). Specific activities were plotted against hGBP concentration fitted using equation 5 (straight lines). For each isoform, maximum specific activity (s_{GTP}) and dimer dissociation constant K_d^{GTP} were obtained (see text).

3.3.2.2. GTPase stimulation is provided by LG-domain interactions

The enzymatic activity of hGBP-1 is strongly driven by intra- and intermolecular interactions. In particular, homo dimerization which in turn stimulates GTPase activity of

Results

hGBP-1 was found to be mediated by intermolecular contacts between LG domains. Studies on enzymatic properties of the isolated LG-domain (1-LG) revealed a cooperative GTP hydrolysis mechanism with both, increased activity and also higher dimer affinity (Praefcke, 2001). In view of the sequence homology among all GBPs which is even higher when narrowed down to the N-terminal LG-domain, comparable interactions were suggested for the isoforms hGBP-2 and hGBP-3. Therefore, constructs consisting of the appropriate regions, namely 2-LG and 3-LG, were investigated with regards to cooperative GTP hydrolysis mechanism.

According to the setup from previous paragraph, specific GTPase activities of 2-LG and 3-LG were determined at varying protein concentrations. Also 1-LG was investigated in the same manner since enzymatic activity under physiological salt conditions had not been determined yet. Results clearly demonstrated that all LG constructs retained entire activity of full-length proteins. Combined plots of respective full-length and LG domain catalyzed GTP hydrolysis curves revealed insights into similarities and differences (figure 3-45). As an indicator for self-assembly stimulated GTPase activity, 2-LG and 3-LG like 1-LG exhibited elevated GTPase activity with increasing concentrations. These data most remarkably suggest that like for hGBP-1 also hGBP-2 and hGBP-3 homo complex formation is initially provided by LG domain interactions.

For hGBP-2, shape of full-length and LG driven GTP hydrolysis curves were perfectly overlapping (figure 3-45 B). As a consequence, dimer dissociation constants and maximum specific activities were almost identical; $s_{\text{GTP}} = 7.4 \text{ min}^{-1}$ and 7.7 min^{-1} , $K_d^{\text{GTP}} = 2.0 \mu\text{M}$ and $1.8 \mu\text{M}$ were obtained values for hGBP-2 and 2-LG, respectively.

Isolated 1-LG was previously shown to distinguish from full-length hGBP-1 by increased activity and also tighter dimer formation. Here, also under physiological salt conditions a higher maximum GTPase activity was obtained (figure 3-45 A). With $s_{\text{GTP}} = 36.7 \text{ min}^{-1}$, 1-LG catalyzed GTP hydrolysis approximately two times faster than hGBP-1 ($s_{\text{GTP}} = 19.1 \text{ min}^{-1}$). As a difference to low salt conditions, formation of 1-LG dimers was evidently impaired by 150 mM NaCl buffer content. While forming approximately four times tighter dimers than full-length hGBP-1 under low salt conditions (Praefcke, 2001), here, $K_d^{\text{GTP}} = 0.39 \mu\text{M}$ was obtained indicating that the 1-LG dimer affinity became even two times lower than the hGBP-1 dimer affinity ($K_d^{\text{GTP}} = 0.20 \mu\text{M}$).

Like for full-length hGBP-3, a concentration dependent increase of the specific activity was obtained also for 3-LG. While apparent dimer constant of $4.3 \mu\text{M}$ was almost the same as for

Results

the full-length protein, maximum GTPase activity provided by 3-LG was $s_{\text{GTP}} = 42.3 \text{ min}^{-1}$ and thus almost three times faster than performed by hGBP-3 ($s_{\text{GTP}} = 14.4 \text{ min}^{-1}$, figure 3-45 C). For completeness, also GTPase activity of truncated hGBP-3 (aa 1-481) was investigated (data not shown). With $s_{\text{GTP}} = 53.5 \text{ min}^{-1}$ the maximum activity was even higher than for 3-LG. Interestingly, also K_d^{GTP} value of hGBP-3 (aa 1-481) being $14.2 \mu\text{M}$ was larger, indicating an approximately 3-fold weaker dimer formation as compared to hGBP-3 full-length and 3-LG (table 3-8).

For the LG domain of hGBP-5, specific activity was determined only for a single protein concentration. At $10 \mu\text{M}$, 5-LG performed GTP hydrolysis with 5.1 min^{-1} .

Isolated LG domains of hGBP-1, hGBP-2 and hGBP-3 demonstrated cooperative GTP hydrolysis. In addition, obtained dimer dissociation constants of respective full-length and truncated proteins were very similar. These data strongly suggest that homo interactions responsible for GTPase stimulation are established by LG domain contacts. Moreover, lacking the helical domain did not reveal any effect on hGBP-2s enzymatic properties, whereby the same loss resulted in elevated activity of 1-LG and 3-LG. Thus, GTPase activity of hGBP-1 and hGBP-3 might be further controlled by intramolecular interactions between LG and helical domains.

Results

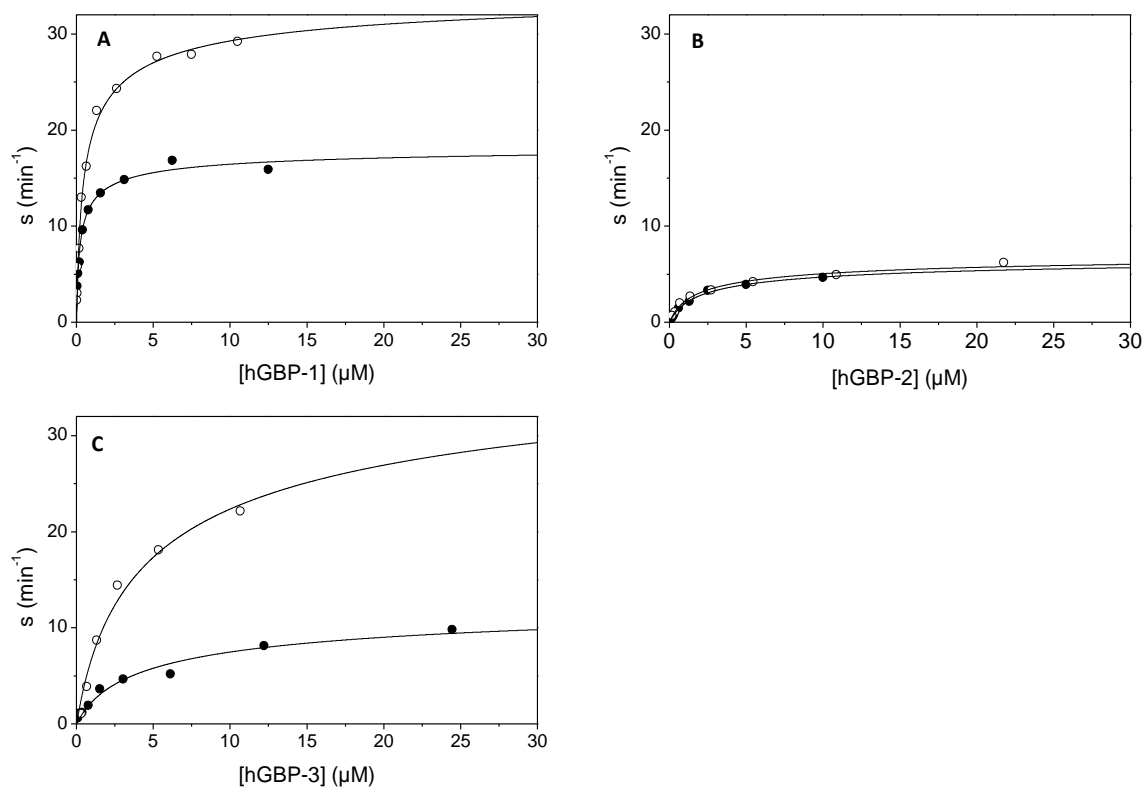


Figure 3-45: GTPase activities of full-length and LG hGBPs. Specific activities were obtained from GTP hydrolysis assay for each LG (open circles) and respective full-length protein (closed circles). (A) hGBP-1, (B) hGBP-2, (C) hGBP-3. Dimer dissociation constants and maximum specific activities resulting from the fits according to equation 5 (straight lines) are listed in table 3-8.

Table 3-8: GTPase activities and apparent dimer dissociations constants of hGBP isoforms.

	hGBP-1	1-LG	hGBP-2	2-LG	hGBP-3	hGBP-3 (aa 1-481)	3-LG
s_{GTP} (min^{-1})	19.1 ± 0.6	36.7 ± 0.7	7.4 ± 0.3	7.7 ± 0.3	14.4 ± 1.3	53.5 ± 3.7	42.8 ± 5.9
K_d^{GTP} (μM)	0.20 ± 0.03	0.39 ± 0.03	2.0 ± 0.2	1.8 ± 0.3	4.4 ± 1.1	14.2 ± 2.1	4.3 ± 1.4

3.3.2.3. *GTP hydrolysis catalyzed by hGBP-1, hGBP-2 and hGBP-3 yields different product compositions*

Hydrolysis of GTP to both GDP and GMP is a unique feature of hGBP-1. In a temperature dependent manner, GMP made up either 40 % (25°C) or 90 % (37°C) of total product (Praefcke, et al., 2004) (Vöpel, et al., 2010). Similarly, hGBP-2 was reported to be a GTPase that also converts GTP in in two successive steps yielding both of the nucleotide products GDP and GMP with latter one being the minor fraction of 10 % (37°C) (Neun, et al., 1996). In contrast and irrespective of the temperature, hGBP-5 catalyzed GTP hydrolysis yielded only GDP but no GMP, clearly indicating that hGBP-5 does not undergo the second hydrolysis step (Wehner, et al., 2010).

In our experiments consistently performed at 25°C, we compared product formation upon GTP hydrolysis catalyzed by full-length hGBP-1, hGBP-2 and hGBP-3. Like described for hGBP-1 (paragraph 3.1.2.), data from GTP hydrolysis assays were employed to determine also maximum specific activities of product formation, s_{GMP} and s_{GDP} . The ratio $s_{\text{GMP}}/s_{\text{GTP}}$ lastly revealed the share of GMP on total product. Values listed in table 3-9 clearly indicate that hGBP-1 and hGBP-3 share the feature to produce significant amounts of GMP. Calculated proportions of 46 % and 34 % GMP for full-length and truncated hGBP-3, respectively, resemble product amounts of hGBP-1 (36 %). In contrast, only 3 % GMP was detected for hGBP-2.

Table 3-9: GMP formation upon hGBP-1, hGBP-2 and hGBP-3 catalyzed GTP hydrolysis. With the aid of equation 5, maximum activities of GTP turnover (s_{GTP}) and GMP formation (s_{GMP}) were derived from GTP hydrolysis assays at 25°C (previous paragraphs). The percentage of GMP was calculated by the ratio $s_{\text{GMP}}/s_{\text{GTP}}$.

	hGBP-1	hGBP-2	hGBP-3	hGBP-3 (aa 1-481)
s_{GTP} (min⁻¹)	19.1	7.4	14.4	53.5
s_{GMP} (min⁻¹)	6.9	0.19	6.6	18.1
GMP (%)	36	3	46	34

Since previous data indicated that hGBP-2 was capable to form higher GMP amounts, we performed also long term hydrolysis assays. Like usually, varying hGBP-2 concentrations and either 500 μM GTP or GDP were incubated for 24 hours at 25°C. Plots of nucleotide composition at each concentration point clearly confirmed our previous observation. No considerable amounts of GMP occurred upon GTP hydrolysis (figure 3-46, upper panel). Obviously, at concentrations above 10 μM hGBP-2 became capable of utilizing also GDP as

Results

substrate; increasing amounts of GMP were yielded consequently (figure 3-46), upper and lower panel). Thus, detected GMP only arose upon GDP hydrolysis but not upon GTP hydrolysis.

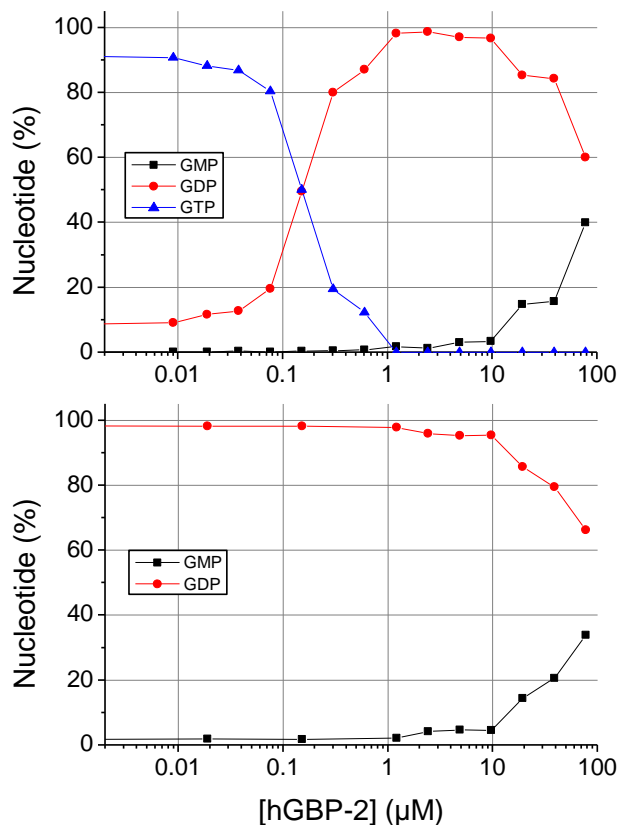


Figure 3-46: Long term GTP and GDP hydrolysis catalyzed by hGBP-2 at 25°C. For 24 hours, varying concentrations of hGBP-2 were incubated with either 500 μM GTP (upper panel) or 500 μM GDP (lower panel). Relative nucleotide amounts (GMP: black, GDP: red, GTP: blue) were derived from rp-HPLC analysis. Decrease and increase of substrate and products, respectively, occurred in concentration dependent manner.

In contrast to studies of Neun et al. (Neun, et al., 1996), our experiments were performed at 25°C and not at 37°C. And also in contrast, we obtained maximal 3 % instead of 10 % GMP. To finally figure out whether hGBP-2 yields product ratio in temperature dependent manner, we performed one measurement at 37°C. Therefore, 10 μM hGBP-2 was incubated with 500 μM GTP. After 30 and 150 minutes samples were analyzed via rp-HPLC (figure 3-47). Within 30 minutes all substrate was hydrolyzed and resulted in 98 % GDP and 2 % GMP, clearly indicating that GMP amounts also at higher temperature unalteredly remained at very low

Results

levels. Since product ratio did not change further after 150 minutes of incubation, additional GDP hydrolysis could be excluded. This is in reasonable agreement with the results from long term hydrolysis studies –even though performed at 25°C- demonstrating that hGBP-2 at a concentration of 10 μ M does not considerably utilize GDP as substrate (figure 3-46).

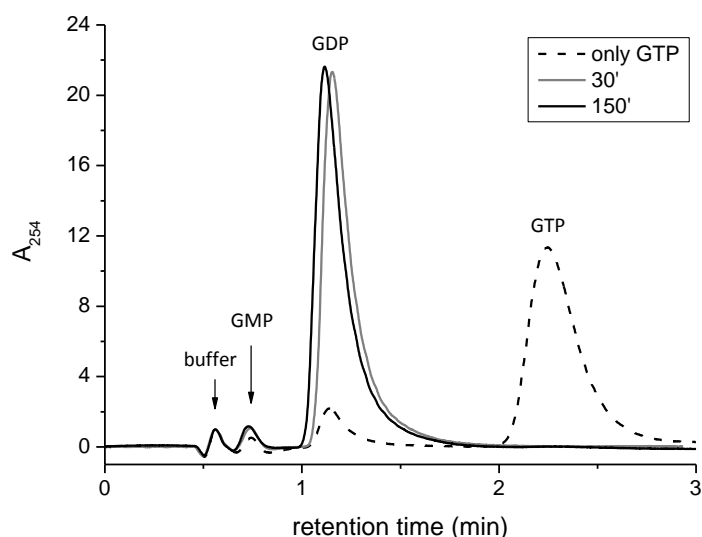


Figure 3-47: Analysis of product formation upon hGBP-2 catalyzed GTP hydrolysis at 37°C. 500 μ M GTP and 10 μ M hGBP-2 were mixed and incubated at 37°C. After 30 minutes (gray solid line) and 150 minutes (black solid line) of incubation product composition was analyzed via rp-HPLC. Elution of the nucleotides was monitored at 254 nm. Compared to GTP only (black dotted line), substrate was consumed completely after 30 minutes yielding 98 % GDP and only a minor fraction of 2 % GMP. Product ratio did not change over time indicating that GDP was not further hydrolyzed. Each chromatogram was normalized by the value of buffer peak eluting after 0.6 minutes.

3.3.2.4. Substrate specificity and product patterns of isolated LG domains

GMP and GDP are both products typically arising upon hGBP-1 catalyzed GTP hydrolysis. Similar product formation was observed also for hGBP-3. For hGBP-2, in contrast, GTP hydrolysis was already completed after the first step of γ -phosphate cleavage resulting in 97-98 % GDP and just a small fraction of GMP.

When deleting the elongated C-terminus of hGBP-1 (aa 328-592), the protein (1-LG) acquires particular characteristics that significantly alter from full-length features. Besides higher GTPase activity and a shift of product ratio in favor of GMP, 1-LG utilizes also GDP as substrate. GDP hydrolysis, like GTP hydrolysis is strongly protein concentration-dependent, working more efficiently at higher concentrations (see paragraph 3.1.2.1). In order to

Results

investigate whether deletion of the corresponding C-terminal domain induces similar effects on hGBP-2 and hGBP-3, long term hydrolysis experiments were performed with 2-LG and 3-LG. Either 500 μ M GTP or GDP were applied, results from rp-HPLC analysis are depicted in figure 3-48.

Like also described in 3.1.2.1., upon GTP hydrolysis product formation of 1-LG occurred in two steps; first, GMP and GDP increased to a ratio of 70:30, second, GMP increased to 100 % while GDP disappeared completely (figure 3-48, left, upper panel). The second step proposed to mark the start of GDPase activity was confirmed by applying GDP as substrate (figure 3-48, left, lower panel). Of note, 1-LG concentration at which half of GTP was consumed was almost ten-fold lower than the concentration at which half of GDP was consumed. This suggests that GDP dependent dimerization and thus efficient GDP hydrolysis sets in at correspondingly higher protein concentration.

In paragraph 3.3.2.2., GTPase activities provided by 2-LG and full-length hGBP-2 were found to be almost identical. In contrast, deletion of the C-terminus resulted in elevated activity of 1-LG and 3-LG. Thus, helical domain of hGBP-2 was suggested not to contribute to the enzyme machinery. Also here, when product pattern was focused, 2-LG demonstrated almost the same picture (figure 3-48, middle panels) as its full-length variant (figure 3-46), emphasizing once more that the C-terminus of hGBP-2 might play only a minor role. At levels between 1 % and 2 %, only neglectable amounts of GMP developed upon 2-LG catalyzed GTP conversion. The same as for full-length hGBP-2, significant amounts of GMP emerged only upon GDP hydrolysis which in turn was established only at protein concentrations above 10 μ M. These data at the same time give evidence for hGBP-2's capability of GDP hydrolysis which might occur in a dimer stimulated manner, as well. However, protein concentrations at which half amount of GTP and half amount of GDP are consumed differ by a factor of approximately 400 which suggests an accordingly weaker GDP bound dimer. For 1-LG, remarkably, the same concentration points differed by only 10 times.

Up to a protein concentration of almost 50 μ M, also 3-LG was assayed for its specific pattern of GTP or GDP hydrolysis and product formation (figure 3-48, right panels). Results revealed two major properties: Firstly, GTP hydrolysis yielded only 12-15 % GMP. Compared to full-length and truncated hGBP-3 (aa 1-481) which were capable of producing even 46 % and 34 % GMP (previous paragraph), GMP amounts in presence of 3-LG were significantly reduced. The more of the C-terminal parts of hGBP-3 were truncated, interestingly, the less GMP arose as GTP hydrolysis product. Secondly, 3-LG just hardly utilized GDP as substrate. Merely above

Results

10-20 μM of 3-LG a slight decrease of GDP indicated putative set in of GDPase activity. Nevertheless, dissociation constant of 3-LG-GDP might be similar to that of 2-LG-GDP dimer, probably even higher.

Although long term hydrolysis assay was not performed on 5-LG, upon GTPase activity measurements we could not detect any GMP at all. GMP deficiency of full-length hGBP-5 has been reported earlier (Wehner, et al., 2010). Resembling results of hGBP-2, full-length and LG domain, C-terminal deletion of also hGBP-5 did not enable 5-LG to produce higher GMP amounts.

Previous experiments focusing GTPase activity already enlightened differences among all tested hGBP isoforms. In the same manner, differences were also found between full-length and truncated LG constructs of a single isoform. Particularly, C-termini of hGBP-1 and hGBP-3 were proposed to be involved in GTPase activity in a certain manner since 1-LG and 3-LG performed significantly elevated GTP turnover than the corresponding full-length proteins hGBP-1 and hGBP-3, respectively. Composition of products emerging from GTP turnover provided further evidence. While 1-LG formed more GMP than hGBP-1, interestingly, 3-LG yielded even less GMP than hGBP-3. Thus, C-termini of hGBP-1 and hGBP-3 might contribute to the enzymatic activity in different, rather opposite ways. In contrast, neither catalytic activity nor product pattern of hGBP-2 changed upon C-terminal deletion.

Lastly, 1-LG among all tested LGs was the only truncation that gained additional GDPase capability. Indeed, when increasing concentrations sufficiently also 2-LG and most probably 3-LG could be forced to perform GDP hydrolysis. However, these were protein concentrations at least 400 times as high as the 1-LG concentration, which in turn raises the question of any biological relevance.

Results

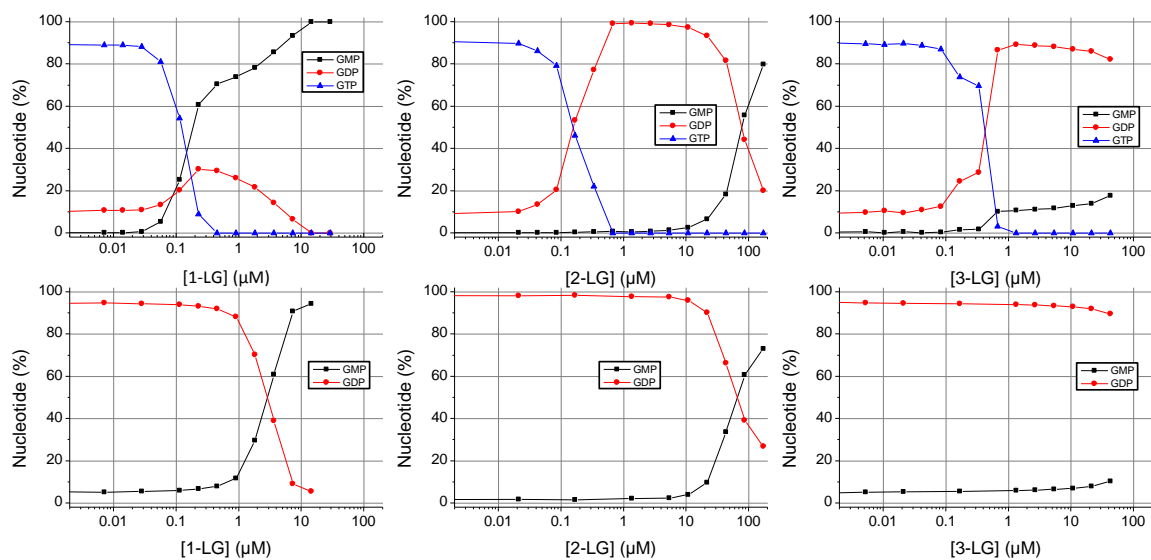


Figure 3-48: Long term GTP and GDP hydrolysis catalyzed by 1-LG, 2-LG and 3-LG. At 25°C and for 24 hours, varying concentrations of 1-LG, 2-LG, and 3-LG (panels from left to right) were incubated with either 500 μM GTP (upper panels) or 500 μM GDP (lower panels). Relative nucleotide amounts (GTP: blue, GDP: red, GMP: black) were derived from rp-HPLC analysis. Decrease and increase of substrates and products, respectively, occurred in concentration dependent manner.

3.3.3. Nucleotide binding properties of hGBP isoforms

All investigated GBP isoform, namely hGBP-1, hGBP-2 and hGBP-3 were shown to exhibit cooperative GTP turnover, whereby deviations were found with respects to maximum levels of activity, dimer dissociation constant and product formation. Differences were also obtained between full-length and LG constructs of a single isoform, indicating specific contribution of the helical domain (see previous paragraph). To further understand these differences, we also investigated nucleotide binding properties of each isoform, performing both stopped-flow measurements and equilibrium titration with mant-nucleotides (mant-GMP, mant-GDP, mant-GppNHp, mant-GTP γ S).

3.3.3.1. Nucleotide binding affinities of hGBP-2 and 2-LG

Nucleotide binding affinities of hGBP-2, full-length (hGBP-2) and LG domain (2-LG), were initially determined by equilibrium fluorescence titrations at 25°C. Therefore 0.5 μ M mant-nucleotide (excited at 366 nm) was titrated with protein (up to 1 mM) until saturation was reached (figure 3-49 A and B). The increase of fluorescence upon binding was monitored at 435 nm. Fitting the data according to a quadratic binding equation 2 revealed K_d values that deviated strongly between full-length and isolated LG domain. Full-length hGBP-2 had a high affinity to all investigated nucleotides, particularly to mGDP ($K_d = 0.049 \mu$ M) and mGTP γ S ($K_d = 0.050 \mu$ M). Interactions with the other non-hydrolysable GTP analog mGppNHp was found to be slightly weaker ($K_d = 0.16 \mu$ M). Still in low micro-molar range, highest K_d value obtained was 1.7 μ M for mGMP and hGBP-2 interaction.

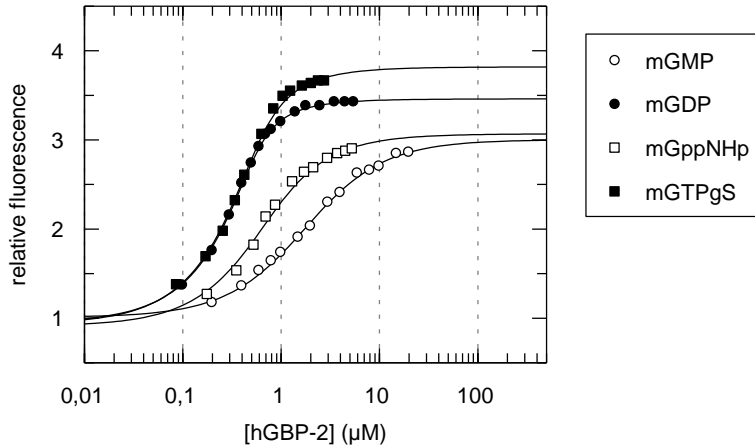
Nucleotide binding studies with the isolated hGBP-2 LG-domain (2-LG), strikingly, unraveled weaker affinities for all nucleotides. In comparison to full-length protein, binding affinities were weakened by at least one order of magnitude. Already visible by the shape of binding curves (figure 3-49 A and B), obtained K_d values in figure 3-49 C were plotted logarithmically to illustrate remarkable deviations. The lowest impact by 12-fold resulting in $K_d = 0.59 \mu$ M was found for mGDP binding which is still an effect of one order of magnitude. Yielding $K_d = 3.1 \mu$ M, interaction of mGTP γ S and 2-LG was even 43-fold weaker as compared with interaction of mGTP γ S and full-length protein. Lack of the helical domain, most notably, led to more than 100-fold weaker binding of mGppNHp and mGMP. Determined K_d values were 27 μ M and 200 μ M, respectively.

In order to address the negative impact that the C-terminal truncation had on the on nucleotide binding affinity of hGBP-2, dynamics of binding were investigated by stopped-flow experiments. Association and dissociation rate constants (k_{on} and k_{off}^*) were derived from

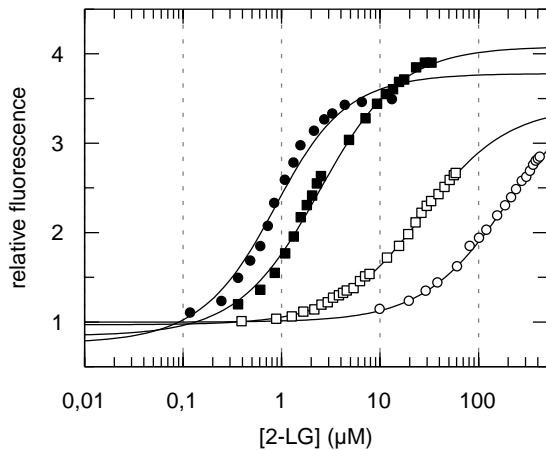
Results

concentration dependent association kinetics and displacement experiments, respectively. All parameters listed in table 3-10 are also depicted in bar charts (figure 3-50).

A



B



C

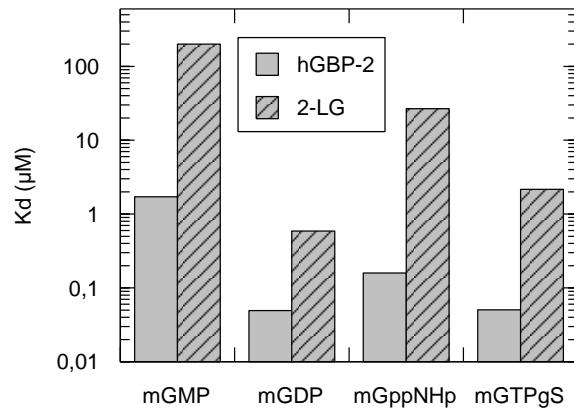


Figure 3-49: Fluorescence equilibrium titration of hGBP-2 constructs and mant-labelled nucleotides. 0.5 μM nucleotide was titrated with either full-length hGBP-2 (A) or 2-LG (B). Mant-nucleotide was excited at 366 nm and fluorescence increase upon binding was detected at 435 nm. Fitting the data according to equation 2 (straight lines) yielded equilibrium dissociation constant (K_d) for complex of protein and mant-nucleotide. For comparison, determined K_d values for hGBP-2 and 2-LG were plotted logarithmically (C). Values are listed in table 3-10.

Dissociation constants (K_d^*) obtained from the ratio $k_{\text{off}}^*/k_{\text{on}}$ were in good agreement with the K_d values resulting from fluorescence titration experiments. The major finding of kinetic analysis was that C-terminal deletion of hGBP-2 dramatically impaired the association rates: For all nucleotides association was approximately 50 times slower, mGMP and 2-LG associated even 120 times slower. On the other hand, dissociation rates were affected to different extent. For instance, mGMP and mGTP γ S dissociation was virtually not affected. Thus, higher

Results

dissociation constants of 2-LG·mGMP and 2-LG·mGTPyS, respectively, resulted almost exclusively from impact on association. Taken together, mGTPyS affinity still localized in low micro-molar range while mGMP affinity was almost lost ($K_d^* > 200 \mu\text{M}$). Isolated 2-LG had the highest affinity to mGDP. Kinetic parameters clearly demonstrated that decelerated mGDP association was largely compensated by also decelerated dissociation. Compared to corresponding full-length parameters association and dissociation rate constants were reduced by approximately 50-fold and 10-fold, respectively. Lastly, binding of mGppNHp which suffered the highest impact was a result of both, remarkably slower association (almost 60-fold) accompanied by an even 6-fold faster dissociation. While a dissociation constant of $0.10 \mu\text{M}$ was obtained for the interaction of full-length hGBP-2 and mGppNHp, consequently, for 2-LG and mGppNHp the value increased to $35 \mu\text{M}$.

Apparently having no effect on enzymatic properties, the C-terminus of hGBP-2 indeed engaged essentially in nucleotide binding. Although harboring all the conserved motifs necessary for nucleotide binding, isolated 2-LG in contrast to the full-length protein had in some cases dramatically weakened binding affinities principally resulting from slower association rates.

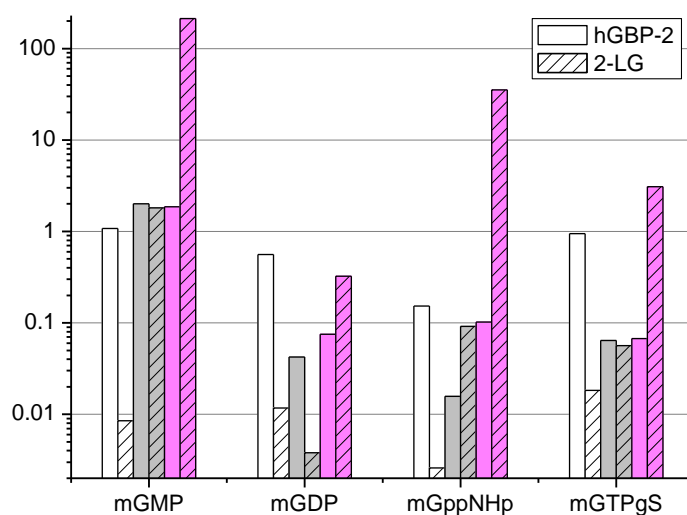


Figure 3-50: Dynamics of mant-nucleotide binding to hGBP-2 and 2-LG. Kinetic parameters k_{on} ($\mu\text{M}^{-1}\text{s}^{-1}$; white) and k_{off}^* (s^{-1} ; from displacement; gray) were derived from stopped-flow experiments (setup identical to 3.1.1.). Including $K_d^* = k_{off}^*/k_{on}$ (μM ; magenta), values for full-length hGBP-2 (non-hatched bars) and 2-LG (hatched bars) were plotted according to indicated mant-nucleotide.

3.3.3.2. Nucleotide binding properties of hGBP-3 constructs

Determined by equilibrium fluorescence titration, all hGBP-3 constructs, full-length, truncation aa 1-481 and also 3-LG, illustrated almost same affinities for all tested mant-nucleotides (figure 3-51). Largest difference, for instance, was found for mGMP binding performed by either full-length or truncated hGBP-3. Even in that case, obtained K_d values deviated by a factor of three only (17 μM versus 5.7 μM). Nucleotides mGMP, mGDP, mGppNHp, and mGTP γ S were bound in order of increasing affinities. K_d values of the nucleotides mGMP and mGTP γ S, which show the weakest and strongest interaction with hGBP-3, are approximately 20 to 50 times apart.

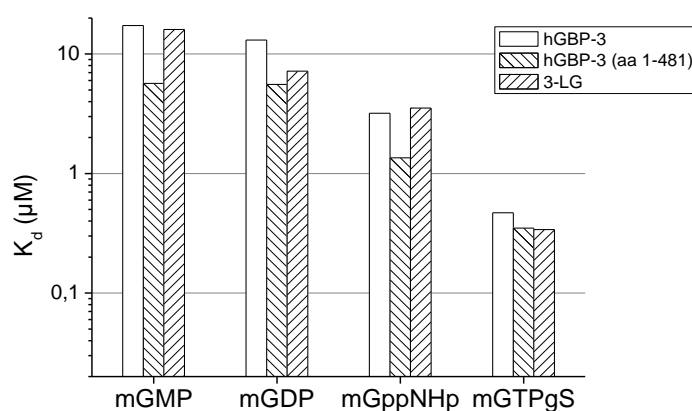


Figure 3-51: Fluorescence equilibrium titration of hGBP-3 constructs and mant-labelled nucleotides. 0.5 μM nucleotide was titrated with either full-length hGBP-3, hGBP-3 (aa 1-481) or 3-LG. Mant-nucleotide was excited at 366 nm and fluorescence increase upon binding was detected at 435 nm. Fitting the data according to equation 2 yielded equilibrium dissociation constant (K_d) for complex of protein and mant-nucleotide. A bar chart was created with determined K_d values for all hGBP-3 constructs (patterned as in legend).

Only for mant-nucleotide binding of 3-LG were performed an entire set of stopped-flow measurements, including concentration dependent association kinetics (figure 3-52, table 3-10). From that association rate constants were derived which were similar for mGMP, mGDP and mGTP γ S (1.2, 0.57 and 1.1 $\mu\text{M}^{-1}\text{s}^{-1}$). According dissociation rate constants of 11, 4.4 and 0.81 s^{-1} showed larger differences instead. Thus, likely dissociation rather than association was the determining factor for different nucleotide binding affinities provided by 3-LG. Lastly 3-LG and mGppNHp interaction which can be classified as the second strongest affinity, was characterized by an almost 5 to 10-fold slower association than seen for other nucleotides ($k_{\text{on}} = 0.10 \mu\text{M}^{-1}\text{s}^{-1}$) and also by a relatively slow dissociation ($k_{\text{off}}^* = 0.31 \text{s}^{-1}$), finally resulting in $K_d^* = 3.1 \mu\text{M}$.

Results

On both other hGBP-3 constructs, full-length and truncation, only mant-nucleotide displacement experiments were performed. Most remarkably, dissociation rate constants (k_{off}^*) obtained for each nucleotide were very similar among all hGBP-3 constructs (figure 3-52, table 3-10). Mant-GDP, for instance, dissociated from hGBP-3, hGBP-3 (aa 1-481) or 3-LG with a rate constant of either 4.7, 4.9 or 4.4 s^{-1} . Considering now that both, binding affinities and also dissociation rate constants among hGBP-3 constructs were very similar, conclusively association rates might not differ remarkably. Specifically concerning nucleotide binding properties, taken together hGBP-3 unlike hGBP-2 remained unaffected by C-terminal truncations.

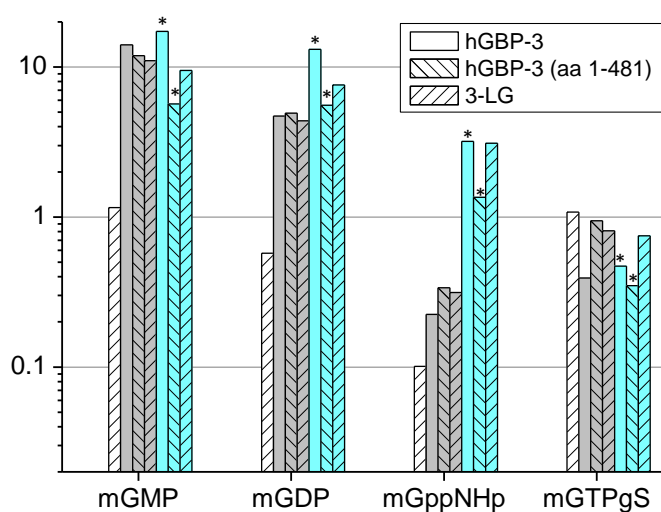


Figure 3-52: Dynamics of mant-nucleotide binding to hGBP-3 constructs. Kinetic parameters k_{on} ($\mu\text{M}^{-1}\text{s}^{-1}$; white) and k_{off}^* (s^{-1} ; gray) were derived from stopped-flow experiments (setup identical to 3.1.1.). Including $K_d^* = k_{\text{off}}^*/k_{\text{on}}$ (μM ; cyan), values obtained for full-length hGBP3, hGBP-3 (aa 1-481) and 3-LG (patterned as in legend) were plotted according to indicated mant-nucleotides. K_d values derived from titration experiments only are labelled with asterisks. All corresponding values are listed table 3-10.

3.3.3.3. Nucleotide binding properties of 1-LG and 5-LG

Compared to full-length hGBP-1, 1-LG had weaker affinities for all nucleotides. Binding of mGMP, mGDP and mGppNHp was 7-fold, 3-fold and 5-fold weaker. Highest deviation by 14-fold was obtained for 1-LG and mGTP γ S interaction. Like previously also seen for 2-FL and LG, also for hGBP-1 upon C-terminal truncation primarily nucleotide association rates were decelerated (figure 3-53 A). Of note, decelerating effects were not nearly as pronounced as for hGBP-2, dissociation rate constants for 1-LG compared to hGBP-1 were merely four to seven times slower. Effects on dissociation rates varied depending on the nucleotide. While mGMP and mGppNHp dissociated from 1-LG with almost same rates, mGDP dissociated 3-fold slower

Results

and mGTPγS even 3 times faster than obtained for full-length hGBP-1. Taken together, 4.3 μM, 14 μM, 20 μM and 2.8 μM were determined K_d values of 1-LG binding to mGMP, mGDP, mGppNHp and mGTPγS. Still in the same manner as its full-length counterpart, also 1-LG bound to mGMP and mGTPγS with higher affinities while binding of mGDP and mGppNHp was weaker.

Finally, also nucleotide binding parameters of 5-LG were determined. Equilibrium titration experiments revealed that 5-LG among all tested protein constructs provided weakest interactions with all nucleotides (figure next, B). The highest affinities were found for 5-LG-mGTPγS (19 μM) and 5-LG-mGDP (9.8 μM). Kinetics of latter complex was additionally investigated by stopped-flow experiments. A very slow association ($k_{on} = 0.045 \mu\text{M}^{-1}\text{s}^{-1}$) and almost ten times faster dissociation ($k_{off} = 0.44 \text{ s}^{-1}$) were obtained. Binding of mGppNHp and mGMP required significantly higher protein concentrations resulting in respective dissociation constants above 100 μM. Although 2-LG already was shown to bind mGMP only weakly, obtained K_d value of 604 μM for 5-LG-mGMP indicated even weaker binding. In fact, dissociation constant being at least one order of magnitude higher than obtained for any other hGBP construct calls into question whether 5-LG provided GMP binding has any biological relevance. Also for full-length hGBP-5 under low salt conditions GMP binding could not be ascertained (Wehner, et al., 2010).

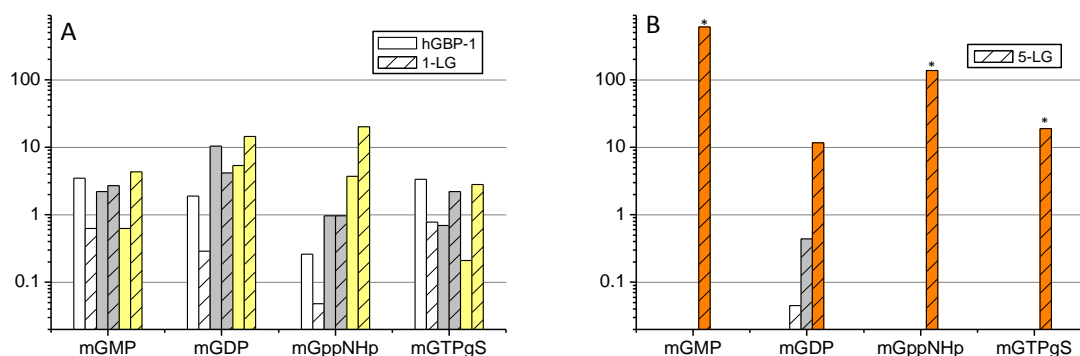


Figure 3-53: Dynamics of mant-nucleotide binding to hGBP-1 constructs and 5-LG. Kinetic parameters k_{on} ($\mu\text{M}^{-1}\text{s}^{-1}$; white) and k_{off} (s^{-1} ; gray) were derived from stopped-flow experiments (setup identical to 3.1.1.). (A) Kinetic parameters of either full-length hGBP-1 or 1-LG provided mant-nucleotide binding were plotted for comparison (pattern as indicated in legend). K_d values (μM , yellow) were calculated by the ratio k_{off}/k_{on} . (B) Equilibrium dissociation constants of 5-LG-mant-nucleotide (orange) were derived from titration experiments as indicated by asterisks. Kinetic parameters were determined only for mGDP binding. All corresponding values are listed in table 3-10.

Results

Table 3-10: Kinetic and equilibrium constants for mant-nucleotide interactions with hGBP constructs. Stopped-flow measurements yielded k_{on} , k_{off} (intercept), and k_{off}^* (displacement) values. Dissociation constant K_d^* was calculated by the ratio k_{off}^*/k_{on} , only when k_{off}^* was not determined the ratio k_{off}/k_{on} was used instead. Corresponding dissociation constants K_d obtained via fluorescence equilibrium titration are listed in the very right column. (–): not determined; (**): no detectable signal. All measurements were carried out at 25°C and in buffer C containing 150 mM NaCl.

		k_{on} ($\mu\text{M}^{-1} \text{s}^{-1}$)	k_{off} (s^{-1})	k_{off}^* (s^{-1})	K_d^* (μM)	K_d (μM)
hGBP-1	mGMP	3.5	2.2	2.2	0.63	
	mGDP	1.9	9.8	10.4	5.4	
	mGppNHp	0.26	1.1	0.96	3.7	
	mGTPyS	3.3	0.69	---	0.21	
1-LG	mGMP	0.63	2.1	2.7	4.3	3.7
	mGDP	0.29	4.2	---	14	---
	mGppNHp	0.048	1.5	0.97	20	16
	mGTPyS	0.78	2.2	---	2.8	---
hGBP-2	mGMP	1.1	1.7	2.0	1.9	1.7
	mGDP	0.56	(-0.39)	0.042	0.075	0.049
	mGppNHp	0.15	(-0.023)	0.016	0.10	0.16
	mGTPyS	0.95	(-0.26)	0.064	0.067	0.050
2-LG	mGMP	0.0085	2.4	1.8	212	200
	mGDP	0.012	0.0053	0.0038	0.32	0.59
	mGppNHp	0.0026	0.061	0.092	35	27
	mGTPyS	0.018	0.030	0.056	3.1	2.2
hGBP-3	mGMP	---	---	14	---	16.3
	mGDP	---	---	4.7	---	12.7
	mGppNHp	---	---	0.22	---	3.58
	mGTPyS	---	---	0.39	---	0.49
3-LG	mGMP	1.2	10	11	9.5	16
	mGDP	0.57	4.5	4.4	7.6	7.2
	mGppNHp	0.10	0.22	0.31	3.1	3.5
	mGTPyS	1.1	(-0.52)	0.81	0.75	0.34
hGBP-3 (aa 1-481)	mGMP	---	---	12	---	5.7
	mGDP	---	---	4.9	---	5.6
	mGppNHp	---	---	0.34	---	1.4
	mGTPyS	---	---	0.94	---	0.35
5-LG	mGMP	**	**	---	---	604
	mGDP	0.045	0.4403	---	9.8	12
	mGppNHp	**	**	---	---	138
	mGTPyS	---	---	---	---	19

3.3.4. Nucleotide dependent homo interactions of hGBPs - analytical SEC

3.3.4.1. Analytical SEC of full-length hGBPs bound to different GTP analogs

In order to investigate the complexes formed by all protein constructs in the absence and presence of nucleotides, 20 μ M protein was applied to analytical gel filtration column. Besides nucleotide-free state, GTP analogues GDP·AlF_x, GTP γ S and GppNHp were investigated for their capacity to induce homo interactions. Elution buffer (buffer C) contained either no or 250-320 μ M nucleotide.

In paragraph 3.1.3., nucleotide dependent SEC of hGBP-1 was already presented in detail. To summarize, hGBP-1 being monomeric in the nucleotide-free state remained so when either GppNHp or GTP γ S were offered. Derived from elution volumes, obtained weights were 94, 97 and 90 kDa respectively. Only when bound to GDP·AlF_x was hGBP-1 enabled to form a complex, probably a dimer, with a corresponding weight of 274 kDa. For comparison, elution chromatograms are depicted in figure 3-54 and corresponding values are listed in table 3-11.

Almost same results as for hGBP-1 were obtained for hGBP-2. In the absence of nucleotide, hGBP-2 eluted at an apparent size of 97 kDa which is most likely a monomer in view of hGBP-1s monomer elution size. A clear hGBP-2 complex with a molecular weight of 287 kDa emerged only in presence of GDP·AlF_x. Again, protein was mainly monomeric when bound to GppNHp or GTP γ S, obtained molecular weights were 89 kDa and 97 kDa. Interestingly, hGBP-1 and hGBP-2 having a theoretical molecular weight of 68 kDa and 67 kDa, constitute also very similar apparent monomer sizes on SEC. That might give a hint to similar structural arrangement of both proteins, with special allusion to the elongated shape of hGBP-1.

The third member investigated, namely hGBP-3 illustrated an entirely deviating picture. Independent from the nucleotide offered and also in absence of any nucleotide elution volumes were always around 1.4 ml. Apparent weights of hGBP-3 were determined to 147, 166, 122 and 146 kDa when nucleotide-free, bound to GDP·AlF_x, GppNHp or GTP γ S. Due to known instability of hGBP-3, before going to interpretation same protein batch was analyzed by SDS-PAGE first (data not shown). Since appearing as a dimer under denaturing SDS conditions, upon storage obviously covalent dimers were formed, thus analytical SEC data were not suitable.

Results

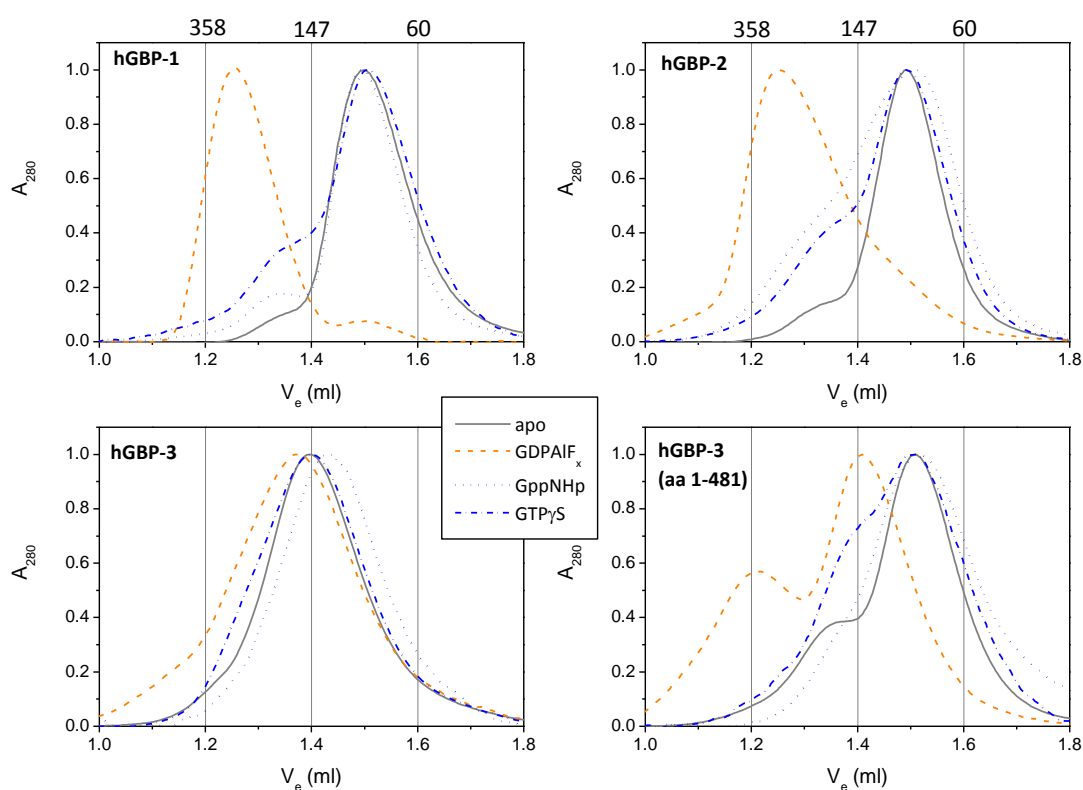


Figure 3-54: Analytical SEC of full-length hGBP isoforms in absence and presence of GTP-analogs. 20 μM of hGBP-1, hGBP-2, hGBP-3, or truncated hGBP-3 (aa1-481) were applied to SEC column containing either no or 250 – 320 μM of nucleotide (GDP-AlF_x, GppNHp, GTP γ S; colors and line style as denoted). Each run normalized by its maximum value was plotted according to indicated protein isoform. Obtained elution volumes as well as according molecular weights are summarized in table 3-11. To orientation, MW_{SEC} of 358, 147, and 60 kDa at elution volumes 1.2, 1.4 and 1.6 ml (grid lines), respectively, are denoted.

To ever gain any information about the complex formation behavior of hGBP-3, alternatively, the truncated protein hGBP-3 (aa 1-481) was examined under same conditions (figure 3-54). Although truncated by 114 amino acids and thus comprising a theoretical molecular weight of 54 kDa, protein in nucleotide-free state eluted at same volume as full-length hGBP-1 and hGBP-2 monomers. This behavior was previously observed also for corresponding construct of hGBP-1 (Benscheid, 2005) (Syguda, et al., 2012). Lack of helices α 12-13 obviously did not alter overall elongated shape and hydrodynamic radius of hGBP-1 so that by elution volume only truncation was not distinguishable. The same might be true also for hGBP-3 which would give a hint to the structural arrangement. However, obtained value of 90 kDa for nucleotide free hGBP-3 (aa 1-481) was exactly the same also for GppNHp or GTP γ S bound protein. A smaller peak at elution volume around 1.4 ml indicating a minor fraction of

Results

apparently bigger complex was visible already in the nucleotide-free state. Upon binding to GppNHp, however, it disappeared but became even more pronounced in presence of GTP γ S. Offering GDP·AlF_x clearly led to a shift of elution profile which suggested homo complex formation of the protein. Two peaks were detectable that due to proportions most probably emerged out of the two species already observed in the nucleotide-free state. Minor and major peaks comprised molecular weight of 329 kDa and 141 kDa, respectively. It was difficult to classify the resulting peak at 141 kDa as dimer since it altered from assumed monomer of 90 kDa by only 51 kDa. On the other hand, the covalent dimer of full-length hGBP-3 had the same apparent size. Therefore, the 141 kDa species is most likely a dimer.

Among all GTP-analogs tested, GDP·AlF_x was the most potent complex inducer for all hGBP isoforms hGBP-1, -2 and -3. However, this is in clear contrast to hGBP-5 which does not form higher complexes in presence of GDP·AlF_x, most likely due to impaired binding of AlF (Wehner, et al., 2010).

Table 3-11: Results of analytical SEC performed with full-length hGBP isoforms. Elution volumes (V_e) of the proteins in the absence or presence of indicated nucleotides were divided by the void volume (V_0) obtained with Blue Dextran. The ratio V_e/V_0 evaluated according to calibration in paragraph 3.1.3.1. yielded listed molecular weight (MW_{SEC}). The last column indicates the nature of the complex, marked with (*) if not well definable.

	Nucleotide	V_e (ml)	V_e/V_0	MW_{SEC} (kDa)	Complex
hGBP-1	No	1.5	1.563	94	Monomer
	GDP·AlF _x	1.26	1.313	274	Dimer
	GppNHp	1.492	1.554	97	Monomer
	GTP γ S	1.51	1.573	90	Monomer
hGBP-2	No	1.492	1.554	97	Monomer
	GDP·AlF _x	1.25	1.302	287	Dimer
	GppNHp	1.511	1.574	89	Monomer
	GTP γ S	1.492	1.554	97	Monomer
hGBP-3	No	1.399	1.457	147	*Dimer*
	GDP·AlF _x	1.373	1.430	166	*Dimer*
	GppNHp	1.442	1.502	122	*Dimer*
	GTP γ S	1.401	1.459	146	*Dimer*
hGBP-3 (aa 1-481)	No	1.509	1.572	90	Monomer
	GDP·AlF _x	1.219 (34%)	1.270	329	*Tetramer*
		1.409 (66%)	1.468	141	Dimer
	GppNHp	1.51	1.573	90	Monomer
	GTP γ S	1.51	1.573	90	Monomer

3.3.4.2. Oligomerization of LGs in the presence of GTP analogs

The complex formation of the hGBP LG domains was investigated by analytical SEC in the presence or absence of nucleotides. Therefore, 20 μ M protein diluted in buffer C without or with respective nucleotide was applied onto the column. As preliminary study for LGs homo and hetero interaction, in particular, GTP analogs GDP·AlF_x, GppNHp and GTP γ S were investigated for their potency to induce LGs complexes. All obtained elution volumes as well as the correlating molecular weights are summarized in table 3-12.

All LGs having a theoretical molecular weight of approximately 35 kDa eluted as monomer in the nucleotide-free state (figure 3-55). According to a calibration curve 1-LG, 3-LG and 5-LG eluted at volumes corresponding to a calculated molecular weight (MW_{SEC}) of 39 kDa, 38 kDa and 42 kDa, respectively. Also most likely a monomer, 2-LG eluted earlier and revealed an apparent size of 50 kDa. Being significantly above the theoretical molecular weight of a monomer but not sufficient to categorize as a dimer, 2-LG compared to the other LGs might have a larger hydrodynamic radius.

While all the full-length hGBP constructs formed complexes only in the presence of GDP·AlF_x (see paragraph 3.3.4.1.), remarkably, some of the LGs dimerized also in the presence of GppNHp and GTP γ S. The LG domains of hGBP-1 and hGBP-2, particularly, dimerized irrespective of the GTP analog offered (figure 3-55). The experimentally obtained molecular weights of 1-LG dimers spread within the range of 69-76 kDa, whereas dimers of 2-LG appeared to be slightly bigger, namely, between 82 and 86 kDa.

Unlike 1-LG and 2-LG, 3-LG and 5-LG dimerized only in the presence of particular GTP-analogs. A clear homo dimer of 3-LG was observed only in presence of GDP·AlF_x (MW_{SEC} = 76 kDa). When bound to GTP γ S, 3-LG resembled the 2-LG monomer. It became apparently bigger than monomeric 3-LG (MW_{SEC} = 50 kDa) but was still smaller than the GDP·AlF_x induced dimer. In order to assign, whether the peak comprised a mixture of monomeric and dimeric 3-LG, an equilibrium shift was intended by increasing protein concentration (data not shown). Also at 3-LG concentration five-fold higher than before, neither V_e nor the shape of the peak altered. Consequently, whether GTP γ S bound 3-LG is either a very dense dimer or a bulky monomer remains elusive. And finally, 3-LG other than all the tested LGs remained monomeric when bound to GppNHp (MW_{SEC} = 37 kDa).

Results

Among the investigated LG domains, remarkably, 5-LG was the only one that did not form dimers in presence of GDP·AlF_x. With an apparent size of 41 kDa, it is perfectly comparable to the nucleotide free monomer (MW_{SEC} = 42 kDa). Similar results have been obtained for full-length hGBP-5 previously and the defective homo assembly has been assigned to impaired binding of AlF_x (Wehner, et al., 2010). The same impact appears most likely to prevent also 5-LG from dimerization. However, binding of either GppNHp or GTPγS induced similarly enlargement of the 5-LG size (63 and 66 kDa) which was most likely due to homo dimerization

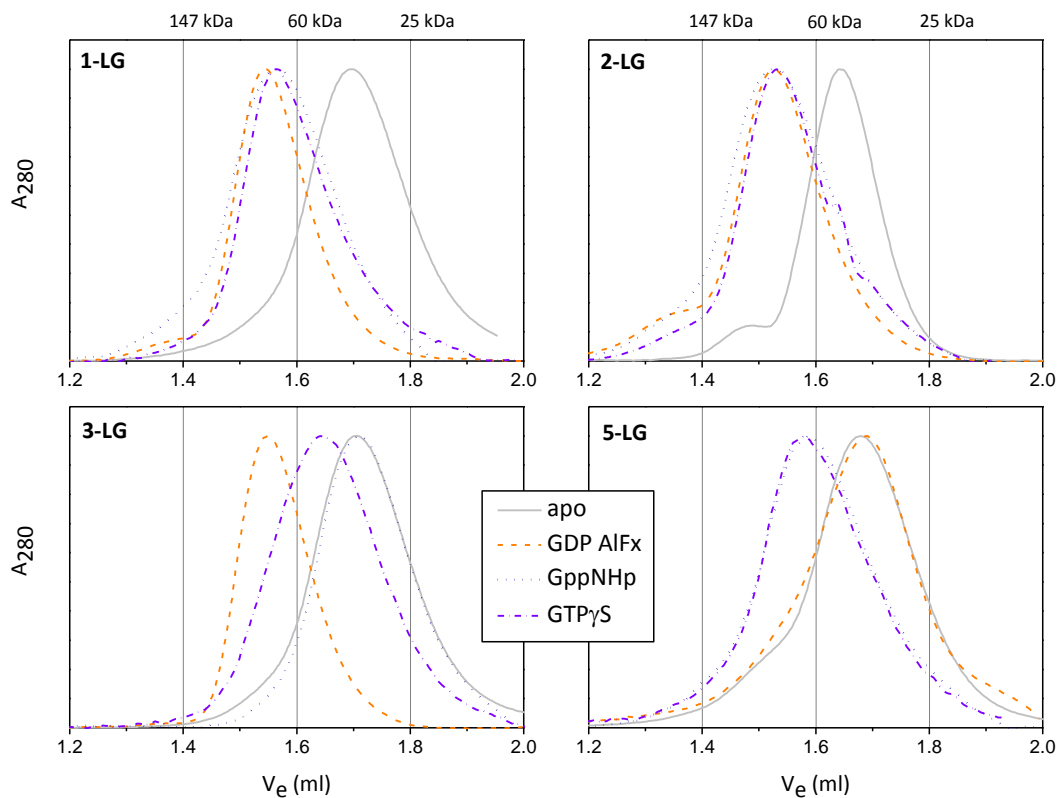


Figure 3-55: Analytical SEC of hGBP LG domains in the absence and presence of GTP-analogs. 20 μM of 1-LG, 2-LG, 3-LG and 5-LG were applied to the SEC column containing either no (apo, gray) or 250 – 320 μM of indicated nucleotide (GDP·AlF_x (orange), GppNHp (blue), GTPγS (violet)). Each run normalized by the maximum value was plotted according to the protein isoform as indicated. Obtained elution volumes as well as according molecular weights are summarized in table 3-12. To orientation, MW_{SEC} of 147, 60 and 25 kDa at elution volumes 1.4, 1.6 and 1.8 ml are depicted.

Results

Table 3-12: Results of analytical SEC performed with hGBP LG domains. Elution volumes (V_e) of the proteins in the absence or presence of indicated nucleotides were divided by the void volume (V_0) obtained with Blue Dextran. V_e/V_0 was put into the linear equation of calibration (see paragraph 3.1.3.1.) yielding the listed molecular weight (MW_{SEC}). The last column indicates the nature of the complex; not clearly definable complexes are marked with an asterisk.

	<i>Nucleotide</i>	V_e (ml)	V_e/V_0	MW_{SEC} (kDa)	<i>Complex</i>
1-LG	<i>No</i>	1,699	1,770	39	Monomer
	<i>GDP·AIF_x</i>	1,548	1,613	76	Dimer
	<i>GppNHp</i>	1,57	1,635	69	Dimer
	<i>GTPγS</i>	1,563	1,628	71	Dimer
2-LG	<i>No</i>	1,642	1,710	50	Monomer
	<i>GDP·AIF_x</i>	1,53	1,594	82	Dimer
	<i>GppNHp</i>	1,52	1,583	86	Dimer
	<i>GTPγS</i>	1,53	1,594	82	Dimer
3-LG	<i>No</i>	1,702	1,773	38	Monomer
	<i>GDP·AIF_x</i>	1,549	1,614	76	Dimer
	<i>GppNHp</i>	1,709	1,780	37	Monomer
	<i>GTPγS</i>	1,642	1,710	50	*Dimer*
5-LG	<i>No</i>	1,679	1,749	42	Monomer
	<i>GDP·AIF_x</i>	1,688	1,758	41	Monomer
	<i>GppNHp</i>	1,591	1,657	63	Dimer
	<i>GTPγS</i>	1,579	1,645	66	Dimer

3.4. Homo and hetero interactions of hGBPs measured by intermolecular FRET

In vivo, human GBPs were shown to homo and hetero dimerize in a nucleotide dependent and hierarchical manner (Britzen-Laurent, et al., 2010). Using recombinant proteins, we intended to elucidate the GBPs interaction network *in vitro*. In particular, we were interested in the quantitative parameters which ground the basis for the hierarchy of homo and hetero interactions. Therefore, a setup needed to be established that easily and reliably allows monitoring and quantifying GBPs interactions.

The GTP hydrolysis assay and SEC were the common approaches to investigate the complex formation of the hGBP isoforms, particularly the homo interactions. Due to altering elution volumes of different sizes, SEC is a qualitative method that allows monitoring whether complex is formed or not. The GTP hydrolysis assay is an indirect method exploiting the stimulation of GTP turnover accomplished by concentration dependent dimerization of the protein. Although latter one allows quantifying the monomer-dimer equilibrium when an appropriate protein concentration range is assayed, it fails for example when the GTPase activity is deficient.

Both methods have limitations that become even more pronounced when it comes to studies of hGBP hetero interactions, which in fact are crucial to understand the proteins intracellular communication and function. When two putative GBP interaction partners are mixed to assay their GTPase activity, the hardest challenge is to extract the contribution of a single isoform. A multiple set of varying concentrations of each partner is then required to obtain reliable quantitative parameters. As an alternative, one could introduce mutations such as R48A for hGBP-1 that have an impact on the GTPase activity. Thus, one partner could be silenced while the altering GTPase features of the other could be monitored. Even then, interaction of different isoforms does not necessarily need to stimulate GTP turnover. In other words, no difference in the enzymatic activity does not mean, that different investigated isoforms do not interact at all. However, to initially state whether hetero dimerization *in vitro* occurs or not, each approach based on the enzymatic activity is far too complicated.

The size exclusion chromatography on the other hand is not suitable at all, since all isoforms share similar molecular weights. Even when different hGBP isoforms dimerize, the formed homo dimers will elute at the same time, so that a clear assignment to homo or heterodimers becomes impossible.

Consequently FRET turned out to be the method of choice to investigate the intermolecular interactions between two different hGBP isoforms. Depending on the spatial proximity of fluorescently labelled proteins, the change in fluorescence signal gives a direct measure of the interaction.

3.4.1. Unspecific labelling of hGBP LG domains with fluorescent dyes

In our lab, site selective coupling of hGBP-1 with sulfhydryl-reactive Alexa dyes for subsequent inter- and intramolecular FRET measurements was successfully established. Therefore, human GBP-1 carrying nine cysteine residues distributed all across the protein was mutated such that all natural cysteines were replaced. Instead, at the positions of interest one or two new cysteine residues were introduced for site specific fluorophore coupling. Here, we tried to establish the unspecific labelling of hGBP-1 and other hGBP isoforms, using the same fluorophores but wild type proteins containing all natural cysteine residues (at least nine), instead. For the purpose of hGBP hetero interaction studies, the unspecific labelling is advantageous for several reasons. In the first line, fluorophore can covalently bind to any accessible cysteine, so that an extended area of the proteins can be elucidated for involvement in interaction. Additionally, mutagenesis constituting the risk of impact on proteins structure and function can be avoided.

On the other hand, unspecific labelling unlike specific labelling does not give the opportunity to control the dyes localization within the protein. In the worst case, donor and acceptor within the protein complex could be too distant for energy transfer to occur. That risk remains at least for full length hGBP-1 having an elongated shape but an unknown dimer arrangement. In contrast, structures of isolated LG domain (1-LG) dimers could be solved successfully (Ghosh, et al., 2006). According to the GDP·AIF_x bound LG dimer, the largest obtainable distance between two cysteine residues was found to be 60.4 Å (C α -C α ; figure 3-56). Thus, FRET couple Alexa488 and Alexa647 with a Förster radius of 52 Å should be capable of monitoring 1-LG dimers. Further, the LG domains of hGBP-1, -2 and -3 were shown to mediate homo dimerization (see paragraph 3.3.4.2.). Since they comprise also a high level of sequence homology, it is highly probable that also hetero interaction is mediated by the same. Thus, we decided to establish the FRET-based hGBP interaction studies first on the isolated LG domains.

Results

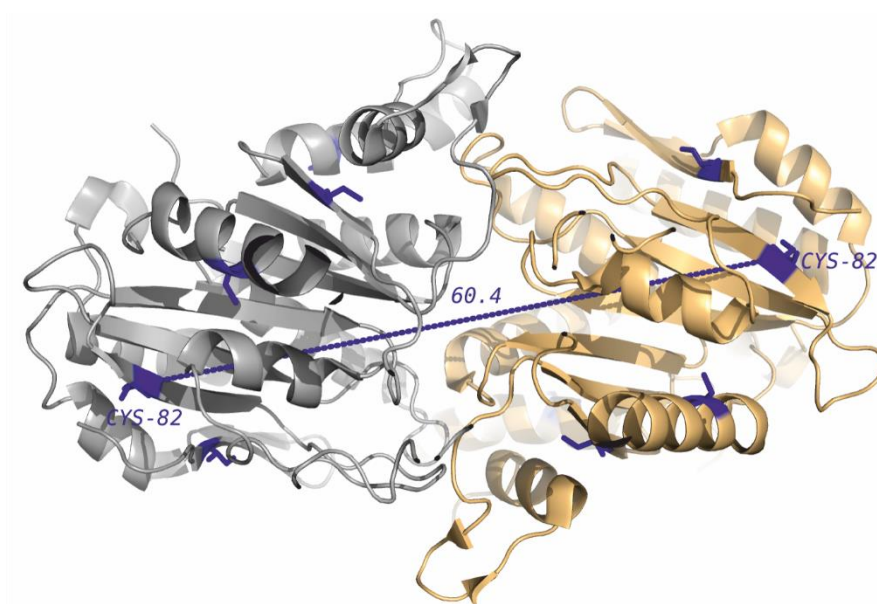


Figure 3-56: Cysteine residues within the dimer structure of GDP-AIF_x bound 1-LG dimer with highlights (pdb:2b92). Each of the monomer (Chain A: gray, chain B: yellow) contains five cysteine residues highlighted in blue. The largest intermolecular distance was obtained between two cysteines each at position 82 (C_{α} - C_{α} = 60.4 Å).

3.4.1.1. Determining concentrations and labelling efficiency

For labelling, two to three fold molar excess of fluorophore over 50-100 μ M protein (LG domains of hGBP-1, -2, -3, -5) was applied. After incubation for 1 hour at 4°C, non-bound fluorophores were removed using desalting spin columns or centrifugal concentrators (10,000 MW cutoff). Protein and fluorophore concentration as well as labelling efficiency were determined as described in paragraph 2.3.11.4. Obtained values together with the molar extinction coefficient for individual LG isoform (Gasteiger, et al., 2005) (H_2O as solvent) are summarized in table 3-13.

While all the other proteins were optically in good shape after labelling, for unknown reasons, 1-LG turned out to be very sensitive to Alexa488; by the end of the labelling procedure, the protein was highly precipitated. Thus, labelling procedure of 1-LG with Alexa488 in the second trial was optimized with respect to several parameters. First, 500 μ M GMP was added to 100 μ M 1-LG, considering that nucleotide binding stabilizes the protein. Additionally, fluorophore concentration was reduced to 1.5-fold over protein. Also incubation time was reduced to 30 minutes while incubation temperature was kept at 4°C. Indeed, visibly no precipitation occurred, so protein was concentrated with a centrifugal concentrator, until the volume was $\leq 100 \mu$ l. Then protein was diluted with 4 ml buffer C containing DTT and

Results

concentrated in the same manner. This cycle was repeated for two more times in order to completely remove both unbound fluorophore and GMP previously added to the reaction mixture.

Finally, constructs 1-LG, 2-LG, 3-LG and 5-LG could be successfully labelled with dyes Alexa488 (donor, D) and Alexa 647 (acceptor, A), respectively. The protein concentration was at least 36 μM (1-LG labelled with donor). More efficiently than acceptor fluorophore Alexa647, donor fluorophore Alexa488 could be coupled to each LG domain, yielding always a higher labelling efficiency for the same construct. In general, labelling efficiency ranged between 0.69 and 2.88 for acceptor labelled 3-LG (3A) and donor labelled 5-LG (5D), respectively (table 3-13). When fluorophores within a protein molecule are assumed to be equally distributed, only 69 % of 3-LG molecules might carry a single acceptor dye while 31 % remained unlabelled. Accordingly, each 5-LG molecule is supposed to carry at least two up to three donor dyes.

Table 3-13: Obtained protein concentrations and labelling efficiencies (LE) of labelled hGBP LGs. Listed extinction coefficients were calculated by Expassy - ProtParam⁴ (an online tool considering water as solvent) and used to determine the protein concentration according to the Beer-Lambert law. LG domain constructs are abbreviated by their isoform number and the fluorophore dye they carry, D and A for donor Alexa488 and acceptor Alexa647, respectively.

<i>Protein</i>	<i>Protein concentration</i> (μM)	<i>LE</i>	ϵ_{280} $\text{M}^{-1} \text{cm}^{-1} (\text{H}_2\text{O})$
1D	36	1.83	35,410
1A	61	0.88	
2D	98	2.40	39,420
2A	92	1.26	
3D	85	1.35	35,410
3A	51	0.69	
5D	105	2.88	30,940
5A	55	1.57	

⁴ <http://web.expasy.org/protparam/>

3.4.1.2. Impact of labelling on basic features of the protein

Representative for the other LGs, 1-LG was tested for any impact that labelling might had on the protein. First, to test whether aggregates were formed, 20 μM protein was analyzed by analytical size exclusion chromatography. None of the protein contained considerable amounts of aggregates since no significant peak was detected at V_0 (0.96 ml). The same as non-labelled protein, acceptor (1A) and donor (1D) labelled protein eluted as monomer (figure 3-57 B). As a difference, the peak of 1D appeared broader with a tailing to higher elution volumes. However, any degradation could be excluded after analyzing the same proteins by denaturing SDS-PAGE showing no more bands than the one corresponding to monomer protein (figure 3-57 A).

Subsequently, GTPase activity of the labelled proteins was determined for 1.5 μM protein concentration. While non-labelled 1-LG had a catalytic activity of 20.5 min^{-1} , it was 18.0 min^{-1} and 2.7 min^{-1} for 1A and 1D, respectively. Although optimizing the labelling with Alexa488 (donor fluorophore) apparently diminished 1-LGs precipitation, a significant impact by almost one order of magnitude on the GTPase activity could be found, nevertheless. However, time dependent FRET measurements with GTP and analogs demonstrated that 1D being impaired in enzymatic activity is still competent to dimerize (see paragraph 3.4.2.).

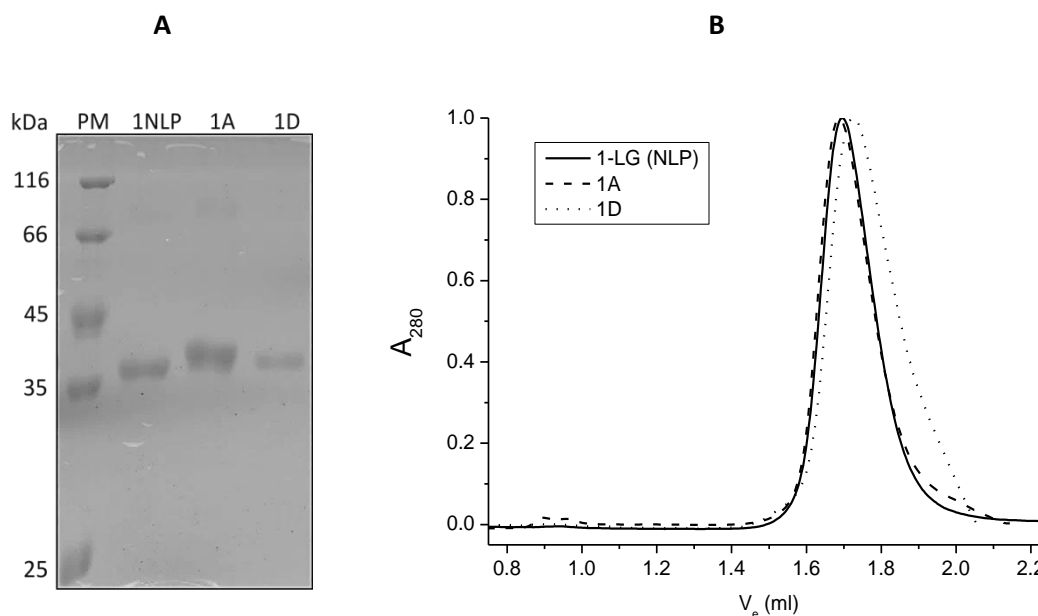


Figure 3-57: Analysis of Alexa labelled 1-LG via SDS-PAGE and analytical SEC. Protein was diluted to 20 μM and applied to the gel filtration column (B) and to an SDS-polyacrylamide gel (A) after mixing 1:1 with 2x sample buffer. Non-labelled protein (NLP) as well as labelled proteins (1A, 1D) elute as monomer, no considerable amounts of aggregates were detected (Expected at $V_0 = 0.96$ ml). Also SDS-PAGE shows a single prominent band for each protein corresponding to monomer size.

3.4.2. Nucleotide dependent homo dimerization of 1-LG

Until now, a lot of effort was made to characterize the LG domain mediated homo dimerization of hGBP-1. For the isolated LG domain, dimerization was shown to appear in a nucleotide dependent fashion. Serving as substrate, GTP induces dimerization of the LG domain and so do all non-hydrolysable GTP-analogs, namely GDP·AlF_x, GppNHp, GTPγS. Exactly that dependency was exploited to check if kinetic FRET measurements with fluorescently labelled 1-LG is a suitable approach to monitor dimerization. As only donor was excited (498 nm) but acceptor emission was detected (664 nm), an increase of the fluorescence was expected to occur only when the donor comes in sufficient proximity of the acceptor molecule to provide energy transfer. Thus any fluorescence increase detected here is supposed to be a direct reporter of proteins dimerization. Since dimerization is also concentration dependent, we decided to perform the measurements with 1.5 μM protein. As known from the GTPase assay, at a protein concentration of 1.5 μM equilibrium is shifted almost completely to the dimer state. Therefore, 0.75 μM donor and 0.75 μM acceptor labelled 1-LG (referred to as 1D and 1A, respectively), in sum, 1.5 μM of protein was mixed and preincubated before dimerization was started by nucleotide addition.

When a stable signal was obtained either 250 μM GTPγS or GDP (for formation of GDP·AlF_x, buffer contained already 10 mM NaF and 300 μM AlCl₃) was added at t₀ = 0 seconds. Due to the weaker binding, GppNHp was adjusted to a final concentration of 500 μM. All GTP analogs succeeded to induce a significant increase in fluorescence being most probably a result of nucleotide dependent 1-LG dimerization (figure 3-58, left panel). The usage of the genuine hydrolysable substrate GTP (650 μM), instead, yielded a reversible FRET signal (figure 3-58, right panel) confirming that obtained fluorescence increase is a direct reporter of 1-LG dimers formed; 1-LG dimers associate upon substrate binding and dissociate after substrate conversion, both steps represented by an increase and a subsequent decrease of the fluorescence, respectively.

Moreover, depending on the GTP analog added, fluorescence increased to different levels (figure 3-58). Taking into account that, firstly, 1-LG concentration was kept constant in each run and, secondly, fluorescence increase is proportional to 1-LG dimer concentration, the different levels of final fluorescence can give an idea about the strength of the 1-LG dimers induced by individual analog. Thus, GDP·AlF_x bound dimers are supposed to have the highest affinity, followed by the GTPγS bound dimers. GppNHp induced dimers, instead, seem to have the lowest affinity. These comparisons, indeed, need to be considered with care since there

Results

are some critical factors that can distort the FRET signal. Exemplarily, each of the nucleotide might induce dimers that have different arrangements which can affect both the environment of a single dye and also the relative orientation of FRET couple dyes, consequently leading to altering FRET efficiencies. Particularly when fluorophores are located in more flexible protein regions the effects might be even more pronounced. Thus, comparison of K_d values for different GTP analog bound dimers, like done here, need to be confirmed at least by protein concentration dependent studies for each. Kinetics and total change in fluorescence, however, can be considered to define the most suitable nucleotide for the following interaction studies.

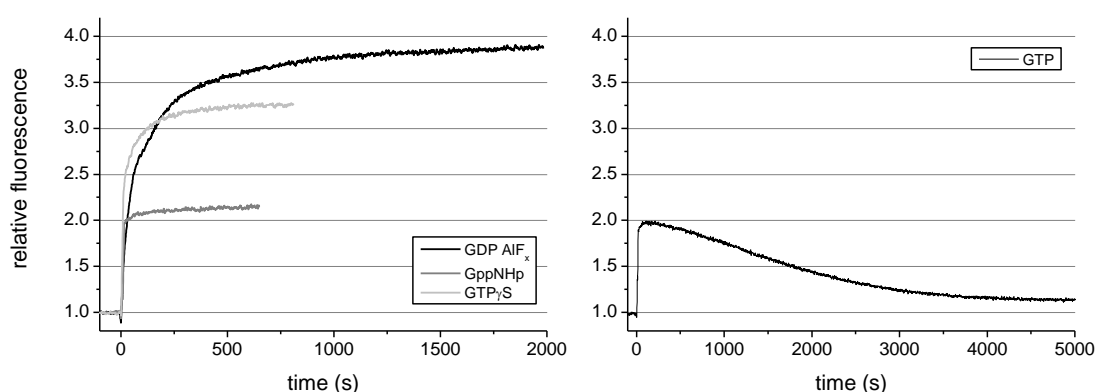


Figure 3-58: Nucleotide dependent dimerization of labelled 1-LG measured by FRET. 0.75 μM 1A, 0.75 μM 1D were mixed and monitored for 2-5 minutes until fluorescence signal was stable. Donor was excited at 498 nm, acceptor emission was detected at 664 nm. Dimerization reported by an increase of fluorescence was started by addition of nucleotide at $t_0 = 0$ s (250 μM GDP and GTP γ S, 500 μM GppNHp, 650 μM GTP). Analogs yielded an irreversible increase to different levels depending on the nucleotide added (left panel). GTP due to hydrolysis yielded a reversible increase; signal decreased upon GTP conversion and dimer dissociation (right panel).

In the next step, we investigated whether dimer dissociation seen in the course of GTP turnover can be shown also for the GTP analog bound dimers. Therefore, 3 μM non-labelled 1-LG was added to the preformed complexes from figure 3-58 (left panel), in order to generate mixed dimers (LP:NLP) which are not detectable FRET pairs and thus should cause fluorescence decrease (figure 3-59). Remarkably, only a two-fold excess of NLP over LP succeeded to dissociate a significant amount of the GTP γ S bound LP:LP dimers, indicated by a slow fluorescence decrease. A single exponential fit yielded the rate constant $k_{\text{diss}} = 0.0093 \text{ s}^{-1}$. Strangely, only a little fraction of the dimers could be dissociated when bound to GppNHp or GDP·AIF $_x$, faster than could be resolved by the setup.

Results

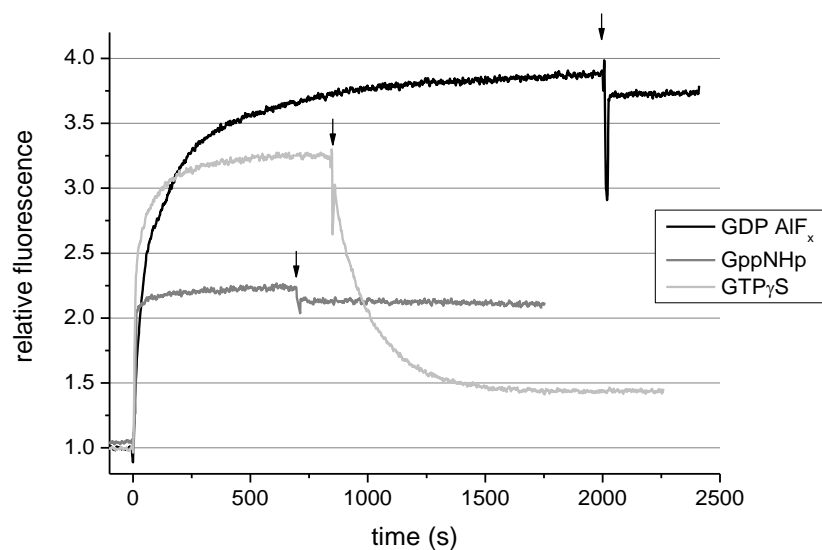


Figure 3-59: Dissociation of GTP analog bound 1-LG dimers. At indicated time points (arrows) 3 μM NLP 1-LG was added to preformed LP dimers (see figure 3-58). Indicated by decreasing fluorescence, upon LP:NLP interactions LP dimers dissociated to different extent, mostly pronounced for GTP γ S bound dimers.

Taken together, GTP and all its analogs applied to fluorescently labelled 1-LG induced an increase of the fluorescence signal that could be assigned to 1-LG dimerization. Consequently, the choice of Alexa488 and Alexa647, a couple with a Förster radius of 52 Å, revealed to be suitable for FRET based dimerization studies, at least for 1-LG.

3.4.3. GDP·AlF_x dependent homo and hetero dimerization of LG domains

3.4.3.1. Homo dimerization of LGs with GDP·AlF_x

Homo dimerization of 1-LG, 2-LG and -3-LG was previously confirmed via GTP hydrolysis assay. Obtained K_d values for dimer formation revealed the hGBP-1 dimer to be the tightest, followed by the hGBP-2 and hGBP-3 homo dimers being weaker by one order of magnitude. Further, size exclusion chromatography demonstrated that 1-LG, 2-LG and 3-LG dimerize when bound to GDP·AlF_x. Here we used Alexa labelled LG domains to address the same issue under FRET conditions. For comparison, donor and acceptor concentration was kept at 0.75 μM each, and dimerization was induced by addition of 250 μM GDP into the AlCl₃ and NaF containing buffer. A significant increase in fluorescence was observed for the LG domains of hGBP-1, -2,

Results

and -3, respectively (figure 3-60), indicating that a considerable amount of the protein forms homo dimers at given concentration. The FRET signal of 5-LG, instead, remains almost at the same level as the initial fluorescence (before nucleotide addition). Like previously observed by analytical SEC (paragraph 3.3.4.2.), also FRET data here confirm that 5-LG is the only isoform that in the presence of GDP·AlF_x does not form detectable amounts of dimers.

Considering only fluorescence intensity is not sufficient to judge about the strength of the homo dimers. Labelling efficiency and location of the dyes, for instance, have already been mentioned as distorting parameters. However, it is likely that 1-LG in comparison to the other LGs forms the tightest homo dimers since the maximum fluorescence levels here are accompanied by kinetics which is the fastest for 1-LG homo dimerization and slower for 2-LG and 3-LG.

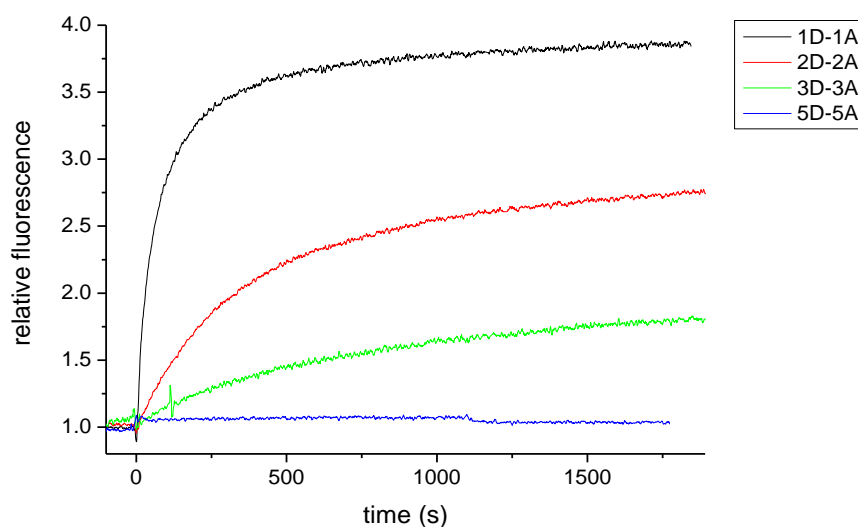


Figure 3-60: Time traces of GDP·AlF_x induced LG homo dimerization. In buffer C containing 10 mM NaF and 300 μ M AlCl₃, donor (D) and acceptor (A) labelled proteins were diluted to a final concentration of 0.75 μ M, each. Initial fluorescence was recorded and at time point zero dimerization was started by adding 250 μ M GDP. 1-LG yielded the fastest dimer association with the highest fluorescence level. Kinetics and the overall fluorescence change was slower and less for 2-LG and 3-LG, respectively. Fluorescence of 5-LG did not increase significantly, suggesting that the protein does not dimerize under given conditions.

3.4.3.1.1. *Correction for the labelling efficiency*

The maximum fluorescence levels obtained in the last figure, theoretically, should reflect the dimer concentration and thus, the different affinities of each homo dimer. Accordingly, 1-LG dimers with the highest fluorescence value should have the highest affinity, followed by 2-LG, 3-LG and 5-LG dimers in decreasing order. These results are in good agreement with the K_d values obtained by GTP hydrolysis assay. Nevertheless, the fluorescence signal is controlled by a series of other parameters that constraint to analyze the data reliably. One of the parameters that need to be considered is the number of fluorescent dyes that each labelled protein contains. As summed up in table 3-13, the labelling efficiency of each labelled LG protein was different, ranging between 0.69 (3A) and 2.88 (5D). While not even each molecule carries a dye in the one construct, another construct contains almost three. To consider this effect for evaluating the FRET data, following procedure is suggested to process the data (see figure 3-61):

1. Normalize the data by constant initial fluorescence like usually done for presentation (A)
2. Divide values from (A) by the labelling efficiency of each interaction partner (B).
E.g. 1-LG values divided by 1.83 and 0.88 being the respective labelling efficiencies of donor and acceptor
3. Subtract the minimum value (C)
4. Take the result for comparison of the affinities (D).

Processing the data in the described way still yields the highest value for 1-LG dimers. In contrast to the raw data, the final value of 3-LG becomes even higher than the value of 2-LG, indicating a weaker 2-LG dimer. As a consequence affinities of homo dimers are rather $K_d (1-LG)_2 < K_d (3-LG)_2 < K_d (2-LG)_2 \ll K_d (5-LG)_2$.

Although correction for labelling efficiency provides an appropriate way to make the FRET data comparable, this method does not cover any other disruptive factors. Quantum yield, for instance, which is 0.92 and 0.33 for Alexa488 and Alexa647, respectively, was not considered so far (Molecular probes handbook), but similar to labelling efficiency it could be easily handled by mathematical operations. However, there is no way to consider dye localization within the protein which might be the main critical factor. Taken together, direct FRET measurement with subsequent processing of the data offers an option to gain information about homo and hetero interactions; but to obtain more reliable data concerning different affinities, additional setups are required.

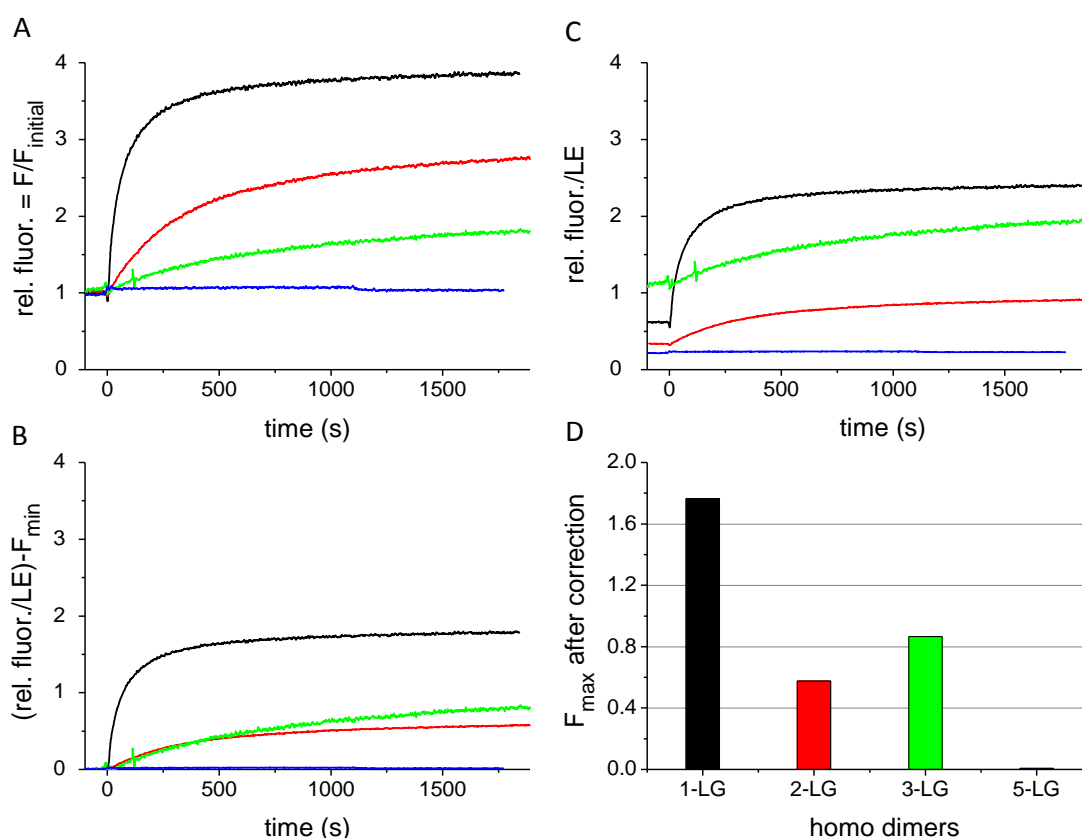


Figure 3-61: Correcting FRET traces by labelling efficiency of the proteins. (A)-(C) Data were corrected and plotted as described in the text. (D) Bar chart of the final fluorescence ($t = 1890$ sec) obtained for each homo dimer after correction procedure.

3.4.3.2. Hetero dimerization of 1-LG in presence of $\text{GDP}\cdot\text{AlF}_x$

Homo and hetero interactions were investigated using fixed equimolar concentrations of donor and acceptor and $\text{GDP}\cdot\text{AlF}_x$ as GTP-analog. The cuvette was filled with $0.75 \mu\text{M}$ of each interaction partner diluted in buffer C containing 10 mM NaF and $300 \mu\text{M AlCl}_3$. Dimerization was induced by $250 \mu\text{M GDP}$. Donor was excited at 498 nm and acceptor fluorescence was detected at 664 nm .

Indicated by a significant fluorescence increase after GDP addition, 1-LG formed hetero dimers with 2-LG and 3-LG, but not considerably with 5-LG (figure 3-62). Each time trace for hetero dimerization (gray) was plotted with the according time traces for homo dimerization (figure 3-62, upper panel). Considering the total changes in fluorescence, 1-LG dimers still

Results

remained the tightest, but, remarkably, 1-LG:2-LG and 1-LG:3-LG hetero dimers were even dominant over the respective 2-LG and 3-LG homo dimers. Even after correcting the data for labelling efficiency, the tendency remained the same (figure 3-62, lower panels). Hetero dimers 1-LG:3-LG, particularly, appeared to be almost as tight as the 1-LG homo dimer. Correction of the data also revealed a more pronounced value for 1-LG:5-LG than obtained for 5-LG homo dimers. Taken together, following order of affinities can be established: $K_d (1-LG)_2 < K_d (1-LG:3-LG) < K_d (1-LG:2-LG) \approx K_d (3-LG)_2 < K_d (2-LG)_2 \ll K_d (1-LG:5-LG) < K_d (5-LG)_2$.

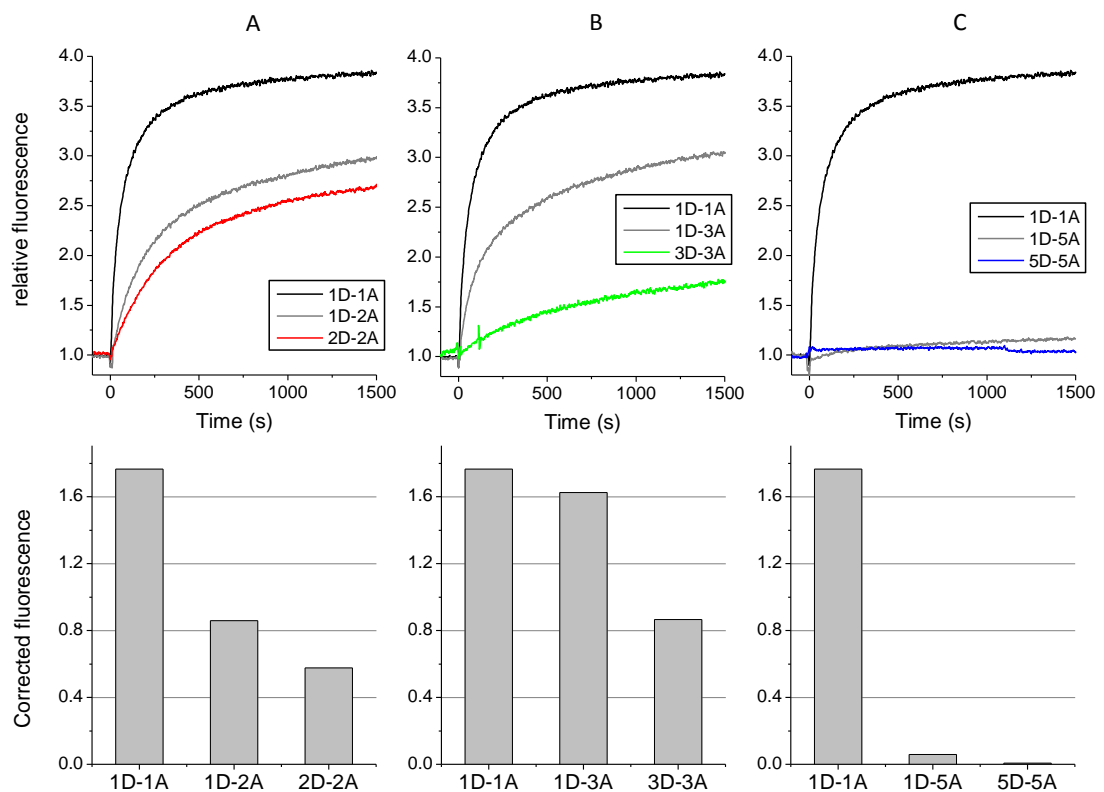


Figure 3-62: GDP·AlF_x induced FRET of 1-LG hetero dimers. Upper panels: Donor labelled 1-LG (1D, 0.75 μM) was combined with (A) acceptor labelled 2-LG (2A), (B) 3-LG (3A), and (C) 5-LG (5A), each having a concentration of 0.75 μM. Time traces of hetero dimerization induced by 250 μM GDP·AlF_x (gray), were plotted with the traces of respective homo dimerization (colors as indicated). Each, 1-LG:2-LG and 1-LG:3-LG hetero dimers were weaker than the 1-LG, but stronger than 2-LG and 3-LG homo dimers. 5-LG did not homo dimerize significantly, while the hetero dimerization with 1-LG appeared slightly higher. Lower panels: Final values from upper panel corrected for the LE are presented in bars.

3.4.3.3. Competitive FRET measurements to address GDP·AlF_x driven 1-LG hetero interactions

As discussed in the previous paragraph, different labelling efficiencies especially when it comes to pairwise combination of GBPs complicate the semi-quantitative estimation of dimer affinities. Although a method was suggested to correct the data for labelling efficiencies, still there is a remnant of uncertainty, e. g. caused by labelling positions. To avoid the uncertainties, another setup was generated that monitors the hetero interaction by mixing labelled and non-labelled interaction partners. When both interaction partners of interest are labelled with fluorescent dyes, the increase in fluorescence is a direct measure of the partner coming in closer proximity upon intermolecular interactions. Vice versa, one of the putative interaction partners when not labelled should be capable to interfere with the FRET couple, resulting in altering FRET efficiency.

Accordingly, the homo and hetero interactions of 1-LG was investigated using fixed equimolar concentration of donor and acceptor labelled protein (1D, 1A), and a two-fold excess of competing non-labelled interaction partner. All compounds were mixed and preincubated prior to nucleotide addition. Any interaction of non-labelled partner (NLP) with the labelled protein (LP) was expected to cause an impact on FRET and thus to decreased levels of fluorescence compared to reference measurement without NLP. All measurements based on the GDP·AlF_x induced dimerization of 0.75 μM 1A and 0.75 μM 1D. The maximum increase in fluorescence signal by 3.7-fold due to the dimerization of 1D and 1A was yielded in the absence of any competitor (figure 3-63, gray). In fact, all applied LG isoforms affected the FRET negatively, suggesting that 1-LG is able to form hetero dimers with each. Depending on the competitor protein applied, the total change in 1-LG signal was impaired to different extent, in parts deviating from the previous experiment. For instance, after correction of LE, hetero interaction of 1-LG:3-LG appeared to be similarly tight as the 1-LG homo interaction. Here, remarkably, the highest impact on 1D-1A FRET was obtained for 3-LG as competitor (1.2-fold increase), meaning that the 1-LG:3-LG hetero dimers are even tighter than the 1-LG homo dimers. The competitive effect of NLP 1-LG, instead, led to a 1.9-fold fluorescence increase. The presence of non-labelled 2-LG made the 1-LG fluorescence increase by 2.3-fold. Thus, 1-LG:2-LG hetero dimers, being in line with the previous experiment, could be categorized as weaker than 1-LG homo and 1-LG:3-LG hetero dimers.

The time trace of 1-LG FRET in presence of NLP 5-LG interactions is interesting with respect to two observations. First, 5-LG interferes with 1-LG homo dimers only slightly weaker than

Results

2-LG does, indicating similar affinities for 1-LG hetero dimers. This in fact is surprising, since previous experiment with labelled proteins only, revealed a very weak FRET between 1-LG and 5-LG, whereas FRET between 1-LG and 2-LG was significantly stronger. One explanation might be that the high labelling efficiency of 5-LG impaired proteins structure or even interface for dimerization. Second, 5-LG was shown to remain monomeric in presence of GDP·AlF_x (analytical SEC and FRET measurement, see figure 3-55 and 3-60). The observed interaction here clearly suggests that hetero interaction with 1-LG occurs nevertheless.

Competitive FRET in contrast to direct FRET measurement is a setup with substantially reduced inaccuracy. Since for the demonstrated example 1D:1A was the constant detectable FRET couple, each run was tainted by the same error caused by proteins labelling efficiency, quantum yield or dye localization. Moreover, the concentration of non-labelled competing partner was also constant. Thus, any effect monitored was assumed to be an exclusive result of different dimer affinities that more reliably than in direct FRET measurements could be estimated as following:

$$K_d (1\text{-LG}:3\text{-LG}) < K_d (1\text{-LG})_2 < K_d (1\text{-LG}:2\text{-LG}) < K_d (1\text{-LG}:5\text{-LG}).$$

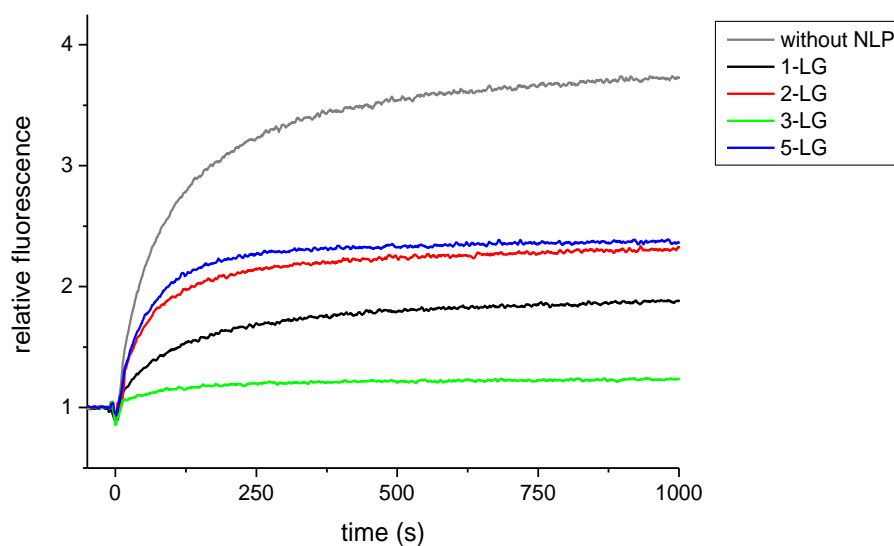


Figure 3-63: Competitive study on GDP·AlF_x driven 1-LG dimerization. 1-LG being the detectable FRET couple (0.75 μM 1D + 0.75 μM 1A) was mixed with 3 μM non-labelled 1-LG (black), 2-LG (red), 3-LG (green) or 5-LG (blue) before nucleotide addition (t₀ = 0 s). In comparison to reference measurement without NLP (gray), each competing LG led to significantly reduced FRET efficiency. The different extent of effect indicates accordingly different hetero dimer affinities.

3.4.4. *GTP γ S dependent homo and hetero dimerization of LG domains*

3.4.4.1. *Homo dimerization of 2-LG in presence of GTP γ S*

Homo dimerization of 2-LG was investigated with GTP γ S, being the GTP analog, at a protein concentration of 0.75 μ M each, 2A and 2D. First, compounds were added in varying orders to check if the maximum FRET signal is reached anyway. Donor was excited at 498 nm and acceptor fluorescence was detected at 664 nm. Cuvette was filled either with both interaction partners, 2A and 2D (figure 3-64, gray line) or with only one interaction partner, 2D or 2A. Then, first GTP γ S and afterwards the complementary partner were added (figure 3-64, orange and blue line). A significant increase of fluorescence could be obtained in each run resulting in almost same final values. This indicates that the order of supplement is not important. The linear drift, visible when 2A and 2D are mixed prior to dimerization, becomes diminished when one of the partners is preincubated with the nucleotide before the second partner is added. This might be due to reshaping of the protein upon binding to the nucleotide. The effect is mostly pronounced when 2A is preincubated and 2D is added later, then plateau is reached within 500 seconds and the fluorescence signal remains stably constant.

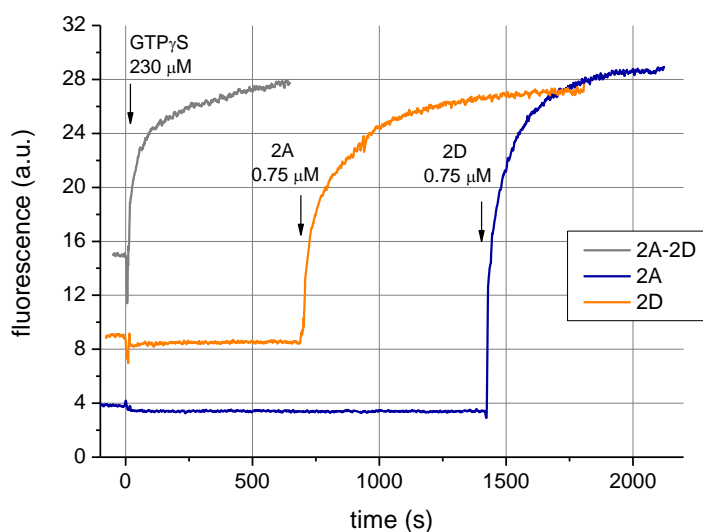


Figure 3-64: Homo dimerization of 2-LG in presence of GTP γ S. Dimerization was checked by supplement of interaction partners in varying order. Gray: 2D (0.75 μ M) and 2A (0.75 μ M) were mixed from the very beginning and GTP γ S (230 μ M) was added afterwards (time point 0 seconds). Orange: At same concentrations as before, first, 2D was present, then GTP γ S and finally 2A (arrow) were added successively. Blue: first, 2A was present, then GTP γ S and finally 2D (arrow) were added successively. Always, donor was excited at 498 nm and acceptor fluorescence was detected at 664 nm. The experiments were carried out at 25°C.

3.4.4.2. *GTP γ S driven 2-LG homo and hetero dimerization monitored by competitive FRET*

As presented for GDP-AIF_x driven hetero interactions of 1-LG (paragraph 3.4.3.3.), hetero interaction provided by GTP γ S bound 2-LG was also investigated via competitive FRET. Accordingly, all measurements based on the GTP γ S induced dimerization of 0.75 μ M donor labelled 2-LG (2D) and 0.75 μ M acceptor labelled 2-LG (2A). Labelled protein (LP) was mixed with 3 μ M of non-labelled protein (NLP) prior to nucleotide addition. Any interaction of NLP with LP was expected to interfere with the FRET detectable 2-LG couple resulting in decreased levels of fluorescence compared to reference measurement without NLP. As expected, maximum increase in fluorescence signal by 2.3-fold due to dimerization of 2D and 2A was yielded in the absence of any competitor (figure 3-65, gray). In fact, all applied LG isoforms effected the FRET efficiency negatively, suggesting that 2-LG is able to form hetero dimers with each of them (figure 3-65). Depending on the competitor protein applied, the total change in 2-LG signal was impaired to different extent. A high impact was obtained for 2-LG as competitor (1.3-fold increase), meaning that 2-LG homo dimerization and therefore inhibition of labelled couple is comparably high. In the presence of 5-LG or 1-LG, the fluorescence increase of 2D-2A was 1.6-fold and 2.0 fold, respectively, indicating that 2-LG:5-LG hetero dimers have a higher affinity than 2-LG:1-LG hetero dimers. Remarkably, NLP 3-LG competes even stronger than 2-LG does, suggesting that 2-LG:3-LG dimers dominate over 2-LG homo dimers. Moreover, NLP 3-LG induced a time trace of 2-LG fluorescence that deviates from the other runs; after a fast increase, which was just the half level of the reference measurement, the fluorescence signal decreased continuously, indicating a respective dissociation of the 2-LG dimer.

Here, 2D:2A was kept as constant FRET couple and competitive effects of any applied non-labelled LG protein were studied. Monitored effects assumed to be an exclusive result of the different dimer affinities revealed the 2-LG:3-LG dimer to be the tightest, 2-LG homo dimers being slightly weaker, and both hetero dimers 2-LG:5-LG and 2-LG:1-LG weaker than the homo dimer ($K_d(2\text{-LG:3-LG}) < K_d(2\text{-LG})_2 < K_d(2\text{-LG:5-LG}) < K_d(1\text{-LG:2-LG})$).

Results

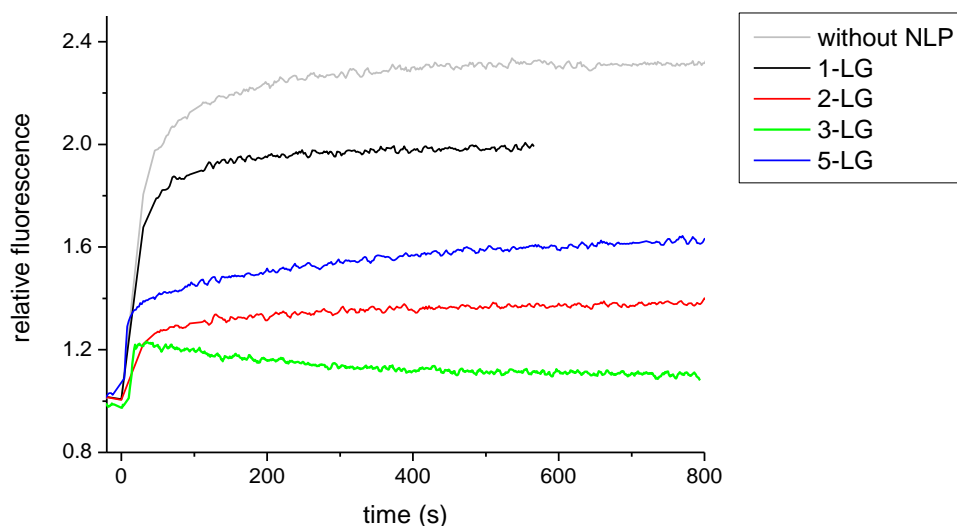


Figure 3-65: Competitive effects of different LG constructs on GTP γ S driven 2-LG homo dimers. GTP γ S induced dimerization of 0.75 μ M 2D and 0.75 μ M 2A was monitored in the absence (gray) and in the presence of competing non-labelled GBP LG constructs. Derived from decreasing fluorescence levels, 3 μ M non-labelled 1-LG (black), 5-LG (blue), 2-LG (red) and 3-LG (green) provided inhibitory effects on 2D-2A dimerization in increasing order.

The dissociative behavior of 2-LG dimers caused by NLP 3-LG led to the idea to modify the competitive FRET study by changing the NLP application order; instead of mixing the competing NLP prior to nucleotide addition, it should be added after GTP γ S induced 2D:2A dimerization was complete. Both directions were tested in two independent runs, each containing 0.75 μ M 2D and 0.75 μ M 2A from the very beginning. In the first run, 230 μ M GTP γ S was added to the labelled proteins allowing 2-LG homo dimers to assemble (figure 3-66 A, black trace). Homo dimerization of 2-LG was indicated by a significant fluorescence increase within the first 5 minutes which was followed by a linear drift monitored for additional 20 minutes. Only then, 3 μ M non-labelled 3-LG was added to the preformed dimers. Being only in two-fold molar excess over labelled protein, 3-LG was capable of triggering remarkable dissociation of the preformed 2-LG homo dimers, indicated by a significant decrease of fluorescence. To ensure that 2-LG dissociation did not occur due to additional 3-LG competing for the nucleotide, another 230 μ M of GTP γ S was added after 2,800 seconds (arrow), having no effect on the trace.

In the second run, like commonly done for the previous competitive FRET measurements, 3-LG was mixed with 2A and 2D before GTP γ S was added (figure 3-66 A, gray trace). Both

Results

signals from the first and second run decreased to almost same levels, being slightly higher than the initial fluorescence and suggesting that virtually no more fluorescently detectable 2-LG homo dimers remained. After shifting the start of the fluorescence decrease to $t_0=0$ s, each decay could be almost perfectly fitted by a single exponential (figure 3-66 B). The obtained rates constants of $4.6 \cdot 10^{-3} \text{ s}^{-1}$ and $4.3 \cdot 10^{-3} \text{ s}^{-1}$, respectively, were almost identical and thus most likely reflected the dissociation rate of 2-LG homo dimers.

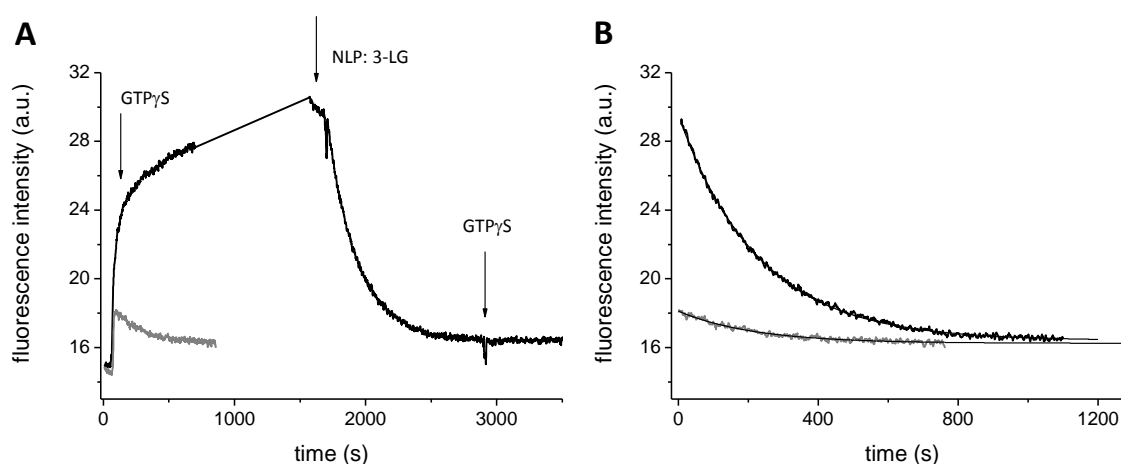


Figure 3-66: Competitive effects of 3-LG on the 2-LG homo dimers induced by GTP γ S. (A) Gray: 3 μ M NLP 3-LG was mixed with 0.75 μ M 2D and 0.75 μ M 2A before dimerization was started with 230 μ M GTP γ S. Black: Initially 0.75 μ M 2D and 0.75 μ M 2A were dimerized with 230 μ M GTP γ S. Addition of 3 μ M NLP 3-LG (arrow) induced dissociation of the preformed homo dimers of 2-LG. (B) Time traces of 2A:2D dissociation obtained from (A) were used to determine the rate constants. The start of the decay was shifted to zero and data were fitted single exponentially yielding the dissociation rate constants $4.6 \cdot 10^{-3} \text{ s}^{-1}$ (black) and $4.3 \cdot 10^{-3} \text{ s}^{-1}$ (gray), respectively.

Competitive FRET measurements were initially established by mixing labelled and non-labelled protein before dimerization was induced with any nucleotide (paragraph 3.4.3.3.). For 3-LG as non-labelled protein competitive effect on 2-LG (LP) interaction could be confirmed independent from the time point of application. When added to 2-LG before dimerization was started, just a little fraction of 2-LG could form some detectable FRET dimers, vice versa, preformed 2-LG FRET dimers were dissociated considerably when 3-LG was added afterwards. Accordingly, competitive effects of all LG constructs on 2-LG homo dimerization (shown in figure 3-65) were tested with the modified competitive FRET setup. For each run 0.75 μ M 2D and 0.75 μ M 2A were mixed and kept for homo dimerization with GTP γ S. After dimerization

Results

was complete, indicated by a fluorescence plateau, 3 μM NLP was added to the system which subsequently led to fluorescence decrease and thus to homo dimer dissociation (figure 3-67). In order to easily compare the amount of dimers dissociated by competitor protein, the total increase in fluorescence upon 2-LG dimerization was scaled to one (figure 3-67). Non-labelled 3-LG was the most potent displacer of 2-LG homo dimers and thus the interaction partner of 2-LG with the highest affinity. At the end, almost no detectable 2-LG FRET dimers were left. Non labelled proteins 2-LG, 5-LG and 1-LG, respectively, made approximately 80 %, 55 % and 25 % of the 2-LG FRET dimers dissociate. These data confirm previously obtained affinities, emphasizing particularly that 2-LG rather than forming homo dimers prefers to hetero dimerize with 3-LG. The affinity of 2-LG homo dimers, however, is higher than the affinity of 2-LG:5-LG hetero dimers, whereas the lowest affinity could be obtained for 2-LG:1-LG hetero dimers.

As already done in the previous section, the decay of fluorescence (figure 3-67) was fitted by a single exponential. For the fluorescence decrease induced by NLPs 1-LG, 2-LG, 3-LG and 5-LG rate constants of 0.0057, 0.0043, 0.0044 and 0.0064 s^{-1} , respectively, were obtained. Considering that deviations might occur due to inaccuracy upon setting the start of the reaction to time point zero, all rate constants appear similarly slow and give an average of $5.2 \cdot 10^{-3} \text{s}^{-1}$ with a relatively high error of $\pm 17\%$. However, to confirm that the obtained rate constants reflect the dissociation of 2-LG homo dimers, the same displacement was induced by the nucleotide GDP, instead, considering that GDP when replacing GTP γ S would facilitate the monomeric state of 2-LG. Therefore, the same concentrations of 2A and 2D (each 0.75 μM) were mixed and homo dimerization was started by addition of only 23 μM GTP γ S (10 times less than usual), which still led to a fluorescence increase but to significantly reduced levels as compared with 3-67 (data not shown). GTP γ S was then displaced with a 50-fold molar excess of monomer inducing GDP which indeed induced dissociation of the FRET dimers. Being almost identical to the average rate constant from above ($5.2 \cdot 10^{-3} \text{s}^{-1}$), most crucially, a rate constant of $5.3 \cdot 10^{-3} \text{s}^{-1}$ was obtained also for GDP as displacer, giving strong evidence that these rate constants describe the dissociation of 2-LG homo dimers.

Results

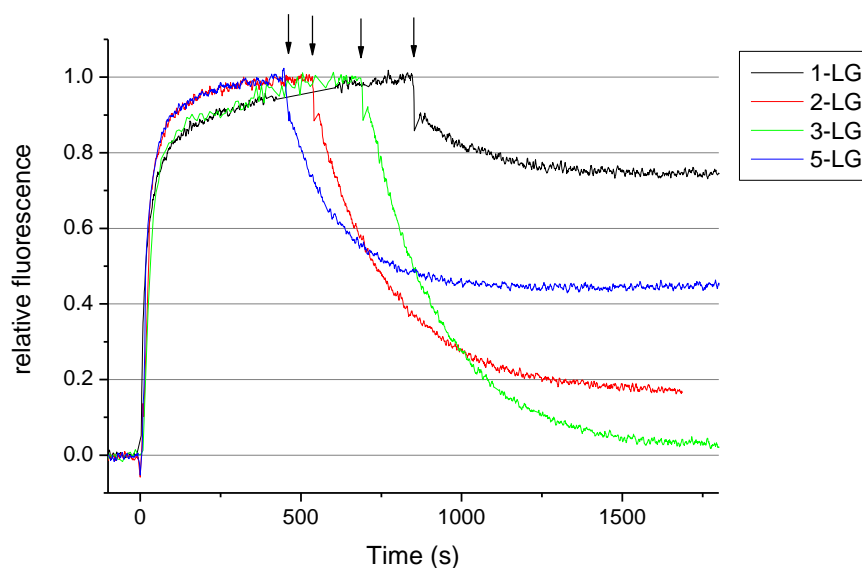


Figure 3-67: Competitive effects of different LGs on preformed GTP γ S bound 2-LG homo dimers. 0.75 μ M 2D and 0.75 μ M 2A were dimerized with 230 μ M GTP γ S. Only then 3 μ M non-labelled 1-LG (black), 2-LG (red), 3-LG (green) and 5-LG (blue) were applied (indicated by arrows) which upon interaction with labelled 2-LG led to dissociation of FRET dimers. Evaluation of the decays as described in figure 3-66 yielded rate constants being 0.0057, 0.0043, 0.0044 and 0.0064 s^{-1} , respectively. In average, a rate constant of $5.2 \cdot 10^{-3} \text{s}^{-1}$ ($\pm 17\%$) can be assumed for the dissociation of 2-LG homo dimers.

3.4.4.3. GTP γ S driven homo and hetero interactions of 1-LG monitored by competitive FRET

Based on labelled 2-LG, affinities for homo and hetero dimers were estimated by studies with non-labelled competitors (previous section). It could be successfully demonstrated that the order of NLP application did not matter; either before or after dimerization of the detectable dimers, the amount of finally remaining homodimers was almost the same directly reflecting the competitive effect of the NLP.

Here, GTP γ S driven homo and hetero interactions of 1-LG were elucidated using labelled 1-LG as constant detectable FRET pair while competing with different non-labelled LG constructs. Also both directions were tested: First, labelled protein (0.75 μ M 1D and 0.75 μ M 1A) and 3 μ M NLP were mixed from the very beginning and 250 μ M GTP γ S was added afterwards (figure 3-68 A). Second, dimerization of labelled protein was started and NLP was added afterwards (figure 3-68 B). Both setups yielded the same results. In comparison to any other LG, 2-LG caused the lowest decrease in fluorescence, namely $\sim 20\%$. Confirming the

Results

results from previous section, consequently, 1-LG and 2-LG form the weakest hetero dimers (compare figures 3-67 and 3-68). Remarkably, 3-LG turned out to be the strongest interaction partner not only for 2-LG but (figure 3-67) but also for 1-LG (figure 3-68). Adding NLP 3-LG before nucleotide yielded the highest impact on 1-LG FRET efficiency (figure 3-67 A) and also adding 3-LG to preformed 1-LG dimers made them dissociate to maximum level (figure 3-67 B). Which is more, competing preformed 1-LG FRET dimers with 1-LG NLP caused also a significant decrease of fluorescence but only additional supplement of 3 μ M of NLP 1-LG (figure 3-68 B, second arrow) made the fluorescence decrease to the same level as NLP 3-LG succeeded to reach with only half of the protein concentration. In sum, the affinity of 1-LG:3-LG hetero dimers is supposed to be even higher than the affinity of 1-LG homo dimers.

By direct FRET measurements in paragraph 3.4.3.2., only weak dimerization of 1-LG and 5-LG was shown. However, the nucleotide used was GDP·AlF_x which was not sufficient to induce 5-LG homo dimers (analytical SEC) and probably due to that it was also not sufficient to induce respective hetero dimers with 5-LG. Here, GTP γ S was used instead, and this nucleotide indeed succeeded to induce considerable amounts of 1-LG:5-LG hetero dimers. The competitive effect of 5-LG was even more pronounced than for 2-LG (figure 3-68), such that 1-LG:5-LG hetero dimers are likely to interact with higher affinity than 1-LG:2-LG hetero dimers. Altogether, these results can be summarized in the following order of K_d values:

$$K_d (1-LG : 3-LG) < K_d (1-LG)_2 < K_d (1-LG : 5-LG) < K_d (1-LG : 2-LG).$$

As already done for 2-LG homo dimers (previous section), the NLP induced decays in figure 3-68 B have been evaluated with a single exponential fit. Yielded rate constants being 0.0063, 0.0075, 0.0065 and 0.0085 s⁻¹ for NLPs 1-LG, 2-LG, 3-LG and 5-LG, respectively, give an average of 7.2·10⁻³s⁻¹ (\pm 13 %) which can be assumed as dissociation rate constant of 1-LG homo dimers.

Results

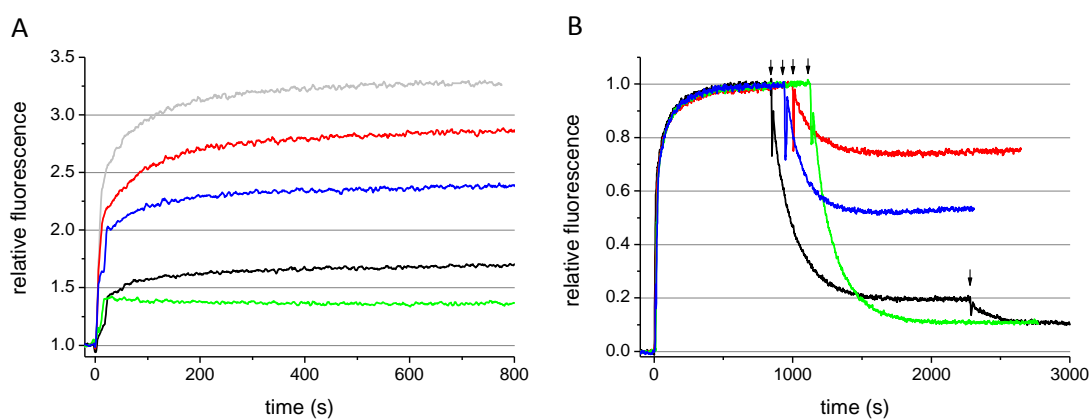


Figure 3-68: Competitive effects of different LG constructs on GTP γ S driven 1-LG homo dimers. 3 μ M NLP 1-LG (black), 2-LG (red), 3-LG (green) and 5-LG (blue) was applied to 0.75 μ M 1D and 0.75 μ M 1A before (A) or after addition of GTP γ S (B). (A) Time traces were normalized by initial fluorescence and compared to reference measurement in the absence of competing NLP (gray). (B) Total change in fluorescence upon 1-LG dimerization was scaled to one. Time points of NLP supplement are indicated by arrows. Of note, additional 3 μ M of NLP 1-LG was added after 2,300 seconds leading to a second decay. Evaluation of the decays as described in figure 3-66 yielded rate constants being 0.0063, 0.0075, 0.0065 and 0.0085 s^{-1} , respectively. In average, a rate constant of $7.2 \cdot 10^{-3} s^{-1}$ ($\pm 13\%$) can be assumed for the dissociation of 1-LG homo dimers.

3.4.4.4. GTP γ S driven homo and hetero interactions of 3-LG monitored by competitive FRET

Performing competitive FRET studies, LG domain of hGBP-3 revealed to be the most potent interaction partner of 1-LG and 2-LG. To enlighten the hetero dimer affinities also from 3-LG's point of view, competitive studies were finally performed on 3-LG being the constant detectable FRET dimer. Since previous experiments demonstrated that same results can be obtained independent from the time point of competing NLP application, here only dissociative effect of the NLPs on 3-LG FRET dimers were investigated. Using same conditions as before, 0.75 μ M 3D and 0.75 μ M 3A were mixed and dimerized with 250 μ M GTP γ S. Adding 3 μ M NLP 1-LG made 40 % of the preformed 3-LG dimers dissociate. NLP 2-LG and 3-LG, similarly, dissociated even 50 % of the preformed dimers, suggesting similar affinities for 2-LG:3-LG hetero and 3-LG homo dimers being slightly tighter than the 1-LG:3-LG hetero dimer. 3-LG and 5-LG instead are supposed to interact much weaker since approximately 80 % of the preformed 3-LG FRET dimers remained after addition of NLP 5-LG. In conclusion,

Results

following order affinities could be identified: K_d (3-LG:2-LG) \approx K_d (3-LG)₂ < K_d (1-LG:3-LG) < K_d (3-LG:5-LG). However, these results were partly contradictory to the previously obtained data indicating that 1-LG:3-LG hetero dimers are stronger than the respective homo dimers. Further, it was unexpected that 2-LG and 1-LG were not sufficient to dissociate larger amounts of 3-LG homo dimers considering that 3-LG conversely was. As observed later, however, it was not possible to dissociate the FRET dimers of 3-LG completely, even if tried with a 20-fold molar excess of non-labelled 3-LG which in fact is the same protein and thus should compete upon homo dimerization. As approximately 40 % of FRET dimers remained anyhow (data not shown), it can be concluded that these amount formed some irreversible complexes. When considering that non-labelled 3-LG revealed as a highly affine interaction partner for 1-LG and also 2-LG (paragraph 3.4.4.2. and 3.4.4.3.) it seems highly probable that the labelling procedure had some impact on 3-LG. However, there was still a considerable amount of 3-LG FRET dimers left that dissociated upon NLP addition (1-LG, 2-LG and 3-LG; figure 3-69). This was exploited to derive rate constants by a single exponential fit. As a result, an average dissociation rate constant of $9.1 \cdot 10^{-3} \text{ s}^{-1}$ ($\pm 7 \%$) could be obtained for 3-LG homo dimers.

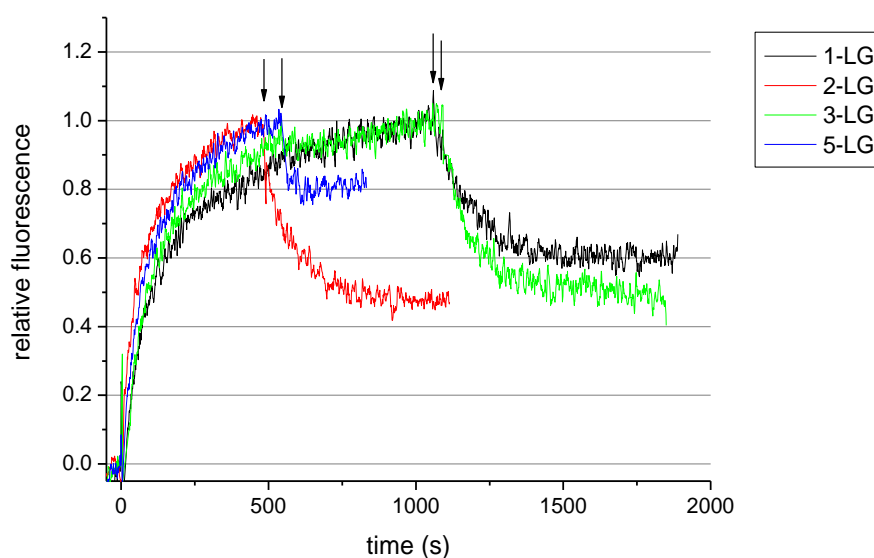


Figure 3-69: Competitive effects of different LGs on preformed GTP γ S bound 3-LG homo dimers. 0.75 μM 3D and 0.75 μM 3A were dimerized with 250 μM GTP γ S. Only then 3 μM of non-labelled 1-LG (black), 2-LG (red), 3-LG (green) and 5-LG (blue) were applied (indicated by arrows), which upon interaction with labelled 3-LG led to dissociation of FRET dimers to different extent. By a single exponential fit to the fluorescence decays, an average dissociation rate constant of $9.1 \cdot 10^{-3} \text{ s}^{-1}$ ($\pm 7 \%$) could be obtained for 3-LG homo dimers.

3.4.5. Competitive FRET studies to address domain involvement in hGBP interactions

The mixed LP-NLP FRET setup - referred to as competitive FRET- opens up a variety of possibilities to study intermolecular interactions. With a plenty amount LP as detectable FRET couple, easily any NLP construct introduced into the system can be assayed for possible interactions in a comparative or even concentration dependent manner.

After confirming homo and hetero interactions based on isolated hGBP LG domains, we exploited the advantages of competitive FRET to address other protein domains being involved in the dimerization. More specifically, we investigated full length hGBP isoforms versus respective LG constructs as competitive interaction partners for labelled 2-LG. The same as before, first, 0.75 μ M 2D and 0.75 μ M 2A served as constant FRET couple that dimerized upon 250 μ M GTP γ S addition (figure 3-70, light gray, reference in the absence of NLP). For the following runs, 3 μ M non-labelled full-length protein was mixed with the FRET couple prior to GTP γ S addition. In paragraph 3.4.4.2., 1-LG among all investigated LG constructs revealed the weakest interaction with 2-LG. Here, replacing 1-LG by its full-length construct diminished the effect even further, since the total change in fluorescence came closer to the level of maximum dimerization (figure 3-70, left panel). One possible explanation is that the helical domain of hGBP-1 probably establishes an LG conformation that is impaired to interact with 2-LG. Hetero interactions of 2-LG and 5-LG were shown to be stronger than 2-LG and 1-LG. Here we showed that the same is true when 5-LG and 1-LG are replaced by the according full-length proteins. Although full-length hGBP-5 more potently than full-length hGBP-1 inhibits 2D-2A homo dimers (figure 3-70, left and right panel), the tendency that full-length proteins basically interact weaker with 2-LG than the LG proteins remain the same. Only for hGBP-2 as competitor the order was reversed; the already strong interaction between 2-LG:2-LG occurred even stronger when one of the interaction partners constituted all subdomains (figure 3-70, middle panel).

Results

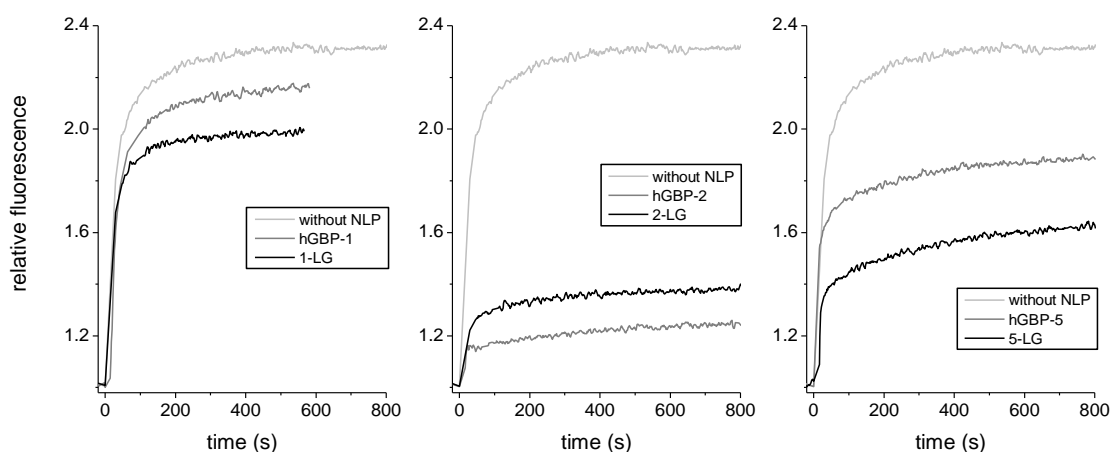


Figure 3-70: Competitive effects of different GBP isoforms (full-length and LG domain) on the GTP γ S driven 2-LG homo dimerization. From left to right, 3 μ M non-labelled hGBP-1, hGBP-2 and hGBP-5 were applied as competitors. Homo dimerization of 0.75 μ M 2D and 0.75 μ M 2A in the absence of competitor (light gray), in the presence of full-length constructs (dark gray), or in the presence of respective LG constructs (black) was detected after addition of 250 μ M GTP γ S.

By the same setup, also hGBP-3 constructs were investigated for their capacity to interact with 2-LG, whereby 3-LG and hGBP-3 (aa 1-481) were found to form significantly stronger hetero dimers than full-length hGBP-3 did (figure 3-71 A). This is in line with the observations that also full-length hGBP-1 and hGBP-5 competed weaker with the FRET dimer than their respective LG variants (figure 3-70).

Notably, the entire change of the 2-LG FRET signal in the absence of any competitor is comparatively reduced in figure 3-71 A (2.3-fold increase in figure 3-70 and only 1.9-fold increase in figure 3-71 A). Most probably, this is due to an additional thawing-refreezing cycle the labelled proteins went through. However, this fact is neglectable since all competing studies with non-labelled hGBP-3 constructs were performed with the same set of labelled proteins, and show significant effects in comparison. For control, nevertheless, dissociative competitive studies were also performed (figure 3-71 B). In reasonable agreement with the results from figure 3-71 A, the truncated forms of hGBP-3 induced more pronounced dissociation of the preformed 2-LG homo dimers. A single exponential fit to the fluorescence decay induced by 3-LG and hGBP-3 (aa 1-481) yielded the rate constants $4.3 \cdot 10^{-3} \text{ s}^{-1}$ and $4.4 \cdot 10^{-3} \text{ s}^{-1}$, respectively, which are in the error range of the previously obtained dissociation

Results

rate constant of 2-LG homo dimers ($5.2 \cdot 10^{-3} \text{ s}^{-1} \pm 17\%$). Only the decay induced by full-length hGBP-3 appeared to be faster ($7.3 \cdot 10^{-3} \text{ s}^{-1}$) but, to remind, all effects observed for full-length hGBP-3 need to be considered with care as the protein was found to be very unstable under given buffer and temperature conditions.

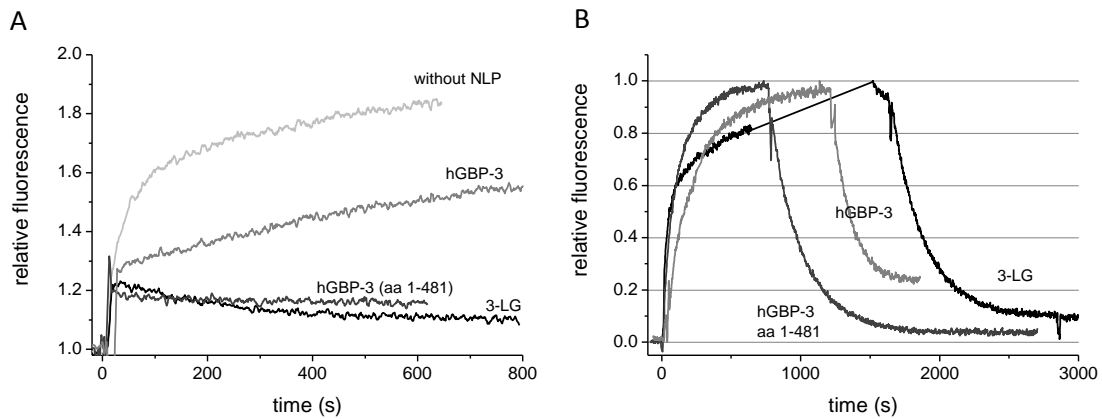


Figure 3-71: Competitive effects of different hGBP-3 constructs on the GTP γ S driven homo dimerization of 2-LG. (A) $0.75 \mu\text{M}$ 2D and $0.75 \mu\text{M}$ 2A were mixed with $3 \mu\text{M}$ NLPs : hGBP-3 full-length, hGBP-3 (aa 1-481) or 3-LG. Dimerization was started with $250 \mu\text{M}$ GTP γ S ($t_0 = 0 \text{ s}$). (B) Using the same concentrations from (A), 2-LG dimers were performed and dissociation was started by addition of indicated hGBP-3 constructs ($3 \mu\text{M}$ NLP).

Using this setup, we confirmed that LG domains are sufficient and dominating to mediate GBP homo and also hetero dimerization. Combining not only LG domains but also full-length constructs of hGBP isoforms with 2-LG unraveled that the C-terminal helical domains mediate altering effects: while the helical domain of other isoforms than hGBP-2 reduced the affinity to 2-LG, the helical domain of the same isoforms even enhanced dimerization. If the same is true for the other isoforms needs to be elucidated in future.

4. Discussion

4.1. Physiological salt conditions do affect the oligomerization but not the catalytic activity of hGBP-1

In previous studies particularly dealing with the biochemical characterization of recombinant hGBP-1, different buffer and temperature conditions have been used which indeed have notable effects on the elucidated features. As driven by electrostatic contacts, the dimerization of hGBP-1 for instance appeared to be very sensitive to the ionic strength of the buffer (Wehner, et al., 2012). Prior to the biochemical characterization of remaining hGBP isoforms and studying their interactions, we switched to a modified buffer system and 25°C as standard temperature to create a basis for reliable comparison. In order to maintain the ionic strength under physiological conditions we supplemented the standard Tris-buffer (pH 7.9) containing 5 mM MgCl₂ with additional 150 mM NaCl. Under these conditions, initially, all basic properties of hGBP-1 such as nucleotide binding, GTPase activity and nucleotide dependent oligomerization were investigated.

We found that the newly established conditions had only neglectable effects on the nucleotide binding properties of hGBP-1. The binding occurred less dynamic since both association and dissociation rates became slower in the presence of higher salt concentration. However, both effects compensated such that resulting equilibrium constants were only 1.3 to 2.5-fold higher as compared with values under low salt conditions. Binding affinities located still in the same micro-molar range with 0.63, 5.4 and 3.8 μM for mGMP, mGDP and mGppNHp, respectively. Similar to the nucleotide binding properties and also as shown in previous studies (Wehner, et al., 2012), the salt content of the buffer had no considerable effects on the cooperative enzymatic activity of hGBP-1. Under low salt conditions and at 25°C, the maximum GTPase activity of 22.8 min⁻¹ was determined yielding 60 % GDP and 40 % GMP as products (Vöpel, et al., 2010). Using additional 150 mM NaCl we obtained the same product ratio and a maximum value of 19.1 min⁻¹ which is only slightly slower but still in the known error range of the technique.

With major contributions of guanine cap residues, the LG-domain mediated dimerization of hGBP-1 is established by electrostatic contacts. These are likely to diminish by increased ionic strength of the buffer. Thus, it appears not surprising that not the nucleotide binding and enzymatic properties of hGBP-1, but rather its capability of GTP dependent self-assembly appears to be mostly affected by increased salt conditions. Employing the dimer dependent

stimulation of the GTPase activity for describing the monomer-dimer equilibrium of hGBP-1, we obtained an apparent dimer constant of 0.20 μM under physiological salt conditions which compared to the respective value of 0.03 μM under low salt conditions indicates an approximately 10 times lower affinity (Wehner, et al., 2012). To directly address the GTP dependent self-assembly of hGBP-1 we performed analytical SEC in the presence of either hydrolysis resistant GTP analog GppNHp or GTP γ S. Using saturating conditions for nucleotide binding (20 μM protein and \geq 250 μM nucleotide) we found that GppNHp or GTP γ S loaded hGBP-1 remained monomeric exactly as the nucleotide-free form. This altogether confirmed that oligomerization of hGBP-1 occurs mostly sensitive to the ionic strength. However, hGBP-1 succeeded to form similar oligomers in the presence of GDP·AlF $_x$ irrespective of the salt content indicating that the transient state of hydrolysis remained rather unaffected. This prompted us to further elucidate the nature of hGBP-1 oligomers induced by either GppNHp, GTP γ S or GDP·AlF $_x$ binding as discussed in the following.

4.2. GDP·AlF $_x$ bound hGBP-1 most likely forms voluminous dimers rather than tetramers

Self-assembly is an essential property that members of the dynamin superfamily require to accomplish their biological function. Purified dynamin, for instance, readily self-assembles into rings or spirals supporting the hypothesis that dynamin wraps around the necks of budding vesicles where it plays a key role in membrane fission (Hinshaw, 2000). For the potent antiviral activity of MxA, on the other hand, oligomerization to ring-like structures is proposed to supply multiple interaction sites for stable binding of viral nucleoproteins to antagonize viral replication (Patzina, et al., 2014). The knowledge of hGBP-1's self-assembly and its biological function is still at the preliminary stage. In general, it is important to distinguish between the farnesylated and the non-farnesylated forms of hGBP-1. As identified in recent results, farnesylated hGBP-1 (fn-hGBP-1) which might be the mostly populated form in eukaryotic cells, is indeed capable of forming higher ordered structures that might be essential for membrane targeting (unpublished data of Shydlovskiy). However, many of the previously published studies and also the experiments of this work are based on bacterially synthesized hGBP-1 which consequently subsists in the non-farnesylated form. For at least two reasons it is still a major concern to quantify the functional complexes formed by non-farnesylated hGBP-1: first, it is not ruled out that parts of cellular hGBP-1 remain in the non-modified form, second and in interdependency with the first point, current data give evidence that non-farnesylated hGBP-1 significantly counteracts polymerization of fn-hGBP-1 which for instance might be a

putative mechanism to redirect accumulated pools of cytosolic hGBP-1 to target membranes (unpublished data of Shydlovskiy).

To the present knowledge, the highest oligomeric form that non-farnesylated hGBP-1 is believed to establish is a tetramer. Many efforts have been done to address the subdomains' involvement in oligomerization. Separately, each of the isolated subdomains and C-terminally truncated forms of hGBP-1, e.g. 1-LG, $\Delta\alpha12-13$, $\alpha12-13$ were shown to homo-dimerize but not capable of forming higher complexes than that (Benscheid, 2005). In contrast, full-length hGBP-1 apparently elevated to dimeric structures when bound to GTP, as mimicked by GppNHp, and even to tetrameric structures in the transient state of GTP hydrolysis, as mimicked by GDP·AlF_x. This was revealed by both approaches analytical SEC and dynamic light scattering (DLS) (Vöpel, et al., 2010). Considering all the oligomerization studies, LG mediated dimers were proposed as the most reasonable building block that upon GTP hydrolysis released $\alpha12-13$ for further assembly to tetramers (figure 4-1 A) (Kunzelmann, et al, 2005).

In this work, we established buffer conditions that from the previously used system distinguished by additional 150 mM NaCl. Towards elucidating the effect of increased ionic strength on the oligomerization capacity of hGBP-1, we used analytical SEC as standard approach to quantify the homo complexes arising from different nucleotides bound to the protein. Strikingly, we observed only two and not three hGBP-1 species as described under low salt conditions: a monomer when hGBP-1 was nucleotide free, bound to GppNHp or GTP γ S, and a complex similar to the proposed tetramer when hGBP-1 was bound to GDP·AlF_x but nothing else that was comparable to the formerly assigned dimer. By repeating the same experiments also under low salt conditions we could indeed observe three different species which on the one hand confirmed the third species as salt dependent effect and on the other hand ruled out any doubts about the resolution capacity of the utilized SEC column. However, these observations raised two questions: First, how is the formation of a hGBP-1 tetramer possible when the dimerization is assumed as required subunit that under increased salt conditions obviously does not emerge? Second, what is the nature of the proposed GppNHp induced dimer which upon increased salt levels is completely abolished?

At this point, the limitations of both methods SEC and DLS for quantifying hGBP-1 and its higher molecular complexes need to be considered. First of all, both methods ground on the hydrodynamic radius of the investigated probes. Here, the elongated shape of hGBP-1, major intramolecular changes of its conformation upon GTP hydrolysis, and also the lacking knowledge about how hGBP-1 arranges into a dimer or a higher oligomer complicate a reliable

Discussion

assignment of the complexes since all of them influence the hydrodynamic radius. In previous studies, it has been investigated how putative arrangements of hGBP-1 could reflect on the hydrodynamic radius (Lüdemann, 2010). Starting from the only dimeric structure available, which is that of the isolated LG domains, two full-length molecules were aligned resulting in an extended dimer over a length of almost 240 Å (figure 1-7 B in the introduction). In order to determine the theoretical hydrodynamic radius both the extended dimer and the experimentally obtained GppNHp bound hGBP-1 monomer (pdb: 1f5n) were applied to the software Hydropro. Indeed did the calculation yield an enlarged radius for the dimer (5.61 nm) as compared with the monomer (3.98 nm). These data, moreover, were in reasonable agreement with the experimentally obtained results from DLS measurements, 5.23 nm and 4.08 nm in the presence and absence of GppNHp, respectively, at first glance supporting the idea of a GppNHp induced dimer of hGBP-1. In the next step it was explored whether there was a scenario where the monomeric protein by putative intramolecular opening only could achieve comparable enlargement of the dynamic radius. For that, a modified version of the monomeric structure was fed into the software. This modification maintained the original arrangement of both the LG and middle domain, but created a relative opening of the helices α_{12-13} by 90°. Most strikingly, the yielded hydrodynamic radius of this monomer was 5.02 nm and thus ranged in between the values of the native monomer and assumed dimer (Lüdemann, 2010). These investigations particularly emphasize the obstacles emerging in evaluating putative protein complexes revealed by analytical SEC and DLS, particularly when the complex structure remains unknown. Calculation of an apparently higher molecular weight based on standard curve which is established on globular proteins, moreover, is consequently not a proof for a real dimer. More precisely, an apparently higher molecular weight of hGBP-1 obtained by SEC or DLS with equal probability can report either a monomer with altering overall arrangement of the subdomains or a dimer that is more densely packed than the theoretically extended version.

To overcome inaccuracies resulting from the hydrodynamic radius, we investigated a covalently bound hGBP-1 dimer on both analytical SEC and SDS-PAGE in the absence of any nucleotide. As performed under denaturing conditions, separation via SDS-PAGE unlike SEC is entirely based on the primary sequence of the protein and thus reflects its real size. Comparison of both runs, as the most interesting fact, revealed that the covalent dimer through SEC eluted exactly at the same volume as the claimed GDP·AIF_x tetramer which clearly contradicts previous assumptions of a tetramer. However, the huge discrepancy between the real size of a hGBP-1 dimer (136 kDa) and the apparent molecular weight (274 kDa) by two-

Discussion

fold implies striking conformational changes that to present knowledge most likely result from the release of α 12-13 (GED). This probability was further confirmed by intramolecular FRET measurements using appropriately labelled hGBP-1 which had a donor and an acceptor dye attached to the LG domain and helix α 13 of the same protein molecule, respectively. Indeed, GDP·AlF_x turned out to induce the most remarkable decrease in FRET efficiency and consequently the largest intramolecular opening as compared with GTP γ S and GppNHp. This is likely to account for the apparently two-fold larger size of the dimer as observed by analytical SEC. This may also explain why it was formerly presumed that the truncation mutant $\Delta\alpha$ 12-13 (Δ GED) formed dimers while the full-length hGBP-1 emerged to tetramers. According to the present results, namely, it can be assumed that both full-length and Δ GED do only dimerize but constitute differentially shaped complexes: full-length hGBP-1 harboring the GED undergoes major structural changes rendering the protein apparently larger, whereas Δ GED due to lacking the GED does not and thus appears as smaller dimer. Restriction of the helical movements of full-length hGBP-1, thus, might lead to similarly 'small' dimers as observed for Δ GED. In fact, the CL-mutant covalently linking the LG and GED support exactly this assumption.

As mentioned above, exclusively binding of GDP·AlF_x did lead to considerable intramolecular opening of hGBP-1. In contrast, GTP γ S caused only a little decrease of the FRET efficiency and GppNHp hardly induced any change indicating only slight or no opening, respectively. By intermolecular FRET studies, further, we addressed the GED:GED interactions which are proposed to require the release of each GED upon intramolecular opening. The generated hGBP-1 constructs carried either a donor or an acceptor dye at the CaaX cysteine in order to exclusively report the distances between two helices α 13 in a nucleotide dependent manner. Consistent with the intramolecular opening, considerable convergence of the C-termini was achieved only by supplement of GDP·AlF_x. Both intramolecular opening and assembly, moreover, occurred with comparable rates suggesting both processes are highly interdependent. The remaining nucleotides GTP γ S and GppNHp failing to induce reasonable intramolecular opening, also in consistency, failed to induce any intermolecular interaction of the GED regions indicating that sufficient release of the GED did not occur.

Assuming now that the nucleotide free and GDP·AlF_x bound forms of hGBP-1 build up both of the extremes, monomer and opened dimer, respectively, still the question remains regarding the apparent GppNHp bound complex emerging only under low salt conditions. The complex is slightly larger than the nucleotide free monomer but completely vanishes when the

Discussion

salt concentration is increased. Performing the same intra- and intermolecular FRET studies (see above) under low salt conditions, indeed, we could see a more pronounced opening of hGBP-1 induced by GppNHp but still it was half of the change yielded with GDP·AlF_x. And still, GED interactions at intermolecular levels did not occur suggesting that the full intramolecular opening and GED release were not sufficiently induced by GppNHp. However, the fluorescence dyes were positioned at the C-terminal parts of hGBP-1, which made the intermolecular FRET setup blind for LG:LG interactions. As the GppNHp induced hGBP-1 conformation in contrast to the GDP·AlF_x induced one was highly sensitive to the ionic strength of the buffer and due to other reasons as will be discussed in the next paragraph, it appears probable that GppNHp induces weak hGBP-1 complexes only involving LG domain contacts. Following scenario is conceivable: (1) Under low salt conditions, GppNHp induces weak dimers exclusively involving the LG domains. (2) At a certain protein concentration applied to analytical SEC only a minor fraction of hGBP-1 is dimeric while the majority remains monomeric, in sum resulting in a single peak apparently shifted to correspondingly larger complex. (3) Increasing the salt concentration weakens the LG:LG interaction driven by electrostatic contacts even more. (4) At the same protein concentration, thus, only monomeric forms are detectable that are perfectly matching with the elution peak of nucleotide free protein.

These data altogether suggest that first, dimers are most likely the highest complexes that non-farnesylated hGBP-1 can form and, second, that different GTP analogs induce different dimers: it seems that GppNHp and GTPγS induce weak dimers that involve the LG domain interface only (figure 4-1 B, left panel). In contrast, GDP·AlF_x facilitates major structural changes and thus involves GED interactions in addition to the LG interactions for establishing tight dimers that are detectable by analytical SEC (figure 4-1 B, right panel). The major structural changes, furthermore, are likely to account for a voluminous appearance which by SEC corresponds to a molecular weight of ~270 kDa.

Discussion

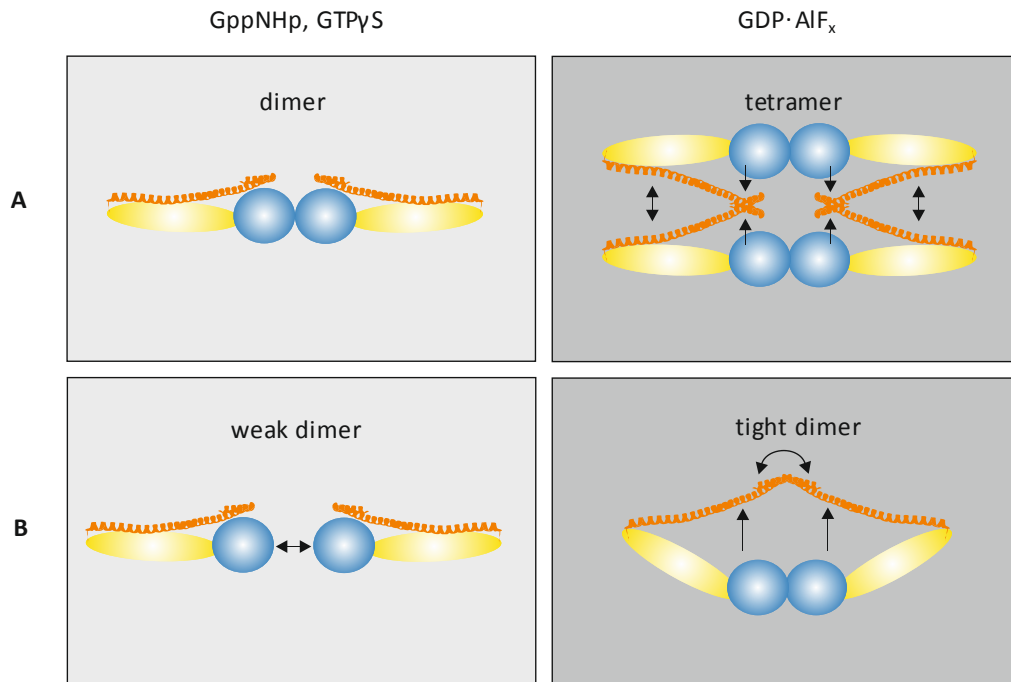


Figure 4-1: Hypothesized models of hGBP-1 self-assembly. (A) According to results and interpretations from previous studies, GppNHp and GTP γ S binding induces stable dimerization of hGBP-1 via LG:LG contacts (left panel). GDP·AlF $_x$ binding in contrast induces the release of the GED and enables two dimers to form tetramers via GED:GED contacts (right panel). (B) According to data of this work, the highest oligomeric form hGBP-1 can build is a dimer: a weak dimer when only LG:LG contacts are involved (as induced by GppNHp and GTP γ S; left panel) and a tight and opened dimer when LG:LG and GED:GED contacts are involved simultaneously (as induced by GDP·AlF $_x$ upon GED release; right panel). Each hGBP-1 molecule is colored according to the subdomain; LG domain: light blue, middle domain: yellow; GED: orange.

4.3. Dimerization of hGBP-1 relies on mutual regulation of the subdomains LG and GED which is nucleotide dependent

Like dynamin-1 or MxA, also hGBP-1 was found to possess locally distinct interfaces for establishing homo complexes; LG:LG domain interactions responsible for stimulated GTPase activity, on the one hand, and interactions of the carboxy-terminal domains responsible for forming higher order oligomers, on the other hand (Faelber, et al., 2011) (Gao, et al., 2011) (Syguda, et al., 2012). However, dynamin-1 and MxA other than hGBP-1 are proposed to assemble through C-terminal interactions first to coordinate the N-terminal domains for subsequent LG:LG interactions. In addition, higher order oligomers of dynamin-1 and MxA already exist in the nucleotide-free state likely to be related to an extended, open ground state. hGBP-1 to present knowledge is believed to be subject to a reversal mode of action as already described in paragraph 4.1. and illustrated in figure 4-1 A. Roughly outlined, in the absence of any nucleotide hGBP-1 is monomeric and provides a closed (safety pin like) conformation established by intramolecular contacts between the LG (particularly helix $\alpha 4'$) and GED ($\alpha 12-13$). These contacts prevent the GED interface from being accessible in the ground state while the LG interface seems readily available. Thus, GTP binding initially facilitates LG:LG interactions which in turn provide the necessary conformational changes, particularly movements of $\alpha 4'$, for release and subsequent interaction of the GEDs. From this perspective, flow and direction of the events along self-assembly of hGBP-1 seem to be well defined: beginning from dimerization of the LG domains a chain of conformational changes within one molecule is transmitted towards the GED for release and downstream events. Altering dimerization of selected mutants compared to wt hGBP-1, however, suggests that not only accessibility of the GED depends on the LG interface but also vice versa. In this regard, intramolecular contacts between the LG domain and the GED appears to play a central role.

For the truncation mutants of hGBP-1 either lacking the GED ($\Delta\alpha 12-13$) or the entire helical domain (1-LG = $\Delta\alpha 7-13$) all the GTP analogs GppNHp, GTP γ S and GDP·AlF $_x$ are capable of inducing dimerization (Vöpel, 2010; Ghosh 2006, present data). As these mutants are devoid of the GED interface for dimerization, LG:LG contacts seem to be sufficient and particularly strong enough to be detectable by analytical SEC. In full-length hGBP-1, controversially, only GDP·AlF $_x$ but none of the other analogs is potent to force dimerization (see paragraph 4.1.). As only difference, here, the presence of the helical domain and correspondingly its intramolecular interaction with the LG domain comes into play which in the case of GTP γ S and GppNHp seems to interfere with the dimerization of the protein. However, intramolecular LG:GED interactions are mediated by an interface that is spatially distinct from the

intermolecular LG:LG interface. The LG:GED interaction allosterically influencing the LG:LG interface, thus, occurs as a reasonable explanation for the different dimerization behavior of wt and truncated hGBP-1 although applying the same nucleotides.

The particular nucleotide and probably the step each of the nucleotide represents along the course of GTP binding and hydrolysis seems to act as key mediator of the allosteric mechanism, considering that differences were observed for GppNHp and GTP γ S but not for GDP·AlF_x. Binding of any GTP analog, obviously, can transform the isolated LG domain (free from any helical regulation) into a conformation capable of dimerization. In the full-length protein, in contrast, LG domain mediated dimerization is restricted deducing that the same nucleotides cannot fully develop the conformational changes for preparing the LG:LG interface. Therefore, it seems that intramolecular tensions between the LG domain and the GED need to be relieved for adapting an LG interface competent to mediate LG:LG interaction. Relieve of the tension probably accomplished by intramolecular opening (release of α 12-13) seems to depend on the particular nucleotide. In the FRET studies from this work, we could see only less or no intramolecular opening of hGBP-1 in presence of GTP γ S and GppNHp, respectively, supporting that binding of these nucleotides cannot overcome the intramolecular tensions and consequently are incapable of forming an appropriate LG interface. GDP·AlF_x inducing large intramolecular opening, in contrast, could also induce dimerization of the full-length protein. Further evidence comes from the dimerization behavior of the 'open' hGBP-1 mutants RK and 3-Phe, respectively. These mutants ground on the full-length sequence but upon substitution of particular residues provide weaker intramolecular LG:GED interactions. These mutants similar to the helical truncated ones dimerize irrespective of the GTP analog offered which suggests that reduced internal tension positively influences rearrangements of the LG domain and particularly the interface for establishing LG:LG contacts. Although the mutants due to the open ground state could be assumed to dimerize via GED:GED directly, nucleotide dependency of dimerization excludes this option and, moreover, emphasizes that the GED:GED interaction reciprocally requires LG:LG interactions.

4.4. Formation of GMP upon hGBP-1 catalyzed GTP hydrolysis is controlled by helical motions

The series of events including GTP binding and hydrolysis, nucleotide dependent regulation of self-assembly to higher order oligomers and their disassembly, as well as oligomer dependent stimulation of the GTP turnover are features that all members of the dynamin superfamily including hGBP-1 have in common. Comprising a multi-domain

architecture with particular role of each domain is the structural basis for a coordinated regulation of the multitude of interdependent processes described. Gaining further insights into the basic biochemical and structural properties of the proteins at molecular levels and correlating these data with their physiological and pathophysiological functions at cellular levels is still a major topic of ongoing research.

Although sharing all the characteristics that members of the dynamin superfamily have in common, their manifestation and additional properties render hGBP-1 unique. One of the most striking features of hGBP-1 is its capability to hydrolyze GTP in two successive steps, both of which are accomplished by cleaving a single phosphate group. The finally yielded nucleotide product is a mixture of GDP and GMP with a certain ratio that strongly depends on the reaction temperature. While at the temperature optimum of 37°C GMP with 90 % is the predominant product, decreasing the temperature to 25°C shifts the share of GMP to 40 %. In this process, dissociation of the GDP bound dimer intermediate has been proposed as a critical factor for the incomplete hydrolysis of GTP to GMP (Kunzelmann, et al., 2005).

Further, hGBP-1 has an altering folding topology that in the nucleotide free ground state adapts a closed conformation. Intramolecular contacts between the amino terminal LG domain and carboxy terminal GED (α 12-13) provide major contributions to this arrangement. GTP binding and hydrolysis, however, trigger conformational changes, disruption of internal contacts, and particularly release of the GED. As being directly linked to the course of GTP hydrolysis, these reversible intramolecular movements suggest an important regulation mechanism of hGBP-1. Like discussed in the previous paragraph, at least dimerization of hGBP-1 seems to be an interdependent process. In this work, we further focused the interdependency of C-terminal motions and the enzymatic activity of hGBP-1. For that, we selected mutants that were previously generated and moreover designed to modify the C-terminus of hGBP-1. Revisiting their enzymatic properties, we could identify a striking dependency between the open state of hGBP-1 and its capacity to produce GMP which prompted us to hypothesize that opening is an essential prerequisite for the unique second hydrolysis step catalyzed by hGBP-1.

In the series of hGBP-1 mutants starting from the closed and going to the most open variant, the mutants CL and 1-LG, respectively, build the two extremes. While the CL-mutant (full-length protein) due to intramolecular cross-linking is constitutively trapped in the closed conformation, 1-LG consists of the catalytic LG domain (aa 1-327) only and thus can act entirely free from any helical regulation. In line with that, CL catalyzed GTP hydrolysis yielded

Discussion

only 3 % of GMP while it was 75 % for 1-LG. Wild type hGBP-1 under the same tested conditions (150 mM NaCl in the buffer, 25°C), in comparison, yields a GMP proportion of 40 %.

To further elucidate the correlation we created a number of mutations at different positions of hGBP-1 that with high probability could engage into the β -phosphate cleavage step of GTP hydrolysis. The first set of mutations relates to the GED: mutations affected either the GED itself (truncation of helix α 13) or they were placed into its close proximity (phenylalanine point mutants within the LG domain). The other mutation K76A was the most distant at sites of the LG dimer interface apparently not being directly related to the GED. However, a deficiency in the second hydrolysis step has been reported for K76A earlier which rendered that mutant as an interesting candidate for our studies (Praefcke, et al., 2004). We found that all of these mutants had some significant, albeit different effects on the second hydrolysis step which altogether supported our initial hypothesis and, moreover, supplied further insights how the helical movements are regulated as will be drawn below and in the next paragraph.

The very C-terminal helix α 13, so far, was simply handled as an extended part of the elongated helix α 12 of hGBP-1. However, the putative stretching out upon dimerization suggested by structural analysis (Annamalai, 2013), as well as the most recent data revealing involvement of α 13: α 13 interactions in hGBP-1's self-assembly suggest a more particular role of the helix (Vöpel, et al., 2014). With respect to the intramolecular motions, α 13 as part of the GED participates in establishing key ionic contacts with the LG domain for maintaining the closed conformation. In line with that, deletion of helix α 13 created a number of differences in comparison to the wild type protein: besides an enhanced GTPase activity by almost 2-fold, GMP was the predominating product accounting for 75 % of the total. Since specific activities for GMP and GDP formation added up to almost exactly 100 % of the GTP turnover, pyrophosphate cleavage could be ruled out as putative reason for the enhanced GMP formation. Consequently, absence of α 13 did not alter the successive mechanism of GTP hydrolysis. hGBP-1 $\Delta\alpha$ 13 also retained the cooperative mechanism of GTP hydrolysis with a slightly weaker dimer affinity than wt hGBP-1. Dimerization could be confirmed directly by analytical SEC in presence of GDP·AlF_x. Considering further that α 12 but not α 13 is predicted to maintain the coiled-coil interaction of GEDs (Syguda, et al., 2012), α 13 appears dispensable for forming LG and GED involved opened dimers.

The listed features of hGBP-1 $\Delta\alpha$ 13 do perfectly overlap with the parameters obtained for 1-LG which, to remind, is the isolated LG domain free from any C-terminal control. Accordingly,

Discussion

one could assume that deletion of $\alpha 13$ might be sufficient to shift the protein to the completely open state (an equilibrium at which an open safety pin like conformation is majorly populated) ensuring that the catalytic domain can undergo all GTP hydrolysis steps to comparable extent as 1-LG without underlying intramolecular control mechanisms of the GED. This can be at least proven by the specific activities of product formation: GMP is generated almost four times faster than GDP which is reversal to the wild-type behavior. However, both known mutants lacking the entire GED (1-LG and Δ GED) have one striking additional feature which $\Delta\alpha 13$ does not have: utilizing external GDP as substrate for cooperative hydrolysis. Due to that it seems reasonable that helix $\alpha 13$ has a particular role in regulating the GTP hydrolysis with respects to defined GDP to GMP product ratio while major contributions to substrate specificity (GTP or GDP) are provided by helix $\alpha 12$. Latter one can be considered as main indicator for the GED-loss-of-control or, more precisely, as marker for the open conformation devoid of any intramolecular control.

But how is this enhanced GMP production explainable when the additional feature to take up GDP for further hydrolysis is excluded? Based on the nucleotide-free crystal structure of hGBP-1 (pdb: 1gd3), $\alpha 13$ after a helical turn forms a coiled-coil type of interaction with $\alpha 12$ but each of the helices provide individual residues to establish a network of salt bridges to the LG domain which finally connects the C-terminus to the N-terminus. Deletion of $\alpha 13$ consequently results in an overall weaker association of the GED and LG domain which is best demonstrated by analytical SEC performed with GTP γ S or GppNHp; Wild type hGBP-1 eluted as dimer in presence of either GTP γ S or GppNHp. Following the line of argument in the previous paragraph, neither analog succeeded to establish intramolecular release of GED for intermolecular GED:GED interaction required to form stable dimers. However, both of the analogs managed to shift the hGBP-1 $\Delta\alpha 13$ equilibrium to a partly dimeric state suggesting a more open conformation upon $\alpha 13$ deletion. Although tested only for the GTP bound state, the enhanced capability of hGBP-1 $\Delta\alpha 13$ to dimerize is conceivable to positively influence also the lifetime of the GDP bound intermediate during GTPase cycle which would explain the enhanced GMP production. However, lifetime of the intermediate and in particular its dissociation to release GDP as product and the particular effects that several mutations probably have on this step is definitely a feature that needs to be assessed in further studies.

Moving from the very C-terminus of the protein into the LG domain adjacent to the GED, we could identify a cluster of phenylalanine residues that upon mutational analysis turned out as key players in transmitting nucleotide induced conformational changes from the LG domain

Discussion

towards the GED and/or vice versa. The triple mutant 3-Phe (F171A/F174A/F175A) in contrast to the deletion mutant $\Delta\alpha 13$ completely adapted 1-LG characteristics, meaning a high GTP turnover number yielding 75-80 % of GMP as resulting product, and above all, exploiting external GDP as substrate which was hydrolyzed in a cooperative manner. In view of the obtained K_d value (0.04 μM) and the maximum specific activity (4 min^{-1}), 3-Phe catalyzed GDP hydrolysis appeared even more efficient than observed for 1-LG. All these data already implicate a loss of control between the LG and GED. Above all, intermolecular FRET measurements and analytical SEC in presence of any tested GTP analog, GppNHp, GTP γ S, and GDP \cdot AlF $_x$ yielded C-terminal approach and tight dimer formation, respectively, altogether confirming enhanced availability of the GED and relaxation of constraints in the LG domain. Deletion of the GED (3-Phe Δ GED), consistently, did not yield any alterations in the basic properties of full-length 3-Phe. Moreover, 3-Phe other than wt hGBP-1 appeared very sensitive to trypsin cleavage which strongly suggests a more open conformation incapable of shielding the multiplicity of putative cleavage sites.

Further pronouncing the similarity to 1-LG, we found that 1-LG, 3-Phe and 3-Phe Δ GED have remarkably decelerated nucleotide binding dynamics. However, decelerated rates of association and dissociation compensated such that the resulting affinity remained mainly unaffected as compared with wt hGBP-1. Dissociation rate of GDP, nevertheless, occurred as an interesting parameter as it was perfectly correlating with the GDPase activity of either protein. Having the smallest k_{off} values (1 s^{-1}), 3-Phe and 3-Phe Δ GED performed the highest GDPase activity (3.7 min^{-1}). At the same protein concentration tested, 1-LG had a catalytic activity of 1.6 min^{-1} and a correspondingly faster k_{off} value for GDP dissociation (3 s^{-1}). Also consistent with the very slow activity of hGBP-1 (0.04 min^{-1} ; from Vöpel, et al., 2010), dissociation of GDP and hGBP-1 occurred as the fastest (10 s^{-1}). For sure, it is not favorable for the β -phosphate cleavage step when GDP dissociates faster than it can be hydrolyzed. On the other hand, longer lasting of the nucleotide can be neglectable, when the GDP dependent dimer dissociates faster. However, the correlation above might be suitable to judge the capacity of hGBP-1 mutants to utilize GDP as substrate, but as proven by hGBP-1 $\Delta\alpha 13$, it is useless for having an idea about the GDP intermediate and its lifetime in the course of GTP hydrolysis: both wt and $\Delta\alpha 13$ have similarly fast GDP dissociation rates but $\Delta\alpha 13$ yields definitely higher GMP amounts.

We also investigated the hGBP-1 point mutant K76A which is in the elongated switch I region and as part of the phosphate cap in close proximity to the γ -phosphate group. Although

being at the opposite site of the intramolecular interaction region, the particular mutation caused a production of only 3 % GMP upon GTP hydrolysis. Thus, we proposed a relationship to the intramolecular opening. The mutant has been reported to hydrolyze GTP in a cooperative manner. Although stimulated activity of K76A was reduced by 25 %, the apparent dimer dissociation constant nevertheless appeared undistinguishable from the wt (Praefcke, et al., 2004). These results clearly indicate dimerization of K76A which is the essential requirement for GMP formation; monomeric protein, in contrast, exhibits only slow basal GTPase activity which yields GDP as exclusive product (Kunzelmann, et al., 2006) (Abdullah, et al., 2010). Our analytical SEC experiments with GDP·AlF_x to directly address dimerization, however, suggested a weaker dimerization of K76A. The protein eluted as both dimer and monomer, with latter one being the dominant proportion (~60 %). Theoretically, 40 % of dimeric protein should be sufficient to yield considerable amounts of GMP but, nevertheless, not more than 3-6 % could be obtained which strongly suggests another reason for the observed deficiency.

As the enzymatic properties of K76A resembled the constitutively closed CL-mutant also being incapable of GMP formation, a trapped conformation appeared as possible option. In fact, introducing the same mutation into the isolated LG domain (LG-76) in order to eliminate any influences from the GED restored all the typical characteristics: LG-76 with respect to dimerization, dimer-dependent GTPase activity and particularly GMP formation behaved very similar to its non-mutated counterpart 1-LG. This in sum gave strong evidence that K76 is not a catalytic residue important for the second hydrolysis step. It seemed rather that K76A on basis of the full-length protein caused a trapped conformation. Intramolecular opening in K76A and intermolecular GED:GED approach, further measured by FRET, demonstrated at least ten times decelerated kinetics as compared to wt. These results suggest a restriction of the GED from release, and consequently, from GED:GED interaction for stable dimerization.

A few more positions within the switch I and switch II regions have been reported to have characteristics similar to K76A. Mutation H74A is one of them, and we obtained the same results as for K76A when comparing full-length and LG variants of the mutant (data not shown). Position H74 and K76 flank the conserved threonine T75 (G2) but interestingly, substitution of the threonine leads to almost completely abolished GTPase activity and cooperativity while it is still maintained when either H74 or K76 are replaced implicating that latter ones might be important in coordinating the conserved residue. The switch II region (aa 99-112) including the G3 motif (DxxG) harbors various residues that are also essential in GMP

production. Forming the beginning and the end of the switch, both positions E99 and D112 when replaced by an alanine yielded only 8 % or 2 % GMP, but noteworthy, they performed also significantly reduced GTPase activity as compared with wt. Having slightly reduced GTPase activity but dramatically reduced GMP levels, K106A was very similar to the switch I mutants H74A and K76A. Further, GTP hydrolysis catalyzed by the single mutants D103A and D108A still yielded reasonable amounts of GMP, however, the double mutant turned out incapable of GMP production (Praefcke, et al., 2004) (Abdullah, et al., 2010). Abdullah and others proposed that conformational changes of the switch II allosterically regulate the connecting region of hGBP-1 for further dimerization and efficient GMP production. As a conclusion, GMP deficiency of the switch II mutants was related to disturbed allostery and consequently inhibited dimerization (Abdullah, et al., 2010). However, stimulated GTPase activity is a strong indicator for dimerization and contradicts the constitutive monomeric state. It seems rather that dimers assemble to catalyze the first hydrolysis step yielding GDP, but probably due to reduced stability tend to dissociate much faster than the second hydrolysis step can occur. This is further supported by an overall reduced GTPase activity and our FRET data illustrating significantly slower intramolecular opening and GED:GED interaction. Latter one has already been discussed as essential property for stable dimer formation while the intramolecular opening itself revealed mutually essential for stabilizing the LG interface. An inappropriate arrangement of the switches due to particular mutations is conceivable to counteract the LG:LG dimers, as well. In fact, crystal structures suggest major conformational changes within the switch regions when comparing GTP and GDP bound forms of hGBP-1, and furthermore, major parts of switch I and switch II appear completely buried in the LG dimers (Prakash, et al., 2000b) (Ghosh, et al., 2006). Taken together, switch regions of hGBP-1 appear essential to the dynamics of dimer formation, either acting directly in the LG:LG interface or indirectly by triggering conformational changes towards the GED for intramolecular opening which in turn stabilizes the LG interface and facilitates GED:GED interactions.

4.5. Additional structural elements in the LG domain of hGBP-1 mediate intramolecular motions

Resolving the first crystal structure revealed a multidomain architecture of hGBP-1 consisting of a LG domain, a middle domain and a GTPase effector domain (GED). Although built on the canonical Ras topology, the large G (LG) domain of hGBP-1 includes a series of insertions which in whole enlarged the subdomain by almost 100 amino acids as compared with Ras. Besides the insertions that caused larger switch loops of hGBP-1 there were two

Discussion

more insertions, insertion 3 (I3) and 4 (I4), adjacent to the GED (figure 4-2) and predicted to be important in stabilizing the GED (Prakash, et al., 2000a). Helix $\alpha 4'$ corresponding to I4 indeed turned out as essential part of the LG:GED interaction. Particularly residues R227 and K228 within $\alpha 4'$ were shown to establish key ionic contacts with $\alpha 12$ and $\alpha 13$ involving the residues E556, E563, E568, and E575. Mutational analyses indicated that movement of $\alpha 4'$ during GTP binding and hydrolysis led to disruption of the ionic contacts necessary for GED release and further interaction. The charge reversed mutant (RK-mutant: R227E/R228E), in accordance, created a permanently open state of the protein which compared to the wt showed increased dimerization, GTPase activity, GMP production and, moreover, GDPase activity utilizing external GDP as substrate (Vöpel et al., 2010) (Syguda, et al., 2012). All these characteristics found as typical indicators for a permanently open state of hGBP-1 were also maintained by the mutant 3-Phe (paragraph 3.2.3.). The substituted phenylalanines of 3-Phe (F171A/F174A/F175A), however, reside in $\alpha 3'$ which is actually part of insertions 3 (figure 4-2). Due to comparable biochemical consequences that mutations 3-Phe and RK have and due to their particular localization close to the GED, altogether, both insertion elements $\alpha 3'$ and $\alpha 4'$ can be assumed as essential mediators of hGBP-1's intramolecular movements.

Although the nature of intramolecular interaction provided by the positions R227 and K228 is well understood, it remains elusive for the phenylalanine residues. It is also not clear, whether the tested phenylalanines provide direct interactions to the GED or rather assist in coordinating neighboring residues. In this context it might be noteworthy to redirect the focus to the preceding sequence that harbors several negatively charged amino acids (D159, E160, E162, E164, E166, D167, and D170) potent to establish ionic contacts to the GED. Being also part of insertion 3 this region seems to be highly flexible as it is not solved in any crystal structure of hGBP-1 (depicted as dotted line in figure 4-2). However, only recently have Persico and others published a molecular model of hGBP-1 which delivers all the missing elements including the mentioned loop. Further, the model might provide insights into the structural organization during GTP hydrolysis as it was built in complex with GDP·AlF_x (Persico, et al., 2015). This model at least validates disruptions of the key ionic interactions between $\alpha 12$ -13 (E556, E563, E568, and E575) and helix $\alpha 4'$ (R227 and K228) during GTP hydrolysis as previously suggested from experimental data (Vöpel, et al., 2010) (Syguda, et al., 2012). What is more, $\alpha 13$ in the GDP·AlF_x bound model utilizes its positively charged residues (R584, R585, R586, and K587), instead, to establish ionic contacts to the negatively charged residues of the loop adjacent to helix $\alpha 3'$. As $\alpha 13$ also appears more detached from the LG domain, one could speculate about a particular role of the loop in intramolecular opening, even about a

nucleotide dependent switch function to sense and/or transmit conformational changes from the LG toward the GED, or the other way around. For sure, the model needs to be confirmed experimentally but considering the observations to be real, the loop might have an essential role in regulating intramolecular interactions of hGBP-1. As a central element, above all, the loop could conduct all the regions that we have separately identified as critical participants in LG:GED interactions to a single network, probably acting in a coordinated manner: the loop precedes helix $\alpha 3'$ (3-Phe) and interacts with helix $\alpha 13$ ($\Delta\alpha 13$) which in turn interacts with helix $\alpha 4'$ (RK).

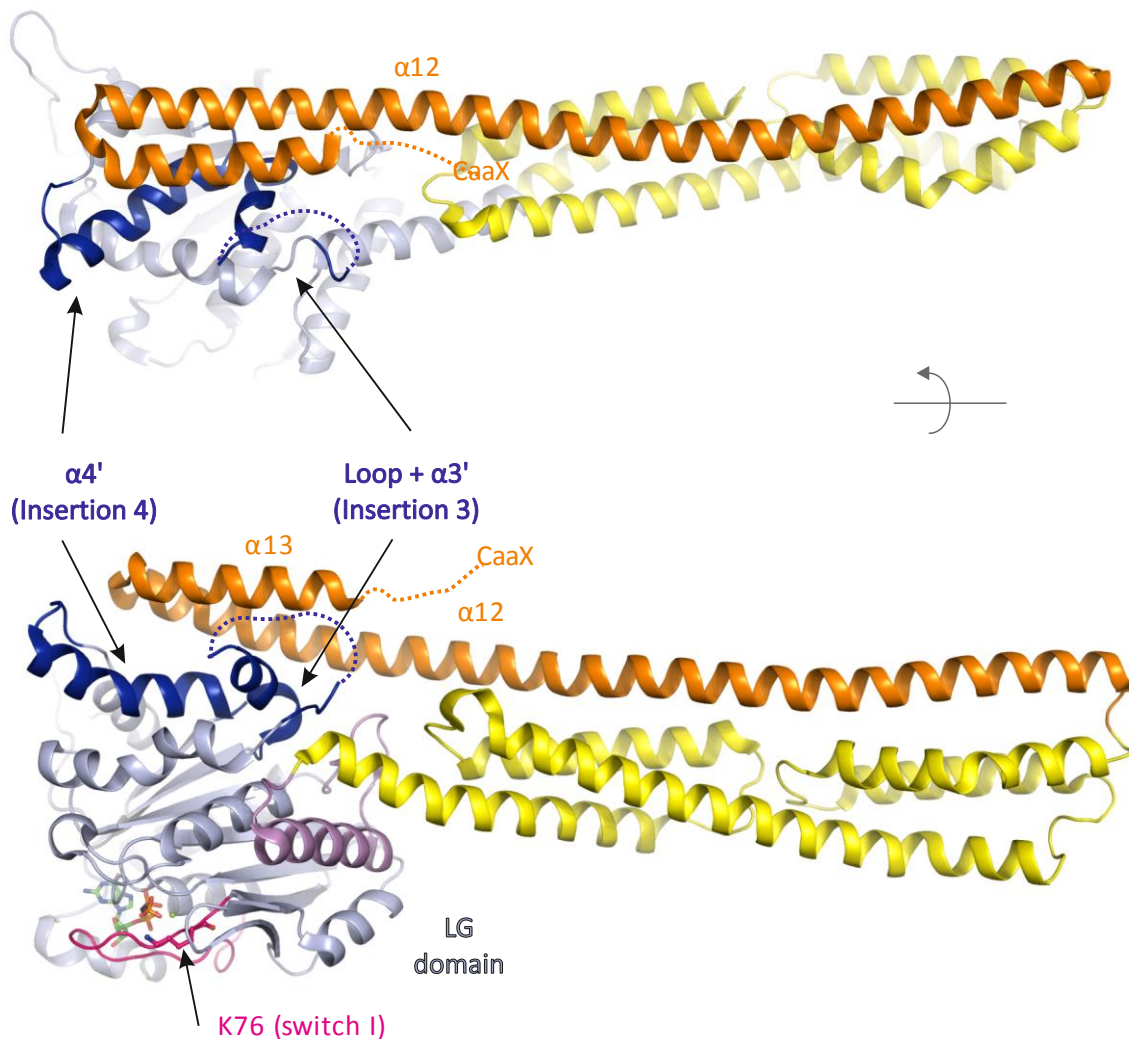


Figure 4-2: Structural elements with critical role in intramolecular LG:GED interactions of hGBP-1. The structure of hGBP-1 (pdb: 1fn5) colored according to the subdomains (LG: light blue, middle domain: yellow; GED consisting of $\alpha 12$ - $\alpha 13$: orange, and non-resolved C-terminus with the CaaX motif: dotted orange line) is depicted in top and side view. Helices $\alpha 4'$ and $\alpha 3'$ (dark blue) from the LG domain harbor the critical residues R227/K228 (RK) and F171/F174/F175 (3-Phe), respectively. The loop preceding $\alpha 3'$ (dotted dark blue line) is predicted to interact with $\alpha 13$ (Persico, et al., 2015). Exact sequences can be looked up in figure 4-5. Although located at the opposite site, K76 (switch I: pink) is also involved in intramolecular interactions (see 4.4.).

4.6. Substrate specificity and product formation serve as indicator for the structural ground state of hGBP-1

By systematic exploration of different site specific and truncation mutants of hGBP-1 we could figure out a dependency between structural arrangements and enzymatic properties. They were helpful towards understanding how particular structural elements regulate the unique enzymatic mechanism. Depending on the ground state, e.g. open versus closed conformation, we obtained a particular pattern of product ratio (certain ratio of GDP to GMP) and substrate specificity (exploiting only GTP or also GDP as substrate). The dimer equilibrium constant is another parameter that defines the protein concentration required for stimulated GTPase or GDPase activity. All these parameters can be reciprocally exploited to judge a novel mutant with special respects to the structural arrangement.

Therefore, we established the long term GTP/GDP hydrolysis studies which revealed as powerful tool to screen all the parameters at one glance as illustrated for 1-LG and wt hGBP-1 (figure 4-3). In a typical setup, serial dilutions of the protein were mixed with 500 μM of GTP or GDP and incubated at 25°C for 24 hours. The nucleotide composition, analyzed via rp-HPLC, was then plotted as function of protein concentration. Decreasing levels of substrate (GTP: upper panel; GDP: lower panel) obviously mark the protein concentration at which efficient hydrolysis becomes relevant. For 1-LG, remarkably, GDP hydrolysis sets in at higher protein concentrations than GTP hydrolysis which perfectly reflects the weaker affinity of catalytic competent 1-LG·GDP dimers as compared with 1-LG·GTP dimers. Although this setup is not sufficient to quantify dimer affinities, nevertheless, x_1 and x_2 (protein concentrations at which half amount of either substrate is consumed) can serve as benchmarks to relate the affinities to each other. For 3-Phe having also GDPase activity, x_1 and x_2 are almost overlapping which indicates very similar affinities. For wt having only poor GDPase activity, in contrast, x_2 is not even resolved in the tested concentration range (figure 4-3, right panel).

Further, the particular product composition yielding from GTP hydrolysis can be detected directly at the protein concentration where GTP is completely converted. For 1-LG this is just a small concentration slot since set in of GDPase activity leads to further GMP production as indicated by a kink (figure 4-3, left upper panel). For wt hGBP-1, in contrast, the product ratio remains mainly constant up to 10 μM (figure 4-3, right upper panel).

In conclusion, the long term hydrolysis study revealed as fast screening method requiring only little protein amount and workload. Although not capable of replacing kinetic studies, this

Discussion

method rather acts as preliminary study supplying a clear picture about substrate specificity and product formation in a strictly concentration dependent manner as exemplified on 1-LG. Especially for newly generated mutations, this presents a helpful tool to detect particular properties and also to adjust concentration ranges for subsequent experiments, accordingly.

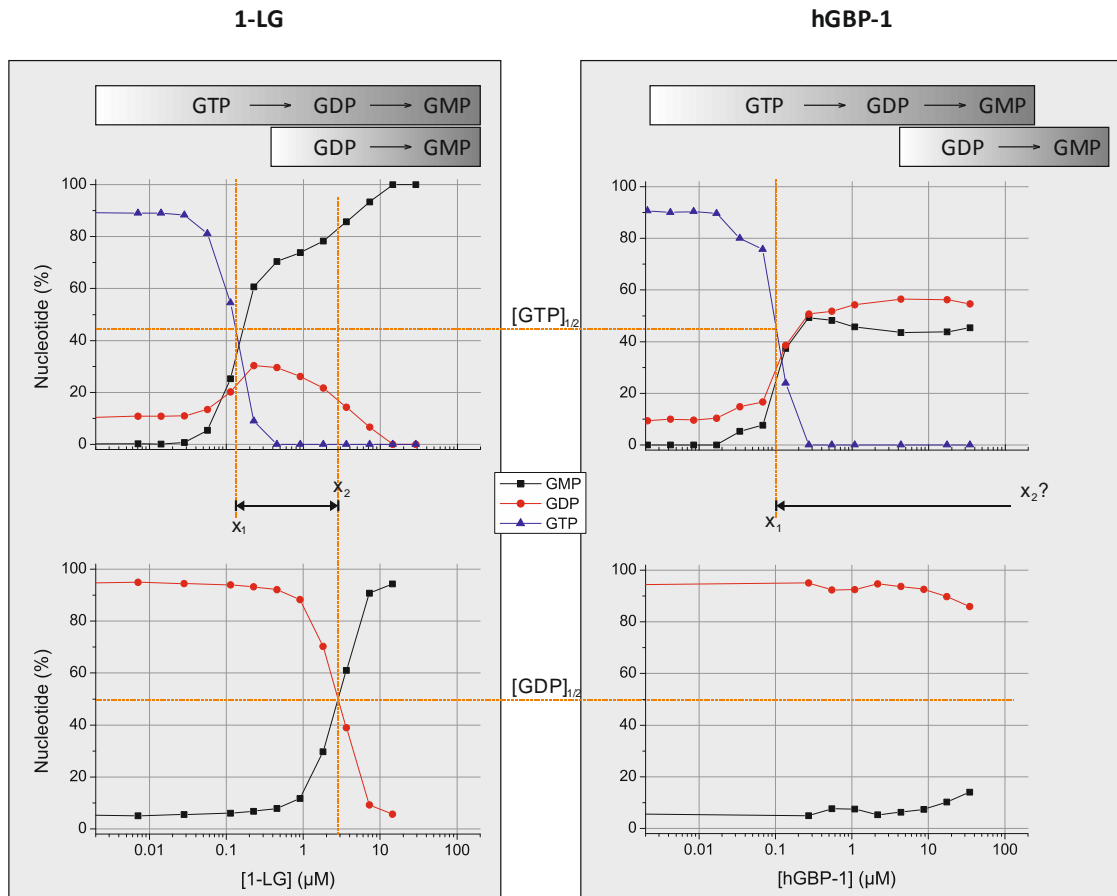


Figure 4-3: Long term GTP/GDP hydrolysis catalyzed by 1-LG (left) and wt hGBP-1 (right). Varying concentrations of 1-LG or wt hGBP-1 were mixed with either 500 μM GTP (upper panels) or GDP (lower panels) to dissect both possible reactions: GTP hydrolysis ($\text{GTP} \rightarrow \text{GDP} \rightarrow \text{GMP}$) and GDP hydrolysis ($\text{GDP} \rightarrow \text{GMP}$). The plots reflect the nucleotide composition at each concentration point. Decreasing levels of substrate (GTP: upper panel; GDP: lower panel) obviously mark the protein concentration at which efficient, dimer dependent hydrolysis becomes relevant. Corresponding to the protein concentrations at which half amount of GTP and GDP is consumed ($[\text{GTP}]_{1/2}$ and $[\text{GDP}]_{1/2}$), respectively, x_1 and x_2 can be used as relative measure for GTP and GDP dependent dimer affinities (orange dotted lines). For the GDPase active 1-LG, GDP dependent dimers appear almost 10-fold weaker than GTP dependent dimers ($x_2/x_1 \approx 10$). For the poorly GDPase active wt hGBP-1 the discrepancy appears even larger considering that x_2 is not even resolved.

4.7. Characterization of the isoforms hGBP-2, hGBP-3 and hGBP-5

Human GBPs are immuno-related proteins that are strongly upregulated in response to pathogenic infection and cytokine release, in particular by IFN- γ (Olszewski, et al., 2006) (Tripal, et al., 2007). Many different cellular functions have been reported for hGBP-1 over the past decades, and recent studies also provide insights into particular roles of other members, for instance, tumor-related hGBP-2 and hGBP-5, or, a newly identified splice variant of hGBP-3 with antiviral activity (Nordmann, et al., 2012). Further, five of the isoforms (hGBP-1 to hGBP-5) revealed capable of forming homo as well as hetero complexes with the consequence of subcellular translocation (Britzen-Laurent, et al., 2010). Suggesting homo and hetero interactions of hGBPs as essential feature for developing full functionality, understanding of their cellular networking relies on quantitative data which to date are not present. Also biochemical and biophysical characterization of individual hGBPs as fundamental prerequisite for insights into molecular details are at rudimentary stage. To present, features of hGBP-1 and hGBP-5 are well-documented but only initial experiments were performed on hGBP-2 while entirely lacking for the remaining members. In this work, biochemical properties of the hGBP family members hGBP-1, hGBP-2, hGBP-3, and hGBP-5 were focused and yielded an individual pattern for each member suggesting particular role within the network (paragraph 4.7.2.). Moreover, a fluorescence based setup was established to further characterize particularly hetero interactions of hGBPs *in vitro*. Initially, labelling procedure and experimental conditions were tested for the isolated LG domains only, and indeed were hetero interactions detectable. Obtained by semi-quantitative analysis, further, these hetero complexes were found to have different affinities as will be discussed in paragraph 4.9.

4.7.1. Purification

For studies of this work full-length and truncated constructs of hGBP-1, hGBP-2, hGBP-3, and hGBP-5 (only isolated LG domain) were synthesized in *E. coli* strains Rosetta (DE3) and BL21 (DE3) according to the standard protocol of hGBP-1. Also in accordance with the standard protocol of hGBP-1, proteins were successively purified by affinity chromatography and preparative gel filtration. All proteins were highly soluble and purification and enrichment worked out without obstacles. Finally ~10 mg of highly pure, amino-terminally hexa-histidine tagged protein was obtained from 1 liter of *E. coli* culture.

Concerning stability, handling of full-length hGBP-3 revealed as the hardest challenge as it had a high tendency to precipitate at some non-definable point; either during protein

purification, ultrafiltration or even during measurements. Although precipitation virtually disappeared when for example up to 1 M NaCl was supplemented to the stock solution, however, it did not prevent the protein from repeated precipitation at any another stage. Different buffer compounds such as glycerol, varying salt and DTT concentrations have been tested extensively (data not shown) but none of them did reliably improve the stability. Probably, hGBP-3 other than the remaining isoforms requires some unknown factor to remain stable: this could be additional nucleotide or even another isoform as interaction partner as will be figured out and optimized in future studies. At least, comparable impairments were not observed for the C-terminally truncated variants of hGBP-3 (hGBP-3-(aa 1-481) and isolated 3-LG), thus, the instability may be related to the C-terminus. However, to have as accurate data as possible also for full-length hGBP-3 under given conditions, enzymatic activity and nucleotide binding properties were exclusively performed with freshly prepared and non-frozen protein. As shown by SDS-PAGE and analytical gel filtration, a cycle of freezing and thawing caused hGBP-3 to react to covalent dimers which makes it impossible to identify or dissect dimer dependent processes.

4.7.2. Individual biochemical fingerprint for each isoform

Human GBP-1, hGBP-2, hGBP-3 and hGBP-5 are four of the seven isoforms sharing a high sequence identity. The deviations are mainly caused by C-terminal diversity while the catalytic LG domain appears highly conserved. In line with the latter fact, all the investigated hGBP isoforms revealed to have one commonsense in their enzymatic function, namely accelerated GTPase activity in the course of concentration dependent self-assembly. Moreover, the LG domain of all investigated hGBPs occurred as the functional unit responsible for mediating both self-assembly and stimulated GTPase activity, as already shown for hGBP-1. This was clearly demonstrated by the fact that the isolated LG domains were sufficient to provide the same enzymatic activity with almost identical dimer dissociation constants as the respective full-length counterparts. For hGBP-1, LG-mediated dimerization has been identified to stabilize catalytic residues for efficient GTP hydrolysis. Based on structural and mutational analysis, dimerization-dependent repositioning of the arginine finger (R48) into the catalytic pocket turned out to be an essential mechanism (Ghosh, et al., 2006). The same mechanism is conceivable also for hGBP-2, hGBP-3 and hGBP-5 since their sequence motifs for GTP binding and hydrolysis are absolutely identical.

Despite the general mechanism of cooperative GTP hydrolysis, however, each of the investigated hGBP yielded a unique pattern regarding maximum GTPase activity, homo dimer

Discussion

affinity and product composition (figure 4-4 A). As illustrated in figure 4-4 A (left panel), hGBP-1 and hGBP-3 appeared highly active in catalyzing GTP turnover which yielded a stimulated activity of 19.1 min^{-1} and 14.4 min^{-1} , respectively. In contrast, hGBP-2 provided almost half of the activity (7.4 min^{-1}) and hGBP-5 even less (3.5 min^{-1} , adapted from unpublished data of Kutsch). Further, hGBP-2 catalyzed GTP hydrolysis did not yield considerable amounts of GMP (2-3 %). The same has been reported for hGBP-5 previously (Wehner, et al., 2010), giving evidence that successive cleavage of GTP to a mixture of GDP and GMP is not a mechanism that all hGBPs have in common (see paragraph 4.8.). However, hGBP-3 being the closest homolog of hGBP-1 (sequence identity of 88 %) succeeded to produce similar amounts of GMP like hGBP-1 (figure 4-4 A, right panel). Apparently sharing very similar characteristics, however, GTP dependent dimerization of hGBP-3 and hGBP-1 revealed one crucial difference: Homo dimers of hGBP-3 had a 20-fold weaker affinity than homo dimers of hGBP-1. This impressively demonstrates that the remaining differences in the sequence were sufficient to alter the dimerization behavior of hGBP-3 significantly, probably by causing deviations in the LG interface. Similarly reduced dimer affinities determined also for hGBP-2 (10-fold) and hGBP-5 (45-fold) indicate a putative distinct role of higher affine hGBP-1 dimers which cannot be specified yet. Considering the important role of hGBP-1's guanine cap in dimer formation, closer inspection of the corresponding amino acids of hGBP-2, -3 and -5 revealed some differences probably responsible for weaker dimerization. Particularly, substitution of the hGBP-1 residues R240 or R244 by an alanine has been shown to cause striking decrease in dimer affinity (Wehner, et al., 2012) (figure 4-4 B, bold type). At corresponding position to hGBP-1's R240, the isoforms hGBP-2, hGBP-3 and hGBP-5 have a tryptophan or leucine, instead, which might be responsible for weaker dimer affinities. The second position R244 may be critical only for hGBP-5 as it has a glutamine instead of a positively charged residue like the others have. However, back mutation to an arginine might shed light on the particular role of mentioned residues. It needs to be further assessed if post-translational prenylation -relevant for the CaaX-box containing isoforms hGBP-1, hGBP-2 and hGBP-5- might have any effect on dimerization. At least for hGBP-1 corresponding results are contradictory: while yeast two-hybrid experiments clearly demonstrate enhanced self-assembly upon farnesylation, in contrast, K_d values derived from GTP hydrolysis assay suggest a 2-fold weaker self-assembly of farnesylated hGBP-1 (Benscheid, 2005) (Fres, et al., 2010). Comparable experiments for the other isoforms have not been performed yet. Anyhow, for hGBP-3 the situation remains unchanged as it does not contain a CaaX sequence and thus will not be further modified.

Discussion

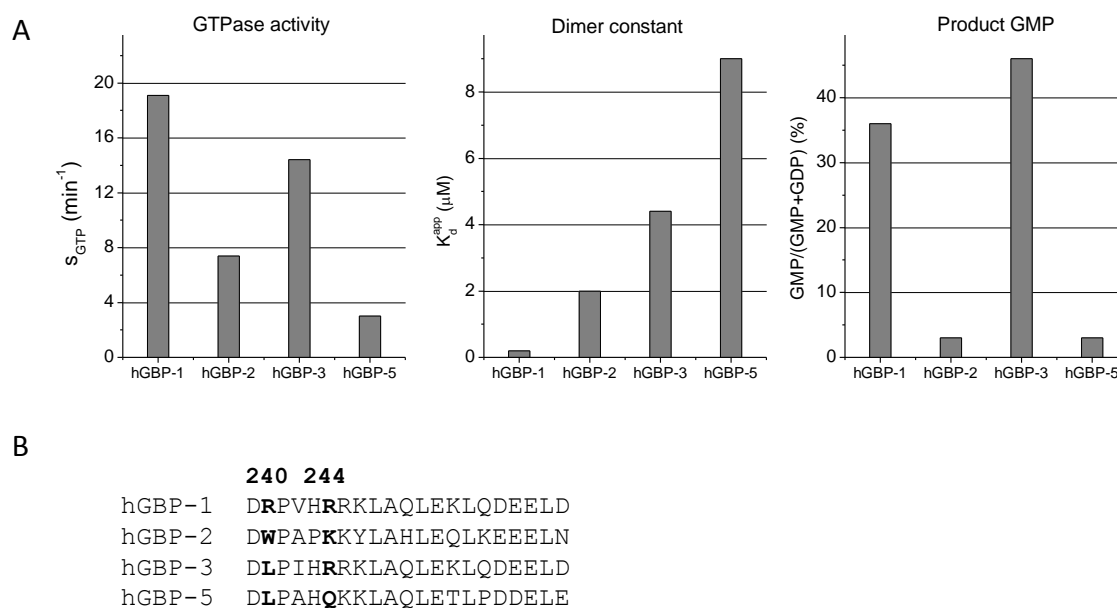


Figure 4-4: Enzymatic activity of hGBP-1, -2, -3, -5 and sequence alignment of guanine cap residues. (A) Bar charts of enzymatic parameters of hGBP-1, -2, -3, -5 that were derived from GTPase activity assays and listed in table 3-8 and 3-9. Panels left to right depict the maximum activity of GTP hydrolysis (s_{GTP}), apparent dimer constant (K_d^{app}) and GMP formation (%) obtained for each hGBP isoform. The enzymatic parameters were derived from the same dataset of concentration dependent measurements performed under physiological salt conditions at 25°C. Respective data of full-length hGBP-5 are adapted from Miriam Kutsch (unpublished data). (B) Sequence alignment guanine cap residues. Major constituents of hGBP-1's homo dimerization are R240 and R244 as indicated. These and corresponding residues of hGBP-2, -3 and -5 are depicted in bold type.

Understanding nucleotide binding as a key feature of nucleotide dependent interactions and considering the potential of human GBPs to switch between three different states (GTP, GDP and GMP bound forms), also nucleotide binding affinities of all proteins –including truncation mutants- have been analyzed within this work. Besides similarities, large variations could be identified in binding affinities which span a range of four orders of magnitude, from 0.05 μM to 604 μM . In view of a roughly constant nucleotide composition within the cell, these huge disparities are likely to account for a certain distribution of hGBPs into a particular nucleotide state. Even subsisting in the nucleotide-free state becomes conceivable when considering that nucleotide amount is limited (see paragraph 4.9.).

However, to have a condensed view, obtained K_d values of the protein:mant-nucleotide complexes (listed in table 3-13) were classified according to a logarithmic scaling as listed and

Discussion

described in table 4-1. Although having rather similar enzymatic features, strikingly, hGBP-2 and hGBP-5 revealed as isoforms with the highest and lowest nucleotide binding affinities, respectively. hGBP-2 interacted with both mGDP and GTP γ S (reflecting the exclusive product and substrate, respectively) with equally high affinity ($K_d = 0.05 \mu\text{M}$). This was mainly caused by crucially reduced dissociation rates as obtained by kinetic studies: for instance, dissociation of hGBP-2 and mGDP was decelerated by 250-fold as compared with hGBP-1. Interestingly, hGBP-2 also provided fairly high mGMP binding affinity which is not consistent with the lacking GMP production upon GTP hydrolysis. hGBP-5 being also incapable of producing GMP, has been shown to be incapable of mGMP binding, accordingly (Wehner, et. al., 2010). Based on the truncation mutant 5-LG we obtained a dissociation constant of $604 \mu\text{M}$ which confirmed previous results and, further, demonstrated that truncation of helical parts did not remarkably alter hGBP-5's capacity to bind nucleotides. Only for 5-LG and mGDP, slightly decreased affinities were identified. Likewise, hGBP-3 did not display remarkably altering nucleotide binding affinities upon C-terminal truncation. The apparent differences in the table merely result from the classification system. In contrast, C-terminal truncation of hGBP-2 (2-LG) crucially affected nucleotide binding, particularly binding of mGMP and mGppNHp. Mainly caused by reduced association rates, interactions of 2-LG with nucleotides occurred up to 240-fold weaker than obtained for hGBP-2. This suggests an important role of the C-terminal domain in facilitating nucleotide binding.

Table 4-1: Classification of hGBPs' nucleotide binding affinities. Depending on K_d values, affinities were classified in logarithmic manner and highlighted by both symbols and color codes: $0.01\text{-}0.099 \mu\text{M}$ (+++, dark blue), $0.1\text{-}0.99 \mu\text{M}$ (++, blue), $1.0\text{-}9.9 \mu\text{M}$ (+, light blue), $10\text{-}99 \mu\text{M}$ (0, light orange), $\geq 100 \mu\text{M}$ (-, orange).(*) Values for hGBP-5 and its truncation (aa 1-489) adapted from (Wehner, et al., 2010); (n.d., white) not determined.

	<i>mGMP</i>	<i>mGDP</i>	<i>mGppNHp</i>	<i>mGTPγS</i>
<i>hGBP-1</i>	++	+	+	++
<i>1-LG</i>	+	o	o	+
<i>hGBP-2</i>	+	+++	++	+++
<i>2-LG</i>	-	++	o	+
<i>hGBP-3</i>	o	o	+	++
<i>hGBP-3 (aa 1-481)</i>	+	+	+	++
<i>3-LG</i>	o	+	+	++
<i>*hGBP-5</i>	-	+	n.d.	o
<i>*hGBP-5 (aa 1-489)</i>	-	+	n.d.	o
<i>5-LG</i>	-	o	-	o

4.7.3. Lacking GMP production of hGBP-2 is in apparent contradiction to the previously published data

In a previous study, Neun et al reported that hGBP-2 was sufficient to produce GMP as reaction product from GTP hydrolysis (Neun, et al. 1996). At 37°C, a share of approximately 13 % on total product was obtained which is strikingly reduced compared to hGBP-1 capable of producing even 90-95 % under same conditions (Neun, et al., 1996) (Praefcke, et al., 2004). However, in experiments of the present work we found almost no GMP production (2-3 % at 25°C), and even increasing the temperature to 37°C did not yield larger amounts. In addition to the reaction temperature, we used NaCl in the buffer system while Neun and others used KCl, instead. In order to ensure that not the ions might cause a difference we also tested GTPase activity of hGBP-2 using KCl (data not shown) but the results did not alter. Consequently, we could not confirm the previous results. Further, dimerization was shown to be absolutely necessary also for hGBP-2 to produce GMP (Abdullah, et al., 2010). In fact, concentration dependent GTP hydrolysis assay and analytical SEC in presence of GDP·AlF_x clearly demonstrated dimerization of hGBP-2, nevertheless, no considerable amounts of GMP was detected. Data of Neun et al. even ground on hGBP-2 concentrations below the here obtained dimer dissociation constant of 2^oμM, while we scanned a range up to concentrations 10-fold above where dimerization is expected to be fully established and could not detect considerable amounts of GMP.

Searching for a reasonable explanation, we had a more detailed look at how the protein was prepared. Recombinant hGBP-2 used in the former studies was bacterially synthesized and had an N-terminal hexa-histidine tag. Emerged from cloning via BamHI, two additional residues glycine and serine connected tag and the first amino acid of hGBP-2. This is exactly the same conditions as we have at present. The only explanation is thus the hGBP-2 clone used: Several natural variants of hGBP-2 are described in the database⁵, namely S281P, P285A and S303G which all apply to the catalytic competent LG domain. In our construct, we have none of these mutations included but considering the reference Neun and others denoted as template cDNA, they most probably worked with the P285A variant. This position, consequently, might be an interesting residue putatively determining the GMP formation capability. If this explains the discrepancy between the presence and absence of GMP in hGBP-2 catalyzed GTPase reaction, one could further elucidate corresponding positions of remaining isoforms. For hGBP-1 through hGBP-7, corresponding residues Q287, P285, K285, I302, M285, T286 and L286,

⁵ <http://www.uniprot.org/uniprot/P32456> [09.04.2015]

respectively, display a high diversity in line with the different product ratios obtained for the so far characterized hGBPs. At least for hGBP-1 this residue is positioned within the amino acid region 279-310 which has been proposed critical for GMP formation (Abdullah, et al., 2010) (Rani, et al., 2012).

Based on the many putative steps occurring during cooperative GTP hydrolysis mechanism of hGBP-1 many steps appear conceivable to cause altered product levels (figure 1-8 in introduction): (1) rate of the second cleavage step, (2) rate of GDP dimer dissociation after the first hydrolysis step, (3) repositioning of the intermediate GDP for the second hydrolysis step, and (4) rate of P_i release. Whatever effects the particular variants of hGBP-2 might have on the GTP hydrolysis mechanism, the results from previous studies clearly indicate that also hGBP-2 is principally capable of catalyzing successive hydrolysis of GTP while the obtained proportion of GMP is crucially lower than for hGBP-1 and hGBP-3. Obviously, there are also variants (used in this work) that do not produce GMP at all suggesting a particular role of GMP production for biological function.

4.8. GTPase activity of hGBP-3 is controlled by the C-terminus

For hGBP-1, regulatory effect of the C-terminus on the enzymatic activity has already been described in detail (paragraph 4.4.). This effect is mostly demonstrated by the enzymatic differences that either 1-LG or full-length hGBP-1 exhibit; structurally, 1-LG is devoid of the helical parts α 7-13 but, enzymatically, it catalyzes enhanced GTP turnover which results in GMP as predominant product. And most crucially, 1-LG can utilize also GDP as substrate. The latter fact could not be found in any other isoform, 2-LG, 3-LG or 5-LG. Gain of GDPase function upon helical truncation is thus a unique property of hGBP-1.

Effects of C-terminal truncation on the GTPase activity, interestingly, could not be observed for either hGBP-2 or hGBP-5. Respective truncations 2-LG and 5-LG retained the same GTPase activity with lacking GMP production. This indicates that the C-terminal domain is not involved in the catalytic machinery and, moreover, supports that impaired GMP production of hGBP-2 and hGBP-5 is not due to a trapped conformation which in case of some hGBP-1 mutants was observed to counteract GMP formation. In contrast to hGBP-2 and hGBP-5, helical truncation of hGBP-3 indeed caused enzymatic alteration. Full-length hGBP-3 was competent to catalyze efficient GTP turnover similar to hGBP-1. Deletion of the helical domain, either only α 12-13 (hGBP-3 Δ GED) or the entire C-terminal domain (3-LG), enabled the protein to act even 3 to 4 times faster, like observed for hGBP-1. As a remarkable

Discussion

difference to hGBP-1, however, GMP amounts produced by hGBP-3 did not increase but rather decreased upon deletion. In analogy to hGBP-1, this altogether suggests that also hGBP-3 is subject to intramolecular interactions between the LG domain and the GED capable to regulate the enzymatic activity.

A closer look at the regions that are identified to regulate intramolecular interactions of hGBP-1 unravel that hGBP-3 and also hGBP-2 harbor both of the important residues R227/K228 (helix $\alpha 4'$) also corresponding negatively charged residues within $\alpha 12-13$ to establish the key ionic contacts between LG domain and GED (figure 4-5). They do also harbor the three phenylalanines (F171/F174/F175) that have been identified as critical residues within this work. Nevertheless, hGBP-1 and hGBP-3 but not hGBP-2 appeared sensitive to C-terminal truncation, giving support to the critical role of the loop region in mediating intramolecular opening as already discussed in paragraph 4.5. Obviously, amino acid composition of the isoforms strongly deviate in this region (figure 4-5). However, hGBP-3 except for deletion of two amino acids adapts the same composition of hGBP-1. In total, hGBP-3 retains five of the six negatively charged residues in the loop and, above all, several positively charged residues within $\alpha 13$ that altogether appear suitable to establish ionic contacts to maintain intramolecular opening as proposed by Persico and others (Persico, et al., 2015).

Although appropriately equipped on primary sequence basis, it is unknown whether hGBP-3 has the same folding topology as hGBP-1 that allows the putative contacts to occur. The high sequence identity of 88 %, at least, could suggest similar structural arrangements of hGBP-3 and hGBP-1. Experimentally, SEC analysis of the GED truncated variants (hGBP-3 (aa 1-481) and hGBP-1 (aa 1-481)) give evidence for a similarly elongated shape of hGBP-3: In the monomeric form, both proteins eluted with an apparent size of ~90 kDa which is similar to the elution behavior of full-length protein (hGBP-1 wt) and, moreover, much larger than the calculated size of 55 kDa. For hGBP-1, the middle domain was found to account for the elongated shape and thus for the apparently larger size through SEC (Prakash, et al., 2000a) (Benscheid, 2005). Consequently, the same appearance becomes likely also for hGBP-3.

Discussion

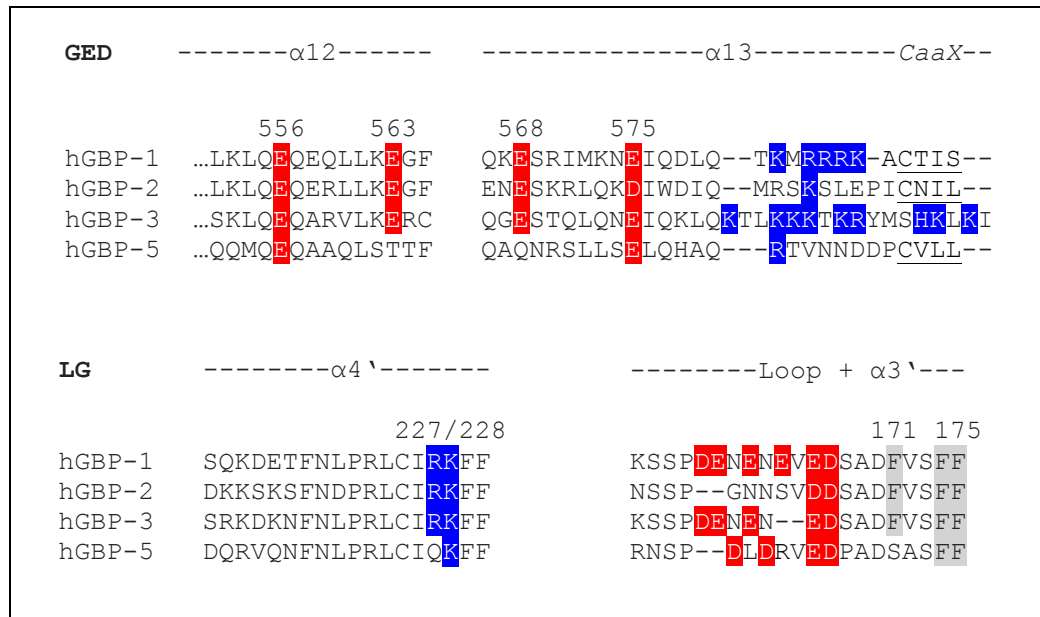


Figure 4-5: Sequence alignment of the regions that have been identified as critical for intramolecular LG:GED interactions of hGBP-1. Amino acids sequences of hGBP-1, -2, -3 and -5 were compared with regards to structural elements from the N-terminal LG domain ($\alpha 4'$ and Loop+ $\alpha 3'$) and from the C-terminal GED domain ($\alpha 12-13$) of hGBP-1 as depicted in figure 4-2. Except for hGBP-5, all isoforms harbor the critical residues R227/K228 in $\alpha 4'$ (blue) and likewise four negatively charged residues in $\alpha 12-13$ (red) which together were shown to establish ionic contacts in hGBP-1. The critical phenylalanines F171/F174/F175 are also conserved (gray), only hGBP-5 has F171 replaced by a serine. For hGBP-1, the negatively charged residues from the loop (red) are predicted to form ionic contacts to the series of positively charged residues in $\alpha 13$ (blue). In these regions, all the isoforms display larger deviations, whereas hGBP-1 and hGBP-3 provide the highest similarity particularly concerning the number of charged residues. The CaaX motifs of hGBP-1, -2 and -5 are underlined.

Going further, a novel splice variant of hGBP-3 has been identified in lung epithelial cells, which beside wt hGBP-1 and hGBP-3 was strongly upregulated in the course of Influenza A virus (IAV) infection (Nordmann, et al., 2012). The protein, termed hGBP-3 Δ C, is lacking parts of the C-terminus and also the sequence aa 357-383 (alignment figure 4-6). Implementation of these elements into the full-length structure hGBP-1 visualizes that truncations include parts of $\alpha 12$ and the whole helix $\alpha 13$, and also the helix $\alpha 8$ of the middle domain (figure 4-6). In view of our experimental results, particular truncation of $\alpha 12-13$ already resulted in significantly enhanced GTPase activity which might apply to the splice variant, as well. This seems consistent with the finding that hGBP-3 Δ C provided the most potent anti-viral activity against IAV as compared with wt hGBP-1 and hGBP-3 (Nordmann, et al., 2012). Even more interesting is the fact that both hGBP-1 and hGBP-3 could be forced to provide similarly high antiviral activity when their isolated LG domains were applied. This together with findings of this work suggest that, first, antiviral activity correlates with the GTPase activity becoming enhanced

Discussion

upon C-terminal truncation and, second, that the GTPase activity of both hGBP-1 and hGBP-3 are regulated by the C-terminus.

In view of the sequence analysis above (figure 4-5) it appears conceivable that hGBP-3 requires the same regions as hGBP-1 to establish and to control intramolecular interaction as could be enlightened by mutational studies in future. Considering that hGBP-1 and hGBP-3 are the only isoforms, so far, capable of forming significant amounts of GMP, and, assuming that hGBP-3 is subject to the same LG:GED control mechanism as hGBP-1, one could speculate about a putative role of GMP production in supplying energy for mechanic actions.

hGBP-3	1	MAPEIHMTGPMCLIEN	TNGELVANPEALKIL	SAITQPVVVVAIVGL	YRTGKSYLMNKL	AG
hGBP-3ΔC	1	MAPEIHMTGPMCLIEN	TNGELVANPEALKIL	SAITQPVVVVAIVGL	YRTGKSYLMNKL	AG
hGBP-3	61	KNKGFSLGSTVKSHT	KGIWMWCVPHPKPE	HTLVLLDTEGLGDV	KKGDND	SWIFTLAV
hGBP-3ΔC	61	KNKGFSLGSTVKSHT	KGIWMWCVPHPKPE	HTLVLLDTEGLGDV	KKGDND	SWIFTLAV
hGBP-3	121	LLSSTLVYNSMGTIN	QQAMDQLYYVTELT	HRIRSKSSPDENE	NEDSADFVSFFP	DFVWTL
hGBP-3ΔC	121	LLSSTLVYNSMGTIN	QQAMDQLYYVTELT	HRIRSKSSPDENE	NEDSADFVSFFP	DFVWTL
hGBP-3	181	RDFSLEADGQPLTP	DEYLEYSLKLTQGT	SRKDKNFNLPRLC	IRKFFPKKCFV	FDLPI
hGBP-3ΔC	181	RDFSLEADGQPLTP	DEYLEYSLKLTQGT	SRKDKNFNLPRLC	IRKFFPKKCFV	FDLPI
hGBP-3	241	HRRKLAQLEKLQDE	ELDPEFVQQVADF	CSYIFSNSKTKT	LSGGIKVNGPR	LESVLTYIN
hGBP-3ΔC	241	HRRKLAQLEKLQDE	ELDPEFVQQVADF	CSYIFSNSKTKT	LSGGIKVNGPR	LESVLTYIN
hGBP-3	301	AISRGDLPCMENAV	LALAQIENSAAVQ	KATAHYDQQMGQ	KVQLPAETLQEL	LDLHRVSE
hGBP-3ΔC	301	AISRGDLPCMENAV	LALAQIENSAAVQ	KATAHYDQQMGQ	KVQLPAETLQEL	LDLHRVSE
hGBP-3	361	EATEVYMKN	SFKD	VHDLFQKKLAAQ	LDKKRDDFC	KQNEASSDRCS
hGBP-3ΔC	357	-----	-----	-----	-----	-----
hGBP-3	421	KAGIYSKPGGYCL	FIQKLDLEKKYEE	PRKGIQAEEL	LQTYLKS	KESVTDAILQTDQIL
hGBP-3ΔC	394	KAGIYSKPGGYCL	FIQKLDLEKKYEE	PRKGIQAEEL	LQTYLKS	KESVTDAILQTDQIL
hGBP-3	481	TEKEKIEVECVKA	ESAQASAKMVEEM	QIKYQOMMEE	KEKSYQEHVK	QLTEKMERERAQL
hGBP-3ΔC	454	TEKEKIEVECVKA	ESAQASAKMVEEM	QIKYQOMMEE	KEKSYQEHVK	QLTEKMERERAQL
hGBP-3	541	LEEQEKTLSK	LQEQARVLKER	COGESTIQ	LQNEIQK	LQKTLK
hGBP-3ΔC	514	LEEQEKTLSK	LQVSV-----	KC---	ITLWFVFLFS	LCSS-----

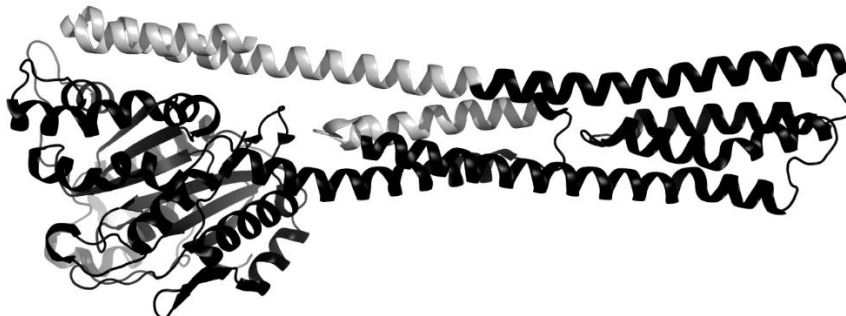


Figure 4-6: Sequential and structural view on the hGBP-3 splice variant hGBP-3ΔC. Sequence alignment of full-length hGBP-3 (NP_060754.2) and splice variant hGBP-3ΔC. (AEI54565.1) with identities highlighted in black. Although X-tal structure of hGBP-3 does not exist, missing parts of the splice hGBP-3ΔC (gray) are visualized on the full-length structure of hGBP-1 (pdb: 1f5n). These include the entire helix α8 and major parts of the GED (α13 and parts α12).

4.9. LG domains do not only mediate homo but also hetero dimerization of hGBPs

Towards elucidating hetero interactions of the hGBPs *in vitro*, we first focused on the isolated LG domain of each isoform (hGBP-1, -2, -3 and -5). Both concentration dependent GTPase activity assay and analytical SEC confirmed that each of the isoforms had at least one interface for homo dimerization within the LG domain. Considering moreover that the primary sequence of all isoforms display the highest degree of conservation in the LG domain, it appeared likely that the LG domains might be also responsible for mediating hetero interactions which have been previously shown on basis of full-length proteins *in vivo* (Britzen-Laurent, et al., 2010). By intermolecular FRET measurements we could indeed show that the LG domains do promote also hetero dimerization.

For the FRET measurements, donor and acceptor labelled LGs were generated using thiol reactive fluorophores Alexa488 and Alexa647, respectively. Although labelling reactions with special respects to the molar excess of fluorophore over protein were identical for all, nevertheless, different labelling efficiencies were obtained. Spanning a range from less than one and up to three suggested that some isoforms remained partly unlabeled while others had even up to three dyes per molecule. This gives evidence for different accessibility and reactivity of cysteines in each isoform which is further supported by deviating number of cysteine residues that each isoform contains: in total, hGBP-1 and hGBP-3 have six cysteine residues in the LG domain, whereas, hGBP-2 has only five, and hGBP-5 has even seven. Both - the labelled LG constructs and FRET as suitable method to monitor intermolecular interactions- were initially validated by nucleotide dependent homo dimerization. In accordance with a classical FRET setup, donor and acceptor constructs of one isoform were mixed and donor was excited while emission of the acceptor was monitored. Basically, only when both partners upon interaction come in sufficient proximity the fluorescence energy transfer can occur. Consequently, increase of fluorescence gives a direct measure for intermolecular interactions. In fact, homo dimerization of 1-LG, 2-LG and 3-LG were deduced from significant increase of fluorescence which occurred exclusively upon addition of GDP·AlF_x or GTPγS. As shown by analytical SEC, 5-LG does form homo dimers only in presence of GTPγS but not in presence of GDP·AlF_x, however, none of these GTP analogs succeeded to induce a fluorescence change when investigating homo dimerization of 5-LG via FRET. Consequently, labelled constructs of 5-LG were not suitable for further investigations.

Discussion

In the same manner as for homo dimerization and using also same concentrations, donor and acceptor labelled isoforms 1-LG, 2-LG and 3-LG were pairwise combined to investigate putative hetero dimerization. Indeed, for all combinations an increase of fluorescence occurred upon addition of either GDP·AlF_x or GTPγS which gave evidence that all tested isoform did form hetero dimers in a GTP dependent fashion and that the LG domains, above all, were sufficient to mediate these interactions. Altering kinetics and total change of fluorescence further suggested that hetero dimers are manifested with different affinities. The same could be observed also for traces reporting homo interactions. In that cases, kinetics and total change of fluorescence apparently correlated with the strength of the homo dimers; for instance, 1-LG having the highest homo dimer affinity (derived from GTPase activity assay) displayed the fastest kinetic and largest fluorescence increase, respectively. Although it appears seemingly plausible to compare all FRET traces likewise (homo and hetero interactions) in order to estimate the affinities, however, different labelling efficiencies, quantum yields of the fluorophores and also position of the labels within the protein do all influence the finally obtained signal thus counteracting a reliable comparison. Although labelling efficiency and quantum yields are parameters that can be corrected by mathematical operations (as suggested in paragraph 3.4.3.1.1.), though, this is not possible for the labelling position. The environment of a single dye within one protein molecule and also the relative orientation of dyes within a protein complex do contribute to the resulting FRET signal. Particularly when fluorophores are located in more flexible protein regions the effects might be even more pronounced. Thus, taking the overall change in fluorescence as a direct measure for estimating differences in affinities appears not reliable, even if the final values are corrected for labelling efficiency and quantum yield. Nevertheless, to yield a semi-quantitative estimation of the LG based hGBP hetero dimers, competitive FRET setups were established as depicted and described in figure 4-7.

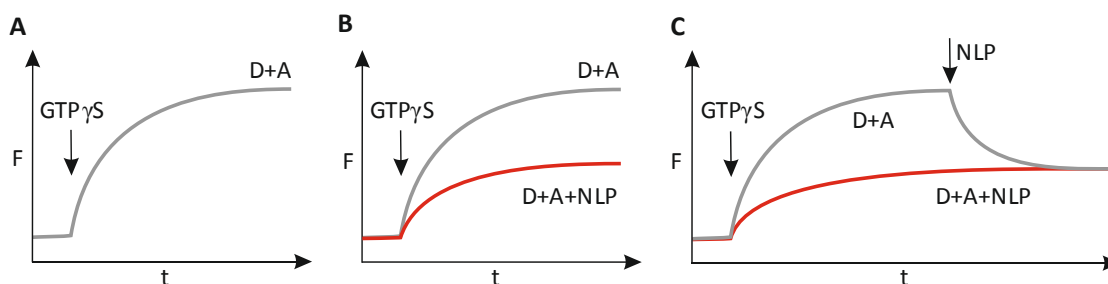


Figure 4-7: Scheme of time-dependent FRET traces according to different experimental setups. All setups ground on initial mixing of donor (D) and acceptor (A) labelled proteins and subsequent addition of GTP γ S (arrow) to induce dimerization. Always, donor is excited and acceptor emission is detected to monitor increase in FRET efficiency as reporter for dimerization. This is basically a classical FRET setup depicted in panel A (gray trace). The final values obtained correspond to the total amount of detectable FRET dimers in the system. (B) Competitive FRET setup 1: The classical FRET system is supplemented with non-labelled protein (NLP) as competitor from the very beginning. If the NLP is capable of forming dimers with the labelled proteins (D and A) the total amount of detectable FRET dimers will be reduced, reflected by decreased levels of fluorescence intensity (red trace). (C) Competitive FRET setup 2: Is a variation of (B) with the difference that NLP is added only after FRET dimers are formed. When NLP is capable of interacting with labelled proteins, preformed dimers dissociate (decreasing fluorescence signal) and the system equilibrates to reduced levels of FRET dimers (gray trace). Using exactly same protein concentrations, competitive FRET variations 1 (red) and 2 (gray) result in almost identical final values. The final value defines the amount of remaining FRET dimers which can be exploited to estimate affinities of different hetero dimers composed of the same LPs and varying types of NLP. Preferentially, D and A are the same type of isoform, such that LP:NLP interactions do not need to be distinguished further.

In contrast to the classical FRET setup, competitive FRET had substantially reduced inaccuracy since homo dimers were used as constant detectable FRET couples and any putative interaction partner was supplemented in its native, non-labelled form (NLP). Thus, each run was tainted by the same error resulting from labelling efficiency, quantum yield or dye localization of labelled proteins (LP). Moreover, the concentration of NLPs was also kept constant in each run. Consequently, any deviation from control measurements in the absence of NLP could be exclusively assigned to LP:NLP interactions. Following the simple relationship ‘the less fluorescence signal, the less detectable FRET dimers, the higher the affinity of LP:NLP’, the amount of remaining homo dimers in competitive FRET measurements were used as direct measure for the strength of LP:NLP and hence for the strength of hetero dimers of hGBP isoforms (figure 4-8). Besides high accuracy, one great advantage of the competitive FRET setup is that many different NLPs can be assayed without relying on additional labelling

Discussion

procedure. This is mostly advantageous for proteins like 5-LG being impaired to dimerize after labelling. Consequently, the labelled form of 5-LG was not useful for performing classical FRET measurements; however, using the non-labelled form in competitive FRET measurements instead, gave some significant effects. In particular, 1-LG and 2-LG hetero dimers with 5-LG revealed to be stronger than hetero dimers of 1-LG and 2-LG (figure 4-8, left and middle panel). Although found to hetero dimerize also with 3-LG, 5-LG had only less competitive effect on 3-LG homo dimers indicating a correspondingly weak hetero dimer affinity (figure 4-8, right panel). In contrast, 3-LG was found to form highly affine hetero dimers with either 1-LG or 2-LG. These hetero dimers intriguingly appeared even stronger than homo dimers of 1-LG or 2-LG (figure 4-8, left and middle panel). Based on the higher apparent K_d value derived from GTPase activity assay and due to incomplete dimerization in presence of GTP γ S via analytical SEC, 3-LG homo dimers are supposed to be even weaker than 1-LG and 2-LG homo dimers. Consequently hetero dimers of 3-LG with 1-LG and 2-LG can be assumed to be stronger than any respective homo dimer. In competitive studies based on 3-LG as detectable FRET dimer, in contrary, 3-LG homo dimers appeared to be even stronger than the mentioned hetero dimers. It was also unexpected that 2-LG and 1-LG were not sufficient to dissociate larger amounts of 3-LG homo dimers considering that 3-LG conversely was. However, it could be identified that complete dissociation of the FRET dimers of 3-LG was not possible, even if tried with a 20-fold molar excess of non-labelled 3-LG which in fact is the same protein and thus should compete upon homo dimerization. Approximately 40 % of the FRET dimers presumably remained as irreversible complexes suggesting that the labelling procedure had some impact on 3-LG's stability. Correspondingly, labelling procedure of 3-LG like for 5-LG need to be optimized for further studies.

Discussion

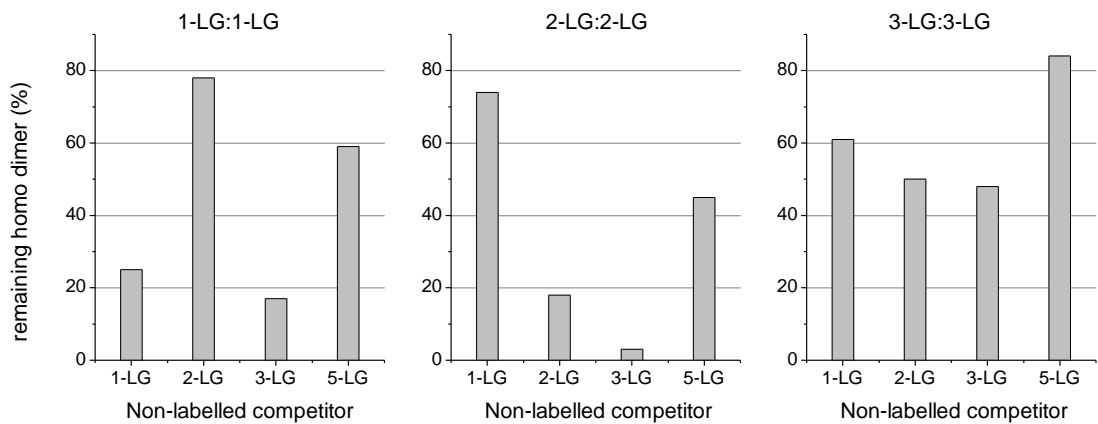


Figure 4-8: Evaluation of homo and hetero interactions between LG domains of hGBP isoforms measured by competitive FRET. The detected FRET dimers are depicted on the top of each panel, whereas, non-labelled competitors are depicted on the bottom. The bar charts present the relative amount of remaining FRET dimers upon competition with the non-labelled interaction partners which can be directly exploited as a measure for the affinity of hetero dimers (LP:NLP). Each labelled homo dimer was also competed with its non labelled counterparts to have a reference value for homo dimer affinity. For instance, competition of NLP 1-LG with the FRET pair of 1-LG (left) yields 25 % of remaining dimers while its only 17 % for 3-LG as competitor, consequently, 1-LG 3-LG hetero dimers are supposed to be stronger than 1-LG homo dimers.

To sum up, by FRET studies we could first of all prove that all isoforms hGBP-1, -2, -3 and -5 do form hetero dimers in a GTP dependent manner. Since all measurements were performed with isolated LG domains, at least one interface for hetero dimers has been identified in this work. If the remaining subdomains do also participate in dimer formation needs to be elucidated in future studies. Further, competitive FRET measurements with a mixture of labelled and non-labelled isoforms uncovered that homo and hetero dimers emerge with different affinities. In this context, 3-LG revealed as the most potent hetero interaction partner for 1-LG and 2-LG while 1-LG and 2-LG formed only weak hetero dimers. How this data might be interpreted and whether tendency of affinities continues also at full-length levels needs to be elucidated in further studies. At least considering that hGBP-1, hGBP-2 and hGBP-5 are targets of prenylation which enables the proteins to associate with membranes, the C-terminal domain together with the prenyl moiety might be required to form higher affine dimers among themselves. Reversely, hGBP-3 is a non-prenylated form which at subcellular levels solely resides in the cytoplasm but upon interaction with either prenylated isoform translocates to respective compartments (Britzen-Laurent, et al., 2010) (Tripal, et al., 2007). Thus, using the LG domain to establish strong interactions with prenylated hGBPs - consistent

with results from competitive FRET - might be a strategy of hGBP-3 to make use of their mobility. However, the here presented FRET setup opens up variety of possibilities to get further insights into the hetero interactions of hGBPs *in vitro*. Particularly competitive FRET variation 2 grounds on dissociation of preformed FRET complexes which can be directly used to determine dissociation rates. Accordingly, we could determine dissociation rate constants of 1-LG, 2-LG and 3-LG homo dimers, being $7.6 \cdot 10^{-3}$, $5.2 \cdot 10^{-3}$, and $9.1 \cdot 10^{-3} \text{ s}^{-1}$, respectively.

In analogy to the presented approach, different protein fragments, full-length proteins and their prenylated forms can be used to identify putative interfaces. Likewise, concentration dependent measurement can be performed to quantify all affinities. The leading question for further studies, above all, is: What is the consequence of hetero interactions on the molecular mechanism of each isoform?

4.10. Cellular concentration of hGBPs as critical determinant for GTP dependent dimerization

Based on the multicity of investigations that have been performed on human GBPs until now, concentration dependency appears as one of the most critical factors in regulating their physiological actions. *In vitro* studies revealed that hGBP-1 stably existing as nucleotide-free monomer is enabled to form homo complexes in a GTP and, above all, in a concentration dependent fashion. This feature seems to be highly relevant since in the majority of tested cell types there are no detectable amounts of basal hGBPs while stimulation with interferons and other inflammatory cytokines lead to remarkable upregulation probably ensuring a protein concentration capable of dimer formation. The formation of dimers, to the present knowledge, acts on two fundamental processes which is the elevation of GTPase activity (homo dimerization) and subcellular translocation (homo and hetero dimerization) to particular compartments which might define the putative places of hGBPs' function.

Biochemically, homo dimerization transfers each of the involved hGBP molecule into a catalytically competent form enabled to perform highly efficient GTP hydrolysis. By this, hGBP-1 reaches a turnover number of almost 100 min^{-1} at 37°C . Underlying the mechanism of dimerization dependent self-stimulation, likewise, all the tested isoforms hGBP-2, hGBP-3 hGBP-5 have been shown to reach comparable ranges at least at 25°C . Considering an average concentration of $250 \mu\text{M}$ free GTP within human cells (Traut, 1994), it seems only reasonable that such a high activity is capable of shifting the entire nucleotide pool to GDP and GMP within a few minutes, provided that substrate saturation and full dimerization is ensured. For

Discussion

judging whether and to which extent these latter points are ensured, protein concentration reveals absolutely critical but, strikingly, only disproportional efforts have been put into quantifying cellular concentrations of the hGBPs until now. With our studies we could further figure out apparent dissociation constants for the GTP dependent homo dimerization of hGBPs revealing remarkable differences among the tested isoforms. All isoforms hGBP-2, hGBP-3 and hGBP-5 ($K_d^{app} = 2 - 9 \mu\text{M}$) unlike hGBP-1 ($K_d^{app} = 0.20 \mu\text{M}$) were significantly attenuated in homo dimer formation, requiring at least ten times higher protein concentration than hGBP-1. Although forming weak homo dimers only, hGBP-3 turned out to form higher affine hetero dimers with either hGBP-1 or hGBP-2. With these findings we have a benchmark at hands that allows estimating the occurrence of particular dimers. Integrating this into the cellular context in order to get insights into the physiological relevance of dimers absolutely requires cellular concentrations of the hGBPs assuming a constant concentration of available GTP (250 μM , see above). Although there are no studies revealing a systematic overview in which concentrations the hGBPs are present after upregulation, however, there are some hints that we will use in the following for estimation.

The first and, to our present knowledge, only estimation of the cellular concentration of human GBPs was done in one of the initial studies 30 years ago (Cheng, et al., 1985). At that stage of research, only recently had hGBP-1 been identified as one of the most abundant proteins in fibroblast cells after treatment with interferons. Exploiting the unique GMP binding ability of the protein, in that study, GMP-agarose affinity chromatography was established to selectively extract hGBP-1 from cellular proteins in a single purification step. From $30 \cdot 10^6$ fibroblast cells previously exposed to optimal concentrations of interferons, Cheng and coworkers routinely yielded 1 μg of highly purified hGBP-1. Based on the molecular weight of the protein (68,000 Da) and Avogadro's number this makes up $9 \cdot 10^{12}$ molecules of hGBP-1 accumulated in $30 \cdot 10^6$ cells and consequently $3 \cdot 10^5$ in a single cell. With the aid of this value corresponding to $3.4 \cdot 10^{-8} \mu\text{g}$ of hGBP-1 per cell and with regards to an average volume of $2 \cdot 10^{-6} \mu\text{l}$ per fibroblast cell (calculated from $2,000 \mu\text{m}^3 = 2 \cdot 10^{-9} \text{cm}^3 = 2 \cdot 10^{-9} \text{ml}$ (Milo, et al., 2010)) we finally obtained 0.017 $\mu\text{g}/\mu\text{l}$ or 0.25 μM as cellular concentration of hGBP-1.

For judging the reliability of this value some of the authors' assumptions about estimating the number of hGBP-1 molecules per cell need to be considered. That the entire amount of hGBP-1 after cell disruption was in the soluble fraction and that no protein was lost in the process of purification are two of these assumptions likely to account for a protein concentration probably being even higher. Arbitrarily, one could assume a loss of 50 % which

Discussion

would yield a two times higher concentration of the protein. Another factor potent to distort the resulting value is the total number of cultivated cells to which the amount of synthesized protein was related to. Above all, noteworthy, none of the remaining hGBP isoforms were yet known during that study. From the following publications over the past decades we recently know that the vast majority of the human GBPs are strongly upregulated by interferons (Tripal, et al., 2007), and that besides hGBP-1 at least hGBP-2 and hGBP-3 provide GMP binding activity (this work). Moreover, hGBP-1 to hGBP-3 sharing almost identical molecular weights of approximately 68 kDa are virtually indistinguishable by SDS-PAGE analysis resulting in apparently a single band. Taken together, affinity chromatography using GMP-agarose to extract interferon induced hGBP-1 as performed by Cheng and others most probably captured not only hGBP-1 but at least also hGBP-2 and hGBP-3. Therefore, the obtained concentration of 0.25 μM (\pm error) is likely to reflect the sum of these proteins emphasizing that the concentration of each isoform is supposed to be even less. To define the particular proportion is complicated since different cytokines have been shown to induce differential levels of particular hGBPs with IFN- γ being the most potent inducer (Tripal, et al., 2007). Moreover, induction occurs in a dose dependent manner and approach of combined cytokines can have synergetic effects even at suboptimal doses (Decker, et al., 1989), which taken together can yield particular proportions of hGBPs depending on the microenvironment. For simplicity, thus, equimolar concentrations for all hGBPs will be assumed and due to lacking knowledge about the features, further, isoforms hGBP-4, hGBP-6 and hGBP-7 will be neglected. The obtained concentration of 0.25 μM total hGBP, consequently, yields maximal 0.08 μM for hGBP-1, -2, -3 and in view of 250 μM GTP each should be substrate saturated. In spite of the substrate excess, the protein concentration is likely to act limiting on dimer formation. Even for hGBP-1, which among the tested isoform has the lowest K_d value (0.20 μM), the monomeric species is expected to dominate at 0.08 μM . As the remaining isoforms hGBP-2, hGBP-3 and hGBP-5 have even weaker dimer affinities with dissociation constants far above the estimated protein concentrations ($K_d^{\text{app}} = 2 - 9 \mu\text{M}$), dimerization of these might not occur at all. This fact occurs strange, considering that these proteins are well equipped to dimerize and perform the related downstream mechanisms like cellular relocation and self-stimulated GTPase activity. From the evolutionary point of view, at least, this implicates a waste of resources.

Humans GBPs, particularly hGBP-1 firstly identified in human fibroblast was later shown to be expressed in many different cell lines to significantly high levels. To have a representative estimation of cellular hGBP concentrations based on these studies and further to have a control for the hGBP quantities obtained by Cheng and others we decided to perform another

approach. Densitometric analyses of published western blots visualizing hGBP levels from cytokine treated cells turned out to be a convenient method. However, there were several requirements to be considered which dramatically reduced the total number of probes: To reflect physiological conditions only, first, we preferred investigations of endogenous hGBP expression levels in cells exposed to cytokines and not results based on cells transfected with hGBP containing vectors. Second, to have a reference value we selected those results using actin as loading control. Being part of the cytoskeleton, actin (42 kDa) is an abundant protein with a cellular concentration of 2-3 mg/ml or approximately 70 μ M (Milo, et al., 2010). By the obtained band intensity of hGBP relative to the actin band, thus, we were able to estimate the hGBP concentration. Figure 4-9 illustrates such a quantification using the free available software GelAnalyzer 2010a. Panel A depicts a western blot analysis of hGBP-1 levels in HUVEC cells differentially induced by indicated inflammatory cytokines (Lubeseder-Martellato, et al., 2002). Selecting a lane (black box) and defining the bands (a and b) results in a plot of respective band intensities (panel B). The area corresponding to the hGBP-1 band (a) was then divided by the area corresponding to the actin band yielding the relative amount of hGBP-1 to actin. For the depicted lane (IL-1 β) hGBP-1 is in 1.8-fold excess over actin which would correspond to 5 mg/ml and consequently 80 μ M of hGBP-1 assuming a concentration of 3 mg/ml for actin. The remaining bands were analyzed analogously and cellular concentrations of hGBP-1 spanning a range from \sim 60 μ M (IL-1 α) to \sim 300 μ M (IFN- γ) were obtained.

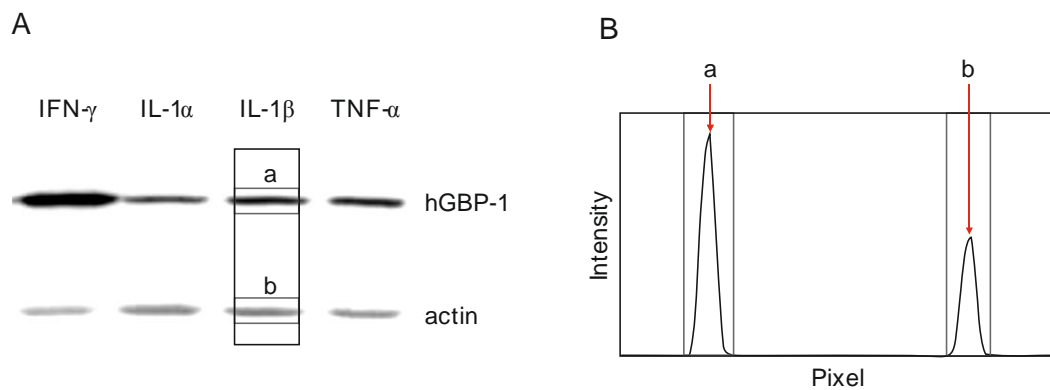


Figure 4-9: Densitometric analysis of cytokine induced hGBP-1 levels detected by western blot. (A) HUVEC cells were treated with indicated cytokines and levels of endogenous hGBP-1 from the cell extract were detected with monoclonal antibodies against hGBP-1. Serving as loading control, actin was detected with specific antibodies as well (adapted from (Lubeseder-Martellato, et al., 2002)). Using the software GelAnalyzer 2010a, bands within a lane were defined (black box, a: hGBP-1 and b: actin) and resulted in an intensity profile with corresponding peaks for each protein band (B). These areas were employed for further quantification as described in the text.

Discussion

Additional results from the same publication were used to estimate the levels of IFN- γ induced hGBP-1 in other cell types. Similar to HUVEC, T-cells, monocytes and embryonic fibroblast contained approximately 200 μM of hGBP-1. These values strikingly differ from the previously obtained concentration of 0.25 μM by approximately 1000-fold and, thus, raise the question which of the both extremes might fairly reflect the real situation. In fact, it could be argued that the quality of the antibodies (specificity, affinity) is a critical determinant of the band intensities which finally served as basis for densitometric analysis. However, even considering that immune labeling of actin was 10 to 100-fold less efficient, the resulting value equal to 20 μM and 2 μM of hGBP-1, respectively, would still distinguish by at least ten-fold compared with 0.25 μM . Staining of the proteins, therefore, does not appear as reasonable explanation for the huge discrepancy obtained by the two different methods. Nevertheless, in order to eliminate the putative inaccuracy upon immunostaining at protein levels, we applied the densitometric analysis to transcriptional levels instead. For that we used results from Decker and others who extracted the total mRNA from cells treated with particular cytokines and separated the cDNA of hGBP-1 and actin obtained by reverse transcription with appropriate primers (Decker, et al., 1989). Identical to the procedure described above and assuming that the yielded intensity of actin transcript accounts for 3 mg/ml cellular actin, we obtained concentration of 40-90 μM hGBP-1. The concentration might be even more considering that one mRNA molecule, depending on the half-life and degradation, is likely to serve as template for more than one protein molecule. However, this result is in good agreement with the densitometric analyses at protein levels, indicating that hGBP-1 might constitute 100-300 μM within the cell.

An additional approximation supporting a concentration range of 100-300 μM hGBP-1 rather than 0.25 μM is setting the hGBP-1 concentration in relation to the total concentration of protein in the cell. We can roughly estimate the concentration of total protein making following assumptions: (1) A human cell has an average volume of $2.0 \cdot 10^{-9} \text{ cm}^3$ (or ml) which at a density of 1.1 g/ml would weigh $2.2 \cdot 10^{-9} \text{ g}$. (2) Protein accounts for approximately 30 % of a cell's weight giving a total weight of $6.6 \cdot 10^{-10} \text{ g}$ which equals $1.25 \cdot 10^{-14} \text{ mole}$, considering that eukaryotic proteins have an average molecular weight of 52,700 g/mol. (3) Referring $1.25 \cdot 10^{-14} \text{ mol}$ of protein to the cellular volume gives a total concentration of 6.3 mM which indeed might deviate depending on the type, size and differentiation state of the cell. However, taking 6.3 mM as a rough benchmark, 100-300 μM of hGBP-1 would correspond to 2-5 % of the total protein. This is an apparently large but not an unreasonable value with regards to electrophoretic analysis of interferon induced proteins from cell extracts (Cheng, et

al., 1983) at which the remarkable share of hGBP is clearly visible by eye only. The alternative value of 0.25 μM hGBPs in view of the total protein concentration accounts for merely 0.004 % and thus should not be visible in such clarity. That cellular concentration of upregulated hGBP-1 is in comparable range of cytoskeletal actin ($\sim 70 \mu\text{M}$) is further supported by immunofluorescence labelling of HeLa cells exposed to IFN- γ (figure 4-10). Irrespective of the antibodies and fluorescence dyes used, obviously, hGBP-1 (green, right panel) enriches to comparable levels as actin (red, right panel). Being even less pronounced than actin might relativize the concentration levels of hGBP-1. In the following we will thus take 100 μM of hGBP-1 as orientation.

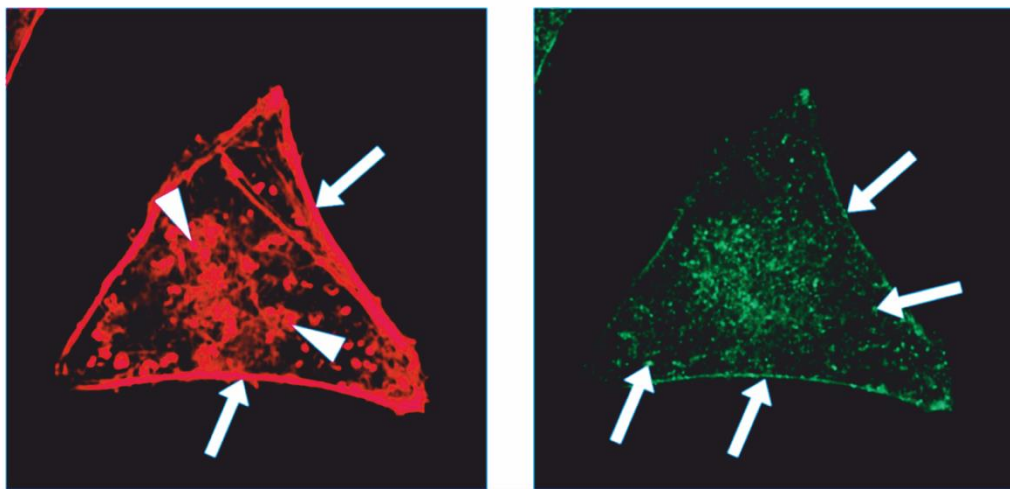


Figure 4-10: Actin and hGBP-1 levels in HeLa cells. HeLa cells were treated with IFN- γ and endogenous actin (left) as well as hGBP-1 (right) were visualized by specific immunofluorescence staining. The image taken from (Ostler, et al., 2014) includes arrows and arrowheads that are not relevant for this work.

Assuming again equimolar concentrations of the hGBPs, they would add up to 700 μM . In this scenario, protein dominates over the GTP concentration which establishes latter one as limiting factor for dimerization. Further, expecting that all the isoform bind GTP with similar affinities, only 35 μM of GTP would be available for each isoform and consequently maximal 35 μM of GTP bound protein would enter the dimeric state. For hGBP-1 having a homo dimer affinity of 0.20 μM this concentration is sufficient for full dimerization. Even having a ten-fold weaker affinity, considerable amounts of hGBP-2, hGBP-3 and hGBP-5 can be expected to form homo dimers, as well. From the enzymatic point of view, this altogether would lead to highly efficient GTP turnover capable of shifting the whole nucleotide pool within several seconds; dimeric hGBP-1 alone (with respects to *in vitro* studies) is sufficient to convert 35 μM GTP in

Discussion

less than one second, considering the turnover number of 100 min^{-1} at physiological temperature. Indeed presumable to have severe consequences for the cell, it remains elusive whether this scenario will ever occur. In particular, there are numerous parameters potent to have regulatory effects on the GTPase cycle of the hGBPs that for simplicity were not considered at all. With respects to GTP, the cellular concentrations of available nucleotide might vary depending on the cell type, other GTPases also competing for the pool of available GTP, and, finally, on the dynamics of GTP depletion and recovery. $250 \mu\text{M}$ of GTP as assumed here is just an average value. With respect to the hGBPs, there are still three more isoforms with not known features. The characterized ones, further, have differentially manifested nucleotide binding affinities and dynamics particularly regarding the GTP hydrolysis products GDP and GMP that were completely left unconsidered. This and also protein complexes emerging in the course of GTP hydrolysis, their lifetimes and rates of disassembly, respectively, are all parameters discouraging a certain proportion of the hGBPs from entering the regular enzymatic cycle. Above all, hetero interactions among the hGBPs have been reported earlier and we could show this to be especially pronounced for hGBP-3 and hGBP-1 or hGBP-2. Besides homo complexes, thus, hetero complexes likely account for a notable amount within the cell. Although not yet knowing the consequences of hetero complexes for particular characteristics such as nucleotide binding and enzymatic activity, one could speculate about an analogy to the GDIs of small GTPases, considering that homo complexes of hGBPs are functional homologues to GAPs.

Irrespective of further efforts necessary -first, to refine the hetero interactions among all hGBP members, and second, to characterize the remaining isoforms- it should be a major concern of upcoming studies to determine the cellular concentration of individual hGBPs. Only then will we have a framework to embed all the biochemical and biophysical knowledge with the chance to get insights into how the hGBP network is regulated in the cellular context.

Summary

Belonging to the dynamin superfamily of large GTPases, human Guanylate Binding Proteins comprise a family of seven members (hGBP-1 to hGBP-7) that are strongly upregulated in response to IFN- γ . Accordingly, several hGBP isoforms have been shown to inhibit replication of Influenza A virus, Hepatitis C virus, and *Chlamydia trachomatis*. While the mechanism of action is yet poorly understood, GTPase activity seems to be crucial in any case. Among the isoforms, hGBP-1 is structurally and biochemically the best characterized member that besides sharing typical features of the dynamin superfamily is unique for its GTP hydrolysis mechanism which is accomplished in two successive cleavage steps yielding a mixture of GDP and GMP as products. Beside hGBP-1 only hGBP-5 has been characterized in biochemical terms, whereas only less or nothing is known about the remaining isoforms. However, yielded differences between hGBP-1 and hGBP-5 in spite of the high sequence homology suggest individual properties and accordingly different functions of all isoforms. At cellular level it has been further shown that hGBP-1 to hGBP-5 do not only form homo but, most strikingly, also hetero complexes. This interplay crucially influences the subcellular localization of each isoform and reveals as important mechanism to direct individual isoforms to the place of their function.

Towards assessing the unique GTPase activity of hGBP-1, particularly the ability to produce GMP, we identified the GTP induced release of the GTPase effector domain as key mechanism that tightly controls the second hydrolysis step. By mutational analysis we could discover a cluster of phenylalanines (F171/F174/F175) in the LG domain that in close proximity to the GED revealed as important region to transmit conformational changes from the LG domain to the GED and vice versa. An open conformation as a result of phenylalanine exchange for alanine was reflected by a GTPase activity resembling that of the isolated LG domain (enhanced GMP production and particularly utilizing GDP as substrate to convert it in a cooperative manner), enhanced dimerization and a higher sensitivity towards trypsin digestion as compared to wildtype. Further, an appropriate arrangement of the switch I region, distant from the GED, was found to be important in initiating conformational changes towards the GED. Replacement of K76 in switch I by an alanine almost abolished GMP production which was suggested to relate to the crucially affected GED release shown by intramolecular measurements. In fact, this was verified by deletion of the GED which accordingly recovered the apparently deficient GMP formation.

Hetero as well as homo dimerization of the hGBPs is a key element of their biological function. In this work, we investigated biochemical features of hGBP-2 and -3 and found LG

Summary

domain mediated homo dimerization as a common mechanism of so far characterized isoforms to stimulate GTPase activity to comparable levels. However, the studies revealed some differences conferring an individual fingerprint for each isoform. As one of the major differences, hGBP-2 and hGBP-3 homo dimers were found to be approximately 10-fold weaker as compared with hGBP-1 homo dimers. Also product composition resulting from GTP hydrolysis occurred differentially manifested for each isoform; while hGBP-3 produced GMP amounts similar to hGBP-1, hGBP-2 similar to hGBP-5 was found to be deficient in GMP production. Unlike hGBP-5, hGBP-2 had still noteworthy GMP binding activity in the micromolar range. Another interesting fact is that hGBP-3 full-length and its isolated LG domain produced altering levels of GMP which resembling hGBP-1 features suggests GED controlled GTPase activity.

Yet not knowing the biochemical and functional consequences, we further elucidated hetero interactions between the isoforms using fluorescently labelled proteins. We could show that all the isoforms hGBP-1, hGBP-2, hGBP-3 and hGBP-5 form GTP dependent hetero complexes confirming cellular results. In addition, we could show that the LG domains known to mediate homo dimerization were also responsible for mediating hetero complex formation. Interestingly, hGBP-3 revealed to be a potent interaction partner of hGBP-1 and hGBP-2 with hetero dimer affinities being similar to or even higher than respective homo dimer affinities. Taken together, although sharing a high sequence identity (up to 88 %), discriminative biochemical features of the GBPs and their tendencies to form homo and hetero interactions give insights into the specific role of each protein in the finely tuned intracellular networking.

Bibliography

Abdullah, N., Balakumari, M. and Sau, A.K. 2010. Dimerization and its role in GMP formation by human guanylate binding proteins. *Biophys J.* 2010, 99(7), pp. 2235-44.

Abdullah, N., et al. 2009. Role of individual domains and identification of internal gap in human guanylate binding protein-1. *J Mol Biol.* 2009, 386(3), pp. 690-703.

Ahmadian, M.R., et al. 1997. Confirmation of the arginine-finger hypothesis for the GAP-stimulated GTP-hydrolysis reaction of Ras. *Nature Structural Biology.* 1997, 4, pp. 686 - 689.

Allin, C., et al. 2001. Monitoring the GAP catalyzed H-Ras GTPase reaction at atomic resolution in real time. *Proc. Natl. Acad. Sci. U. S. A.* 2001, 98, pp. 7754-7759.

Al-Zeer, M.A., et al. 2013. Autophagy restricts Chlamydia trachomatis growth in human macrophages via IFNG-inducible guanylate binding proteins. *Autophagy.* 2013, 9(1), pp. 50-62.

Anderson, N.L. and Anderson, N.G. 2002. The human plasma proteome: history, character, and diagnostic prospects. *Mol Cell Proteomics.* 2002, 1(11), pp. 845-867.

Anderson, S.L., et al. 1999. Interferon-induced guanylate binding protein-1 (GBP-1) mediates an antiviral effect against vesicular stomatitis virus and encephalomyocarditis virus. *Virology.* 1999, 256, pp. 8-14.

Andreoli, M., et al. 2014. Identification of the first inhibitor of the GBP1:PIM1 interaction Implications for the development of a new class of anticancer agents against paclitaxel resistant cancer cells. *J Med Chem.* 2014, 57(19), pp. 7916-7932.

Annamalai, V. 2013. Structural and biochemical studies on members of the dynamin superfamily. *PhD thesis RUB.* 2013.

Asundi, V.K., Stahl,R.C., Showalter,L., Conner,K.J., and Carey,D.J. 1994. Molecular cloning and characterization of an isoprenylated 67 kDa protein. *Biochem. Biophys. Acta.* 1994, 1217, pp. 257-265.

Balasubramanian, S., Nada, S. and Vestal, D. 2006. The interferon-induced GTPase, mGBP-2, confers resistance to paclitaxel-induced cytotoxicity without inhibiting multinucleation. *Cell Mol Biol (Noisy-le-grand).* 2006, 52(1), pp. 43-49.

Bibliography

Benscheid, U. 2005. Biochemische Charakterisierung der Oligomerisierung des Interferon-gamma-induzierten humanen Guanylat-bindenden Proteins 1. *PhD thesis RUB.* 2005. PhD thesis.

Bleiziffer, O., et al. 2012. Guanylate-binding protein 1 expression from embryonal endothelial progenitor cells reduces blood vessel density and cellular apoptosis in an axially vascularised tissue-engineered construct. *BMC Biotechnol.* 2012, 12, p. 94.

Bos, J.L. 1989. Ras oncogenes in human cancer: a review. *Cancer Res.* 1989, 49, pp. 4682-4689.

Bourne, H.R., Sanders, D.A. and McCormick, F. 1990. The GTPase superfamily: a conserved switch for diverse cell functions. *Nature.* 1990, 348, pp. 125-132.

—. **1991.** The GTPase superfamily: conserved structure and molecular mechanism. *Nature.* 1991, 349, pp. 117-127.

Britzen-Laurent, N., et al. 2013. GBP-1 acts as a tumor suppressor in colorectal cancer cells. *Carcinogenesis.* 2013, 34(1), pp. 153-162.

Britzen-Laurent, N., et al. 2010. Intracellular trafficking of guanylate-binding proteins is regulated by heterodimerization in a hierarchical manner. *PLoS One.* 2010, Vol. 5, 12, e14246.

Capaldo, C.T., et al. 2012. IFN- γ and TNF- α -induced GBP-1 inhibits epithelial cell proliferation through suppression of β -catenin/TCF signaling. *Mucosal Immunol.* 2012, 5(6), pp. 681-690.

Carr, J.F. and Hinshaw, J.E. 1997. Dynamin assembles into spirals under physiological salt conditions upon the addition of GDP and gamma-phosphate analogues. *J. Biol. Chem.* 1997, 272, pp. 28030-28035.

Carter, C.C., Gorbacheva, V.Y. and Vestal, D.J. 2005. Inhibition of VSV and EMCV replication by the interferon-induced GTPase, mGBP-2: differential requirement for wild-type GTP binding domain. *Arch. Virol.* 2005, 150, pp. 1213-1220.

Casey, P.J. and Seabra, M.C. 1996. Protein Prenyltransferases. *Journal of Biological Chemistry.* 1996, 271(10), pp. 5289–5292.

Bibliography

- Chakrabarti, P.P., et al. 2004.** Fourier transform infrared spectroscopy on the Rap:RapGAP reaction, GTPase activation without an arginine finger. *J. Biol. Chem.* 2004, 279, pp. 46226-46233.
- Cheng, Y.S., Colonna, R. and Yin, F.H. 1983.** Interferon induction of fibroblast proteins with guanylate binding activity. *J Biol Chem.* 1983, 258, pp. 7746–50.
- Cheng, Y.S., et al. 1985.** Affinity purification of an interferon-induced human guanylate-binding protein and its characterization. *J. Biol. Chem.* 1985, 260, pp. 15834-15839.
- Cheng, Y.S., Patterson, C.E. and Staeheli, P. 1991.** Interferon-induced guanylate-binding proteins lack an N(T)KXD consensus motif and bind GMP in addition to GDP and GTP. *Mol Cell Biol.* 1991, 11(9), pp. 4717-4725.
- Chung, C.T., Niemela, S.L. and Miller, R.H. 1989.** One-step preparation of competent *Escherichia coli*: transformation and storage of bacterial cells in the same solution. *Proc Natl Acad Sci U S A.* 1989, 86(7), pp. 2172-2175.
- Damke, H., et al. 1994.** Induction of mutant dynamin specifically blocks endocytic coated vesicle formation. *J. Cell Biol.* 1994, 127, pp. 915-934.
- Danino, D. and Hinshaw, J. E.. 2001.** Dynamin family of mechanoenzymes. *Current opinion in Cell Biology.* 2001, 13, pp. 454-460.
- Darnell, J.E.Jr., Kerr, I.M. and Stark, G.R. 1994.** Jak-STAT pathways and transcriptional activation in response to IFNs and other extracellular signaling proteins. *Science.* 1994, 264(5164), pp. 1415-21.
- De Donato M, Mariani M, Petrella L et al. 2012.** Class III beta-tubulin and the cytoskeletal gateway for drug resistance in ovarian cancer. *J Cell Physiol.* 2012, 227, pp. 1034–1041.
- Decker, T., et al. 1991.** Cytoplasmic activation of GAF, an IFN-gamma-regulated DNA-binding factor. *EMBO Journal.* 1991, 10, pp. 927-932.
- Decker, T., et al. 1989.** Interactions of alpha- and gamma-interferon in the transcriptional regulation of the gene encoding a guanylate-binding protein. *EMBO J.* 1989, 8(7), pp. 2009-2014.

Bibliography

Dever, T.E., Glynias, M.J. and Merrick, W.C. 1987. GTP-binding domain: three consensus sequence elements with distinct spacing. *Proc. Natl. Acad. Sci. USA.* 1987, Vol. 7, 84, pp. 1814-1818.

Dinareello, C.A. 2007. Historical Review of Cytokines. *European journal of immunology.* 2007, 37(Suppl. 1), pp. S34–S45.

Ding, S., et al. 2014. Epigenetic reprogramming of the type III interferon response potentiates antiviral activity and suppresses tumor growth. *PLoS Biol.* 2014, 12(1), p. e1001758.

Dovengerds, C. 2013. Membraninteraktionen von großen Dynamamin-verwandten GTPasen. *PhD thesis.* 2013.

Dranoff, G. 2004. Cytokines in cancer pathogenesis and cancer therapy. *Nature Reviews Cancer.* 2004, 4, pp. 11-22.

Duan Z, Foster R, Brakora KA, Yusuf RZ, Seiden MV. 2006. GBP1 overexpression is associated with a paclitaxel resistance phenotype. *Cancer Chemother Pharmacol.* 2006, 57, S. 25–33.

Dudek, S.E., et al. 2010. The clinically approved proteasome inhibitor PS-341 efficiently blocks influenza A virus and vesicular stomatitis virus propagation by establishing an antiviral state. *J.Virol.* 2010, 84, pp. 9439–9451.

Faelber, K., et al. 2011 . Crystal structure of nucleotide-free dynamin. *Nature.* 2011 , 477(7366), pp. 556-560.

Fellenberg, F., et al. 2004. GBP-5 splicing variants: New guanylate-binding proteins with tumor-associated expression and antigenicity. *J Invest Dermatol.* 2004, 122(6), pp. 1510-1507.

Fernandez-Sesma, A. 2007. The influenza virus NS1 protein: inhibitor of innate and adaptive immunity. *Infect Disord Drug Targets.* 2007, 7(4), pp. 336-43.

Forster, F., et al. 2014. Guanylate binding protein 1-mediated interaction of T cell antigen receptor. *J Immunol.* 2014, 192(2), pp. 771-781.

Bibliography

Fres, J.M., Müller, S. and Praefcke, G.J. 2010. Purification of the CaaX-modified, dynamin-related large GTPase hGBP1 by coexpression with farnesyltransferase. *J Lipid Res.* 2010, 51(8) , pp. 2454-2459.

Fukumoto, M., et al. 2014. Guanine nucleotide-binding protein 1 is one of the key molecules contributing to cancer cell radioresistance. *Cancer Science.* 2014, 105(10), S. 1351-1359.

Gao, J., Liao, J. and Yang, G.Y. 2009. CAAX-box protein prenylation process and carcinogenesis. *Am J Transl Res.* 2009, 1(3), pp. 312-325.

Gao, S., von der Malsburg, A. and Dick, A., Faelber, K., Schröder, G.F., Haller, O., Kochs, G., Daumke, O. 2011. Structure of myxovirus resistance protein a reveals intra- and intermolecular domain interactions required for the antiviral function. *Immunity.* 2011, 35(4), pp. 514-525 .

Gasper, R., et al. 2009. It takes two to tango: regulation of G proteins by dimerization. *Nat Rev Mol Cell Biol.* 2009, 10(6), pp. 423-429.

Gasteiger, E., et al. 2005. Protein Identification and Analysis Tools on the ExPASy Server. [book auth.] J. M. Walker. *The Proteomics Protocols Handbook.* 2005, pp. 571-607.

Ghosh, A. 2004. Relationship between function and 3D-structure of interferon inducible GTPases. *PhD thesis.* 2004.

Ghosh, A., et al. 2006. How guanylate-binding proteins achieve assembly-stimulated processive cleavage of GTP to GMP. *Nature.* 2006, 440, S. 101-104.

Guenzi, E., et al. 2003. The guanylate binding protein-1 GTPase controls the invasive and angiogenic capability of endothelial cells through inhibition of MMP-1 expression. *EMBO Journal.* 2003, 22, S. 3772–3782.

Guenzi, E., et al. 2001. The helical domain of GBP-1 mediates the inhibition of endothelial cell proliferation by inflammatory cytokines. *EMBO Journal.* 2001, 2, S. 5568–77.

Guimarães, D.P., et al. 2009. Interferon-inducible guanylate binding protein (GBP)-2: a novel p53-regulated. *Int J Cancer.* 2009, 124(2), pp. 272-279.

Bibliography

Haldar, A.K., et al. 2013. IRG and GBP host resistance factors target aberrant, "non-self" vacuoles characterized by the missing of "self" IRGM proteins. *PLoS Pathog.* 2013, 9(6), e1003414.

Haldar, A.K., et al. 2014. The E2-like conjugation enzyme Atg3 promotes binding of IRG and Gbp proteins to Chlamydia- and Toxoplasma-containing vacuoles and host resistance. *PLoS One.* 2014, 9(1), e86684.

Haller, O. and Koch, G. 2002. Interferon-induced Mx proteins: dynamin-like GTPases with antiviral activity. *Traffic.* 2002, 3, pp. 710-717.

Haller, O., et al. 2015. Mx GTPases: dynamin-like antiviral machines of innate immunity. *Trends Microbiol.* 2015, 23(3), pp. 154-163.

Haller, O., Staeheli, P. and Kochs, G. 2007. Interferon-induced Mx proteins in antiviral host defense. *Biochimie.* 2007, 89(6-7), pp. 812-818.

—. **2009.** Protective role of interferon-induced Mx GTPases against influenza viruses. *Rev Sci Tech.* 2009, 28(1), pp. 219-231.

Haller, O., Stertz, S. and Kochs, G. 2007. The Mx GTPase family of interferon-induced antiviral proteins. *Microbes Infect.* 2007, 9(14-15), pp. 1636-43.

Hammon, M., et al. 2011. Role of guanylate binding protein-1 in vascular defects associated with chronic inflammatory diseases. *J Cell Mol Med.* 2011, 15(7), pp. 1582-92.

Hengstenberg, C.S. 2013. Structural dynamics and implications for dimer formation of human guanylate-binding protein 1. *PhD thesis RUB.* 2013.

Hinshaw, J. E. 2000. Dynamin and its Role in Membrane Fission. *Annu. Rev. Cell Dev. Biol.* 2000, 16, pp. 483-519.

Isaacs, A. and Lindemann, J. 1957. Virus interference. I. The interferon. *Proc R Soc Lond B Biol Sci.* 1957, 147(927), pp. 258-67.

Itsui, Y., et al. 2009. Antiviral effects of the interferon-induced protein guanylate binding protein 1 and its interaction with the hepatitis C virus NS5B protein. *Hepatology.* 2009, 50(6), pp. 1727-37.

Bibliography

Itsui, Y., et al. 2006. Expressional screening of interferon-stimulated genes for antiviral activity against hepatitis C virus replication. *J Viral Hepat.* 2006, 13, S. 690–700.

Janeway, C.A. Jr, Travers, P. and Walport, M., et al. 2001. Basic Concepts in Immunology. *Immunobiology: The Immune System in Health and Disease.* 5th. New York : Garland Science, 2001.

Jordan, M.A. & Wilson, L. 2004. Microtubules as a target for anticancer drugs. *Nature Reviews Cancer.* 2004, 4, pp. 253-265.

Kim, B.H., et al. 2011. A family of IFN-gamma-inducible 65-kD GTPases protects against bacterial infection. *Science.* 2011, 332, pp. 717–721.

Kim, B.H., et al. 2012. IFN-inducible GTPases in host cell defense. *Cell Host Microbe.* 2012, 12(4), pp. 432-44.

Kim, B.H., Shenoy, A.R., et al. 2011 . A family of IFN- γ -inducible 65-kD GTPases protects against bacterial infection. *Science.* 2011 , 332(6030), pp. 717-721.

Knight, E. Jr. and Korant, B. D. 1979. Fibroblast interferon induces synthesis of four proteins in human fibroblast cells. *Proc. Natl. Acad.Sci. USA.* 1979, 76, S. 1824-1827.

Kotenko, S.V., et al. 2003. IFN-lambdas mediate antiviral protection through a distinct class II cytokine receptor complex. *Nat Immunol.* 2003, 4(1), pp. 69-77.

Kumar, V. and McNerney, M.E. 2005. A new self: MHC-class-I-independent Natural-killer-cell self-tolerance. *Nature Reviews Immunology.* 2005, 5, pp. 363-374.

Kunzelmann, S. 2006. Molekularer Mechanismus der GTP-Hydrolyse durch das humanen Guanylat-bindende Proteins 1. *PhD thesis RUB.* 2006.

Kunzelmann, S., Praefcke, G.J. and Herrmann, C. 2005. Nucleotide binding and self-stimulated GTPase activity of human guanylate-binding protein 1 (hGBP1). *Methods Enzymol.* 2005, 404, pp. 512-27.

—. **2006.** Transient kinetic investigation of GTP hydrolysis catalyzed by interferon-gamma-induced hGBP1 (human guanylate binding protein 1). *J Biol Chem.* 2006, 281(39), pp. 28627-35.

Bibliography

Kunzelmann, Simone. 2007. Molekularer Mechanismus der GTP-Hydrolyse durch das humane Guanylat-bindende Protein 1. *PhD thesis RUB*. 2007.

Lee, A., et al. 1999. Dominant-negative inhibition of receptor-mediated endocytosis by a dynamin-1 mutant with a defective pleckstrin homology domain. *Curr. Biol.* 1999, 9, S. 261-264.

Lee, S.-H. und Vidal, S. M.. 2002. Functional diversity of Mx proteins: variations on a theme of host resistance to infections. *Genome Research*. 2002, Bd. 12, S. 527-530.

Lenzen, C., et al. 1998. Kinetic analysis by fluorescence of the interaction between Ras and the catalytic domain of the guanine nucleotide exchange factor Cdc25Mm. *Biochemistry*. 1998, 37, pp. 7420-7430.

Lew, D.J., et al. 1991. Overlapping elements in the guanylate-binding protein gene promoter mediate transcriptional induction by alpha and gamma interferons. *Molecular Cell Biology*. 1991, 11, pp. 182-191.

Li, G., et al. 2009. The evolutionarily dynamic IFN-inducible GTPase proteins play conserved immune functions in vertebrates and cephalochordates. *Mol Biol Evol.* 2009, 26(7), pp. 1619-30.

Li, M., et al. 2011. Guanylate binding protein 1 is a novel effector of EGFR-driven invasion in glioblastoma. *J Exp Med.* 2011, 208(13), pp. 2657-2673.

Lipnik K, Naschberger E, Gonin-Laurent N et al. 2010. Interferon gamma-induced human guanylate binding protein 1 inhibits mammary tumor growth in mice. *Mol Med.* 2010, 16, S. 177–187.

Lipnik, K., et al. 2010. Interferon gamma-induced human guanylate binding protein 1 inhibits mammary tumor growth in mice. *Mol Med.* 2010, 16(5-6), S. 177-87.

Lu, Y.P., et al. 2007. Antiviral effect of interferon-induced guanylate binding protein-1 against Coxsackie virus and Hepatitis B virus B3 in Vitro. *Virologica Sinica*. 2007, 22(3), pp. 193-198.

Lubeseder-Martellato, C., et al. 2002. Guanylate-binding protein-1 expression is selectively induced by inflammatory cytokines and is an activation marker of endothelial cells during inflammatory diseases. *Am J Pathol.* 2002, 161(5), pp. 1749–59.

Bibliography

- Lüdemann, Maik-Borris. 2010.** Charakterisierung des humanen Guanylat-bindenden Proteins 1 mit Hilfe von dynamischer Lichtstreuung und Deuteriumaustausch. *PhD thesis RUB*. 2010.
- MacMicking, J.D. 2004.** IFN-inducible GTPases and immunity to intracellular pathogens. *Trends Immunol.* 2004, 25(11), pp. 601-609.
- . **2012.** Interferon-inducible effector mechanisms in cell-autonomous immunity. *Nat Rev Immunol.* 2012, 12(5), pp. 367–382.
- Mandel, M. and Higa, A. 1970.** Calcium-dependent bacteriophage DNA infection. *J Mol Biol.* 1970, 53(1), pp. 159-162.
- Milo, R., et al. 2010.** BioNumbers--the database of key numbers in molecular and cell biology. *Nucleic Acids Res.* 2010, 38(Database issue):D750-3.
- Mirpuri, J., et al. 2010.** Commensal *Escherichia coli* reduces epithelial apoptosis through IFN- α -mediated induction of guanylate binding protein-1 in human and murine models of developing intestine. *J Immunol.* 2010, 184(12), pp. 7186-7195.
- Modiano, N., Lu, Y.E. and Cresswell, P. 2005.** Golgi targeting of human guanylate-binding protein-1 requires nucleotide binding, isoprenylation, and an IFN- γ -inducible cofactor. *Proc Natl Acad Sci U S A.* 2005, 102(24).
- Muhlberg, A.B., Warnock, D.E. and Schmid, S.L. 1997.** Domain structure and intramolecular regulation of dynamin GTPase. *EMBO Journal.* 1997, 16, pp. 6676-6683.
- Nantais, D.E., et al. 1996.** Prenylation of an interferon- γ -induced GTP-binding protein: the human guanylate binding protein, huGBP1. *J Leukoc Biol.* 1996, 60(3), pp. 423-431.
- Naschberger, E., Bauer, M. and Stürzl, M. 2005.** Human guanylate binding protein-1 (hGBP-1) characterizes and establishes a non-angiogenic endothelial cell activation phenotype in inflammatory diseases. *Adv Enzyme Regul.* 2005, 45, pp. 215–227.
- Naschberger, E., et al. 2008.** Angiostatic immune reaction in colorectal carcinoma: impact on survival and perspectives for antiangiogenic therapy. *Int J Cancer.* 2008, 123, pp. 2120–2129.

Bibliography

Naschberger, E., et al. 2006. Human guanylate binding protein-1 is a secreted GTPase present in increased concentrations in the cerebrospinal fluid of patients with bacterial meningitis. *The American Journal of Pathology*. 2006, 169, pp. 1088-1099.

Naschberger, E., et al. 2011. Increased expression of guanylate binding protein-1 in lesional skin of patients with cutaneous lupus erythematosus. *Exp Dermatol*. 2011, 20(2), pp. 102-6.

Naschberger, E., et al. 2004. Nuclear factor-kappaB motif and interferon-alpha-stimulated response element co-operate in the activation of guanylate-binding protein-1 expression by inflammatory cytokines in endothelial cells. *Biochem J*. 2004, 79(Pt 2), pp. 409-420.

Neun, R., et al. 1996. GTPase properties of the interferon-induced human guanylate-binding protein 2. *FEBS Lett*. 1996, 390(1), pp. 69-72.

Niemann, H.H., et al. 2001. Crystal structure of a dynamin GTPase domain in both nucleotide-free and GDP-bound forms. *EMBO Journal*. 2001, 20, S. 5813-5821.

Nordmann, A, et al. 2012. A new splice variant of the human guanylate-binding protein 3 mediates anti-influenza activity through inhibition of viral transcription and replication. *FASEB J*. 2012, 26(3), pp. 1290-1300.

Novelli, G. and D'Apice, M.R. 2012. Protein farnesylation and disease. *Journal of Inherited Metabolic Disease*. 2012, 35(5), pp. 917-926.

Olszewski, M.A., Gray, J. and Vestal, D.J. 2006. In silico genomic analysis of the human and murine guanylate-binding protein (GBP) gene clusters. *J Interferon Cytokine Res*. 2006, 26, pp. 328-352.

Ostler, N., et al. 2014. Gamma interferon-induced guanylate binding protein 1 is a novel actin cytoskeleton remodeling factor. *Mol Cell Biol*. 2014, 34(2), pp. 196-209.

Pammer, J., Reinisch C und Birner P, Pogoda K, Stürzl M, Tschachler, E. 2006. Interferon-alpha prevents apoptosis of endothelial cells after short-term exposure but induces replicative senescence after continuous stimulation. *Lab Invest*. 2006, 86, S. 997–1007.

Pan, W., et al. 2012. Guanylate-binding protein 1 participates in cellular antiviral response to dengue virus. *Virology*. 2012, 27, p. 292.

Bibliography

Patzina, C. and Haller, O., Kochs, G. 2014. Structural requirements for the antiviral activity of the human MxA protein against Thogoto and influenza A virus. *J Biol Chem.* 2014, 289(9), pp. 6020-6027.

Persico, M., et al. 2015. GTP is an allosteric modulator of the interaction between the guanylate-binding protein 1 and the prosurvival kinase PIM1. *Eur J Med Chem.* 2015, 91, pp. 132-144.

Pestka, S. 2007. The interferons: 50 years after their discovery, there is much more to learn. *J Biol Chem.* 2007, 282(28), pp. 20047-51.

Pestka, S., Krause, C.D. and Walter, M.R. 2004. Interferons, interferon-like cytokines, and their receptors. *Immunol Rev.* 2004, 202, pp. 8-32.

Pilla, D.M., et al. 2014. Guanylate binding proteins promote caspase-11-dependent pyroptosis in response. *Proc Natl Acad Sci U S A.* 2014, 111(16), pp. 6046-6051.

Praefcke, G.J. and McMahon, H.T. 2004b. The dynamin superfamily: universal membrane tubulation and fission molecules. *Nature Reviews Molecular Cell Biology.* 2004b, 5, pp. 133-147.

Praefcke, G.J., et al. 2004. Identification of residues in the human guanylate-binding protein 1 critical for nucleotide binding and cooperative GTP hydrolysis. *Journal of Molecular Biology.* 2004, 344, pp. 257-269.

Praefcke, G.J., et al. 1999. Nucleotide-binding characteristics of human guanylate-binding protein 1 (hGBP1) and identification of the third GTP-binding motif. *Journal of Molecular Biology.* 1999, 292, pp. 321–332.

Praefcke, Gerrit J. K. 2001. Das humane Guanylat-bindende Protein 1 : Modell oder Sonderfall der Dynamin-verwandten GTP-bindenden Proteine. *PhD thesis RUB.* 2001.

Prakash, B., et al. 2000a. Structure of human guanylate-binding protein 1 representing a unique class of GTP-binding proteins. *Nature.* 2000a, 403, pp. 567-571.

Prakash, B., et al. 2000b. Tri-phosphate structure of guanylate-binding protein 1 and implications for nucleotide binding and GTPase mechanism. *EMBO Journal.* 2000b, 19, pp. 4555-4564.

Bibliography

Ramachandran, R., et al. 2007. The dynamin middle domain is critical for tetramerization and higher-order selfassembly. *EMBO Journal*. 2007, Vol. 2, 26, pp. 559-566.

Rani, A., et al. 2012. Insight into temperature dependence of GTPase activity in human guanylate binding protein-1. *PLoS One*. 2012, 7(7), e40487.

Robb, R.J. and Hill, G.R. 2012. The interferon-dependent orchestration of innate and adaptive immunity after transplantation. *Blood*. 2012, 119(23), pp. 5351-8.

Robertsen, B., et al. 2006. Molecular and expression analysis of an interferon-gamma-inducible guanylate-binding protein from rainbow trout (*Oncorhynchus mykiss*). *Dev. Comp. Immunol.* 2006, 30, pp. 1023-1033.

Scheffzek, K., et al. 1997. The Ras-RasGAP complex: structural basis for GTPase activation and its loss in oncogenic Ras mutants. *Science*. 1997, 277(5324), pp. 333-8.

Schnoor, M., et al. 2009. Guanylate-binding protein-1 is expressed at tight junctions of intestinal epithelial cells in response to interferon-gamma and regulates barrier function through effects on apoptosis. *Mucosal Immunol.* 2009, 2(1), pp. 33-42.

Schroder, K., et al. 2004. Interferon-gamma: an overview of signals, mechanisms and functions. *J Leukoc Biol.* 2004, 75(2), pp. 163-89.

Schweins, T., Geyer, M., et al. 1995. Substrate-assisted catalysis as a mechanism for GTP hydrolysis of p21ras and other GTP-binding proteins. *Nature Structural Biology*. 1995, 2, pp. 36-44.

Schwemmler, M. and Staeheli, P. 1994. The interferon-induced 67-kDa guanylate-binding protein (hGBP1) is a GTPase that converts GTP to GMP. *J. Biol. Chem.* 1994, 269, pp. 11299–11305.

Schwemmler, M., et al. 1996. Chicken guanylate-binding protein. Conservation of GTPase activity and induction by cytokines. *J. Biol. Chem.* 1996, 271, pp. 10304-10308.

Strehlow, I., Lohmann-Matthes, M.L. and Decker, T. 1994. The interferon-inducible GBP1 gene: structure and mapping to human chromosome 1. *Gene*. 1994, 144(2), pp. 295-299.

Syguda, A., et al. 2012. Tetramerization of human guanylate-binding protein 1 is mediated by coiled-coil formation of the C-terminal α -helices. *FEBS J.* 2012, 279(14), pp. 2544-2554.

Bibliography

Syguda, Adrian. 2008. Strukturelle und biophysikalische Charakterisierung der Oligomerisierung des humanen Guanylat-bindenden Proteins 1. *PhD thesis RUB*. 2008.

Takagi, K., et al. 2011. High TSC22D3 and low GBP1 expression in the liver is a risk factor for early recurrence of hepatocellular carcinoma. *Exp Ther Med*. 2011, 2(3), pp. 425-431.

Taylor, G. A., Feng, C. G. und Sher, A.. 2004. p47 GTPases: regulators of immunity to intracellular pathogens. *Nature Review Immunology*. 2004, Bd. 4, S. 100-109.

Tietzel, I., El-Haibi, C. and Carabeo, R.A. 2009. Human guanylate binding proteins potentiate the anti-chlamydia effects of interferon-gamma. *PLoS One*. 2009, 4(8), e6499.

Traut, T.W. 1994. Physiological concentrations of purines and pyrimidines. *Mol Cell Biochem*. 1994, 140(1), pp. 1-22.

Tripal, P., et al. 2007. Unique features of different members of the human guanylate-binding protein family. *J Interferon Cytokine Res*. 2007, 27(1), pp. 44-52.

Uetani, K., et al. 2008. Influenza A virus abrogates IFN-gamma response in respiratory epithelial cells by disruption of the Jak/Stat pathway. *Eur J Immunol*. 2008, 38(6), pp. 1559-1573.

Vestal, D.J. and Jeyaratnam, J.A. 2011. The guanylate-binding proteins: emerging insights into the biochemical properties and functions of this family of large interferon-induced guanosine triphosphatase. *J Interferon Cytokine Res*. 2011, 31(1), pp. 89-97.

Vestal, D.J. 2005. The guanylate-binding proteins (GBPs): proinflammatory cytokine-induced members of the dynamin superfamily with unique GTPase activity. *J Interferon Cytokine Res*. 2005, 25(8), pp. 435-43.

Vetter, I.R. and Wittinghofer, A. 2001. The guanine nucleotide-binding switch in three dimensions. *Science*. 2001, 294, pp. 1299-1304.

von der Malsburg, A., et al. Stalk domain of the dynamin-like MxA GTPase protein mediates membrane binding and liposome tubulation via the unstructured L4 loop. *J Biol Chem*. 286(43), pp. 37858-37865.

Vöpel, T., et al. 2010. Mechanism of GTPase activity induced self-assembly of human guanylate binding protein 1. *J. Mol. Biol*. 2010.

Bibliography

Vöpel, T., et al. 2014. Triphosphate induced dimerization of human guanylate binding protein 1 involves association of the C-terminal helices: a joint double electron-electron resonance and FRET study. *Biochemistry*. 2014, 53(28), pp. 4590-4600.

Vöpel, T., Kunzelmann, S. and Herrmann, C. 2009. Nucleotide dependent cysteine reactivity of hGBP1 uncovers a domain movement during GTP hydrolysis. *FEBS Letters*. 2009, Vol. 12, 583, pp. 1923– 1927.

Walker, J.E., et al. 1982. Distantly related sequences in the alpha- and beta-subunits of ATP synthase, myosin, kinases and other ATP-requiring enzymes and a common nucleotide binding fold. *EMBO Journal*. 1982, 1, pp. 945-951.

Wehner, M. and Herrmann, C. 2010. Biochemical properties of the human guanylate binding protein 5 and a tumor-specific truncated splice variant. *FEBS J*. 2010, 277(7), pp. 1597-1605.

Wehner, M., Kunzelmann, S. und Herrmann, C. 2012. The guanine cap of human guanylate-binding protein 1 is responsible for dimerization and self-activation of GTP hydrolysis. *FEBS J*. 2012, 279(2), S. 203-10.

Weinländer, K., et al. 2008. Guanylate binding protein-1 inhibits spreading and migration of endothelial cells through induction of integrin alpha4 expression. *FASEB J*. 2008, 22(12), pp. 4168-4178.

Wenneberg, K., Rossman, K.L. and Der, C.J. 2005. The Ras superfamily at a glance. *J.Cell Sci*. 2005, 118, pp. 843-846.

Wennerberg, K., Rossman, K.L. and Der, C.J. 2005. The Ras superfamily at a glance. *J Cell Sci*. 2005, 118(Pt 5), pp. 843-6.

Wittinghofer, A. and Vetter, I.R. 2011. Structure-function relationships of the G domain, a canonical switch motif. *Annu Rev Biochem*. 2011, 80, pp. 943-71.

Yamamoto, M., et al. 2012. A cluster of interferon- γ -inducible p65 GTPases plays a critical role in host defense against *Toxoplasma gondii*. *Immunity*. 2012, 37(2), pp. 302-313.

Yu, C.J., et al. 2011. Identification of guanylate-binding protein 1 as a potential oral cancer marker involved in cell invasion using omics-based analysis. *J Proteome Res*. 2011, 10, pp. 3778–3788.

Bibliography

Zhong, G. 2009. Killing me softly: chlamydial use of proteolysis for evading host defenses. *Trends Microbiol.* 2009, 17(10), pp. 467-74.

Zhu, Z., et al. 2013. Identification of human guanylate-binding protein 1 gene (hGBP1) as a direct transcriptional target gene of p53. *Biochem Biophys Res Commun.* 2013, 436(2), pp. 204-211.

Zhu, Z., et al. 2013. Nonstructural protein 1 of influenza A virus interacts with human guanylate-binding protein 1 to antagonize antiviral activity. *PLoS One.* 2013, 8(2), e55920.

Zimmermann, P., et al. 2011. The viral nucleoprotein determines Mx sensitivity of influenza A viruses. *J Virol.* 2011, 85(16), pp. 8133-40.

Acknowledgement

Ich danke all denjenigen, die mich während dieser Arbeit in irgendeiner Form unterstützt haben.

Allen voran geht mein ganz herzlicher Dank an meine Eltern und meine Geschwister inklusive ‚Schwiegerschwester‘ Kezban, Ismail, Mehmet Akif und Gökçen, die mir jederzeit Halt und Unterstützung und noch so vieles mehr gegeben haben. Ihr seid großartig! Kezban und Ismail danke ich zusätzlich für die tolle Unterstützung technischer und organisatorischer Art und ihre Geduld mit mir. Meiner Mutter danke ich insbesondere für die eine Bewerbung, die sie mich hat schreiben lassen. Diese stellte sich tatsächlich als entscheidender Faktor für meinen gesamten beruflichen Werdegang heraus.

Prof. Dr. Christian Herrmann danke ich für die Chance, in seiner Arbeitsgruppe forschen zu dürfen. Nicht nur während meiner Doktorarbeit, sondern auch lange vorher habe ich fachlich und menschlich viel von Ihnen lernen können. Danke für ein tolles Jahrzehnt!

Prof. Dr. Raphael Stoll danke ich für die Bereitschaft, das Zweitgutachten zu übernehmen.

Weiterhin danke ich meinen Korrekturlesern Miriam, Arzu, Sergii. Die kreativen Kommentare habe ich mit Freude studiert!

Ich danke ehemaligen Mitgliedern der AG Proteininteraktionen, insbesondere Agne, Adrian, Caro und Viji, sowie den aktuellen Mitgliedern Miriam, Sergii, Oktavian, Klaus, Fabian und Linda für ein tolles Arbeitsklima, anregende Diskussionen, Lehrreiches und manchmal sogar weniger Lehrreiches. Miriam und Sergii danke ich vor allem für die tolle Unterstützung in den letzten Zügen der Arbeit, aber auch für die Zeit vorher, in der das Forschen an GBPs eine gemeinsame Herzensangelegenheit wurde.

Und schließlich danke ich meinen Mädels Emel, Hatice, Arzu, Gülhan, Zehra und Banu, die alle auf ihre ganz eigene Weise eine Bereicherung für mich sind. Schön, dass es euch gibt!

Curriculum vitae

Name: Semra Ince
Date of Birth: 17.09.1982
Place of Birth: Dortmund

Education

2011–2015 Ph. D. student at Ruhr-University Bochum
2008-2011 Master studies in Mathematics and Biology (M.Ed.), Ruhr-University Bochum
2005-2008 Bachelor studies in Mathematics and Biology (B.Sc.), Ruhr-University Bochum
2002-2005 Training as biology laboratory technician at the Max-Planck-Institute for molecular physiology in Dortmund
1993-2002 Phönix-Gymnasium, Dortmund

Working experience

2005–2011 Biology laboratory technician in the group of Prof. Dr. Christian Herrmann, Physical Chemistry I, Faculty for Chemistry and Biochemistry, Ruhr-University Bochum

Publications

FEBS J. 2012; 279(14):2544-54.

Tetramerization of human guanylate-binding protein 1 is mediated by coiled-coil formation of the C-terminal α -helices.

Syguda A, Bauer M, Benschaid U, Ostler N, Naschberger E, Ince S, Stürzl M, Herrmann C.

J Med Chem. 2013; 56(23):9664-72.

Bisphenol A binds to Ras proteins and competes with guanine nucleotide exchange: implications for GTPase-selective antagonists.

Schöpel M, Jockers KF, Düppe PM, Autzen J, Potheraveedu VN, Ince S, Yip KT, Heumann R, Herrmann C, Scherkenbeck J, Stoll R.

Mol Cell Biol. 2014; 34(2):196-209.

Gamma interferon-induced guanylate binding protein 1 is a novel actin cytoskeleton remodeling factor.

Ostler N, Britzen-Laurent N, Liebl A, Naschberger E, Lochnit G, Ostler M, Forster F, Kunzelmann P, Ince S, Supper V, Praefcke GJ, Schubert DW, Stockinger H, Herrmann C, Stürzl M.

(Submitted)

Interaction of isolated cross-linked short Actin Oligomers with the Skeletal Muscle Myosin Motor Domain.

Qu Z, Fujita-Becker S, Ballweber E, Ince S, Herrmann C, Schröder RR, Mannherz HG

Conferences attended

Cold Spring Harbor Asia, "Small GTPase Small GTPases at Different Scales: Proteins, Membranes, Cells". September 24 - 28, 2012. Suzhou, China. Poster: Biochemical Characterization of human Guanylate Binding Protein 2.

Molecular Life Sciences 2013 – International Symposium of the German Society of Biochemistry and Molecular Biology. October 03. -06, 2013. Frankfurt am Main, Germany. Poster: Mutations in a hydrophobic cluster in human Guanylate Binding Protein 1 (hGBP-1) induce striking differences in enzymatic activity and intramolecular arrangement.

FEBS EMBO Meeting hosted by SFBBM. 30 August – 4 September 2014. Paris, France. Poster: Molecular insights into interactions between isoforms of human Guanylate Binding Proteins – anti-pathogenic players of the immune system.